N71-23714

SPACE SYSTEMS

GE-SSO-70SD4286
FEBRUARY 1, 1971

FINAL REPORT

ROLLUP SUBSOLAR ARRAY

CASE FILE COPY

Prepared for: Jet Propulsion Laboratory

Prepared Under: Contract 952314

DDC
RECEIVED
MAY 1971
C

VOLUME II

DETAILED TEST RESULTS

GENERAL ELECTRIC

Report No. 70SD4286

Date February 1, 1970

Volume II

DETAILED TEST RESULTS

Prepared for

JET PROPULSION LABORATORY
CALIFORNIA INSTITUTE OF TECHNOLOGY
4800 OAK GROVE DRIVE
PASADENA, CALIFORNIA

Prepared Under: Contract 952314
Contracting Officer: R. G. Curry
Project Manager: W. A. Hasbach

Prepared by: N. Shepard
P. Perez
K. Hanson
Dr. R. Ross (JPL)

Approved by:

K. L. Hanson
Project Manager

THIS WORK WAS PERFORMED FOR THE JET PROPULSION LABORATORY, CALIFORNIA INSTITUTE OF TECHNOLOGY AS SPONSORED BY THE NATIONAL AERONAUTICS AND SPACE ADMINISTRATION UNDER CONTRACT NAS 7-100

GENERAL ELECTRIC
SPACE SYSTEMS ORGANIZATION
Valley Forge Space Center
P O Box 8555 • Philadelphia, Penna 19101

This report contains information prepared by the General Electric Co., Space Systems Organization, under JPL Subcontract. Its content is not necessarily endorsed by the Jet Propulsion Laboratory, California Institute of Technology, or the National Aeronautics and Space Administration.

Volume II

TABLE OF CONTENTS

Section		Page
1	INTRODUCTION	1-1
2	FINAL ASSEMBLY AND BLANKET INSTALLATION	2-1
	2.1 General	2-1
	2.2 Alignment of Drums and Array Blankets	2-1
	2.3 Bonding of Leading Edge Loop	2-4
3	DEVELOPMENT TEST PROGRAM	3-1
	3.1 Introduction	3-1
	3.2 Background	3-1
	3.3 Discussion of Results and Conclusion	3-3
4	SYSTEM TEST PROGRAM	4-1
	4.1 Introduction	4-1
	4.2 Health Checks and Inspections	4-2
	4.2.1 Introduction	4-2
	4.2.2 Test Setup and Special Equipment	4-4
	4.2.3 Test and Inspection Results	4-12
	4.2.4 Conclusions and Recommendations	4-47
	4.3 Deployed Dynamics Tests	4-49
	4.3.1 Introduction	4-49
	4.3.2 Test Approach	4-49
	4.3.3 Test Results	4-66
	4.3.4 Post Test Analysis of Out of Plane Modes Using Revised Mathematical Models	4-127
	4.3.5 In-Plane Results Discussion	4-149
	4.3.6 Summary of Pretest Analysis	4-156
	4.4 Pryotechnic Shock Test	4-162
	4.4.1 Introduction	4-172
	4.4.2 Test Objectives	4-172
	4.4.3 Results and Conclusions	4-172
	4.4.4 Discussion of Testing	4-174
	4.5 Thermal-Vacuum Test	4-180
	4.5.1 Introduction	4-180
	4.5.2 Description of Test Setup	4-180
	4.5.3 Instrumentation	4-187
	4.5.4 Test Procedure	4-195
	4.5.5 Test Results	4-205
	4.5.6 Conclusions and Recommendations	4-243

TABLE OF CONTENTS (CONT.)

Section			Page
	4.6	Acoustic Test	4-244
		4.6.1 Introduction	4-244
		4.6.2 Objectives	4-245
		4.6.3 Results and Conclusions	4-246
		4.6.4 Discussion of Testing	4-248
	4.7	Stowed Dynamics Test	4-266
		4.7.1 Summary	4-266
		4.7.2 Test Objectives	4-266
		4.7.3 Results	4-267
		4.7.4 Test Setup and Test Conduction	4-275
		4.7.5 Discussion of Test Results	4-286
5	REFERENCES		5-1

LIST OF ILLUSTRATIONS

Figure		Page
1.0-1	Final Assembly and System Test Sequence	1-2
2.1-1	RA250 Mechanical Assembly	2-2
2.2-1	Alignment of Storage Drum/Blanket	2-3
2.3-1	Bonding of Leading Edge Loop	2-6
3.1-1	Thermal Bending Test Setup (NASA G-69-4536)	3-2
3.2-1	Test Coordinates	3-7
4.2-1	Sequence of Health Checks	4-3
4.2-2	+Y Blanket Unwrapped on Table for Inspection	4-5
4.2-3	Module Illumination (VF 70323A)	4-6
4.2-4	Uniformity Measurement Setup (VF 70323B)	4-7
4.2-5	Upward Deployment Aid Force-Deflection Curve	4-9
4.2-6	Upward Deployment Aid Installed on Roof Beam (VF 70142)	4-10
4.2-7	Upward Deployment Aid Installation in 32 x 54 Foot Chamber (VF 70249A)	4-11
4.2-8	Solar Cell and Platelet Breakage	4-16
4.2-9	Damage in J6 Module	4-20
4.2-10	Damage in H1 Module	4-22
4.2-11	Fractured Cell at Foot in G7 Module	4-23
4.2-12	Deployment of RA250	4-25
4.2-13	Examples of BI-STEM Current History During Deployment	4-27
4.2-14	Examples of BI-STEM Current History During Retraction	4-29
4.2-15	Examples of BI-STEM Deploy/Retract Time Histories	4-31
4.2-16	BI-STEM Limit Switch Actuator Problem	4-34
4.2-17	BI-STEM Rod Element Crack	4-36
4.2-18	History of Slip Ring Dynamic Resistance	4-39
4.2-19	Thermistor Location on -Y Array Blanket	4-42
4.2-20	+Y Blanket Thermistor Characteristics	4-44
4.2-21	-Y Blanket Thermistor Characteristics	4-45
4.3-1	Deployed Dynamics Test Setup	4-52
4.3-2	Deployed Dynamics Test Setup-View from Top of Chamber (Lid OFF) Showing Shaker Assembly and Modal Test Support Fixture (VF 70180C)	4-53
4.3-3	Deployed Dyanmics Test Setup-View of Array and Handling Frame Mounted on Modal Test Support Fixture. Support Aids Are Mounted on the Handling Frame (VF 70180H)	4-54
4.3.4	Deployed Dynamics Test Setup. View from Bottom of Vacuum Chamber from Back Side of Blankets (Wide Angle Lens). Targets for Displacement Trackers Can Be Seen Through the Blanket. Targets on BI-STEM Are Also Visible (VF 70209F)	4-55
4.3-5	Deployed Dynamics Test Setup. View of Low End of Blankets. BI-STEM Boom and Leading Edge Member Are Not Installed. Fixed Trackers to Measure Motion of Outboard Ends at Leading Edge Member Are Visible	4-56

LIST OF ILLUSTRATIONS (CONT.)

Figure		Page
4.3-6	Deployed Dynamics Test Setup. View of Six Optical Trackers Mounted On Scanning Bar (VF 70193C)	4-57
4.3-7	Array Optical Target and Tracker Distribution	4-58
4.3-8	Target Details	4-61
4.3-9	Deployed Dynamics Test Data Flow	4-63
4.3-10	Frequency Sweep-Out-of-Plane Symmetric Excitation	4-72
4.3-11	Frequency Sweep-Out-of-Plane Symmetric Excitation	4-73
4.3-12	Frequency Sweep-Out-of-Plane Symmetric Excitation	4-74
4.3-13	Frequency Sweep-Out-of-Plane Symmetric Excitation	4-75
4.3-14	Frequency Sweep-Out-of-Plane Symmetric Excitation	4-76
4.3-15	Frequency Sweep-Out-of-Plane Symmetric Excitation	4-77
4.3-16	Mode Shape-First Mode-Out-of-Plane Symmetric Excitation	4-84
4.3-17	Mode Shape-Second Mode-Out-of-Plane Symmetric Excitation	4-85
4.3-18	Mode Shape-Third Mode-Out-of-Plane Symmetric Excitation	4-86
4.3-19	Oscilloscope Records of Input and Response for Symmetric Excitation	4-88
4.3-20	Decay of Vibration in First Symmetric Mode	4-89
4.3-21	Decay of Vibration Mode at 0.6325 Hz Excited by Symmetric Excitation	4-90
4.3-22	Decay of Vibration In Mode at 0.781 Hz Excited by Symmetric Excitation	4-91
4.3-23	Response to Step Input Symmetric Excitation	4-92
4.3-24	Frequency Sweep-Out-of-Plane Antisymmetric Excitation	4-97
4.3-25	Frequency Sweep-Out-of-Plane Antisymmetric Excitation	4-98
4.3-26	Frequency Sweep-Out-of-Plane Antisymmetric Excitation	4-101
4.3-27	Frequency Sweep-Out-of-Plane Antisymmetric Excitation	4-102
4.3-28	Frequency Sweep-Out-of-Plane Antisymmetric Excitation	4-103
4.3-29	Frequency Sweep-Out-of-Plane Antisymmetric Excitation	4-104
4.3-30	Mode Shape-First Out-of-Plane Antisymmetric Excitation	4-107
4.3-31	Damping Co-efficients For Lower Nested Torsional Resonance, Based on Exponental Decay From Suddenly Removed Shaker Excitation	4-110
4.3-32	Oscilloscope Records of Input (LVDT) and Response for Antisymmetric Excitation	4-111
4.3-33	Decay of Vibration from Higher Modes Excited by Antisymmetric Excitation 80% Span-Tracker 8Z	4-112
4.3-34	Response of System to Step Input Antisymmetric (Torsion) Excitation	4-113
4.3-35	Response of System to Sudden Input Antisymmetric (Torsion) Excitation	4-114
4.3-36	Frequency Sweep - In-Plane Excitation	4-116
4.3-37	Frequency Sweep - In-Plane Excitation	4-117
4.3-38	Frequency Sweep - In-Plane Excitation	4-119
4.3-39	Frequency Sweep - In-Plane Excitation	4-120
4.3-40	Characteristics of -Y Blanket Support	4-129
4.3-41	Characteristics of +Y Blanket Support	4-130

LIST OF ILLUSTRATIONS (CONT.)

Figure		Page
4.3-42	Blanket Substructure Discretization	4-132
4.3-43	Complete Finite Element Discretization of the Deployed Roll-up Array	4-133
4.3-44	Effect of Blanket Rigidity on Deployed Natural Frequencies (LEM Tension = 2 lbs/Blanket)	4-136
4.3-45	Effect of Blanket LEM Attachment Tension on Deployed Natural Frequencies (Blanket Rigidity = 0.1 in.-lbs)	4-138
4.3-46	Composite Structural Mode Resulting From Unequal LEM Tensions	4-140
4.3-47	Four Tension Distributions Used to Analyze the Effect of Non-Uniform Blanket Tensions	4-142
4.3-48	Effect of Non-Uniform Blanket Tensions on Deployed Natural Frequencies	4-143
4.3-49	First Blanket Resonance with Non-Uniform Tension Distribution	4-144
4.3-50	Typical Higher Order Mode With Non-Uniform Unequal Tension Distribution	4-146
4.3-51	In-Plane Deflection Mode	4-151
4.3-52	Drum Flexing Caused by In-Plane Displacement	4-154
4.3-53	Predicted Response at Outboard Edge of Blanket (80% Span) Out-of-Plane Symmetric Excitation	4-157
4.3-54	Predicted Response at Outboard Edge of Leading Edge Member (Torsional Excitation)	4-158
4.3-55	Results of Narrow Band Frequency Sweep	4-159
4.3-56	Effect of Damping on Response	4-160
4.4-1	Coordinate System for Use in Shock Discussion	4-165
4.4-2	Shock Spectra Induced by Spacecraft Separation Band Release and RA250 Uncaging	4-167
4.4-3	Shock Pulse	4-169
4.4-4	Comparison of Response Spectrum at Fixture With Sawtooth Shock Pulse	4-170
4.4-5	Comparison of Response Spectrum at Fixture With Sawtooth Shock Pulse	4-171
4.4-6	Comparison of Response Spectrum at Fixture With Sawtooth Shock Pulse	4-172
4.4-7	Comparison of Response Spectrum at Fixture With Sawtooth Shock Pulse	4-173
4.4-8	Shock Test Data System	4-175
4.4-9	Test Set-Up	4-176
4.4-10	Shock Response Spectrum at Fixture (331Y)	4-178
4.4-11	Shock Response Spectrum on Caging Arm (338X)	4-179
4.5-1	IR Lamp Array Under Construction (VF 70208C)	4-180
4.5-2	Lamp Zone Arrangement	4-183
4.5-3	IR Lamp Array Mounted in Chamber (Viewed From Above) (VF 70237A)	4-185
4.5-4	Leading Edge of Fully Deployed Array (VF 70240C)	4-186

LIST OF ILLUSTRATIONS (CONT.)

Figure		Page
4.5-5	Lamp Zones for Heliotek, GE No. 2, and Boeing Modules (VF 70240E)	4-188
4.5-6	Specimen Thermocouple Locations	4-193
4.5-7	Storage Drum Thermocouple Locations	4-192
4.5-8	Thermocouple Installation on BI-STEM Elements	4-196
4.5-9	Deployed Transient Temperature History	4-206
4.5-10	Deployed Transient Temperature History	4-207
4.5-11	Deployed Transient Temperature History	4-208
4.5-12	Deployed Transient Temperature History	4-209
4.5-13	Deployed Transient Temperature History	4-210
4.5-14	Deployed Transient Temperature History	4-211
4.5-15	Deployed Transient Temperature History	4-212
4.5-16	Deployed Transient Temperature History	4-213
4.5-17	Deployed Transient Temperature History	4-214
4.5-18	Deployed Transient Temperature History	4-215
4.5-19	Deployed Transient Temperature History	4-216
4.5-20	Deployed Transient Temperature History	4-217
4.5-21	Deployed Array Heating Transient From -202°F (-130°C)	4-219
4.5-22	Deployed Array Cooling Transient From +284°F (+140°C)	4-219
4.5-23	Low Temperature Stowed Cool-Down History	4-220
4.5-24	Low Temperature Stowed Cool-Down History	4-221
4.5-25	Low Temperature Stowed Cool-Down History	4-222
4.5-26	Outboard End Support Showing Fractured Separation Nut Mounting Base (VF 70244B)	4-224
4.5-27	Both Separation Nuts With Fractured Mounting Bases (VF 70244C)	4-225
4.5-28	Unwrapped -Y Blanket as Viewed From Lamp Array Side (VF70244A)	4-228
4.5-29	Unwrapped -Y Blanket as Viewed From Rear Side (VF70244E)	4-229
4.5-30	Unwrapped -Y Blanket as Viewed From Above (VF70244D)	4-230
4.5-31	Stowed Transient Temperature History	4-231
4.5-32	Stowed Transient Temperature History	4-232
4.5-33	Stowed Transient Temperature History	4-233
4.5-34	Stowed Array Heating Transient From -202°F (130°C)	4-235
4.5-35	Stowed Array Cooling Transient From +284°F (+140°C)	4-235
4.5-36	Scorch Marks on +Y Array Blanket	4-236
4.5-37	Scorch Marks on -Y Array Blanket	4-237
4.5-38	Transmittance of Corning 0211 Microsheet	4-239
4.5-39	Color Temperature Versus Voltage for Quartzline Lamp-Tungsten T3-500 Watt	4-241
4.5-40	Temperature Distribution in Stowed Rollup Array Blanket With Glass Simulated Solar Cells	4-242
4.6-1	Test Setup	4-249
4.6-2	Spectrogram of Input Acoustic Field During Run 2	4-250
4.6-3	Spectrogram of Input Acoustic Field During Run 3	4-251

LIST OF ILLUSTRATIONS (CONT.)

Figure		Page
4.6-4	Acoustic Test Results.	4-252
4.6-5	Acoustic Test Results.	4-253
4.6-6	Acoustic Test Results.	4-254
4.6-7	Acoustic Test Results.	4-255
4.6-8	Acoustic Test Results.	4-256
4.6-9	Acoustic Test Results.	4-257
4.6-10	Acoustic Test Results.	4-258
4.6-11	Acoustic Test Results.	4-259
4.6-12	Acoustic Test Results.	4-260
4.6-13	Acoustic Test Results.	4-261
4.6-14	Acoustic Test Results.	4-262
4.6-15	Acoustic Test Results.	4-263
4.6-16	View of Rollup Solar Array Installed in the Acoustic Chamber (C-70-0115-A).	4-264
4.6-17	Test Facility for Roll-up Solar Array Acoustic Test (C-70-0115-C).	4-265
4.7-1	Control Signal for Y Axis Sinusoidal Vibration - Qualification Level Run.	4-269
4.7-2	Control Signal for Y Axis Sinusoidal Vibration - Qualification Level Run.	4-270
4.7-3	Control Signal for Y Axis Sinusoidal Vibration - Qualification Level Run.	4-271
4.7-4	Control Signal for Y Axis Sinusoidal Vibration - Qualification Level Run.	4-272
4.7-5	Power Spectral Distribution of Control Signal for X-Axis Random Vibration Qualification Level Run.	4-273
4.7-6	Power Spectral Distribution of Control Signal for Z-Axis Random Vibration Qualification Level Run.	4-274
4.7-7	RA250 Stowed Vibration Test Instrumentation.	4-277
4.7-8	Data Processing System	4-281
4.7-9	Y Axis Test Setup (VF 70271B).	4-282
4.7-10	Z Axis Test Setup with X Axis Exciter and Hydrastatic Bearing in Foreground (VF 700275B)	4-283
4.7-11	X Axis Test Setup (VF 70278)	4-284
4.7-12	Frequency Sweep - Excitation Axis - X	4-289
4.7-13	Frequency Sweep - Excitation Axis - X	4-290
4.7-14	Frequency Sweep - Excitation Axis - X	4-291
4.7-15	Frequency Sweep - Excitation Axis - X	4-292
4.7-16	Control Signal for Y Axis Sinusoidal Vibration - Qualification Level Run.	4-295
4.7-17	Control Signal for Y Axis Sinusoidal Vibration - Qualification Level Run.	4-296
4.7-18	Control Signal for Z Axis Sinusoidal Vibration Qualification Level Run.	4-297
4.7-19	Control Signal for X Axis Sinusoidal Vibration - Qualification Level Run.	4-298

LIST OF ILLUSTRATIONS (CONT.)

Figure		Page
4.7-20	Power Spectral Distribution for Control: Signal for X Axis Random Vibration - Qualification Level Run.	4-301
4.7-21	Power Spectral Distribution of Control Signal for Z Axis Random Vibration - Qualification Level Run.	4-302
4.7-22	Power Spectral Distribution of Control Signal for X Axis Random Vibration - Qualification Level Run.	4-303

SECTION 1

INTRODUCTION

Volume II of the Final Report on the 30 Watt Per Pound Rollup Solar Array presents the detailed results of the final four (4) months of the program which consisted of the final assembly and systems tests of the engineering development unit. Test results are described, analyzed and compared with the analyses reported in quarterly reports previously issued on this program. Parallel with the system test activity, the NASA Goddard Space Flight Center continued with thermal bending tests of sections of the BISTEM boom and results are included in this report.

The time phasing for the system test sequence is shown in Figure 1-1. Health checks were performed at selected points in the sequence so that damage or anomalies could be associated with a particular test or environment. Failures were recorded but not repaired before proceeding with the program. No problems occurred which prevented completion of the test program.

Several of the tests resulted in unusual test equipment or required unusual test techniques. These are discussed in this part of the report. The test results have been assessed with respect to future qualification testing of a rollup solar array or integration with a spacecraft and recommendations for future programs are presented.

Volume I summarizes the results of the total program.

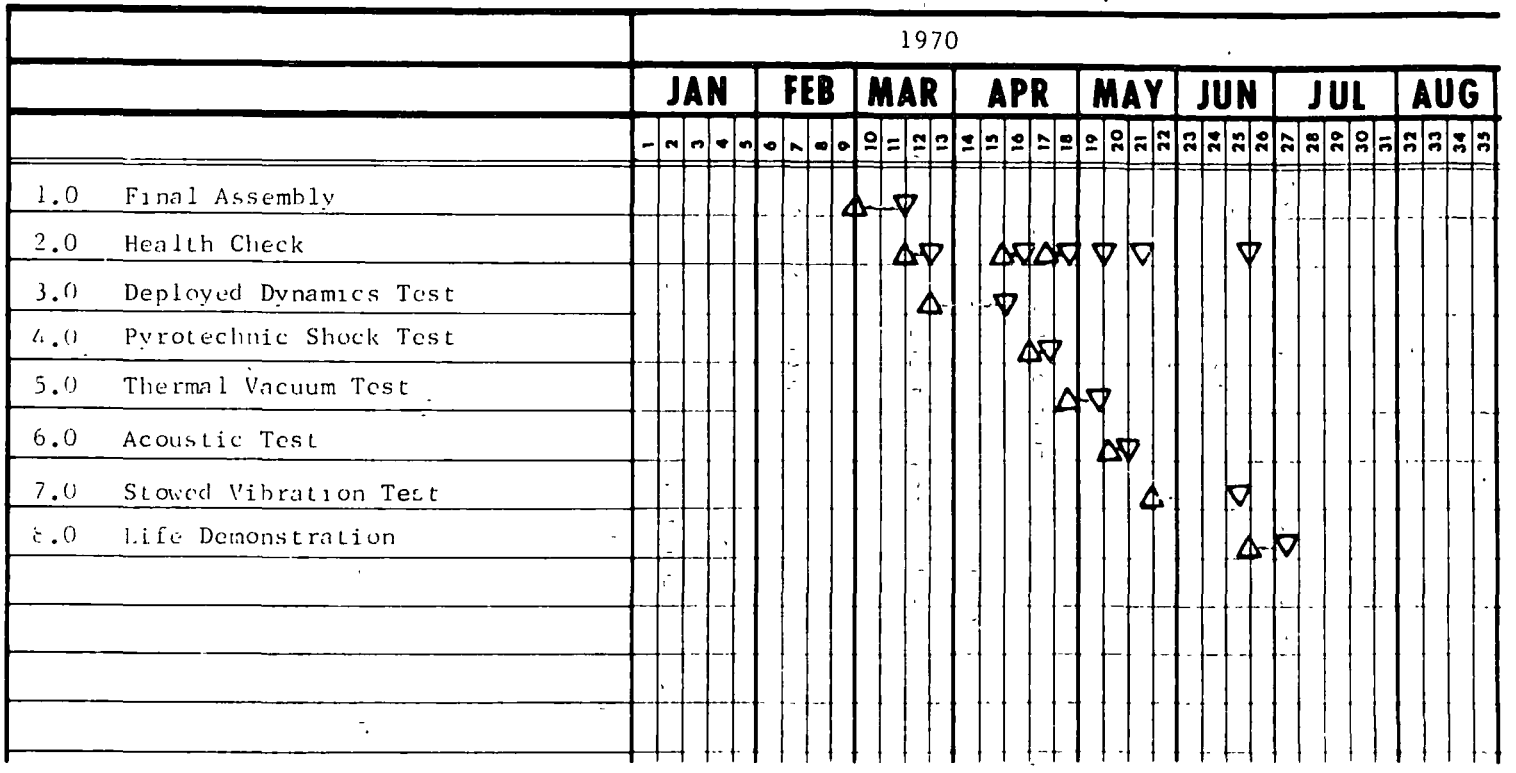

Figure 1.0-1. Final Assembly and System Test Sequence

SECTION 2

FINAL ASSEMBLY AND BLANKET INSTALLATION

2.1 GENERAL

The assembly of the system mechanical components was straight forward and was performed without difficulty. Figure 2.1-1 is a photograph of the completed mechanical assembly prior to the installation of the array blankets. Note that the system was assembled on a holding fixture which served as the interface with all test fixtures and the handling dolly. The array was not removed from this fixture during the test program. A provision for adjusting the outboard end supports with respect to the centerline of the center support tube should be incorporated in any subsequent models which are built to this basic design concept. This alignment is important to avoid difficulty in engaging the tapered plugs of the outboard end supports with the tapered holes in the outboard end caps of the storage drums.

2.2 ALIGNMENT OF DRUMS AND ARRAY BLANKETS

The most important factor which affects the ability of the array blankets to rewrap properly is the initial alignment of the array blankets with respect to the storage drums. During the installation of the blankets on the storage drums, the perpendicularity of the blanket edges with respect to the center line of the storage drums was established by optical methods. The details of this procedure are illustrated in Figure 2.2-1. First, the handling dolly was positioned at one end of the long work table so that the storage drum axis is approximately normal to the edge of the table. The dolly was then leveled so that the storage drum axis is horizontal (Figure 2.2-1(a)). A triangulation transit is then set up

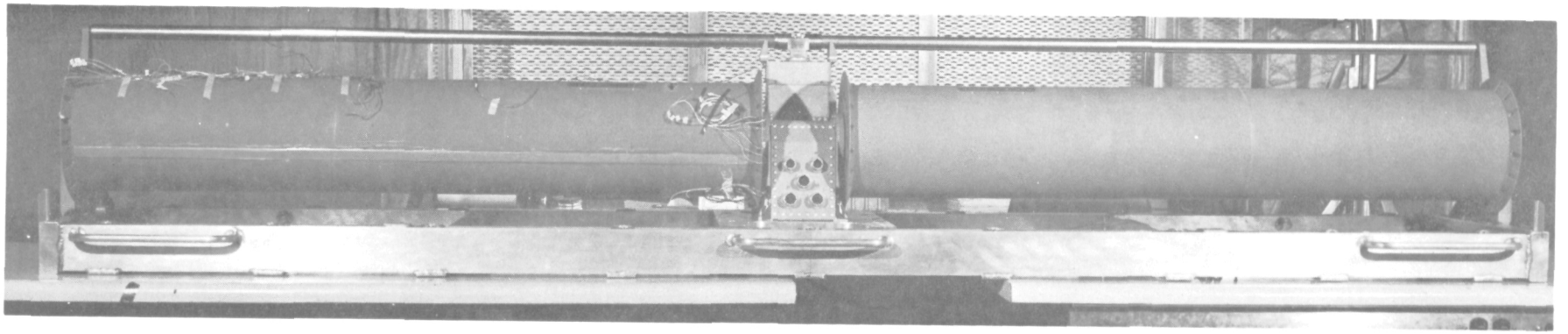

Figure 2.1-1. RA250 Mechanical Assembly

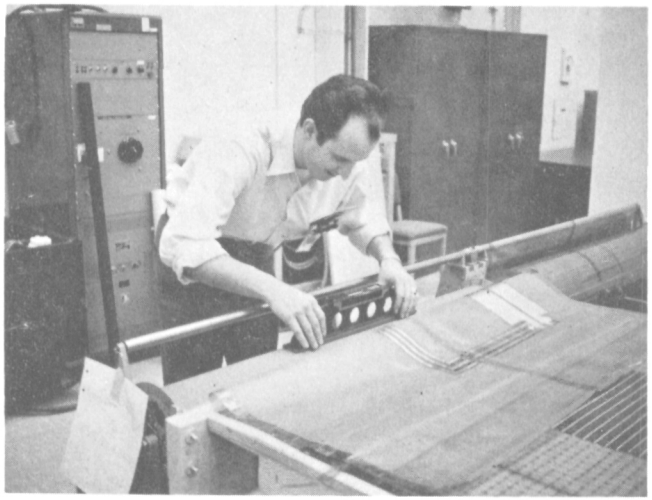

(a) Level Drum Shell

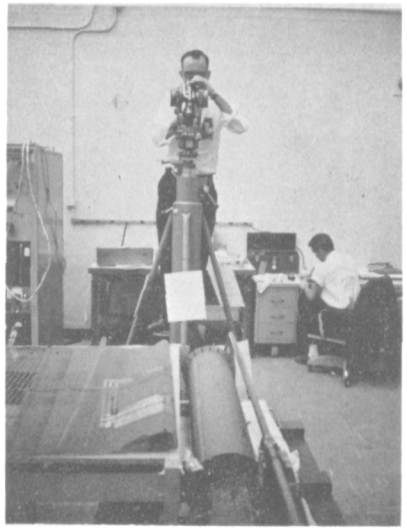

(b) Establish Optical Line of Sight Along Drum Axis

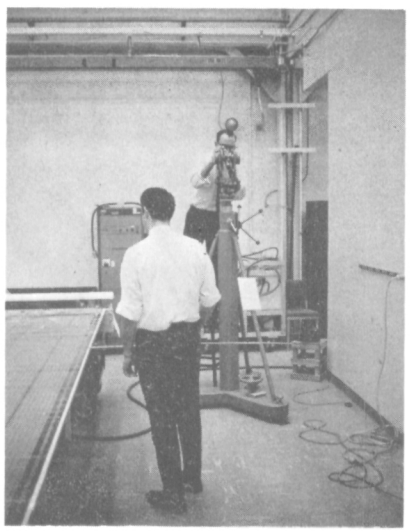

(c) Establsih Blanket Edge Which is Normal to Drum Axis

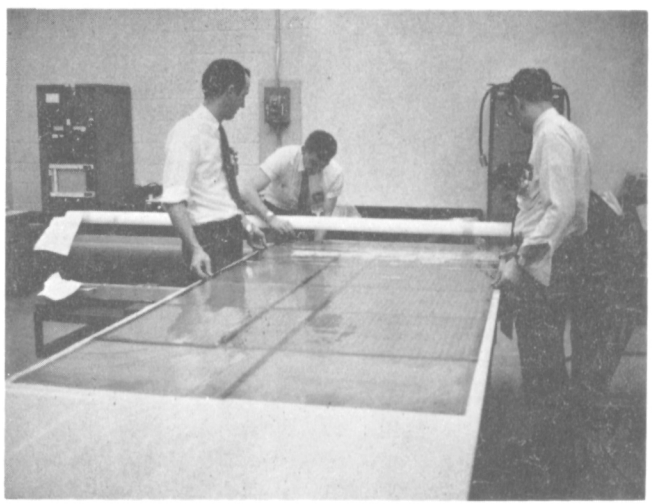

(d) After Securing to Drum Shell, Wrap Up Blanket on Drum

Figure 2.2-1. Alignment of Storage Drum/Blanket

and leveled so that a line of sight is established parallel with the centerline of the storage drum (see Figure 2.2-1(b)). The transit is then turned through a horizontal angle of 90 degrees to establish a line of sight which is normal to the drum axis. The distance between the edge of the array blanket and this line of sight is then measured at 2 foot stations along the length of the blanket (see Figure 2.2-1(c)). The position of the array blanket is then corrected to produce an edge which is everywhere equidistant from the line of sight with the inboard end positioned properly with respect to the drum feedthrough penetrations. This is verified by again measuring at the blanket stations. This straight and parallel edge of the blanket is then transferred to the table by marking along the entire edge. The inboard end of the blanket is then trimmed and taped to the drum shell so that the bus strips coincide with the feedthrough penetrations. Without removing the tape, the substrate was bonded to the drum shell with SMRD 100.* The Schjel-Clad residual adhesive was removed from the blanket substrate in the bond area.

The array blanket was wrapped on drum shell by allowing the Negator spring system to supply the necessary force while the edge of the blanket is guided so that it always remains coincident with the line marked on the table. In this way, the blanket was wrapped so that every layer was directly on top of the previous layer.

2.3 BONDING OF LEADING EDGE LOOP

After the initial wrapping of each blanket, the leading edge termination was made by looping the substrate around the leading edge member and joining it to

---

* SMRD 100 is a flexible epoxy formulated by and available from GE-SSO.

itself by bonding with SMRD 100. The excess Kapton was trimmed off so that the loop could be bonded (see Figure 2.3-1(a)). The residual Schjel-Clad adhesive was removed from the blanket substrate in the bond area (see Figure 2.3-1(b)). The SMRD 100 adhesive was applied and cured with heater blankets for 16 hours at 250°F. The intent was to position the loop with respect to the Loading Edge Member (LEM) so that there was a uniform distribution of load across the substrate width. This technique did not provide a uniform blanket tension distribution and, in general, will not. The load deflection characteristics of the leading edge member must be taken into account to provide a uniform distribution and the load distribution will change as the total blanket tension load changes. A simple leading edge loop was selected over more complex methods that would have provided adjustments to modify the load distribution. As discussed in Section 4.3, the load distribution was modified for special test by stuffing the loop with paper towels to determine the effects of tension distribution.

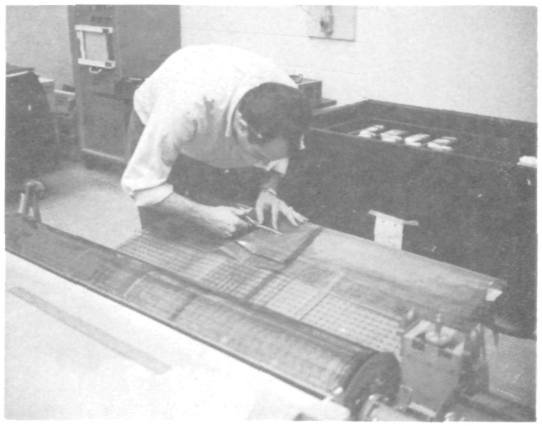

(a) Trimming of Excess Substrate Leader

(b) Removing Residual Schyel - Clad Adhesive Prior to Bonding With SMRD-100

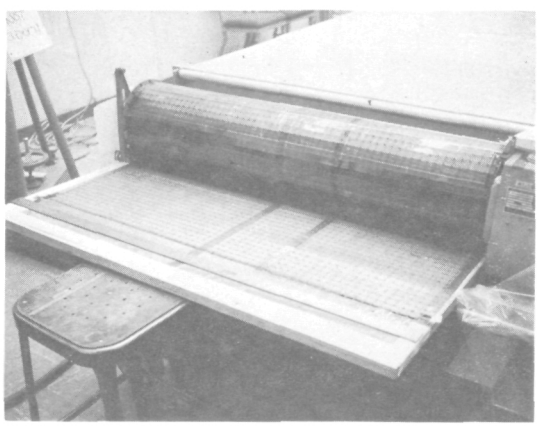

(c) Prior to Application of Heater Blanket to Cure SMRD-100

Figure 2.3-1. Bonding of Leading Edge Loop

SECTION 3

DEVELOPMENT TEST PROGRAM RESULTS

3.1 INTRODUCTION

During the system test phase development testing continued on the thermal bending characteristics of the BI-STEM rod. Partial results of this test were included in Reference 1-6.

The objective of this test was to correlate empirical thermal distortion data obtained on a sample BI-STEM boom to aid analytical prediction of boom thermal distortion under orbital operating conditions.

3.2 BACKGROUND

NASA/GSFC has been studying the bending of deployable booms that results from radiant thermal excitation for several years. To support these studies a specialized facility is maintained.

The thermal vacuum chamber utilized in investigating boom thermal bending behavior consists essentially of a vertical cylinder approximately 1 foot in diameter and 13 feet high, incorporating a liquid N_2 shroud, and a heat source that provides an intensity equivalent to one solar constant over the full length of a 10 foot boom surface with an intensity uniformity of better than ± 5 per cent. The facility is shown in Figure 3.1-1.

In addition, the facility employs a high-speed, low backstreaming pumping system and provision for rotating the suspended test specimen over a range of angular velocities. The degree of bending from thermal excitation can be recorded

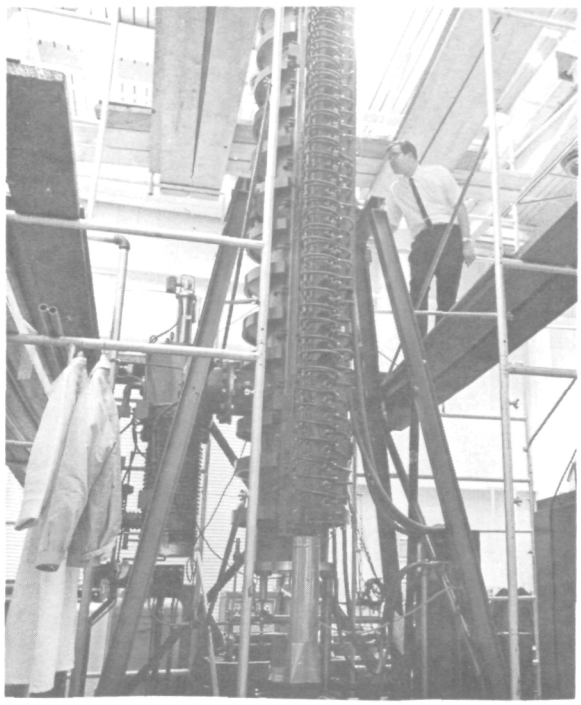

Figure 3.1-1 Thermal Bending Test Setup (NASA G-69-4536)

photographically as well as by optical means. Samples were removed from the test specimen to measure absorptance characteristics necessary to extrapolate the observed bending which resulted from essentially an IR source to solar radiation conditions. Peripheral temperature distribution, time constants relating to heat conductions around the perimeter, and heat flow from the solar source to boom and shroud were recorded.

Over the past 2 years, NASA/GSFC has employed this facility in the development of a technique for measurement of gravity gradient rod deflections under the influence of solar heating and the RA250 BI-STEM is one of many boom configurations that have been tested.

Test results were provided for use in this program and are included in this report. NASA/GSFC will issue a report on the entire boom thermal test program which will include the data on the RA250, 1.34 inch diameter BI-STEM.

3.3 DISCUSSION OF RESULTS AND CONCLUSION

Data presented in Table 3-1 a and b was obtained by repeating the following measurement sequence.

a. With the heat source off and the BI-STEM suspended by upper support, the center location of the BI-STEM lower end was established and nulled on the optical measurement system.

b. The heat source was energized and the position of the free end of the rod was monitored with the final stable location being read. The z and y in-plane and out-of-plane coordinates were read directly through a telescope prism optical system which viewed the free end of the rod along the rod vertical center line.

c. Angular twist data was obtained in the same manner using a quadrant reticle pattern.

TABLE 3-1a

TIP DEFLECTION OF 10' 1 3/8 INCH SILVER PLATED
RA250 BI-STEM

Source Angle	TIP NOT WELDED					
	Z mm	Y mm	θ_t Deg.	Z mm	Y mm	θ_t Deg.
0	+ 9.4	+7.1	N/D	+11.5	+ 9.1	- 4.5
30	+ 8.1	+2.1		+ 7.7	+ .8	+ 1.5
60	+11.5	-0.8		+12.8	+ 0.5	- 6.9
90	+13.1	-1.1		+13.3	- 2.3	- 8.0
120	+ 9.7	-3.8		+10.5	- 4.5	- 3.5
150	+ 6.4	-3.4		+ 7.0	- 2.7	- 2.4
180	+ 5.2	-1.7		+ 5.1	- 1.1	+ 5.7
210	+ 5.6	-1.1		+ 5.0	- 0.4	+11.5
240	+ 7.1	-0.8		+ 8.3	- 0.8	+16.0
270	+ 8.6	-2.3		N/D	N/D	N/D
300	+ 4.8	+1.7		+ 0.3	+ 8.4	- 1.5
330	+ 5.8	+8.3		+ 6.7	+11.8	- 2.5
Comment	a			b		

a - Boom pretwist not determined

b - -26 degree boom pretwist

N/D - No data

TABLE 3-1b

Source Angle	TIP WELDED								
	Z mm	Y mm	θ_t Deg.	Z mm	Y mm	θ_t Deg.	Z mm	Y mm	θ_t Deg.
0	+ 7.5	+10.4	N/D	+ 7.6	+ 3.2	- 0.5	+ 8.9	+10.3	0.0
30	+ 7.9	+ 3.8	N/D	+ 7.0	+ 1.2	+ 1.8	N/D	N/D	N/D
60	+12.8	+ 4.6	N/D	+11.4	+ 2.4	+ 2.0	+10.6	+ 2.9	+2.6
90	+15.5	+ 1.6	N/D	+11.9[a]	- 1.0[a]	N/D	N/D	N/D	N/D
120	+11.0	- 2.5	N/D	+ 7.2	- 3.6	+ 3.5	+14.5	- 3.1	+2.0
150	+ 7.8	- 3.9	N/D	+ 6.5	- 3.3	N/D	+11.5[a]	- 7.8[a]	N/D
180	+ 5.5	- 3.0	N/D	+ 5.2	- 1.3	N/D	+ 5.7	- 1.5	+0.5
210	+ 5.1	+ 0.1	N/D	+ 4.4[a]	+ 1.2[a]	N/D	N/D	N/D	N/D
240	+ 8.2	+ 1.3	N/D	+ 4.1[a]	+ 2.5[a]	N/D	+ 8.1	1.4	+10.5[a]
270	+10.0	+ 3.4	N/D	+ 3.8[a]	+ 3.7[a]	N/D	N/D	N/D	N/D
300	- 3.9	+ 8.4	N/D	+ 3.5	+ 4.8	-2.0	- 0.9	+ 6.7	+1.7
330	+ 8.5	+16.0	N/D	+ 6.1	+ 5.7	0.0	+15.4	+ 3.2	+2.8
Comments	b			c			d		

a - Estimate not data

b - Boom pretwist not determined

c - $+20^{o}$ boom pretwist

d - -26^{o} boom pretwist

N/D - No data

The test coordinate system is shown in Figure 3.2-1. Initial data runs reported in Reference 1-6 did not include angular twist response or pretwist condition of the specimen. It was subsequently noted that the rod can retain a mechanical pretwist and hence these effects were recorded even though in the RA250 configuration the BI-STEM and leading edge member are decoupled for torsion about the boom axis.

Extrapolation of the data from specimen test conditions to array orbital operating conditions was presented in Reference 1-6 where it was concluded that a total deflection of 23 inches would occur at one sun intensity. This compares with an analytical prediction of 35.7 inches at 1.5 suns intensity. Inspection of the data shows the deflection pattern is not symmetrical and that tip motion is not confined to the plane formed by the rod and the light source. A final report on the NASA/GSFC testing program (which included many types and sizes of deployable boom) is planned and should provide much additional data.

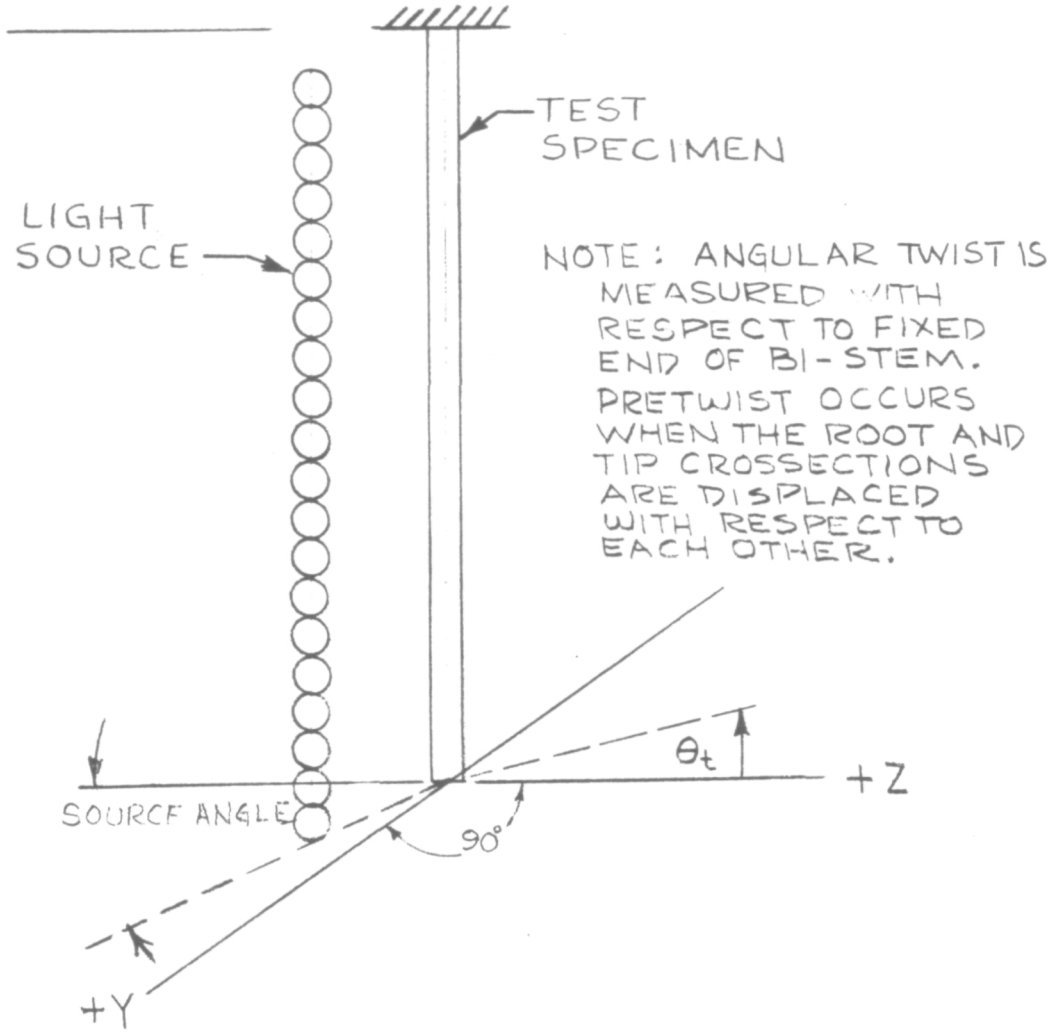

NOTE: AT SOURCE ANGLE OF ZERO DEGREES
THE SPECIMEN-LIGHT RELATIONS ARE
AS FOLLOWS:

Figure 3.2-1. Test Coordinates

SECTION 4

SYSTEM TEST PROGRAM

4.1 INTRODUCTION

The system test program was intended to verify the mathematical modeling and to validate the basic RA250 roll-up solar array design for future flight applications. In order to meet this objective, the RA250 prototype model was subjected to a deployed dynamics test to provide data on the dynamic characteristics of the deployed array. These experimental results could then be compared with the theoretical models which were used to predict the response of the system. Advances in the state-of-the-art for low frequency vibration testing were required to obtain these results since the specimen had resonant frequencies in the region of 0.1 Hz. These tests were conducted in a vacuum chamber at a pressure of approximately 1 torr to eliminate aerodynamic effects. A d.c. coupled exciter was used to provide sinusoidal base excitation. Array displacements were measured with electro-optical trackers (Optron Model 800). These trackers make no physical contact with the specimen and have the capability of measuring displacements in two directions over the frequency range from d.c. to 10 k Hz.

This deployed dynamics test was followed by a series of system level environmental tests which were conducted in the following order:

1. Pyrotechnic Shock Test
2. Thermal Vacuum Test
3. Acoustic Test
4. Stowed Dynamics Test

Intervening health checks were performed to check the status of the system. These health checks included inspection of the array blankets for damage, demonstration of deployment and retraction, and the assessment of the electrical characteristics of the active solar cell modules.

4.2 HEALTH CHECKS AND INSPECTIONS

4.2.1 INTRODUCTION

Throughout the testing program, the RA-250 was subjected to a performance test and detailed inspection in order to determine the "health" of the system after exposure to various environments. A total of seven of these health checks have been performed during the course of the system testing as shown in Figure 4.2-1. In general, each of these health checks included the following:

1. Array blanket inspection for breakage
2. Mechanical inspection of structure for damage
3. Electrical performance of active solar cell modules
4. System deployment and retraction to verify the performance of the BI-STEM actuator, slip ring assemblies, and drum bearing system.

The first health check was performed after the RA250 final assembly and established the initial condition of the test specimen prior to any environmental testing. Because of test schedule constraints, Health Check No. 3 did not include electrical performance measurements of the active solar cell modules.

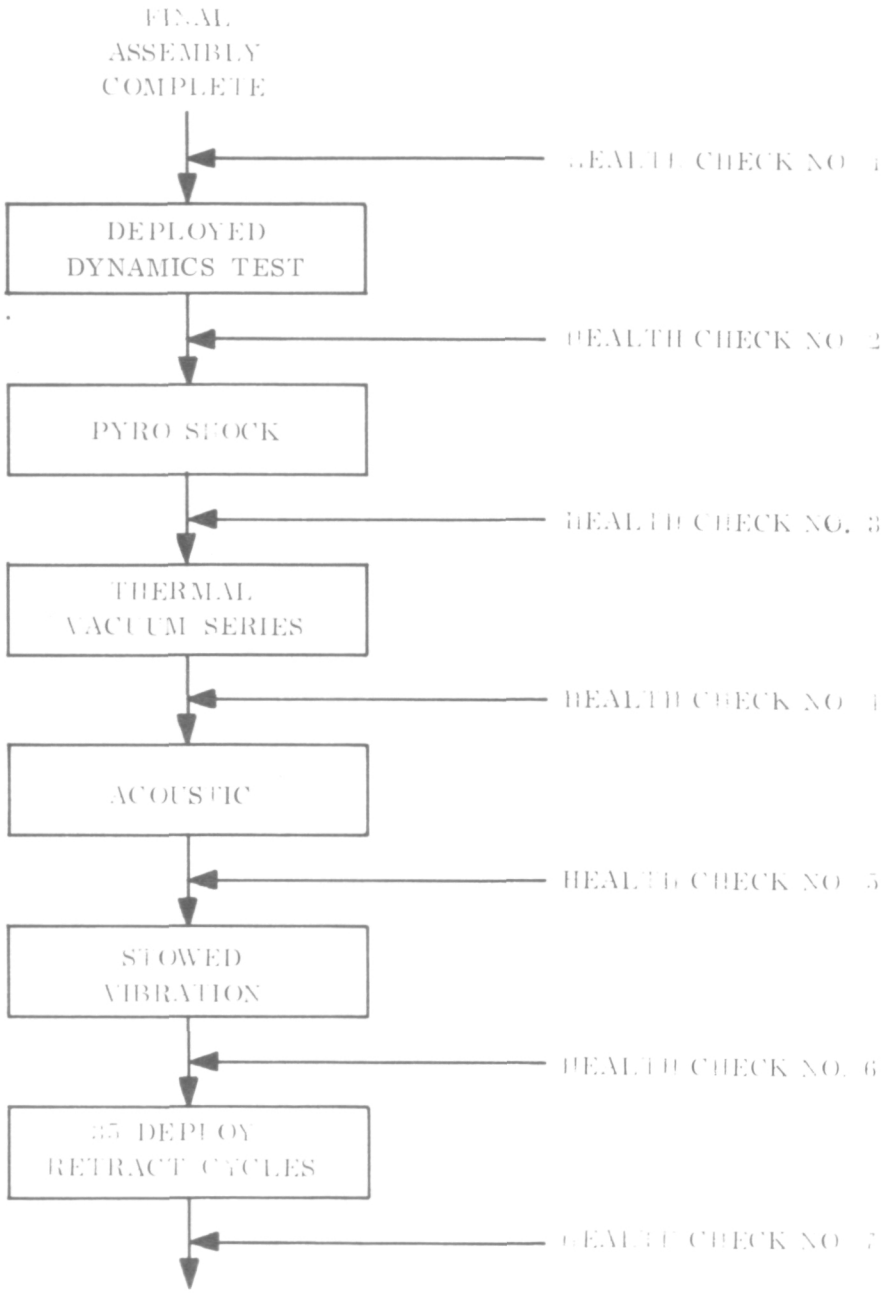

Figure 4.2-1. Sequence of Health Checks

4.2.2 TEST SETUP AND SPECIAL EQUIPMENT

The array blanket inspections were performed on a horizontal table in the laboratory area which served as the home base for the RA250 unit throughout the testing program. For inspection and module illumination, each blanket was unwrapped onto the table as shown in Figure 4.2-2. This horizontal deployment provided a convenient arrangement for the detailed visual inspection of each glass platelet and each solar cell on the blankets. The module illumination was performed with the tungsten lamp array shown in Figure 4.2-3. This lamp array was supported on a rail structure which permitted the illuminator to be traversed across the width of each blanket. This degree-of-freedom in the source coupled with the ability to move the blanket on the table provided the adjustments needed to illuminate any module on the substrate. The lamp array intensity and uniformity were adjusted using a JPL supplied standard cell (BFS 307) as shown in Figure 4.2-4. The lamp array was traversed off the side of the table to a plate which was positioned such that the top of the standard cell was in the same level plane as the modules on the table. Holes in the plate enabled the standard cell to be positioned at each solar cell location within a module. In this way a standard cell output of 61.5 mv $\pm$4% (equivalent to 139.6 mw/cm^2, Air Mass Zero at 28^{o}C) was established across the area of a module. During the module illumination there were no provisions for heat sinking to control module temperature. For each module test sufficient time was allowed for thermal equilibrium to be reached and the module temperature was measured by means of the two thermocouples installed between the cells and the substrate.

For vertical upward deployment of the complete RA250 system it was necessary to use a counterbalance system to reduce the load on the BI-STEM rod due to the 1G

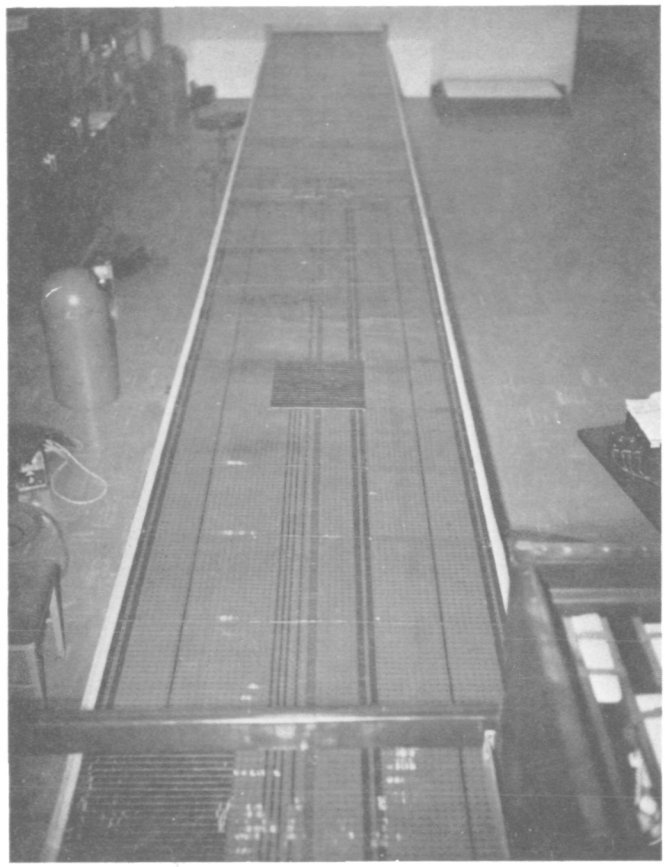

Figure 4.2-2 +Y Blanket Unwrapped on Table for Inspection

Figure 4.2-3 Module Illumination (VF70323A)

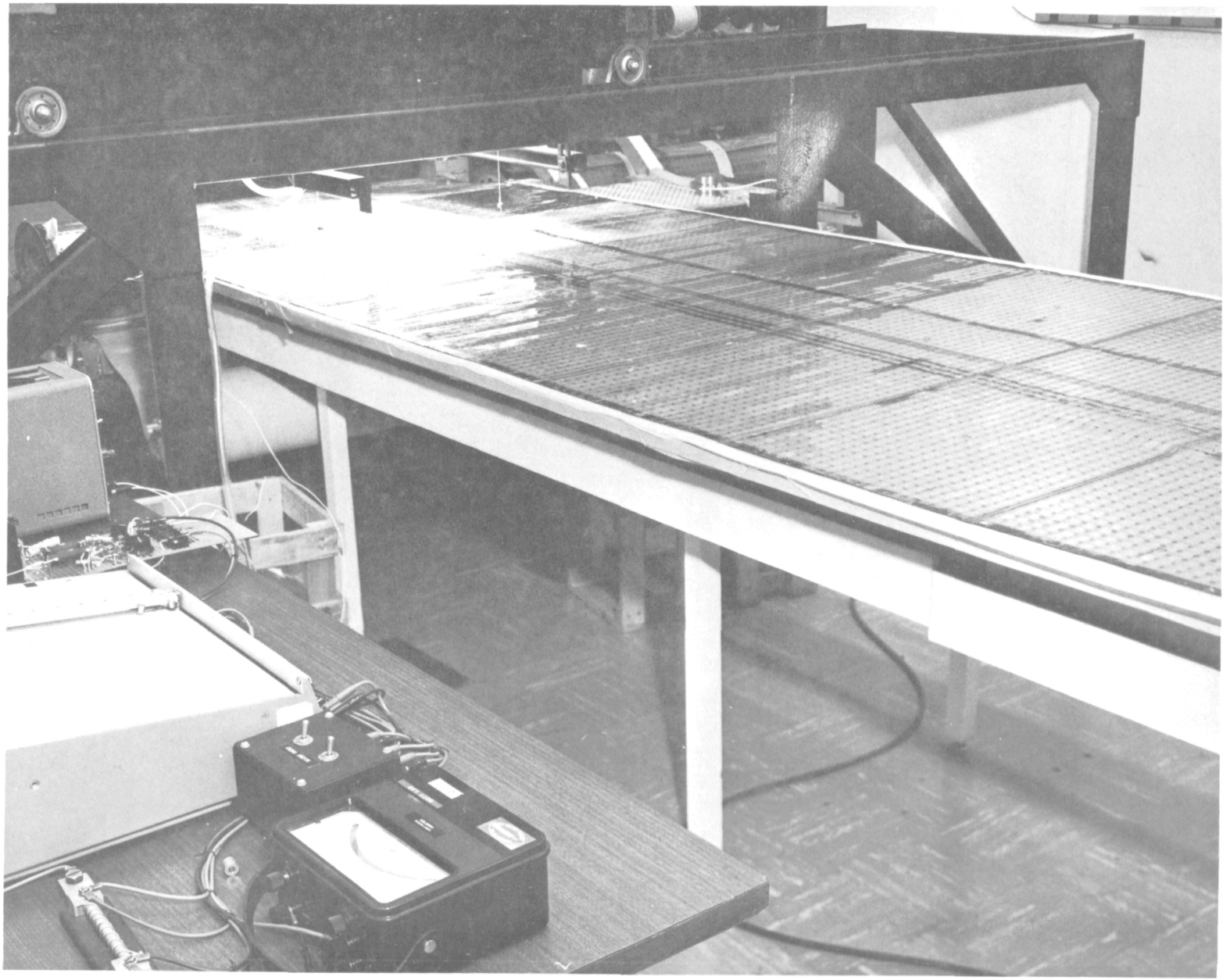

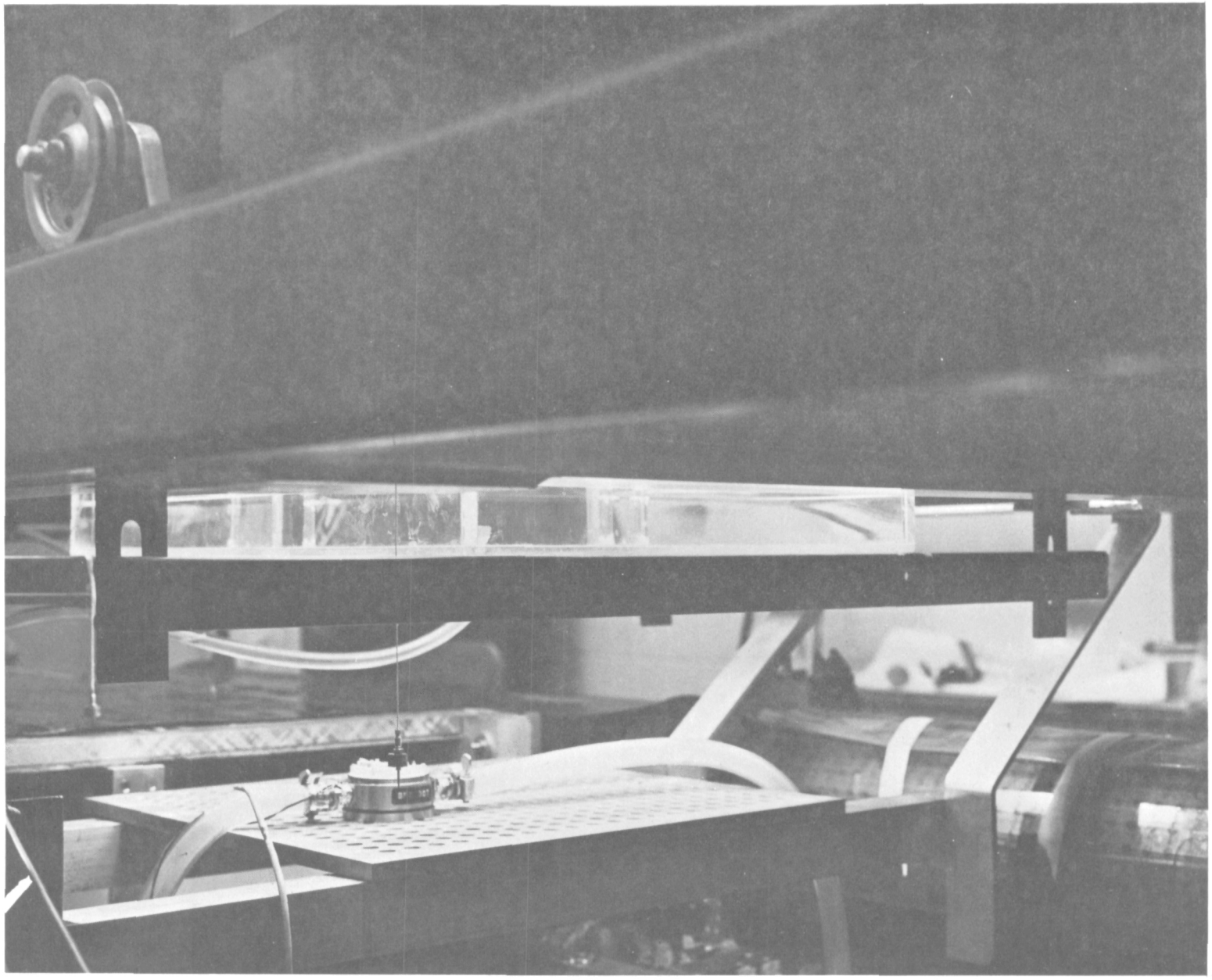

Figure 4.2-4 Uniformity Measurement Setup (VF70323B)

environment. This system was designed to counterbalance the weight of the Bi-STEM rod elements, the leading edge member (LEM), and the array blankets. Figure 4.2-5 shows the desired total counterbalance force-deflection curve for this device. This total is composed of the BI-STEM rod at .0162 lb/in, the LEM at 0.7 lb, and the blankets at .119 lb/in. The weight of the strongback is not shown in this plot. The storage drum Negator spring force was not counter-balanced. The measured force-deflection data points for the upward deployment aid have been superimposed on Figure 4.2-5 to show the close match with the desired curve.

In the test program this deployment aid was mounted in two locations. First the laboratory where it was used for health check deployments. This installation is shown in Figure 4.2-6. Second, the 32' x 54' thermal vacuum chamber where it was used for the high and low temperature deploy/retract test. This installation is shown in Figure 4.2-7.

A potentiometer mounted to the chain wrap-up drum was used to indicate array deployment position. The signal from this potentiometer with a 5.000 VDC input was calibrated vs. array deployed length. Due to a difference in the elevation of the deployment aid with respect to the array, it was not possible to establish the same deployment aid cable position for the fully stowed array in both the chamber and the laboratory. For the chamber set-up the deployment aid is supplying a counterbalance force corresponding to an array which is extended 30 inches when the array is fully stowed. In effect this adds about 4 lb. of net upward force at all times. Thus, during deployment the BI-STEM was assisted by this over-compensating force. During retraction this same force represents an additional load on the actuator motor.

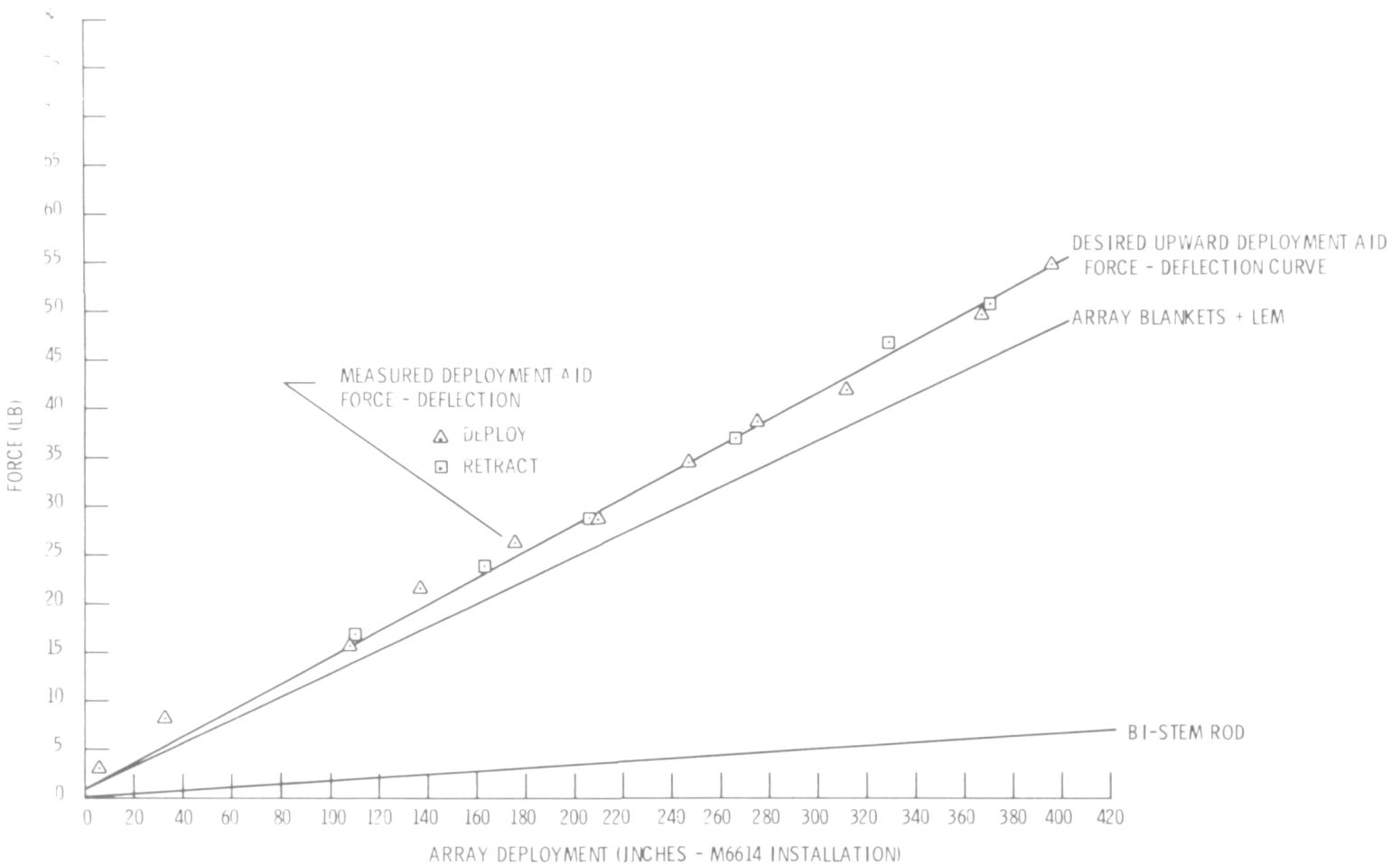

Figure 4.2-5. Upward Deployment Aid Force - Deflection Curve

Figure 4.2-6 Upward Deployment Aid Installed on Roof Beam (VF70142)

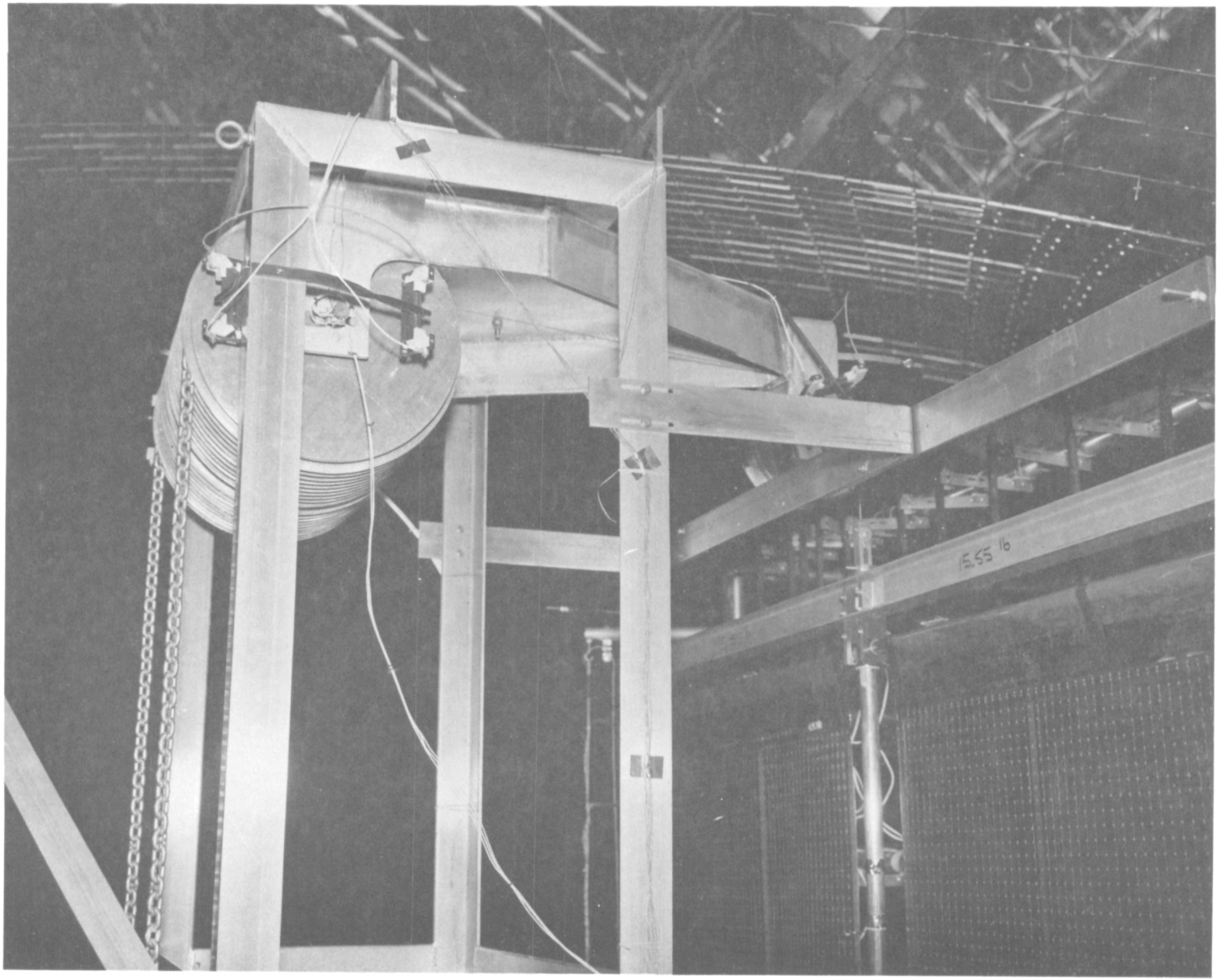

Figure 4.2-7 Upward Deployment Aid Installation in 32' x 54' Space Simulator

4.2.3 TEST AND INSPECTION RESULTS

4.2.3.1 Solar Cell Blankets

4.2.3.1.1 Active Solar Cell Module Performance

As described in Section 3.1 of Volume I, there are eleven active solar cell modules on the RA250. The performance of these modules was assessed during each health check. The I-V characteristic was obtained for each module using the illuminator described in Section 4.2.2. In addition, a detailed visual inspection of each module was performed to detect broken coverglass and cells and to assess the condition of the interconnects and top connections.

Table 4.2-1 summarizes the results of these inspections and electrical performance measurements for each active module. Note that Centralab modules 2, 3 and 4 were installed after the deployed modal test and therefore do not appear in the tabulation until Health Check No. 2. Also, the electrical performance of each module was not measured during Health Check No. 3 due to time constraints imposed by the thermal vacuum test. For each module, the electrical performance is expressed in terms of the short-circuit current (I_{SC}), the open-circuit voltage (V_{OC}), and the maximum power (P_{max}) as obtained from the I-V characteristic. The temperature of the module was read from the two thermocouples installed between the cells and the substrate and the value listed is the average of the two readings. The total accumulative cell and coverglass damage is also listed for each module. Multiple cracks or chips in a cell or coverglass were counted only once. No repairs were made of any solar cell module damage which occurred during this program. Some of the solar cell and coverglass breakage occurred as the result of

Module Identification	No. of Cells	Prior to Substrate Bonding						Health Check No. 1 3/19/70 - Before Deployed Dynamics						Health Check No. 2 4/14/70 - After Deployed Modal Before Pyro Shock						Health Check No. 3 4/24/70 - After Pyro Shock Before T/V						Health Check No. 4 5/11/70 - After TV Before Acoustic						Health Check No. 5 5/18/70 - After Acoustic Before Stowed Vibration						Health Check No. 6 6/12/70 After Stowed Vibration Before 35 Cycles						Health Check No. 7 7/1/70 After 42 Deploy./Retract Cycles						Total Percent Change in P_{max} (%)	Change** in Number of Broken Cells (H, C, & Thru 7)	Change** in Number of Broken Cover Glass (H, C, & Thru 7)
		Average Module Temp (°C)	I_{SC} (amp)	V_{OC} (volts)	P_{max} (watts)	Broken Cells	Broken Cover Glass	Average Module Temp (°C)	I_{SC} (amp)	V_{OC} (volts)	P_{max} (watts)	*Broken Cells	*Broken Cover Glass	Average Module Temp (°C)	I_{SC} (amp)	V_{OC} (volts)	P_{max} (watts)	*Broken Cells	*Broken Cover Glass	Average Module Temp (°C)	I_{SC} (amp)	V_{OC} (volts)	P_{max} (watts)	*Broken Cells	*Broken Cover Glass	Average Module Temp (°C)	I_{SC} (amp)	V_{OC} (volts)	P_{max} (watts)	*Broken Cells	*Broken Cover Glass	Average Module Temp (°C)	I_{SC} (amp)	V_{OC} (volts)	P_{max} (watts)	*Broken Cells	*Broken Cover Glass	Average Module Temp (°C)	I_{SC} (amp)	V_{OC} (volts)	P_{max} (watts)	*Broken Cells	*Broken Cover Glass			
(K11) GE No. 1	380	42	2.27	10.75	18.3	1	0	54	2.32	10.43	18.0	1	0	54	2.35	10.32	17.8	1	1	-	-	-	-	1	1	56	2.38	10.31	18.0	3 / 2	11 / 10	51	2.29	10.42	17.6	3 / 2	14 / 13	48	2.34	10.54	18.3	5 / 4	15 / 14	51	2.36	10.50	18.4	5 / 4	15 / 14	+2.2	4 / 3	14 / 13
(H7) GE No. 2	380	42	2.26	10.74	18.5	1	3	59	2.33	10.41	18.25	1	3	54	2.38	10.40	18.5	1	3	-	-	-	-	1	3	53	2.28	10.45	17.7	3 / 3	3 / 3	52	2.32	10.48	18.1	5 / 5	3 / 3	53	2.34	10.59	18.6	5 / 5	3 / 3	55	2.38	10.46	18.4	6 / 6	3 / 3	+0.8	5 / 5	0 / 0
(E6) GE No. 3	380	48	1.99	10.58	16.6	4	17	62	2.12	10.15	16.2	6	21	58	2.14	10.27	16.3	6	21	-	-	-	-	6	21	51	2.03	10.35	15.6	12 / 8	24 / 24	54	2.16	10.40	16.2	14 / 8	26 / 24	49	2.03	10.48	15.7	17 / 11	45 / 43	50	2.05	10.42	15.4	17 / 11	45 / 43	-4.9	11 / 5	24 / 22
(G7) Heliotek	380	49	2.28	10.47	17.5	3	0	51	2.31	10.51	17.9	6	2	48	2.36	10.68	18.4	7	2	-	-	-	-	7	2	47	2.17	10.60	17.2	19 / 14	8 / 3	45	2.18	10.62	17.5	20 / 15	8 / 3	-	2.17	10.65	17.3	21 / 16	14 / 9	-	2.29	10.39	17.5	24 / 19	17 / 12	-2.2	17 / 12	15 / 10
(H1) Spectrolab	240	48	1.42	10.51	11.0	0	1	52	1.45	10.27	10.7	0	1	48	1.49	10.34	11.3	1	1	-	-	-	-	1	2	54	1.41	10.33	10.4	4 / 2	9 / 7	53	1.39	10.27	10.8	5 / 3	9 / 7	49	1.38	10.48	10.9	19 / 17	26 / 24	47	1.46	10.55	11.5	19 / 17	26 / 24	+7.5	18 / 16	25 / 23
(I7) Boeing	360	42	2.07	10.80	16.8	1	0	48	2.12	10.44	16.6	2	1	46	2.14	10.53	16.8	2	1	-	-	-	-	3	4	48	2.02	10.45	15.9	10 / 3	12 / 5	46	2.00	10.52	16.0	10 / 3	12 / 5	-	2.03	10.56	16.3	11 / 4	19 / 12	48	2.10	10.45	16.4	11 / 4	19 / 12	-1.2	9 / 2	18 / 11
(J6) ECS	360	44	2.14	10.47	16.9	2	5	49	2.21	10.40	17.3	3	10	52	2.27	10.23	17.2	3	10	-	-	-	-	3	10	51	1.64	10.28	13.0	7 / 6	13 / 12	51	1.68	10.27	13.5	7 / 6	13 / 12	54	1.73	10.05	13.4	8 / 7	13 / 12	-	1.57	10.25	12.2	8 / 7	13 / 12	-29.5	5 / 4	3 / 2
(K12) Centralab No. 1	380	48	2.22	10.66	17.4	0	1	56	2.31	10.28	17.2	0	1	58	2.37	10.26	17.5	0	1	-	-	-	-	0	1	55	2.37	10.20	17.4	2 / 0	13 / 11	54	2.31	10.25	17.1	3 / 1	15 / 13	52	2.36	10.35	17.6	4 / 2	25 / 23	53	2.38	10.28	17.5	4 / 2	27 / 25	+1.7	4 / 2	26 / 24
(B12) Centralab No. 2	380	-	-	-	-	-	-	-	-	-	-	-	-	53	2.41	10.40	18.4	1	4	-	-	-	-	1	4	52	2.36	10.50	18.1	4 / 1	7 / 4	56	2.32	10.36	17.6	6 / 3	7 / 4	52	2.30	10.41	17.6	6 / 3	16 / 13	57	2.39	10.40	18.2	6 / 3	16 / 13	-1.1	5 / 2	12 / 9
(D11) Centralab No. 3	380	-	-	-	-	-	-	-	-	-	-	-	-	45	2.40	10.05	17.7	0	0	-	-	-	-	0	0	49	2.33	10.04	17.0	2 / 0	2 / 0	48	2.41	10.07	17.7	5 / 3	2 / 0	49	2.25	10.05	16.9	14 / 12	7 / 5	55	2.25	10.04	16.7	14 / 12	7 / 5	-5.7	14 / 12	7 / 5
(D12) Centralab No. 4	380	-	-	-	-	-	-	-	-	-	-	-	-	49	2.37	10.47	18.3	3	0	-	-	-	-	3	0	52	2.33	10.44	18.0	3 / 3	2 / 2	47	2.42	10.58	18.9	6 / 6	6 / 6	45	2.27	10.55	18.0	10 / 10	11 / 11	47	2.28	10.58	18.1	10 / 10	11 / 11	-1.1	7 / 7	11 / 11
Total	4000					12	27					19	39					25	44					26	48					69 / 42	104 / 81					84 / 55	115 / 90					120 / 91	194 / 165					124 / 95	199 / 174		99 / 70	155 / 130

*Cumulative Total

Total → 17 / 11 ← Total Excluding Known Handling Damage

the installation and removal of test instrumentation and other handling damage. Known damage of this type has been identified in the tabulation of the breakage for Health Checks 4 through 7. Thus, the breakage number in the upper left hand corner of the table is the total accumulative while the number in the lower right hand corner is the total accumulative excluding known handling damage. To arrive at the total damage due to the environmental testing program, the breakage at Health Check No. 2 was subtracted from the breakage at Health Check No. 7. These numbers are tabulated in the last two columns. A total of 70 solar cells and 130 coverglass were broken as a result of the environmental testing program (exclusive of known handling damage). With 4000 solar cells on the array blanket, this amounts to 1.75% and 3.25% breakage of solar cells and coverglass, respectively. It should be mentioned that this total breakage, while excluding known handling damage, does include handling damage from unknown sources. It was not possible to separate this type of breakage from damage due to the actual test environments.

The total percentage change in solar cell module maximum power from beginning to end at the test program is also tabulated for each module. Several factors have contributed to this change: (1) repeatability and uniformity of the illuminator, (2) module temperature variation from one health check to another (3) the number, location and crack geometry of the broken solar cells, and (4) interconnect integrity.

4.2.3.1.2 Inspection Data

Figure 4.2-8 summarizes the results of the seven blanket inspections in bar graph form. After the addition of three active solar cell modules following the deployed modal test there were a total of 4000 solar cells on the blanket. The remaining

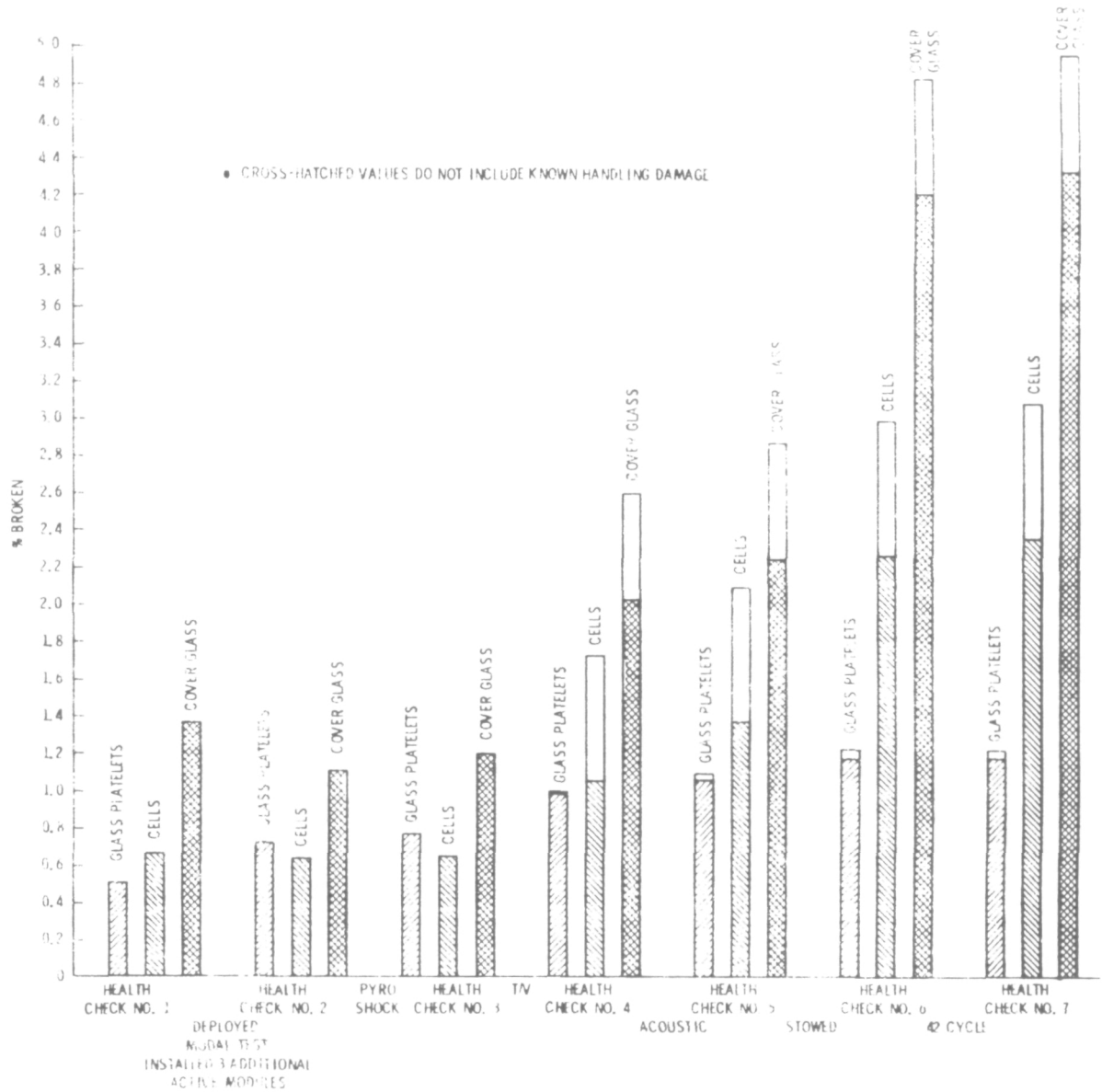

Figure 4.2-8 Solar Cell and Platelet Breakage

area was covered with 51,176 glass platelets which simulated the solar cell mass and stiffness. This addition of 1140 solar cells between Health Check No. 1 and No. 2 accounts for the decrease in the percentage of cells and coverglass broken. For the thermal vacuum test, breakage was caused by the installation and removal of thermocouples. From this test on, known instrumentation damage was segregated from the total as shown in the figure. Similar damage occurred from the installation and removal of accelerometers during the Stowed Dynamics tests.

4.2.3.1.3 Discussion

As a result of the inspections conducted during the course of this program, the total breakage which can be attributed to the environmental test program has been summarized in Table 4.2-2 based on data derived from Table 4.2-1 and Figure 4.2-8. Several observations can be made based on these results.

- The stowed vibration test caused the greatest breakage of cells and coverglass.
- The thermal vacuum test series caused the largest percentage of broken glass platelets.
- The total breakage numbers show that the glass platelets are significantly less vulnerable to breakage than either the cells or coverglass and that the cells are less vulnerable than the coverglass.

The fact that the thermal vacuum test was the most severe environment for the glass platelets may be attributed to the fact that these areas of dummy glass were not temperature controlled during the deploy/retract cycles and therefore were colder than the solar cell modules and/or because many localized areas of the dummy glass were affected by the over-heating which occurred during the stowed high temperature test.

Table 4.2-2

BREAKAGE RESULTING FROM ENVIRONMENTAL TEST PROGRAM

TEST ENVIRONMENT	PERCENT * BROKEN GLASS PLATELETS	PERCENT* BROKEN CELLS	PERCENT * BROKEN COVERGLASS
PYRO SHOCK	0.043	0.025	0.100
THERMAL VACUUM	0.213	0.400	0.825
ACOUSTIC	0.084	0.325	0.225
STOWED VIBRATION	0.121	0.900	1.975
35 AMBIENT DEPLOY/RETRACT CYCLES	0.008	0.100	0.125
TOTAL BREAKAGE	.469	1.750	3.250

*DOES NOT INCLUDE KNOWN HANDLING DAMAGE

The relatively high vulnerability of the coverglass is apparent from the inspection results. There is no breakage pattern to indicate a possible cause for this high proportion of damage, although there are a few examples of parallel adjacent coverglass within a module row which have cracked in a direction parallel to the axis of the storage drum. Two examples of this type of cracking pattern occurred on an inboard module (K12)*. This may be an indication that cushioning is needed between the storage drum shell and the first wrap of solar cells.

The results indicate that the cell/coverglass composite is not as resistant to damage as a corresponding glass platelet mass simulation which is .011 inches thick. The .003 inch thick coverglass appears to break independent of the cell in most cases. The two modules with the most coverglass breakage are K12 and H1, located at the inboard and outboard ends of the -Y blanket, respectively. The H1 module also has the largest percentage of cell breakage. This would tend to indicate that the environment which produces breakage is more severe at both the inner and outer wraps of the stowed array. It is certain that the potential for handling damage is greater on the outer wrap.

The J6 module suffered extensive interconnect damage which was reflected by a 29.5 percent reduction in the maximum power. This damage occurred during a thermal vacuum test series. Figure 4.2-9 shows examples of the various types of damage which occurred within this module. The majority of this damage occurred within the area of the module which was affected by the localized overheating during the stowed high temperature thermal vacuum test. The temperature in this area was high enough to melt the solder and cause the top contact feet to lift as shown in Figure 4.2-9(d). The damaged pictured in Figure 4.2-9(a) and (b) is a

* The module locations are shown in Figure 3.1-4 of Vol. 1, which also lists the active module designations.

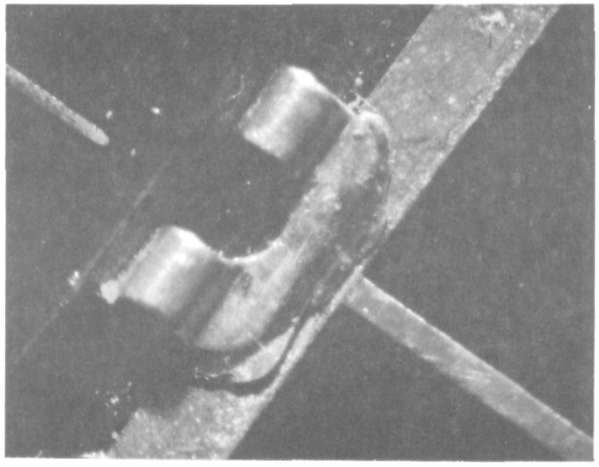

(a) Silicon Flake-out

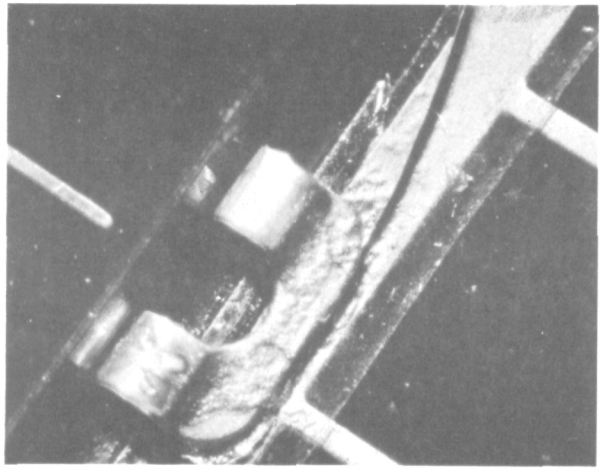

(b) Silicon Flake-out and Splintering

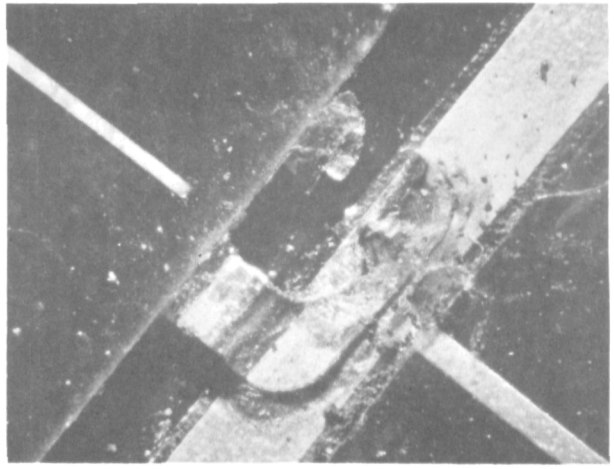

(c) Fractured Interconnect Foot

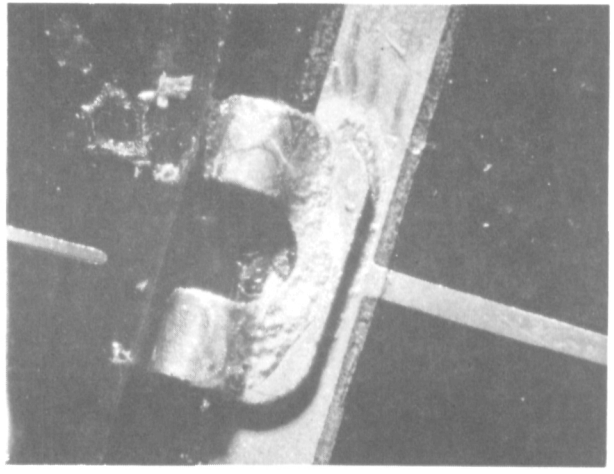

(d) Lifted Interconnect Foot

Figure 4.2-9 Damage in J6 Module

silicon flake-out at the foot which is indicative of a low temperature failure mechanism. The damage mechanism for the fractured conductor in (c) is unknown.

Some interconnect damage on the H1 module was observed after the stowed vibration test. Figure 4.2-10 shows examples of the types of failure. The lifted feet occurred adjacent to a cell which was not securely bonded to the substrate. The fractured conductor pictured in (a) was at the edge of the module.

One example of an interconnect related failure was also observed in the G7 module following the stowed vibration test. This fracture of the cell around a top connection is pictured in Figure 4.2-11.

4.2.3.2 BI-STEM Performance

4.2.3.2.1 Test Results

During the course of the RA250 test program, the BI-STEM actuator was extended and retracted a total of 58 cycles over the entire 400 inches of travel. In addition, 19 partial extension/retraction cycles have been accumulated. The deployment of the BI-STEM was always performed vertically, but there were a variety of loading conditions imposed by the test conditions. These are listed below:

a. Entire array-vertically upward with deployment aid in laboratory (Room M6614).

b. Entire array-vertically upward with deployment aid in 32' by 54' thermal-vacuum chamber.

c. BI-STEM only-vertically upward unaided.

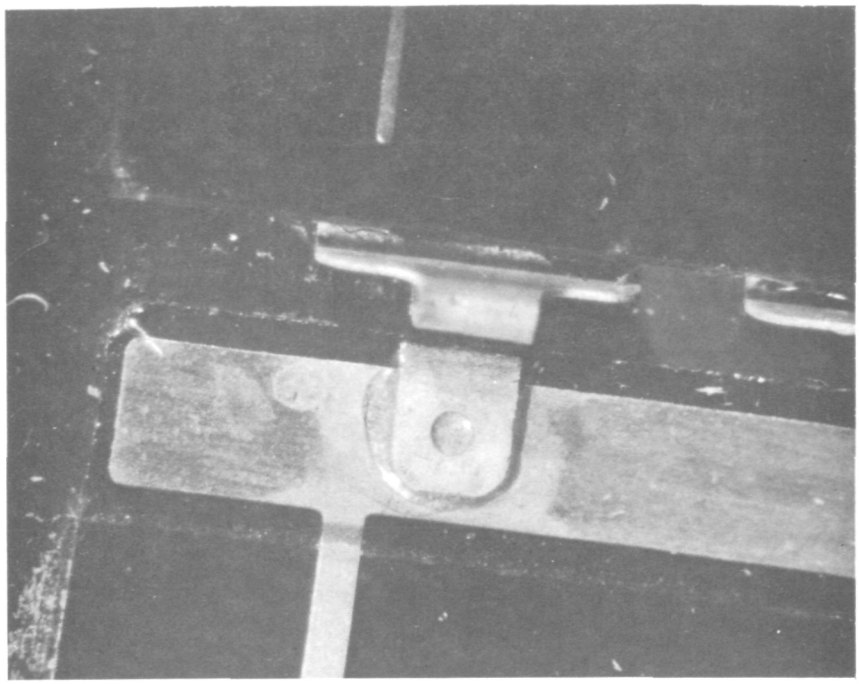

(a) Fractured Interconnect Foot

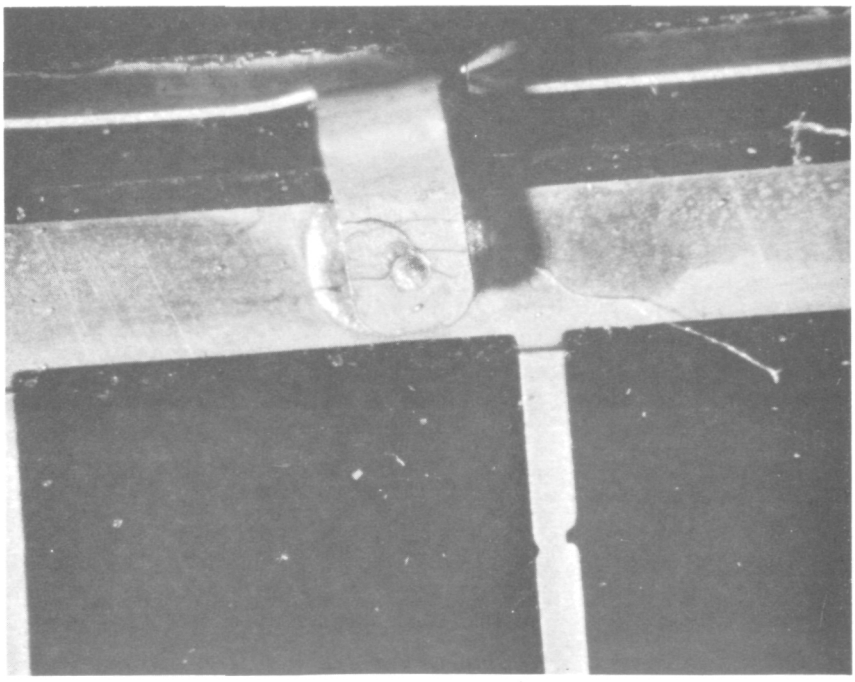

(b) Lifted Interconnect Foot

Figure 4.2-10 Damage in H1 Module

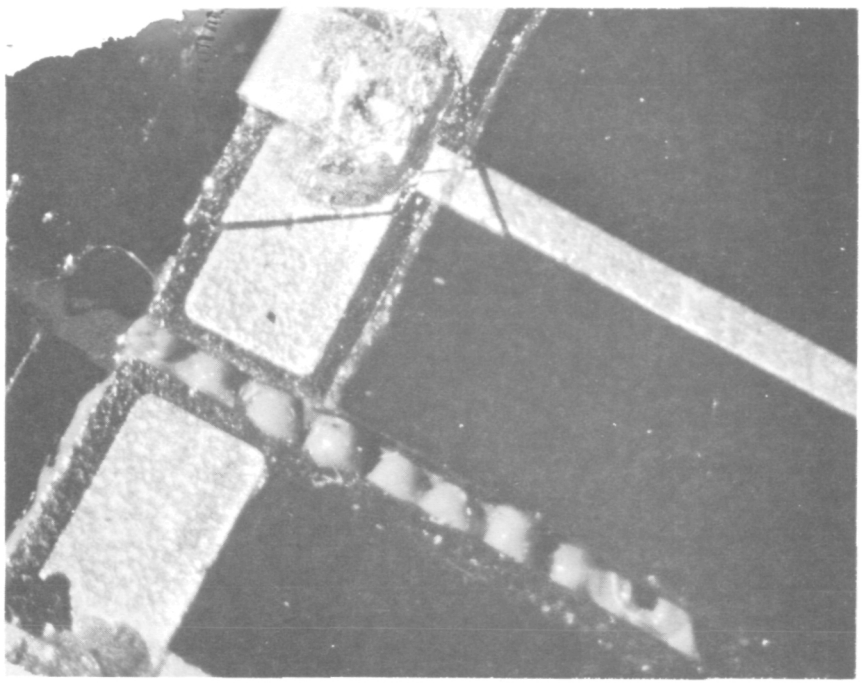

Figure 4.2-11 Fractured Cell at Foot in G7 Module

d. BI-STEM only-vertically downward unaided.

The set-up for array deployment in Room M6614 is shown in Figure 4.2-12. The handling dolly, with the RA250 attached, is first positioned directly under the upward deployment aid cable. The leveling jacks on the dolly are adjusted so that the deployed BI-STEM rod is perpendicular to a level surface. A circular level has been previously adjusted with respect to the deployed rod. After leveling, the strongback is attached to the leading edge member as shown in Figure 4.2-12(a). A safety line is attached to the top of BI-STEM rod as a precautionary measure. During the deployment and retraction of the array, the following parameters were monitored:

1. BI-STEM motor current
2. BI-STEM motor voltage
3. -Y slip ring current
4. +Y slip ring current
5. -Y slip ring voltage drop
6. +Y slip ring voltage drop
7. Upward deployment aid potentiometer signal
8. BI-STEM motor temperature

The first six parameters were recorded on a Brush recorder while the upward deployment aid potentiometer signal was recorded on a X-Y plotter with an X axis time base. The BI-STEM motor temperature was monitored periodically via a hand balance thermocouple potentiometer.

Figure 4.2-13 shows examples of the BI-STEM motor current history during

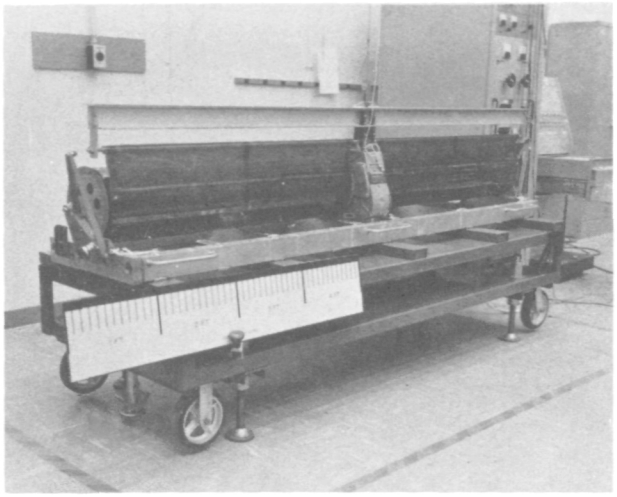

(a) Stowed With Strongback Installed (VF70228A)

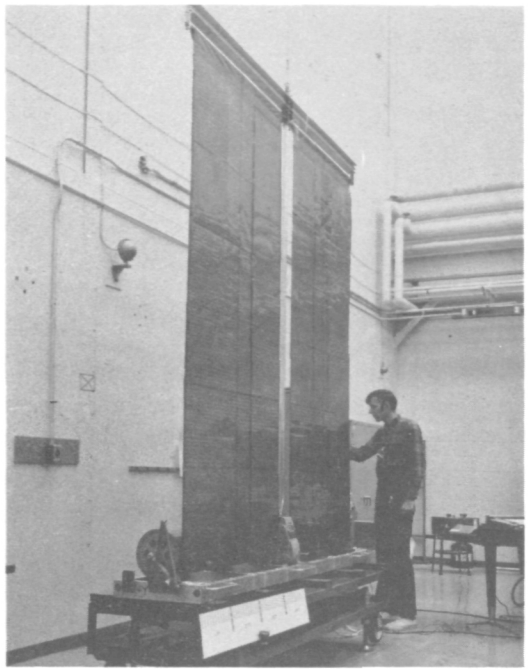

(b) Deployed Approximately 10 Feet (VF70228G)

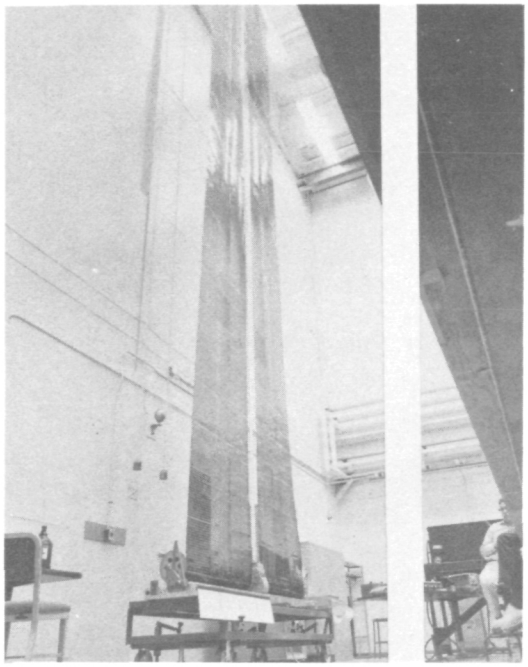

(c) Fully Deployed (VF80228B)

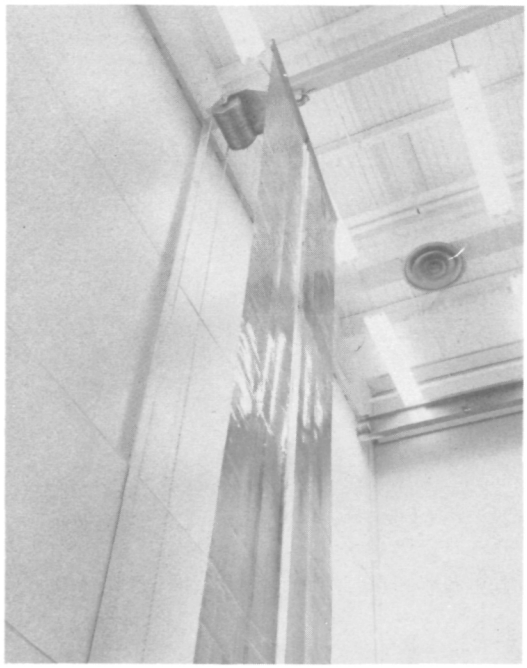

(d) Fully Deployed - Upper Portion (VF70228C)

Figure 4.2-12 Deployment of RA250

deployment at various times in the test program. Part (a) of this figure is for an ambient deployment in the 32' x 54' chamber prior to the thermal vacuum low temperature deployment. Figure 4.2-13(b) shows the current trace for the thermal vacuum low temperature deployment. The next trace is at ambient conditions immediately following the low temperature test. Part (d) was recorded during the thermal vacuum high temperature deployment test. Figure 4.2-13(e) was included to show the trace resulting from the deployment of the BI-STEM only without the array blankets. No deployment aid was used. Figures 4.2-13(f) through (h) show traces recorded during the 35 cycle deploy/retract life test at the end of the program.

The traces of Figure 4.2-14 were recorded during the retraction of the array on these same occasions. Note that the low temperature retraction was stopped approximately 77 inches short of the launch stowed position. Brush noise is a possible cause of the high frequency variations in motor currents.

Figure 4.2-15 shows the upward deployment aid potentiometer signal vs time for each of the above mentioned occasions (except the deployment and retraction of the BI-STEM rod only).

4.2.3.2.2 Discussion

The three microswitches within the BI-STEM actuator perform the following functions:

1. Full Retract Limit Switch - This switch is actuated by a ramp at the tip of the rod to remove power from the motor when the rod reaches the fully retracted position. Note that this switch serves as a backup to the orbital retract limit switch for orbital operation in case it malfunctions.

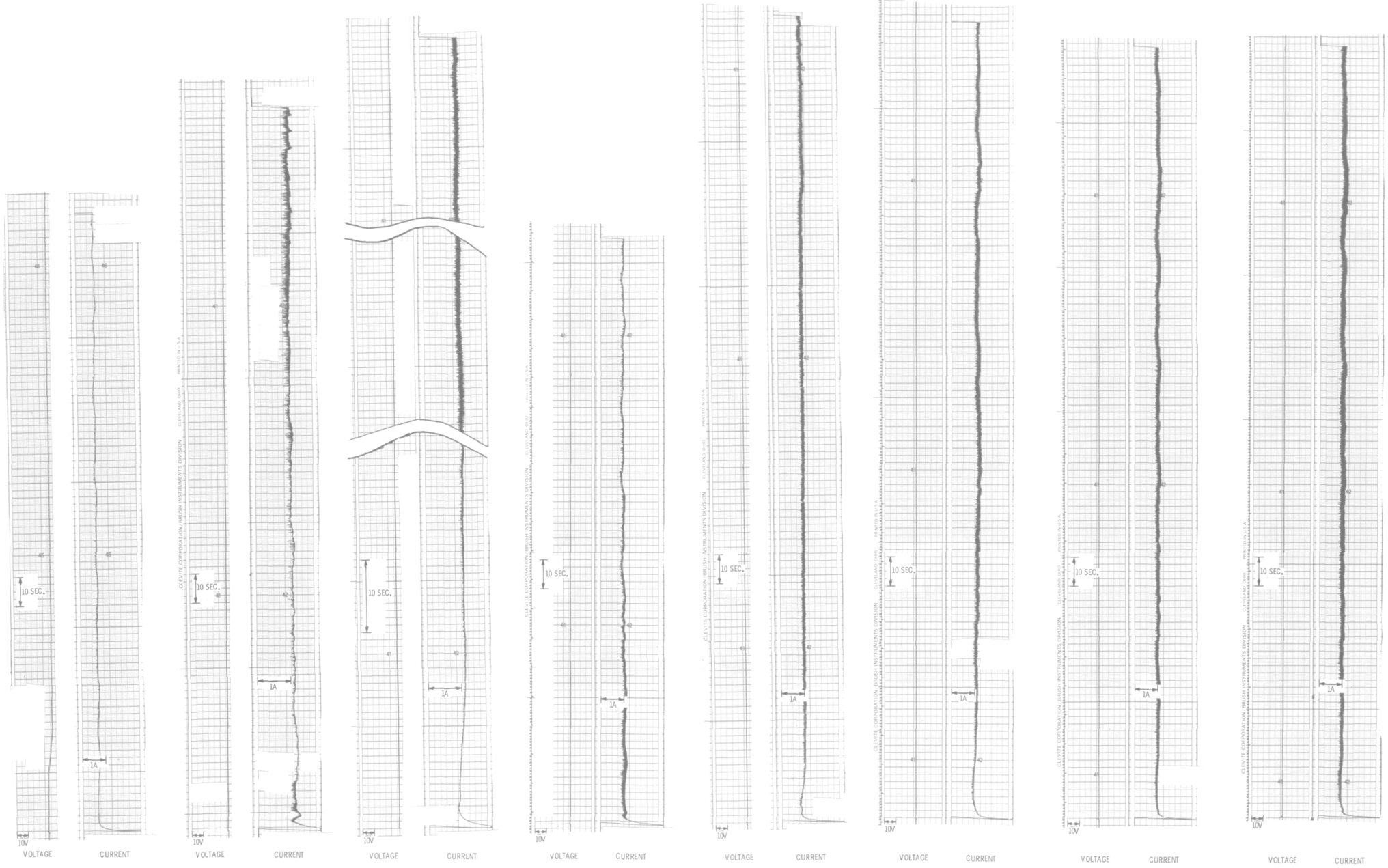

(a) 4/27/70 AMBIENT - CHAMBER

(b) 5/4/70 T/V LOW TEMP

(c) 5/5/70 AMBIENT - CHAMBER

(d) 5/7/70 T/V - HIGH TEMP

(e) 5/18/70 - BI-STEM ONLY NO DEPLOYMENT AID

(f) 6/18/70 AMBIENT - M6614 CYCLE NO. 1

(g) 6/22/70 AMBIENT - M6614 CYCLE NO. 20

(h) 6/23/70 AMBIENT - M6614 CYCLE NO. 35

Figure 4.2-13 Examples of BI-STEM Current History During Deployment

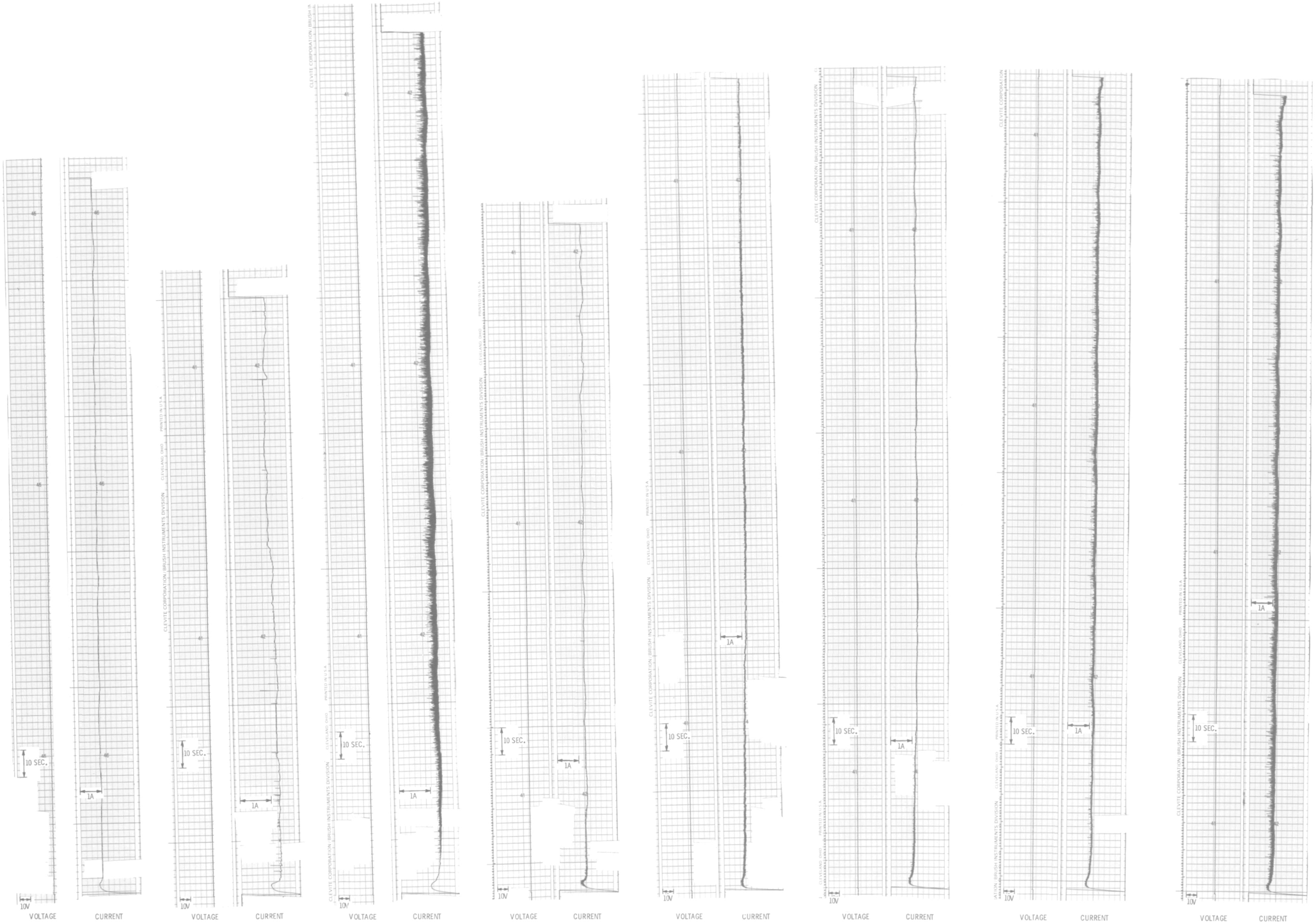

(a) 4/27/70 AMBIENT CHAMBER

(b) 5/4/70 T/V - LOW TEMP

(c) 5/5/70 AMBIENT - CHAMBER

(d) 5/7/70 T/V - HIGH TEMP

(e) 5/18/70 AMBIENT - BI-STEM ONLY NO DEPLOYMENT AID

(f) 6/18/70 AMBIENT - M6614 CYCLE NO. 1

(g) 6/22/70 AMBIENT - M6614 CYCLE NO. 20

(h) 6/23/70 AMBIENT - M6614 CYCLE NO. 35

Figure 4.2-14 Examples of BI-STEM Current History During Retraction

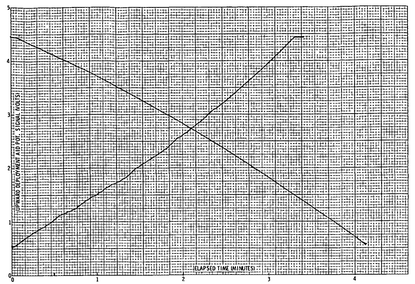

(a) 4/27/70 AMBIENT - CHAMBER

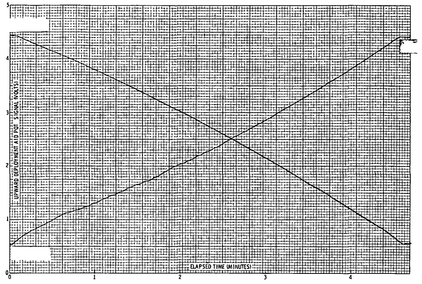

(c) 5/5/70 - AMBIENT - CHAMBER

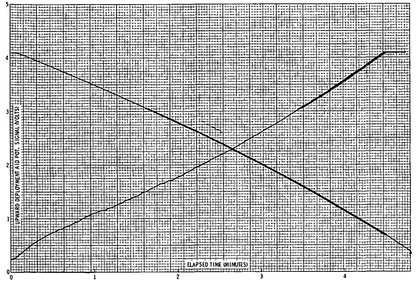

(e) 4/13/70 AMBIENT - M6614
CYCLE NO. 1

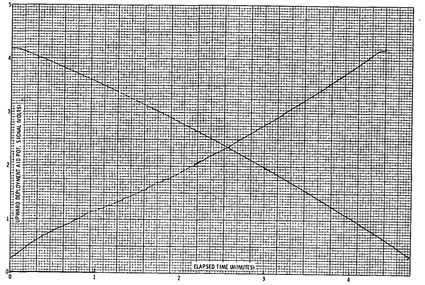

(g) 4/23/70 - AMBIENT - M6614
CYCLE NO. 35

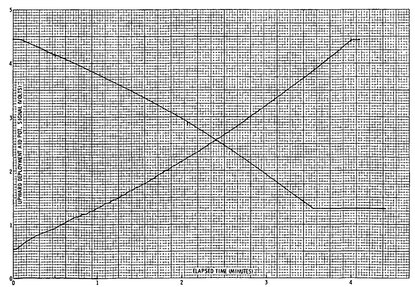

(b) 5/4/70 TIV - LOW TEMPERATURE

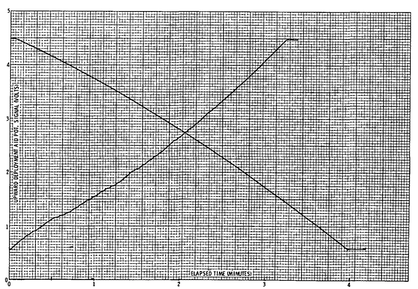

(d) 5/7/70 TIV - HIGH TEMPERATURE

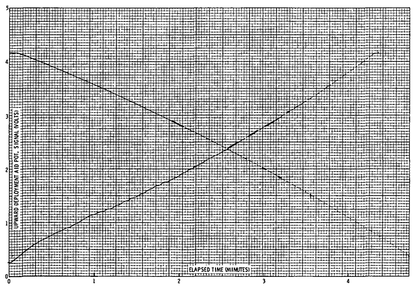

(f) 4/22/70 AMBIENT - M6614
CYCLE NO. 20

Figure 4.2-15 Examples of BI-STEM Deploy/Retract Time Histories

2. Orbital Retract Limit Switch - This switch is actuated by a roller which falls into a slot in the rod element to remove power from the motor when the rod reaches the orbital retracted position (approximately 4 inches from fully retracted).

3. Full Extend Limit Switch - This switch is actuated by a roller which falls into a slot in the rod element to remove power from the motor when the rod reaches the fully extended position.

At the conclusion of the testing program none of these switches was operable. The full retract limit switch mounting bracket was never properly adjusted and became loose during the course of the testing program. Since it does not function during orbital operation of the BI-STEM, no effort was made to fix this switch. The BI-STEM could be manually stopped in the fully retracted position. The orbital retract limit switch roller actuator failed during an ambient deploy/retract of the BI-STEM on March 20, 1970. Figure 4.2-16 shows the location of this switch in the BI-STEM actuator housing. The roller which falls in the slot is the rod element and is attached to a AZ31B-H24 magnesium bracket with a spring pin as shown in the detail sketch. This bracket is, in turn, riveted to a 302 stainless steel leaf spring which deflects to depress the microswitch button. The point of fracture was at the root of the bracket at the outermost rivet hole. It is believed the fitting had cracked during the component vibration test but that the end of the actuator was held in place by the rivet. The assigned cause of this failure is fatigue damage due to the cyclic bending loads imposed during the component vibration test. The stress concentration at the rivet hole is considered a major contributing factor. A possible redesign of this roller bracket is shown on Figure 4.2-16 to illustrate that an adequate fix is not complicated. On June 5, 1970, an identical failure of the roller bracket on the full extend limit switch was discovered while attempting to deploy the BI-STEM following the Z-axis stowed vibration test. This switch is located adjacent to the orbital

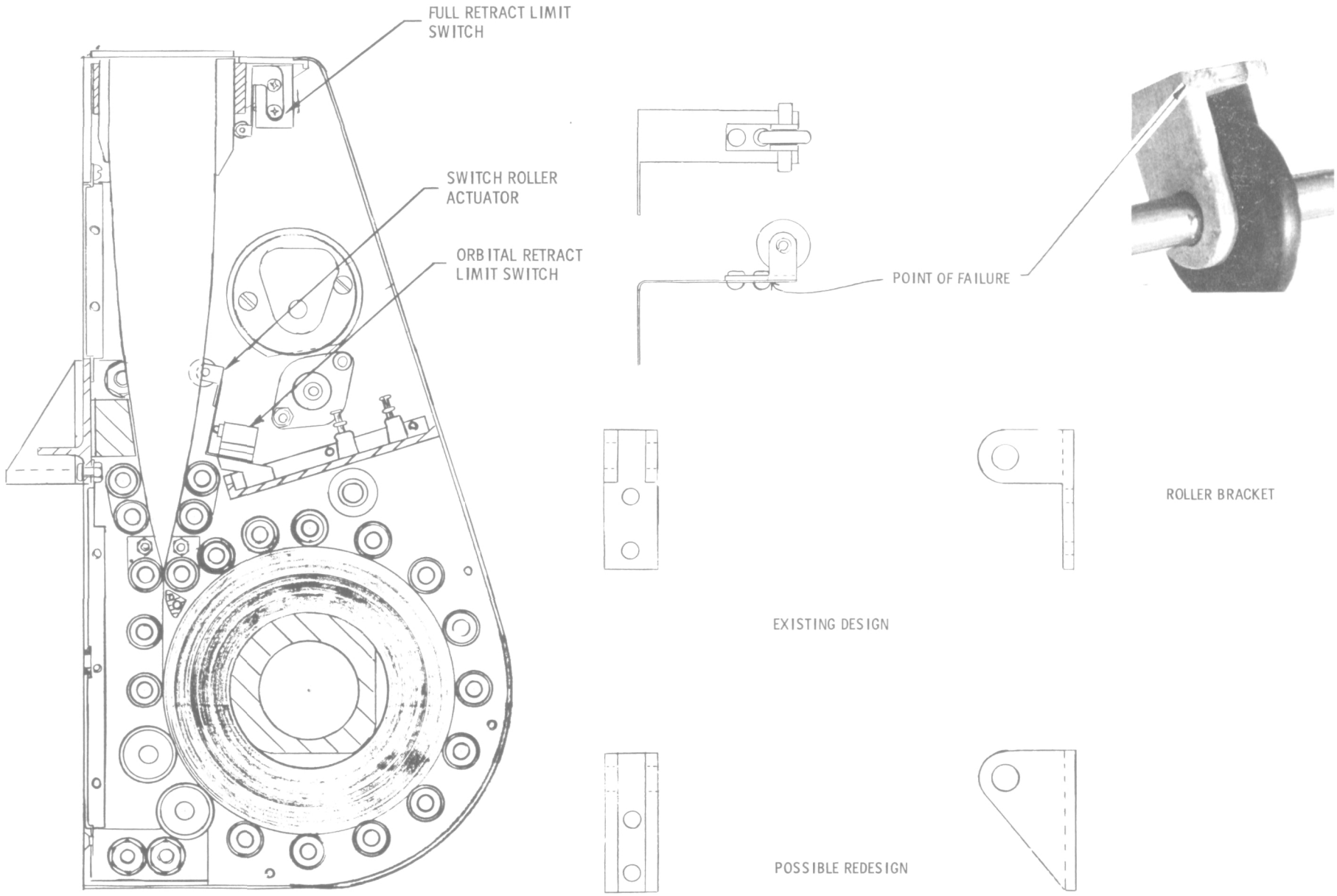

Figure 4.2-16 BI-STEM Actuator Switch Problem

retract limit switch and is actuated in exactly the same manner.

On June 17, 1970 a fatigue crack in the BI-STEM rod outer element was discovered while preparing for the 35 cycle life demonstration following the stowed vibration test. This 1/8 in. long crack is located approximately 7-1/8 inches down from the centerline of the leading edge member at the edge of outer element on +Y side of the rod as shown in Figure 4.2-17. The actuator operated properly during the subsequent 35 cycle life demonstration and approximately 12 additional deployments.

Aside from the failure of the switch actuators, the BI-STEM has performed its function in the system throughout the test program. Figures 4.2-13 and 4.2-14 show a general increase in the noise level on the BI-STEM motor current as the program progressed. The largest change occurred as a result of the thermal vacuum low temperature deploy/retract cycle. This is particularly obvious when comparing the traces of (a) and (c) of Figure 4.2-14. It is also apparent from Figure 4.2-15 that the time to deploy or retract at ambient conditions is greater after the low temperature deploy/retract cycle. Since that increase, however, the total times to deploy or retract at ambient conditions have remained relatively constant.

4.2.3.3 Slip Ring Performance

4.2.3.3.1 *Test Results*

During the deployment and retraction of the array, a current was passed through both power rings of each slip ring assembly and the voltage drop across each

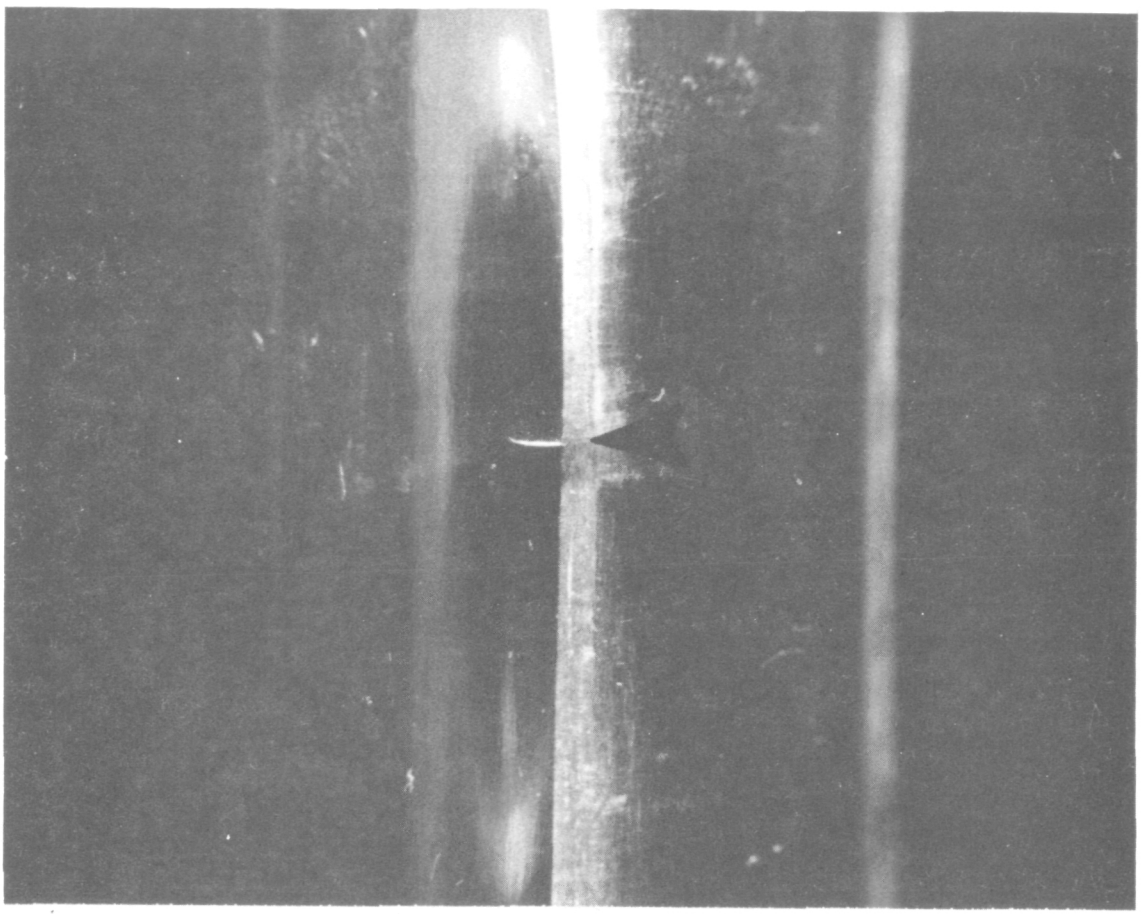

ROLLUP SOLAR ARRAY

Fatigue Crack in Rollup Solar Array BI-STEM Element-Crack is approximately 3/16 inches long and is 5-3/4 inches from end of element

Figure 4.2-17. BI-STEM Rod Element Crack

assembly was recorded. To accomplish this measurement, the power penetrations through both storage drum shells were shorted together with a copper strap during final assembly so that current from an external source could be passed in series through both power rings of each assembly. The voltage drop measurement tap points were placed at the external connectors on the center support, so that the measured voltage drop includes the power circuit slip ring resistance plus the drum internal wiring and the center support interface connector resistance.

Figure 4.2-18 shows examples of the slip ring voltage drop traces at various times during the test program. The equivalent d.c. resistance which reflects the constant current flow through each set of rings has been marked on each trace to indicate the scale factor.

4.2.3.3.2 Discussion

As shown in Figure 4.2-18 at the beginning of the test program, the slip ring resistance remained constant as the storage drums turned during array deployment and retraction. Some slip ring dynamic resistance noise was first noted during the low temperature deploy/retract cycle. Similar fluctuations, along with a slight overall increase in resistance, were recorded during the high temperature deploy/retract cycle. Figure 4.2-18(e) shows the slip ring traces from the first deployment of the 35 cycle life test immediately following the stowed vibration test. Fluctations in resistance of 0.005 ohms are obvious in these traces with spikes which correspond to the period of rotation of the storage drums. After 19 consecutive deploy/retract cycles, the magnitude of these fluctations in resistance had decreased substantially as shown in part (f) of this figure. At the 35th cycle the traces show the same basic characteristics as the 20th cycle except for a slight increase in the higher frequency content of the noise. The

periodic nature of the changes in resistance indicates the possibility of dirt on the power rings which was gradually removed by the brushes as the array was deployed and retracted during the 35 cycle life demonstration. There has been no significant increase in the static resistance of the power rings as a result of the environmental test program.

4.2.3.4 Thermistor Performance

4.2.3.4.1 Test Results

Two thermistors were installed on each blanket to check the survivability of such devices during the environmental test program. The thermistor used is the THINISTOR manufactured by Victory Engineering Corp., Springfield, N. J. Two different resistance values were used at each location to cover the complete temperature range from -130°C to +140°C. The vendor part number and each resistance value is given in Table 4.2-3.

On the -Y array blanket the two thermistors were located on the rear side of the H1 module (Spectrolab), while on the +Y blanket the two thermistors were located at the E6 module (GE No. 3). The installation on the -Y blanket is shown in Figure 4.2-19. At each location the two thermistors were bonded to the rear of the Kapton substrate with SMRD-745.* The thermistor leads were soldered to the three copper bus strips with the center strip being a common connection, and a Kapton insulating patch was then bonded over the two thermistors with SMRD-745. After this bonding operation the resistance of each thermistor as measured at room ambient is given in Table 4.2-3.

---

* SMRD 745 is a flexible epoxy formulated by and available from GE-SSO.

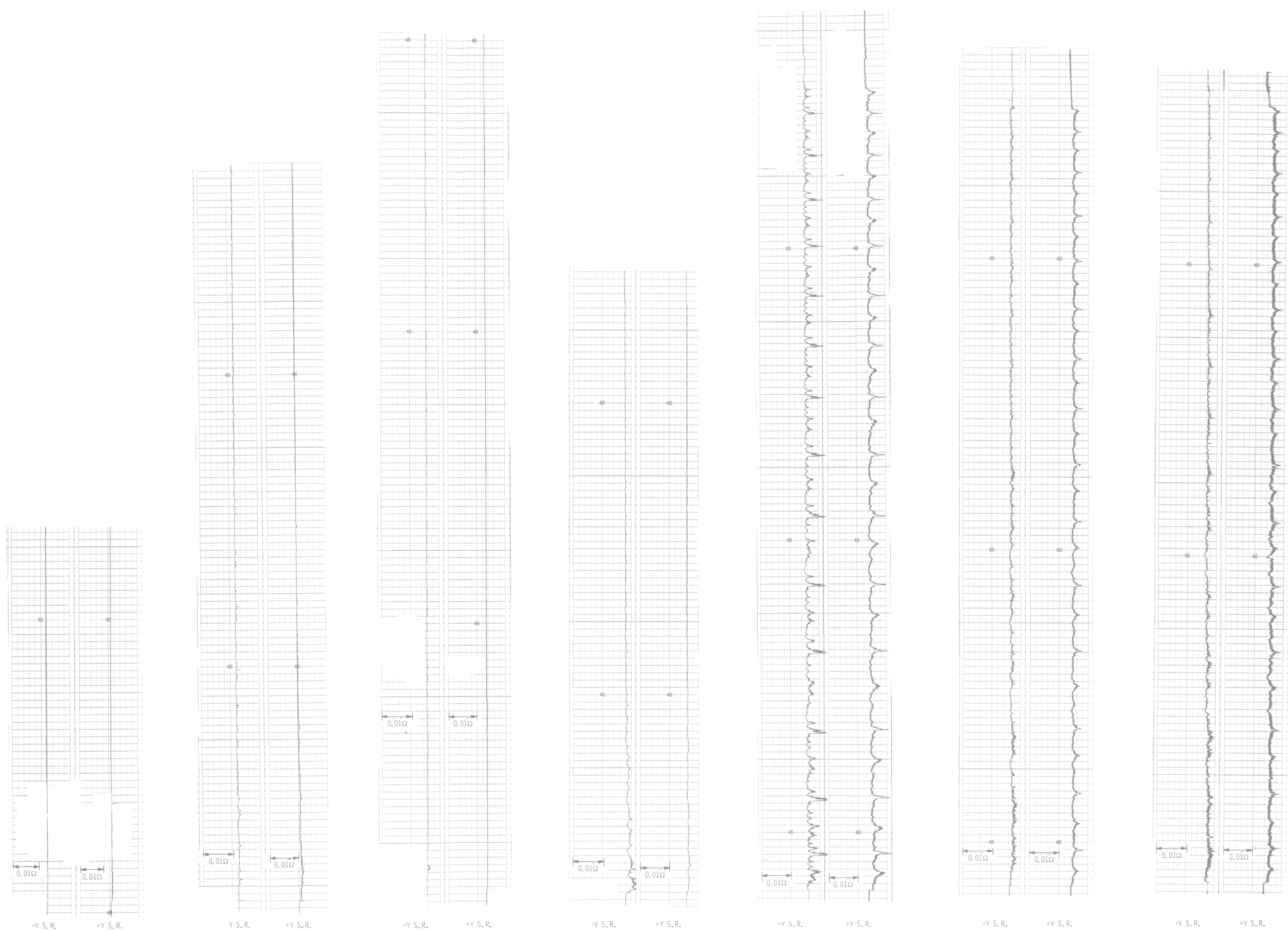

(a) 4/28/70 AMBIENT RETRACTION

(b) 5/4/70 T/V LOW TEMP DEPLOYMENT

(c) 5/5/70 AMBIENT RETRACTION

(d) 5/7/70 I/V HIGH TEMP RETRACTION

(e) 6/18/70 AMBIENT CYCLE NO. 1 DEPLOYMENT

(f) 6/22/70 AMBIENT CYCLE NO. 20 DEPLOYMENT

(g) 6/23/70 AMBIENT CYCLE NO. 35 DEPLOYMENT

Figure 4.2-18 History of Slip Ring Dynamic Resistance

Table 4.2-3 Thermistor Resistance Values

		Victory Part No.	
		FN3C9* OHMS	FN3C15** OHMS
Vendor Value (25°C)		250	25,000
Value after Bonding to Blanket	-Y Blanket (H1)	330	31,000
	+Y Blanket (E6)	420	25,000
Value at Conclusion of Test Program	-Y Blanket (H1)	530	52,000
	+Y Blanket (E6)	6,500	68,000

* For Low Temperature Range

** For High Temperature Range

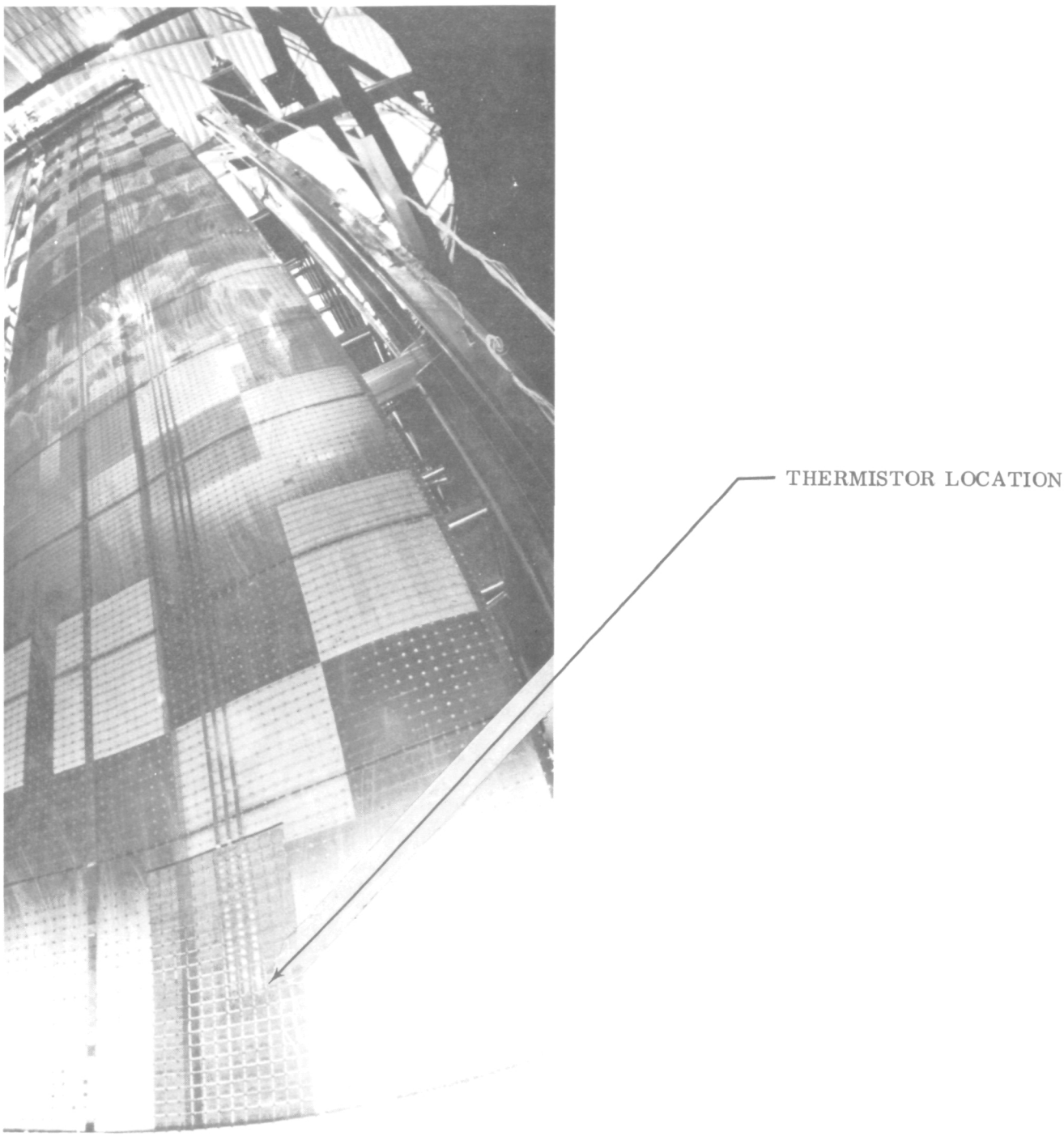

Figure 4.2-19 Thermistor Location on -Y Array Blanket

Prior to the deployed thermal vacuum test, a thermocouple was bonded to the rear of the substrate at each thermistor location. During this test these thermocouple readings and the output voltages from a half bridge circuit for each thermistor were recorded. The results of these measurements are shown graphically in Figures 4.2-20 and 4.2-21. After this operational calibration, the thermistor outputs could be used to monitor temperature. Note that the thermocouples were disconnected immediately after the deployed thermal transient test. The output voltages from the thermistor bridge circuits were also recorded periodically at ambient temperature. These results are summarized in Table 4.2-4.

At the conclusion of the test program the thermistor resistance values at room ambient temperature were again measured with the results given in Table 4.2-3. The slip ring portion of the circuit was checked to verify that the signal resistance had not changed and that the resistance change was occurring in the device. It is evident these thermistors are not stable under the conditions existing in this application. Both thermal vacuum and vibration environments caused significant resistance changes.

4.2.3.4.2 Discussion

The THINISTOR type of thermistor was successfully bonded to the array substrate and used to monitor solar cell module temperature during the thermal vacuum test. An increase in room temperature resistance occurred as a result of the thermal vacuum test environment. This is obvious from the results in Table 4.2-4, if the data recorded on 4/16/70 is compared with the data recorded on 5/11/70.

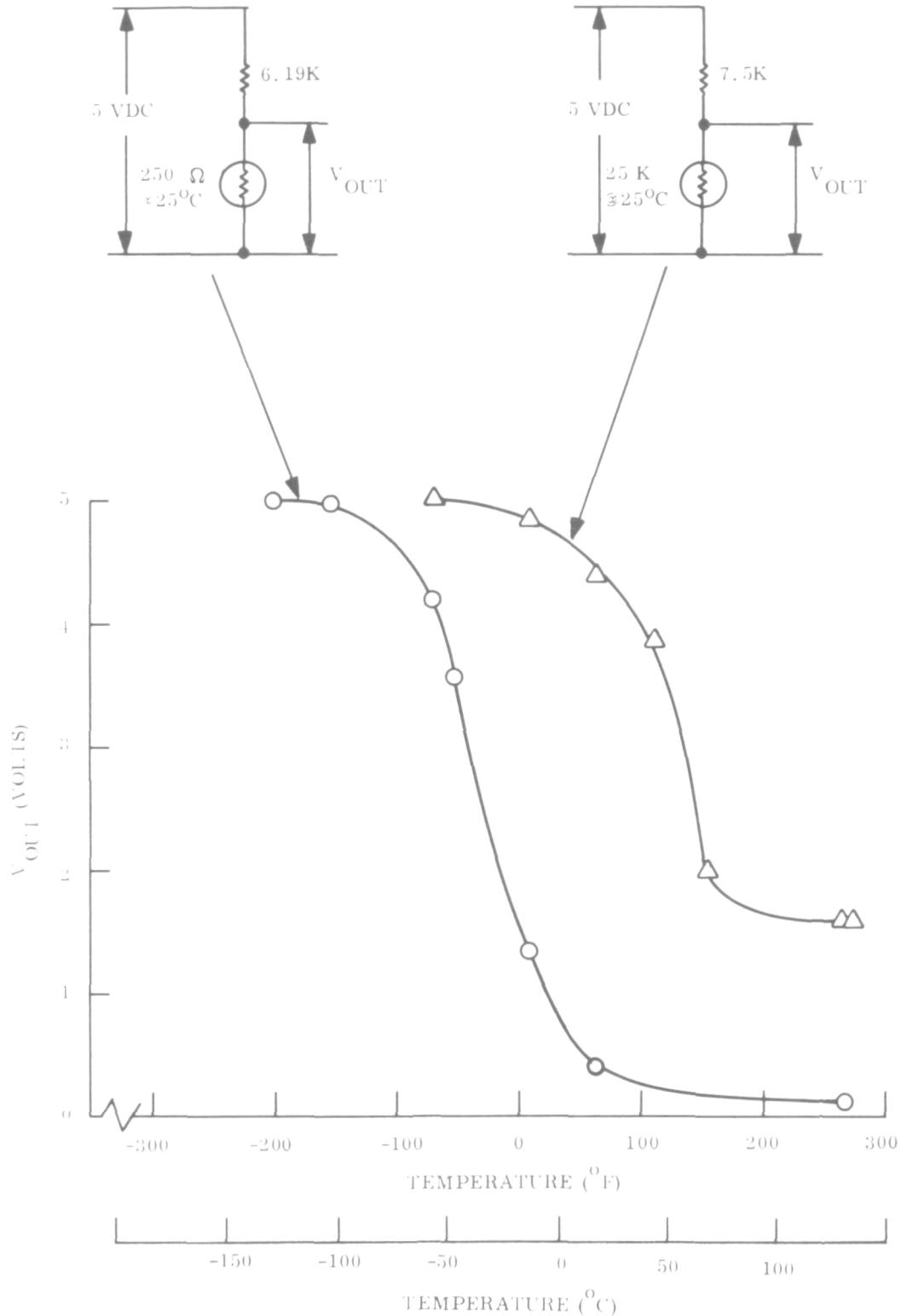

Figure 4.2-20. +Y Blanket Thermistor Characteristics

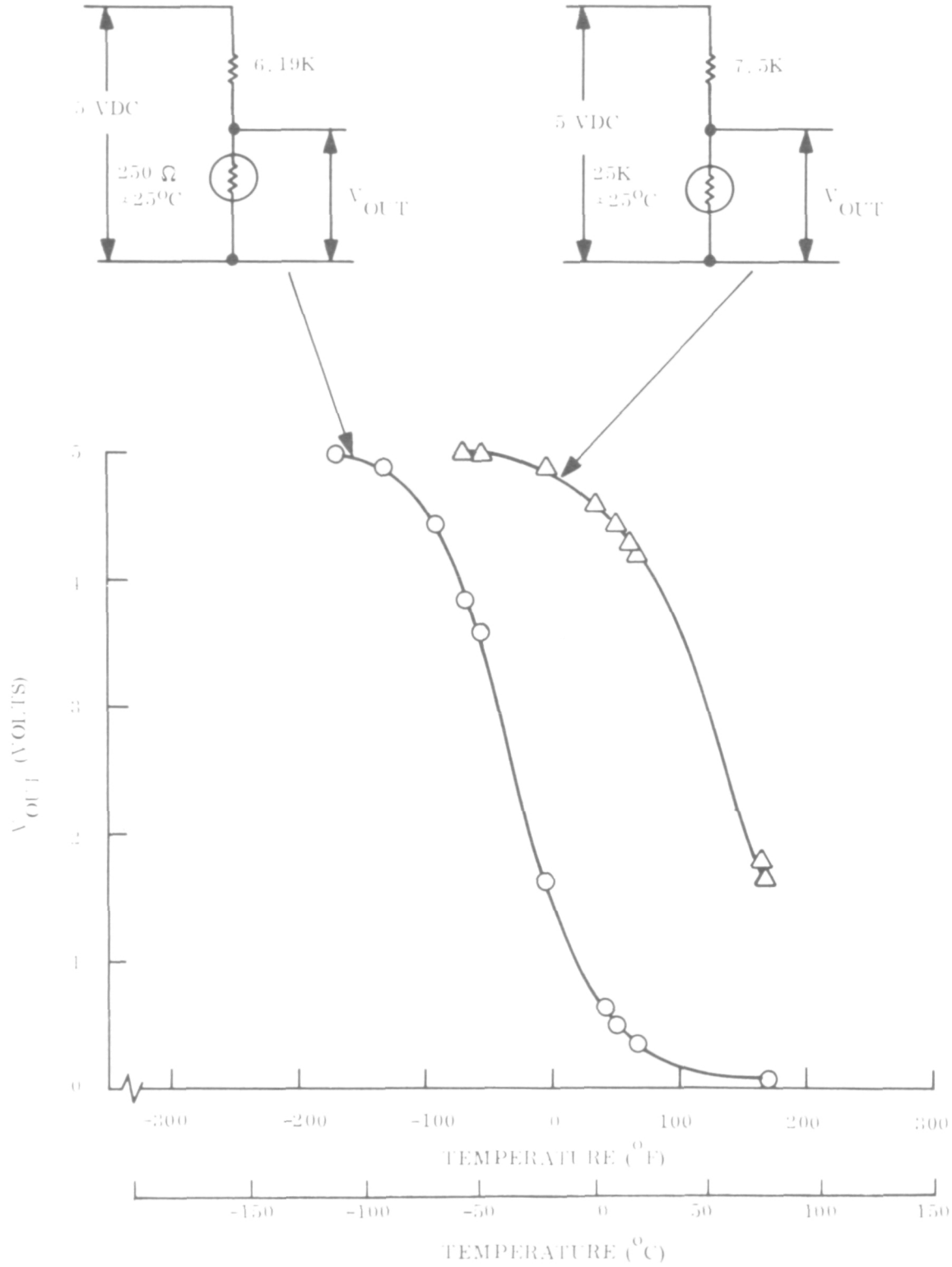

Figure 4.2-21. -Y Blanket Thermistor Characteristics

Table 4.2-4 Summary of Thermistor Outputs at Ambient Temperature

DATE	AMBIENT TEMPERATURE (^{O}F)	Blanket Position		V_{OUT} (vdc)		REMARKS
		-Y BLANKET	+Y BLANKET	-Y	+Y	
4/16/70	75	On Table	Stowed	3.988 .286	4.170 .299	After deployed modal test
4/27/70	80	Stowed	Stowed	4.012 .292	4.173 .297	Before T/V
4/30/70	80	Deployed	Deployed	4.006 .283	4.161 .298	Before T/V
5/11/70	75	On Table	Stowed	4.354 .371	4.546 .468	After T/V
5/20/70	75	Stowed	Stowed	4.369 .398	4.548 .500	After Acoustic
7/8/70	75	Stowed	Stowed	4.370 .408	4.550 2.215	After stowed vibration and 35 cycle deploy/retract

Array Blanket	Thermistor Part Number	Percentage Increase in Room Temperature Resistance
-Y	FN3C9	32.
	FN3C15	71.
+Y	FN3C9	62.
	FN3C15	97.

Inspection of this data reveals that the +Y blanket thermistors experienced a greater change in resistance than the corresponding type thermistors on the -Y blanket. Since the E6 module was affected by the overheating condition which developed during the stowed high temperature thermal vacuum test, there is reason to suspect that this change in thermistor resistance may be linked to a high temperature limitation.

Another resistance change of approximately 670 percent occurred with the FN3C9 thermistor on the +Y blanket. This change was detected after the stowed vibration test and 35 cycle life test. The slip ring portion of this circuit was checked to verify that the signal ring resistance was not contributing to this change.

4.2.4 CONCLUSIONS AND RECOMMENDATIONS

The following conclusions and recommendations can be made as a result of these periodic inspections and performance demonstrations.

1. Before further use in this or other applications, the BI-STEM actuator design requires the redesign of the microswitch actuators.

2. Coverglass and solar cell breakage exceeded the program goal of zero. Results from other solar array development programs are given in Volume I, Section 3.2.2 for comparison.

3. Handling was a severe test environment on this program. For example the edges of the two blankets were particularly vulnerable to handling damage. A count of the broken glass platelets on each edge reveals that there were 11 percent of these broken during the program as compared to only 0.47 percent of the total population of glass platelets. An edge buffer zone which is perhaps a 1/2 inch wide, would serve to eliminate much of this handling damage.

4. The environment which causes breakage of cells and coverglass is most severe at both the inner and the outer wraps. More cushioning between the storage drum shell and the first wrap might be beneficial. A longer leader between the leading edge member and the first row of solar cells might also serve to reduce the outer wrap damage.

5. The electrical characteristics of the thermistors underwent a significant change as a result of the test program. They are not a satisfactory temperature measuring device for this application.

4.3 DEPLOYED DYNAMICS TESTS

4.3.1 INTRODUCTION

The purpose of the deployed dynamics tests was to provide data on the dynamic characteristics of the deployed rollup array. It was to be used in a comparison with analytical results to verify the mathematical models generated in earlier phases of the program or to provide information to improve the mathematical models. The linearity of the system response to different excitation levels was to be determined. Data on damping, non-existent at present, was to be obtained for use in future designs and analyses.

It was recognized that this test was unusual and that several problems had to be solved prior to testing. The effects of gravity were known to be large and had to be taken into account in the selection of the test approach. The large surface area of the array would produce significant aerodynamic forces. The natural frequencies of the system are below the operating range of conventional vibration test equipment and it was anticipated that very slow sweep rates would be needed to determine natural frequencies. Conventional accelerometers and other vibration instrumentation are not suitable for the low frequency, large displacement motion involved in this test and would affect the mass distribution of the test specimen.

4.3.2 TEST APPROACH

The approach to the test was to carry out an integrated effort involving the development of test techniques, the analysis of the array in the test configuration, the identification of instrumentation and equipment requirements, the procurement of new instrumentation and vibration test equipment, and the design and fabrication of the fixtures needed for the test. Development of the test

techniques started in early 1968 and continued through the procurement and checkout of the new equipment. The test plan included the measurement of the natural frequencies, mode shapes, linearity, and modal damping for both in-plane and out-of-plane motion of the array.

It was concluded the best approach to the gravity forces was to test the system in a manner where the effects of gravity could be adequately included in the mathematical model. Correlation of the test results in gravity with a mathematical model that included gravity would provide confidence that the analysis could be extended to the zero gravity case with good results. The test arrangement was to deploy the array vertically downward and excite the system by moving the center support. This arrangement provided a free boundary condition at the leading edge member which is the boundary condition which will exist in an orbiting application. The blankets will have an increasing tension due to the force of gravity but are supported by the relatively rigid drums. The Negator spring motors were supplemented with support aids that individually applied torque to the drums to compensate for the weight of the blankets. The drums were allowed to rotate.

The tests were conducted in a vacuum chamber at ambient pressures of less than 1 mm Hg to eliminate aerodynamic effects. The deployed test length of 26 feet was determined by the work space below the lid of the vacuum chamber.

A DC coupled exciter suitable for vacuum operation was used for the test. Auxiliary equipment to provide stable sinusoidal motion down to 0.008 Hz and 0.0025 inch motion (double amplitude) and a sweep rate capability down to 10^6 seconds per decade was procured.

Array displacements were measured with Optron Model 800 optical trackers modified to allow operation in vacuum. The trackers have no physical contact with the test specimen and have the capability of measuring displacements in two directions over the frequency range from DC to 10 kHz. The sensitivity of the units is a function of the lens system and the setup used for these tests had the capability of resolving motions as small as .001 inch. A total of eight trackers was used for the test. Two were focused on the ends of the leading edge member and were fixed. Six were mounted on a scanning bar which traversed the length of the system and could be positioned at ten equally spaced span locations. White paper targets were mounted on the cell side of the solar array blankets to provide the contrast needed for the operation of the trackers.

The physical arrangement of the test is shown in Figure 4.3-1, which is a sketch of the cross section of the setup in the 32 foot by 54 foot Space Simulator at the General Electric Valley Forge Space Center. The locations of the optical trackers are conceptual and are not specifically correct with respect to location or number. The array is suspended from the Modal Test Support Fixture which includes a linear bearing system that can be arranged to provide motion in either of two directions in the horizontal plane or rotation about a vertical axis. Photographs of the test setup are shown in Figures 4.3-2 through 4.3-6.

The location of the targets for the displacement measurements is shown in Figure 4.3-7. As shown in the figure, one target (and an associated tracker) was mounted at each end of the leading edge member. Targets were located in ten equally spaced spanwise columns with the following chordwise distribution: one column on the BI-STEM, one column at the outboard extremity of the +Y blanket; and

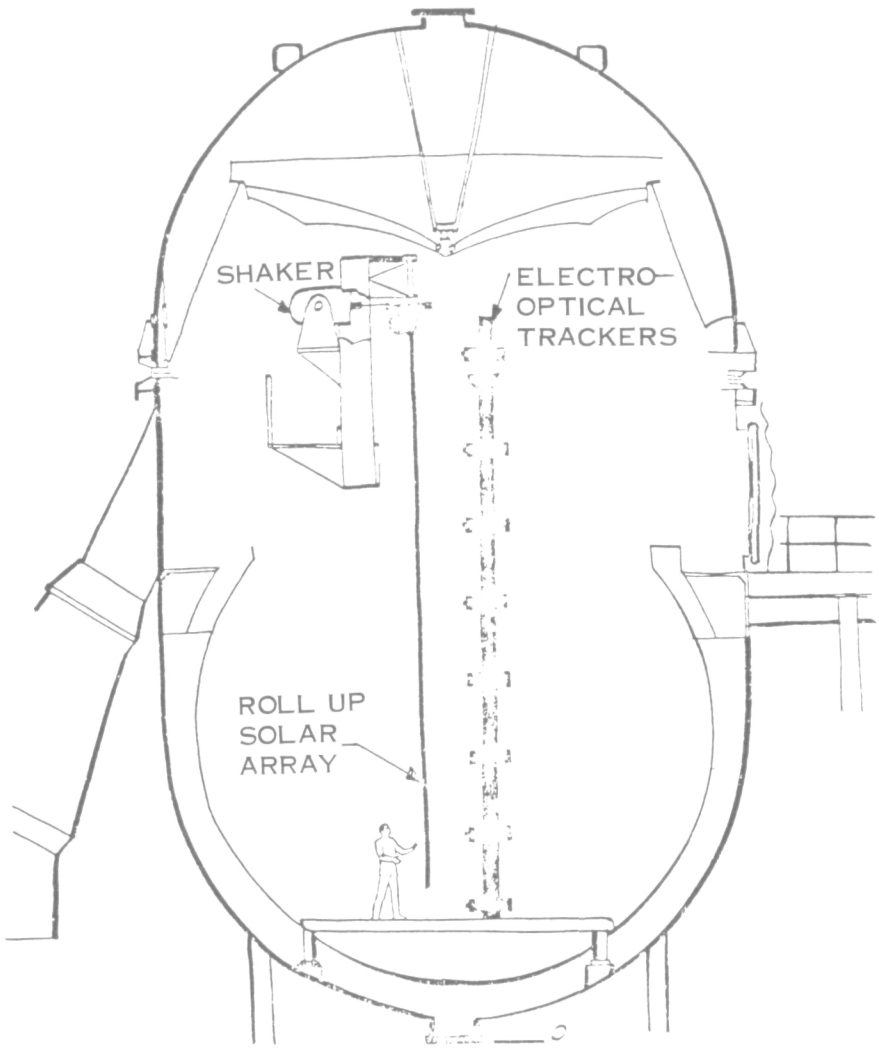

Figure 4.3-1 Deployed Dynamics Test Set-Up

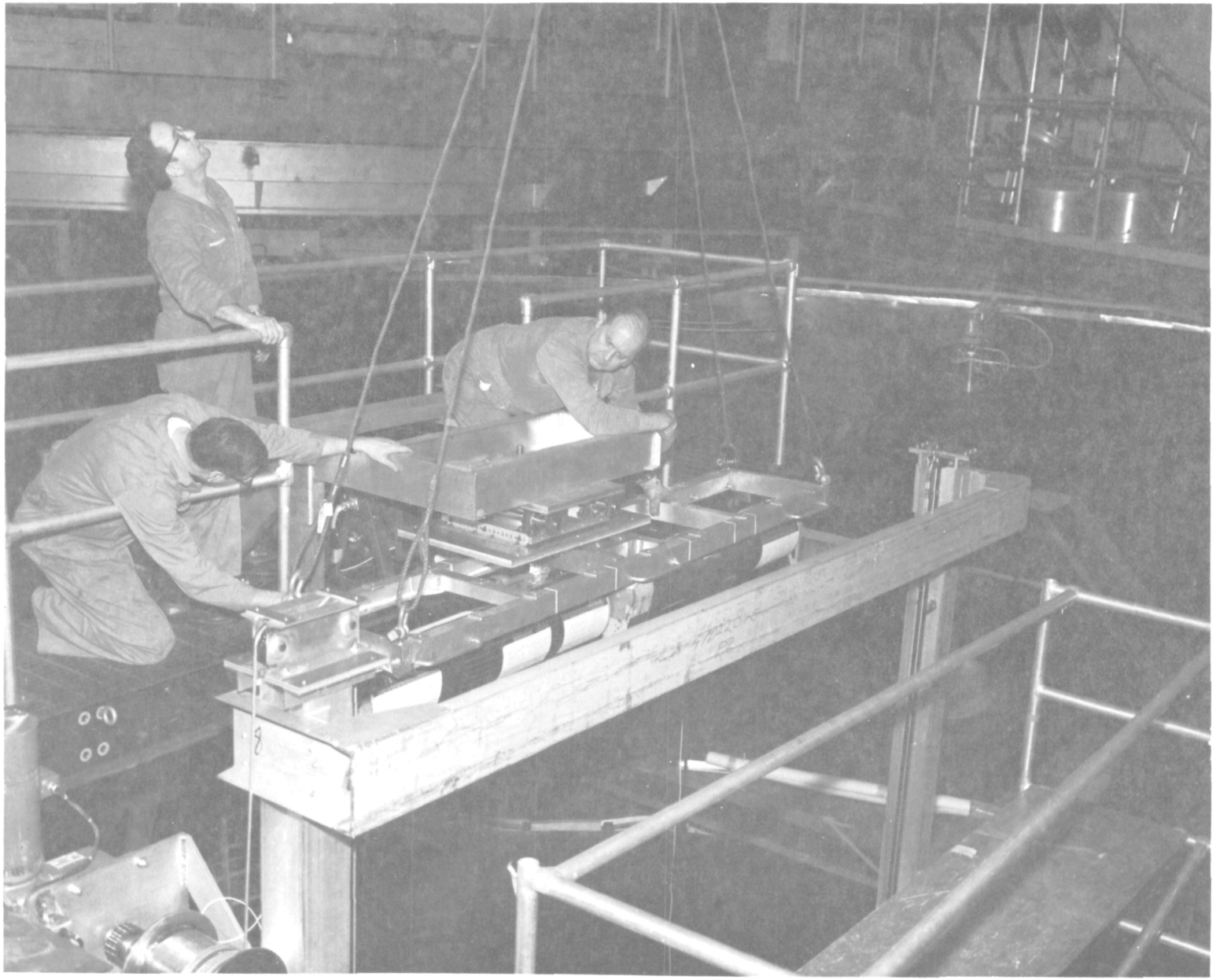

Figure 4.3-2. Deployed Dynamics Test Setup - View from top of chamber (lid off) showing shaker assembly and modal test support fixture (VF70180C)

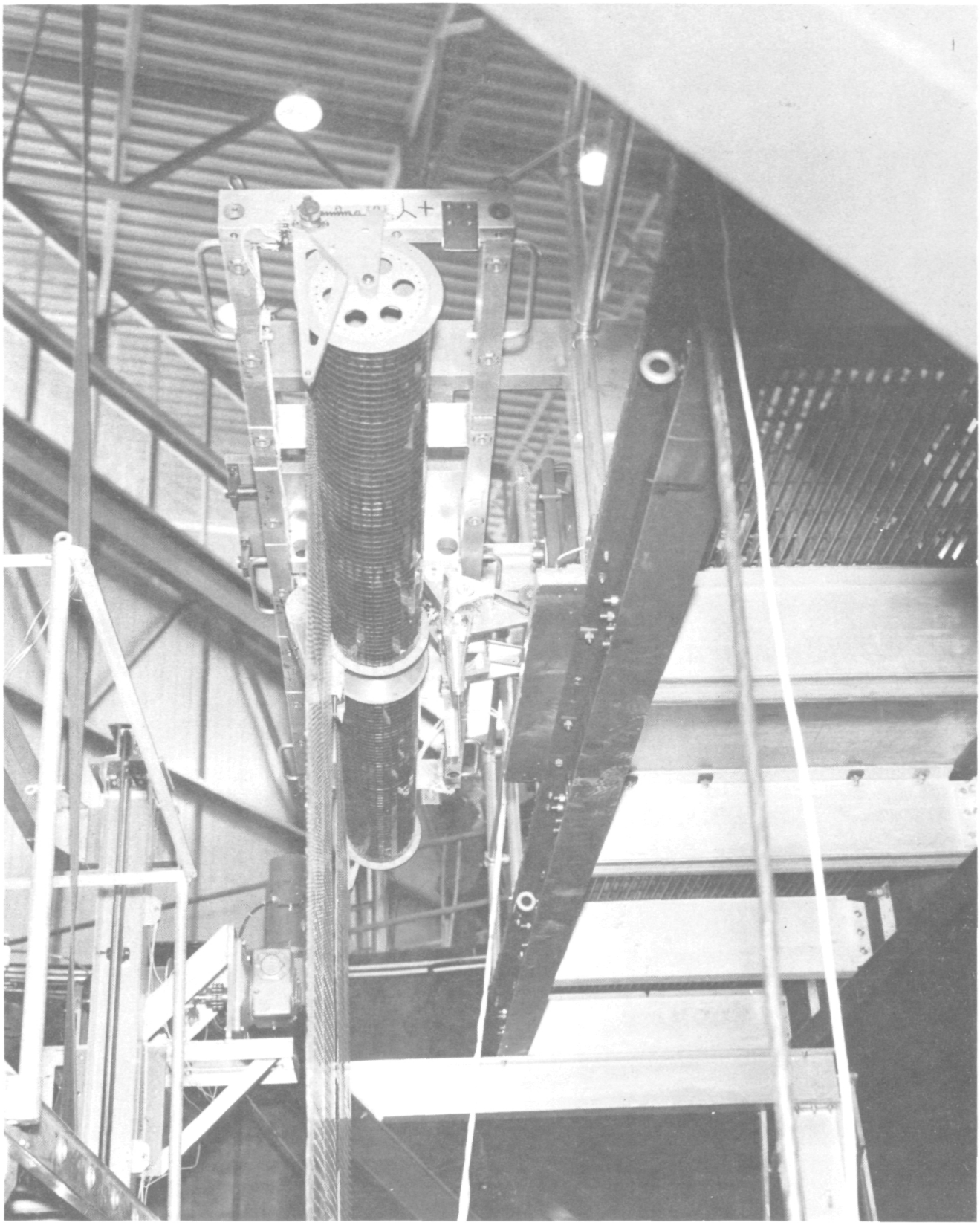

Figure 4.3-3. Deployed Dynamics Test Setup. View of array and handling frame mounted on modal test support fixture. Support aids are mounted on the handling frame. (VF70180H)

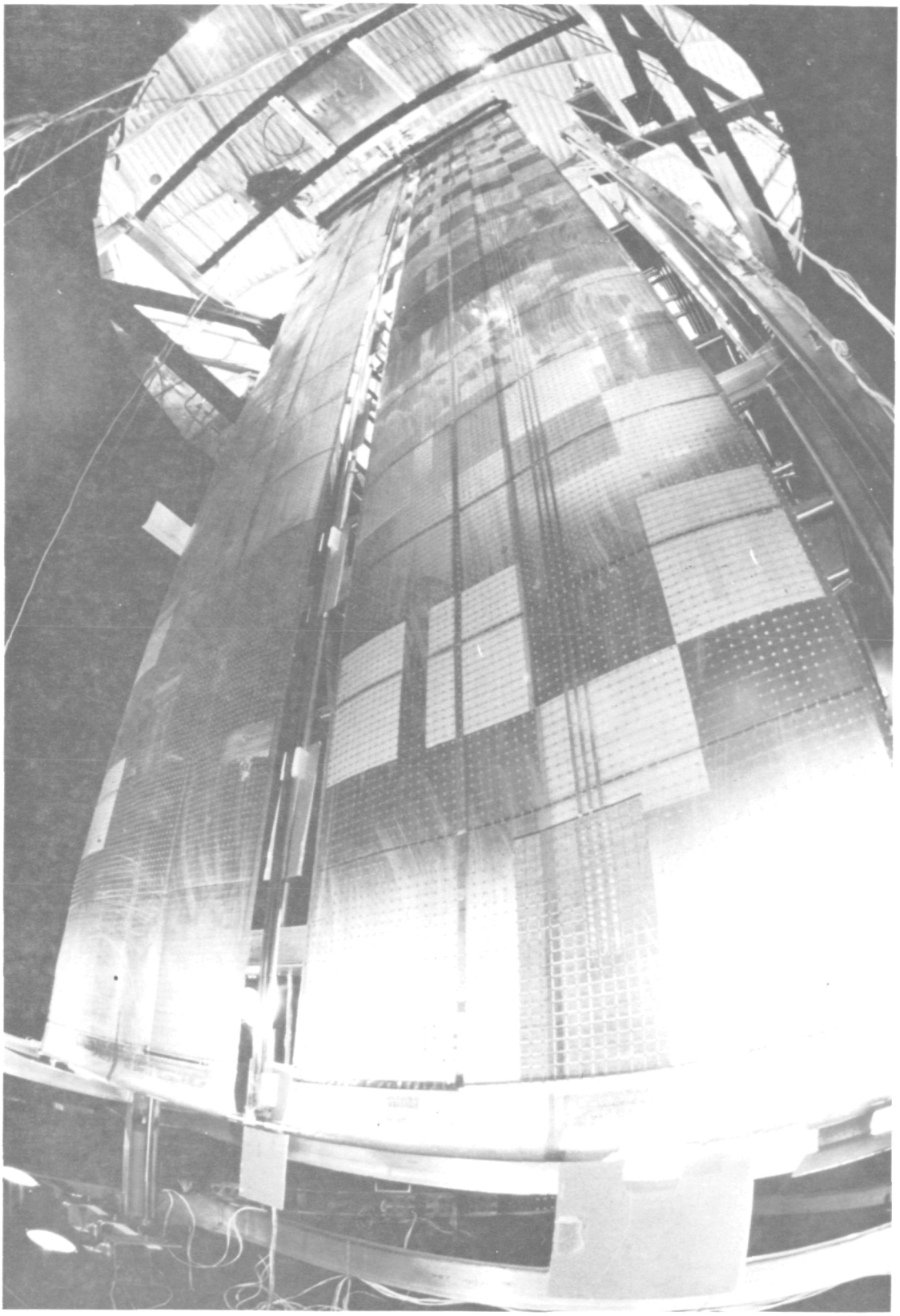

Figure 4.3-4. Deployed Dynamics Test Setup. View from bottom of vacuum chamber from back side of blankets (wide angle lens). Targets for displacement trackers can be seen through the blanket. Targets on Bi-Stem are also visible. (VF70209F)

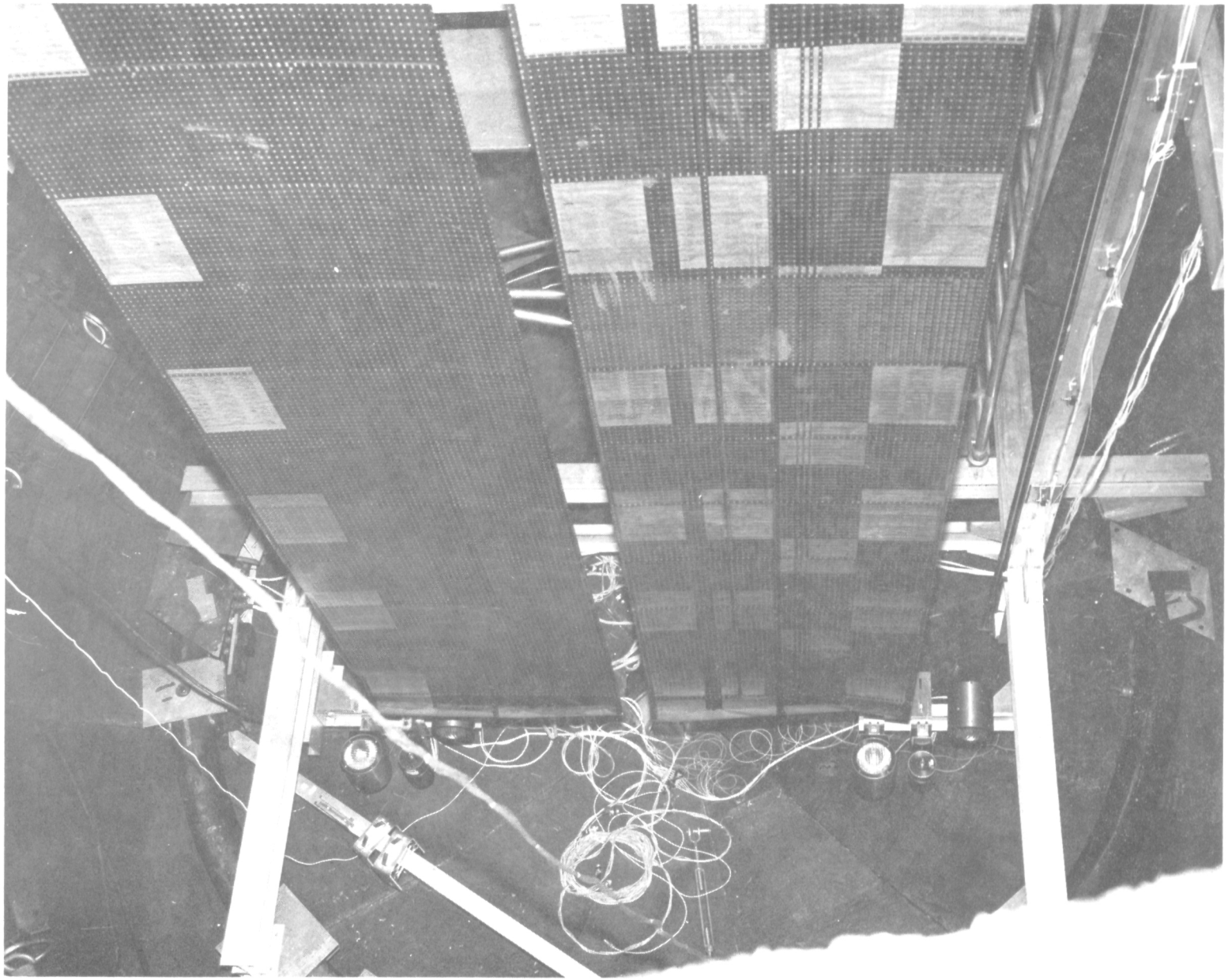

Figure 4.3-5. Deployed Dynamics Test Setup. View of low end of blankets. Bi-Stem boom and leading edge member are not installed. Fixed trackers to measure motion of outboard ends at leading edge member are visible. (VF70180G)

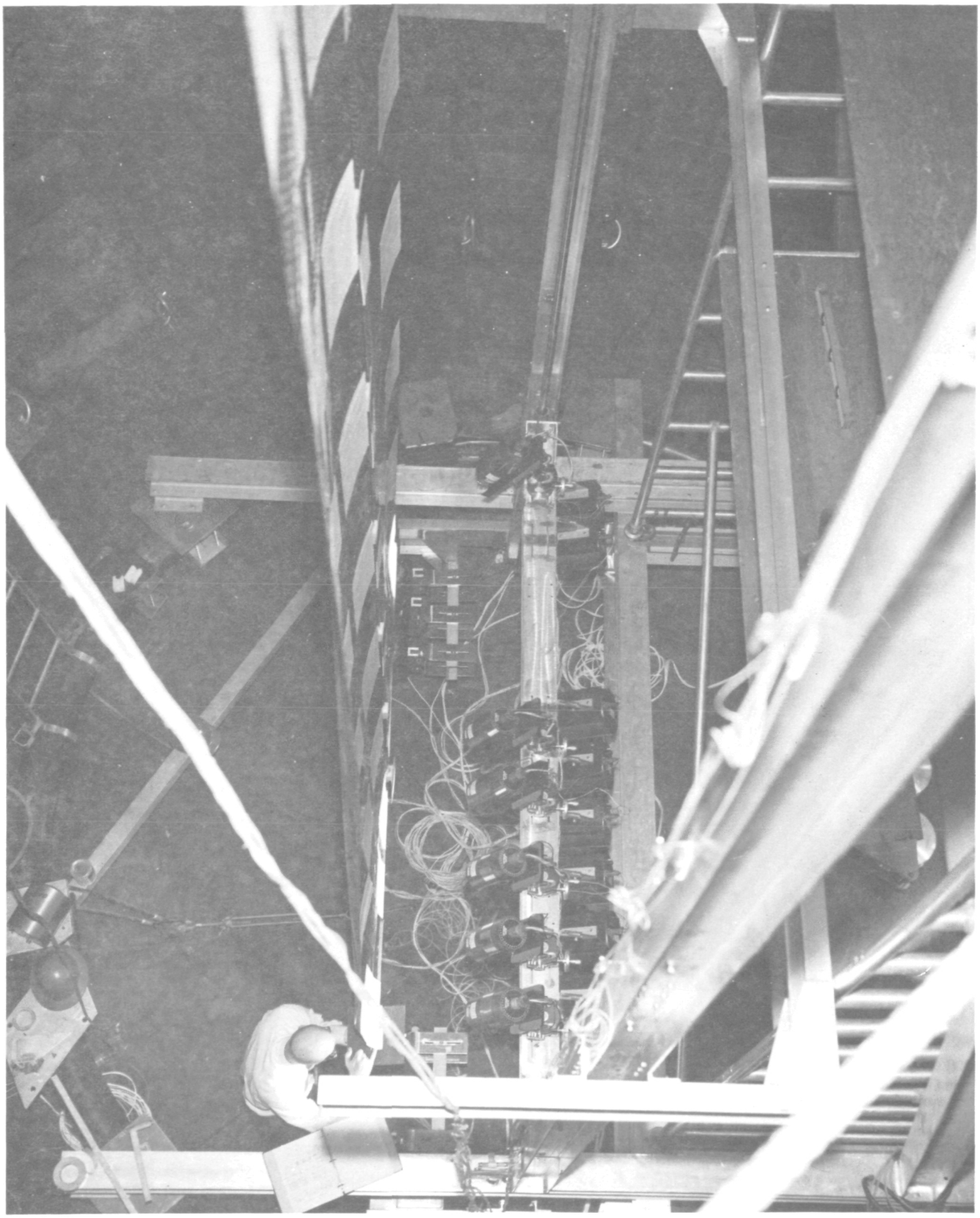

Figure 4.3-6. Deployed Dynamics Test Setup. View of six optical trackers mounted on scanning bar. (VF70193C)

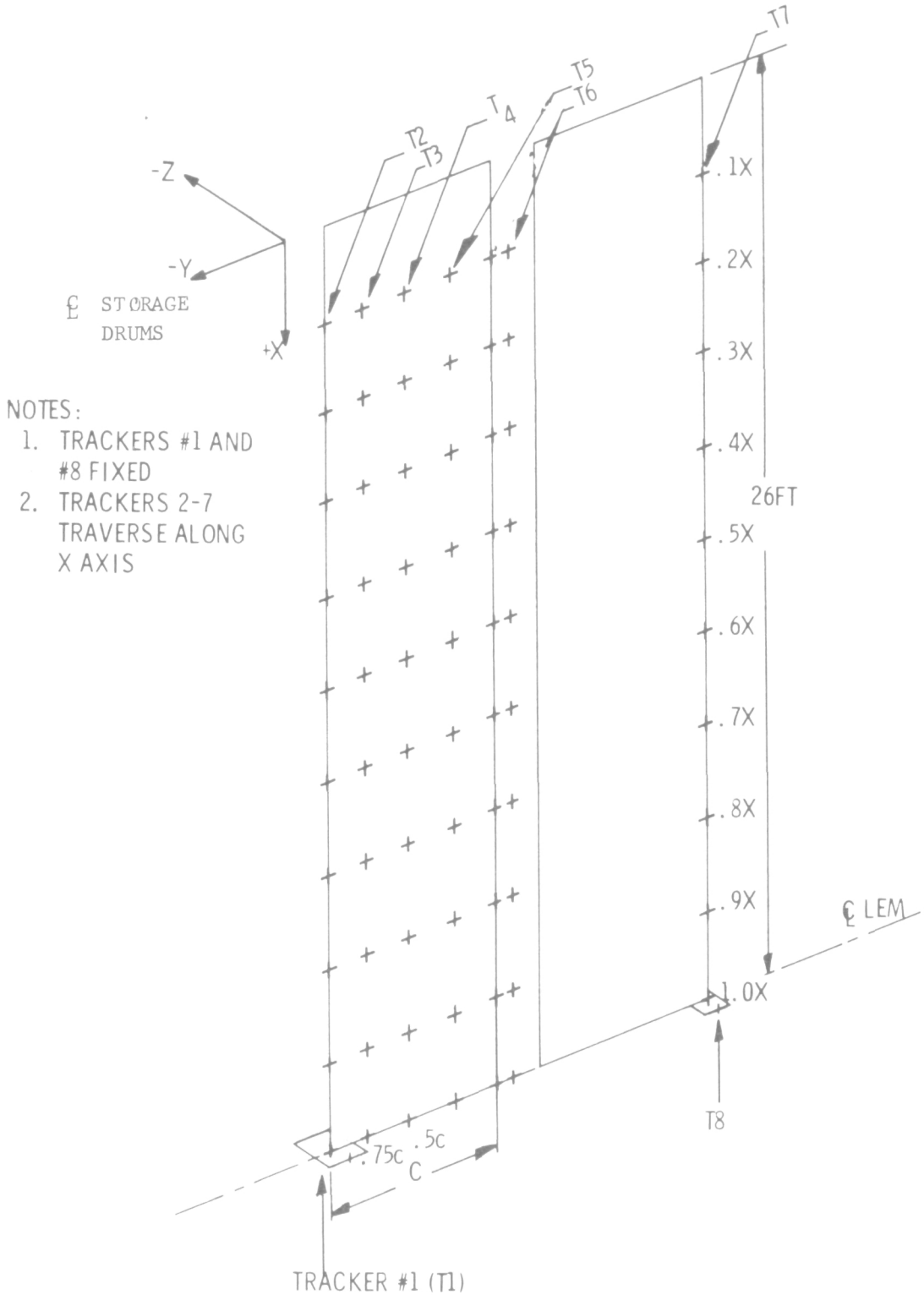

Figure 4.3-7. Array Optical Target and Tracker Distribution

columns at the one-quarter chord (25% chord), the middle (50% chord), the three-quarter chord (75%), and the outboard edge (100% chord) of the -Y blanket. These targets were used with six optical trackers properly located in a row on a scanning bar. The scanning bar could be indexed to each of the spanwise locations. It will be noted the trackers were concentrated on the -Y blanket on the basis that the system would be symmetrical. The identification assigned for data recording is given in Table 4.3-1. Note that the trackers are numbered serially from 1 through 8. Each tracker measures motion in two directions, Y and Z, and the directions are identified as 2 (for Y) and 3(for Z). Note that one row of trackers was rearranged for the in-plane measurements.

The optical trackers monitor the position of a white to black or black to white interface. In this case the interfaces were provided by targets affixed to the blanket. The trackers monitor the position of two interfaces perpendicular to the tracker optical axis. Figure 4.3-8(a) presents a sketch of a representative biaxial optical target. The tracker optical axis is perpendicular to the ξ and η axes.

The tracker monitors the position of the horizontal white to black (W-B) interface to yield ξ displacement data and the position of the vertical white to black interface to supply η displacement data. The tracker was bore sighted approximately on the center of the targeted white field per Figure 4.3-8(b).

Since motion of 8.0 in. DA was desired a minimum offset from pt. A target position identification (span and chord) of 4 inches was required to insure that the moving target always presented the white to black interfaces to the sensing optics. The net result is that while displacements are referenced to position A the displacements

Table 4.3-1. Tracker Stations Identification

Tracker No./Axis for Out-of-Plane Tests	Measurements Taken	Tracker No./Axis for In-Plane Tests
1Y, or 12 1Z, or 13	Outboard extremity of the -Y side of LEM (Fixed Tracker)	Same
2Y, or 22 2Z, or 23	Outboard edge (100% chord) of -Y blanket	Same
3Y, or 32 3Z, or 33	75% chord of -Y blanket	Same
4Y, or 42 4Z, or 43	50% chord of -Y blanket	Same
5Y, or 52 5Z, or 53	25% chord of -Y blanket	None
6Y, or 62	Inboard edge (0% chord) of -Y blanket	
6Z, or 63	BI-STEM	5Y, or 52 5Z, or 53
7Y, or 72 7Z, or 73	Outboard Edge (100% chord) of +Y blanket	Same
8Y, or 82 8Z, or 83	Outboard extremity of the +Y side of LEM (Fixed Tracker)	Same

NOTE 1: Spanwise location denoted by the addition of two digits, 2201, 2202, ... 2210 respectively denote 10%, 20%, ... 100% span locations for Tracker No. 2 (which is at the outboard extremity of the -Y blanket) measurements of displacement in the Y direction.

NOTE 2: Tracker No. 6 not used for In-Plane tests.

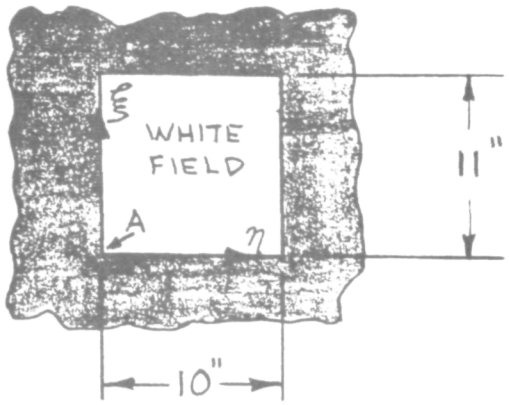

(a) SKETCH OF TARGET

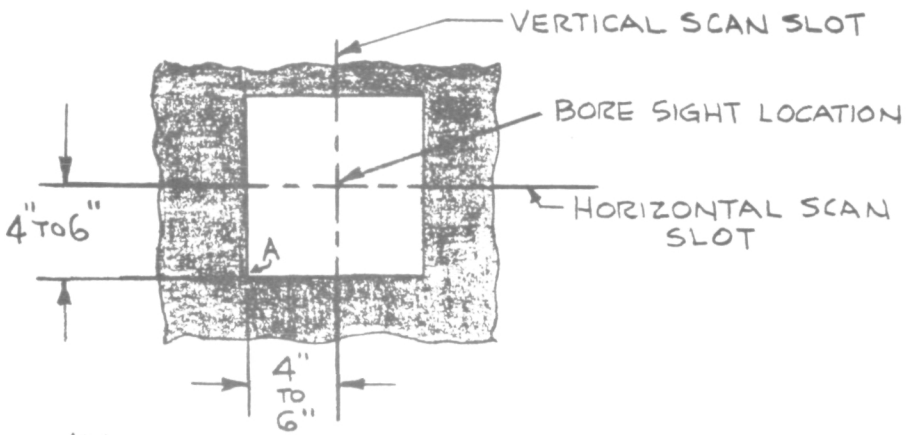

(b) BORE SIGHT LOCATION

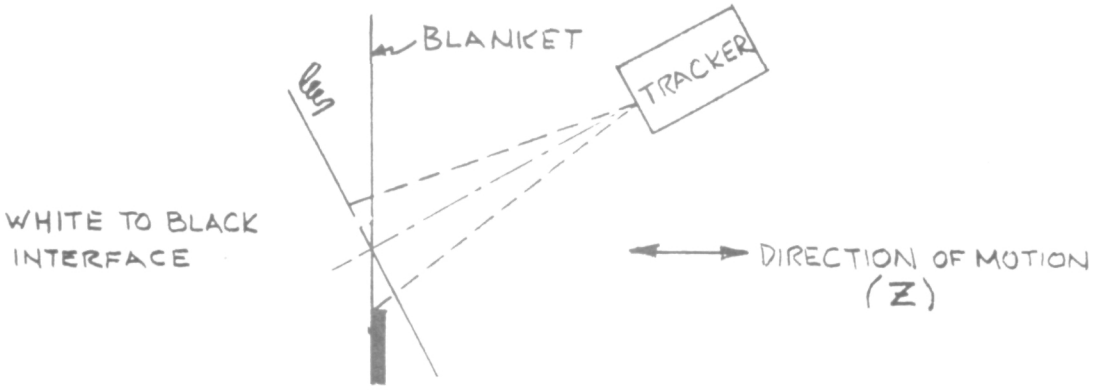

(c) APPARENT MOTION IN ξ DIRECTION

Figure 4.3-8. Target Details

of the targets are actually measured along lines that intersect at A. For example ξ measurements are made four to six inches from A when η displacement is zero. If concurrent η displacement is taking place then the ξ displacement is measured along the portion of the W⟶B horizontal interface which moves into the tracker vertical scan location. Similarly, η measurements are made along the vertical W⟶B interface (ξ axis).

Displacement normal to the blanket plane was measured by tilting the tracker so that motion in Z (array axis reference) produced an apparent ξ motion of the white to black interface as shown in Figure 4.3-8(c).

This approach was successful as actual X motion was negligible and the apparent ξ motion measured by the tracker was the result of blanket Z motion. Each tracker was individually calibrated for the test operation.

Potentiometers were installed on each drum so that rotation could be monitored. The test data flow is shown in Figure 4.3-9. Displacement data from the eight optical trackers and the Linear Variable Differential Transformer (LVDT) mounted on the exciter was recorded on magnetic tape for playback analysis as required. A single channel low frequency wave analyzer was used to provide in-phase and quadrature components of the output of a selected data channel during the test runs. An oscilloscope was also employed to monitor the quality and shape of the input and response waveforms on-line. A direct writing oscillograph was available for recording responses as needed. During resonance dwells the voltmeters reading the output of the trackers were visually read, recorded on data sheets and later converted to displacements to show mode shapes.

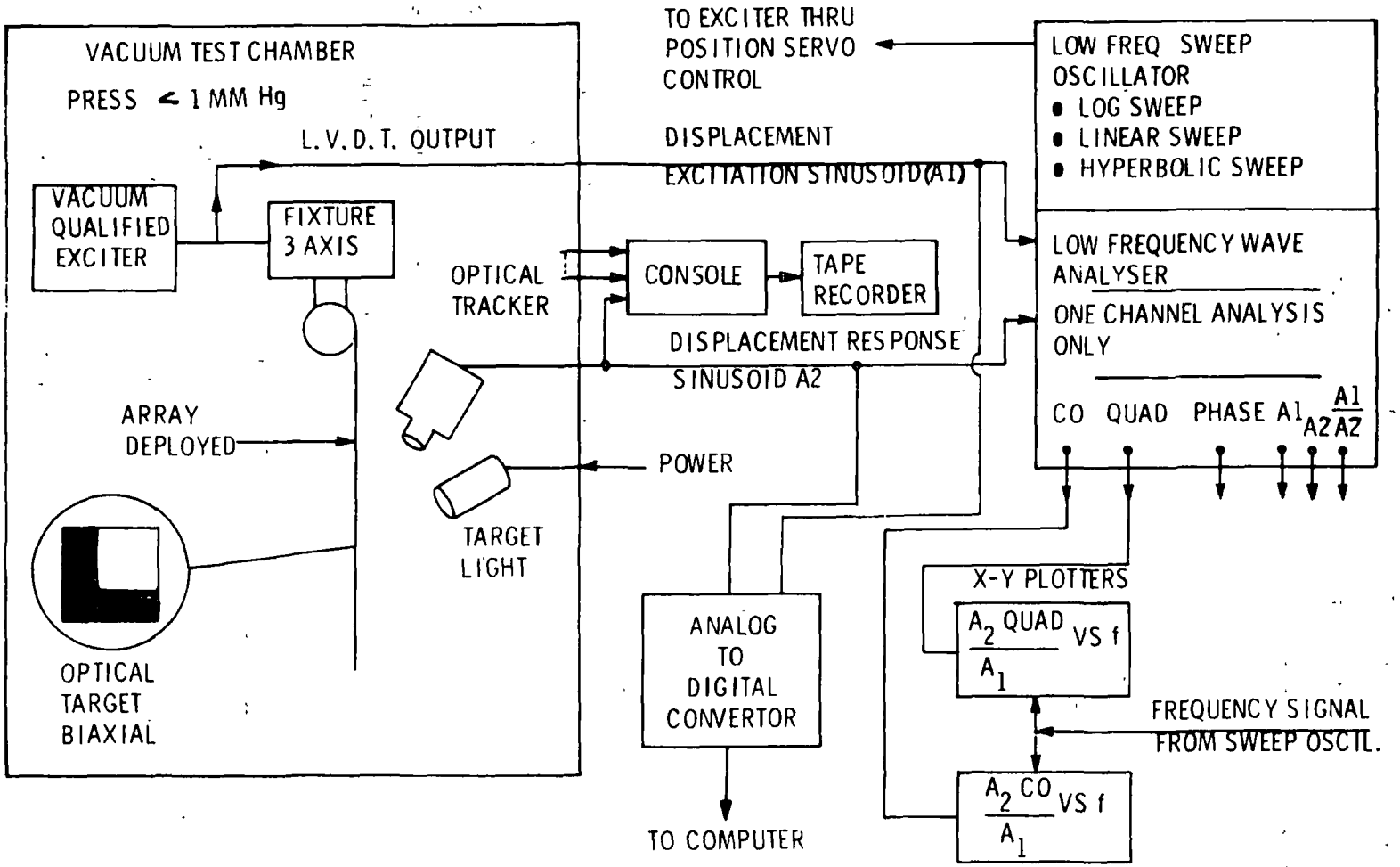

Figure 4.3-9 . Deployed Dynamics Test Data Flow

The test data was also digitized and transmitted in real time to a digital data laboratory, where it was formatted and recorded for further processing. The digital computer provided multi-channel wave analysis and arranged the results in tabular form.

The planned deployed dynamics (deployed modal) test program for each test axis consisted of the following test runs:

1. Resonance searches under ambient conditions
2. Resonance searches under vacuum conditions
3. Measure mode shapes at resonance dwells
4. Linearity evaluation tests
5. Structural damping data tests

4.3.2.1 Ambient Resonance Search Tests

Resonance search tests under ambient conditions were performed to: (a) permit visual and unobstructed observations of array behavior under constant sinusoidal base motion; (b) establish frequency regions for the ensuing resonance searches in vacuum; and (c) establish approximate values of structural damping under ambient conditions for use as a datum in evaluating damping measured in vacuum.

4.3.2.2 Resonance Searches (Sweeps in Vacuum)

The resonant frequencies of the test article were to be determined by exciting the structure with a constant sinusoidal base motion. The frequency of the base motion was hyperbolically swept at rates sufficiently slow to establish the frequencies of peak quadrature. The quadrature (or out-of-phase to the exciting motion) response at selected locations was used to determine the resonant frequencies of the test article for the ensuing dwells.

4.3.2.3 Resonance Dwells

At each of the resonant frequencies (up to the first 4 modes) indicated by the peaking of the quadrature response, the mode shapes of the test article were to be determined. The frequency was slowly varied in the region of the first resonance and tuned to peak the quadrature response. The first mode shape was then determined by scanning all the locations on the test article. The base motion was then abruptly stopped and the free decay of the resonant response measured. This procedure was then repeated for the other indicated resonances in each test axis.

Modal damping data was also obtained from the results of these tests by at least two methods. The decay rate of the resonant response induced by abruptly stopping shaker inputs at each principal resonance, can be related to modal damping. In addition, the frequencies (f_a) and (f_b) at which the in-phase response peaks on either side of a given resonance during sweeps are related to the damping coefficient.

4.3.2.4 Linearity Evaluation Tests

At each of the resonances (per test axis) investigated during resonance dwells, linearity evaluation tests were to be performed. During these tests, the base motion was to be reduced to half the amplitude used for the previous mode shape measurements. The frequency was slowly varied to peak the quadrature response and the resonant frequency determined.

The base motion was to be abruptly stopped, and the free decay of the resonant response measured. Damping coefficients were measured via the same techniques outlined above.

4.3.3 TEST RESULTS

4.3.3.1 Introduction

Testing was initiated per the approach described in the previous section. With no data available on damping coefficient and the use of new testing techniques, initial runs were exploratory. In particular the determination of sweep rates was critical. The rate has to be sufficiently slow to avoid "beating" in the region of a resonant frequency. At the low frequencies involved, the sweep times were long (many minutes to a few hours) so it was desirable to use as high a sweep rate as possible to keep costs down. Test results were used to modify the test plan and additional exploratory tests were added to the sequence to investigate anomalies or to provide information for use in test analysis. The testing sequence is given in Table 4.3-2.

Test results will be grouped with respect to the test axis with certain of the special tests discussed separately. Predicted results are included as appropriate with the tabulations of the test data.

4.3.3.2 Out of Plane - Symmetric Excitation (Z Axis Test)

4.3.3.2.1 Ambient Sweep Test

The deployed dynamics test program was initiated on March 30 by performing an ambient sweep (0.50" D.A. input). The purposes of this sweep were: (1) to obtain data to assess array frequency and damping characteristics under ambient conditions, and (2) to physically observe array vibration patterns "close up".

Table 4.3-2. Testing Sequence

Test Axis	Test Description	Date
Out-of-Plane (Symmetric) Z-Axis Excitation	Ambient Sweep Test (0.1 Hz to 2.8 Hz)	3-30
	Sweep Test in Vacuum (0.13 Hz to 1.0 Hz)	3-31
	Resonance Dwells in Vacuum	4-1 & 4-2
	Linearity Checks and Damping Measurements in Vacuum	4-1 & 4-2
	Ambient Sweep Test with Leading Edge Member Removed	4-9
	Vacuum Sweep Test with Leading Edge Member Removed	4-10
	Vacuum Resonance Dwell with Leading Edge Member Removed	4-10
Out-of-Plane (Antisymmetric) Torsional Excitation About X-Axis	Ambient Sweep Test (0.05 Hz to 1.0 Hz)	4-3
	Sweep Test in Vacuum (0.15 Hz to 1.0 Hz)	4-4
	Resonance Dwell in Vacuum	4-6
	Narrow Band Sweep Tests in Vacuum	4-7
	Linearity Checks and Damping Measurements in Vacuum	4-7
	Movies of Resonance Dwells	4-8
	Ambient Sweep	4-8
	Ambient Sweep Modified Tension Distribution at the Leading Edge	4-8
In-Plane Motion Y-Axis Excitation	Ambient Sweep Test (0.1 Hz to 2.3 Hz)	4-8
	Sweep Test in Vacuum (0.6 Hz to 1.6 Hz)	4-9
	Ambient Sweep with Drums Locked	4-9
Static	Mapping of Static Shape of System	4-9

The frequency sweep was hyperbolic, i.e., $\frac{df}{dt} = K_n^2$ and the constant, K_n was selected so that 26 minutes were required to sweep from 0.13 Hz to 1.0 Hz. This rate was selected on the basis of an assumed damping ratio ($\xi = C/C_{cr}$) of 0.10 and a Hok's sweep rate parameter (φ) in excess of 2.0. (See Reference 1-7)

$$\varphi = \xi f_n \sqrt{\pi / \frac{df}{dt}}$$

φ = Hok's sweep rate parameter

ξ = C/C_{cr}, the damping coefficient

f_n = resonant frequency, Hz

df/dt = sweep rate, Hz per second

The reference concludes the sweep rate is sufficiently slow to allow the response to build up with acceptable distortion of the quadrature response when $\varphi \geq 2.0$.

For the test, the optical tracker assembly was positioned to measure motions at the 80% span station. This location was selected on the basis of analysis as the best position for detecting array modes. Data from Tracker No. 2 (identification 2308) at the 100% chord station of the -Y blanket was monitored. Test results (including comparisons with analytical predictions) are given in Table 4.3-3.

At 2.80 Hz, the tracker support structure began to visibly vibrate, indicating the presence of a resonance on that scaffolding. Consequently, this sweep was terminated at that frequency. This scaffolding resonance results in an upper limit of approximately 1.5 Hz to obtain test data unaffected by test set up motions.

Table 4.3-3. Summarized Test Results Ambient Sweep-Out of Plane Symmetric

Analytical Mode Number	Analytical Predicted Frequency (Hz)	Apparent Resonant Frequency (Hz)
1	0.17**	0.16
2/3*	0.39	0.42
4	0.56	0.55
5/6*	0.81	0.80
7	0.92	0.94
-	-	1.00
8/9*	1.24	1.15
10	1.32	1.36
-	-	-
11/12*	1.72	-
-	-	1.70

* Analytical predictions show two modes at these frequencies. These modes involve only blanket motion and the number of modes at a given frequency depends on the number of elements in the mathematical model. The analysis predicts these modes would not be excited by base motion.

** This represents the first predicted frequency (C.248 Hz), corrected to reflect apparent air mass influences. From unsteady aerodynamic theory involving subsonic flutter of high-aspect ratio lifting surfaces, the effective air mass is described by a cylinder of air, whose center is located at the 50% chord line. The height of this cylinder is equal to the length of the span (26 ft. for the array) and its diameter is equal to the length of the chord (1.83 feet for each blanket). At ambient conditions, (ρ = .002378 slug/ft^3), the weight (W_A/C) of the air cylinder is 21 lbs. Each blanket (W_b) weighs 18.5 lbs. The frequency (f_{corr}) of the array, compensated for air mass effects, is related to the computed frequency (f_{comp}) in terms of weights involved, i.e.,

$$f_{corr} = f_{comp} \sqrt{\frac{W_b}{W_b + W_{A/C}}}$$

Only the first array mode was corrected for this aerodynamic effect.

The on-line in-phase response and quadrature response plots are presented by Figures 4.3-10 and 4.3-11 respectively. At the fundamental resonance (.17 Hz), a peak response of 3.06 in D.A. was recorded. Assuming the analytically predicted mode shape to be correct, this corresponds to a damping ratio $\xi = c/c_c = 0.10$. This validates the assumption of the damping value in evaluating rates for this ambient sweep. The apparent jitter in the plots is due to an equipment characteristic in the hyperbolic sweep mode.

4.3.3.2.2 Vacuum Sweep Tests

Sweep tests in vacuum were performed to:

(1) Locate regions containing resonances for subsequent slow sweeps and dwells,

(2) Establish and/or verify concepts for establishing sweep rate criteria.

Hyperbolic sweep rates were initially used and adjustments to both rate and input amplitude were made on the basis of test results. Final runs were made with linear sweep rates. The optical trackers were positioned at the 80% span point. The sweeps are summarized in Table 4.3-4 and selected analyzed response plots are shown in Figures 4.3-12 through 4.3-15.

Inspection of the data produced the results in Table 4.3-5. The measured frequencies have been assigned to the appropriate predicted frequencies. The blankets modes of the analysis were not excited which agrees with the response

analysis. These modes are a function of the method of discretization of the finite element analysis.

The results of sweep rate studies are given in Table 4.3-6. Note the long times required for the sweeps that accurately define the natural frequencies.

Table 4.3-4. Summary of Vacuum Sweeps - Out-of-Plane-Excitation

Identification Number	Frequency Range (Hz)	Duration (minutes)	Sweep Rate (Seconds to sweep Decade)	Input Level (D.A. inches)	Comments
9	0.13 to 0.25	14	2,050*	0.25	Terminated at 0.25 Hz because response exceeded tracker range.
10	0.20 to 1.0	15.3	2,050*	0.10	Severe beating noted
11	.145 to .22	31.2	7,200*	0.25	Terminated at 0.23 Hz because of beating
12	.29 to 1.0	32.6	7,200*	0.10	
13	.22 to .29	29.9	14,700*	0.05	No beating
14	.236 to .256	71	175,100**	0.05	No beating
15	0.55 to 0.66	18	8,800**	0.25	Refined natural
16	0.72 to 0.90	29.5	8,800**	0.10	Refined frequency to 0.781 Hz.

* Hyperbolic Sweep Rate
** Linear Sweep Rate

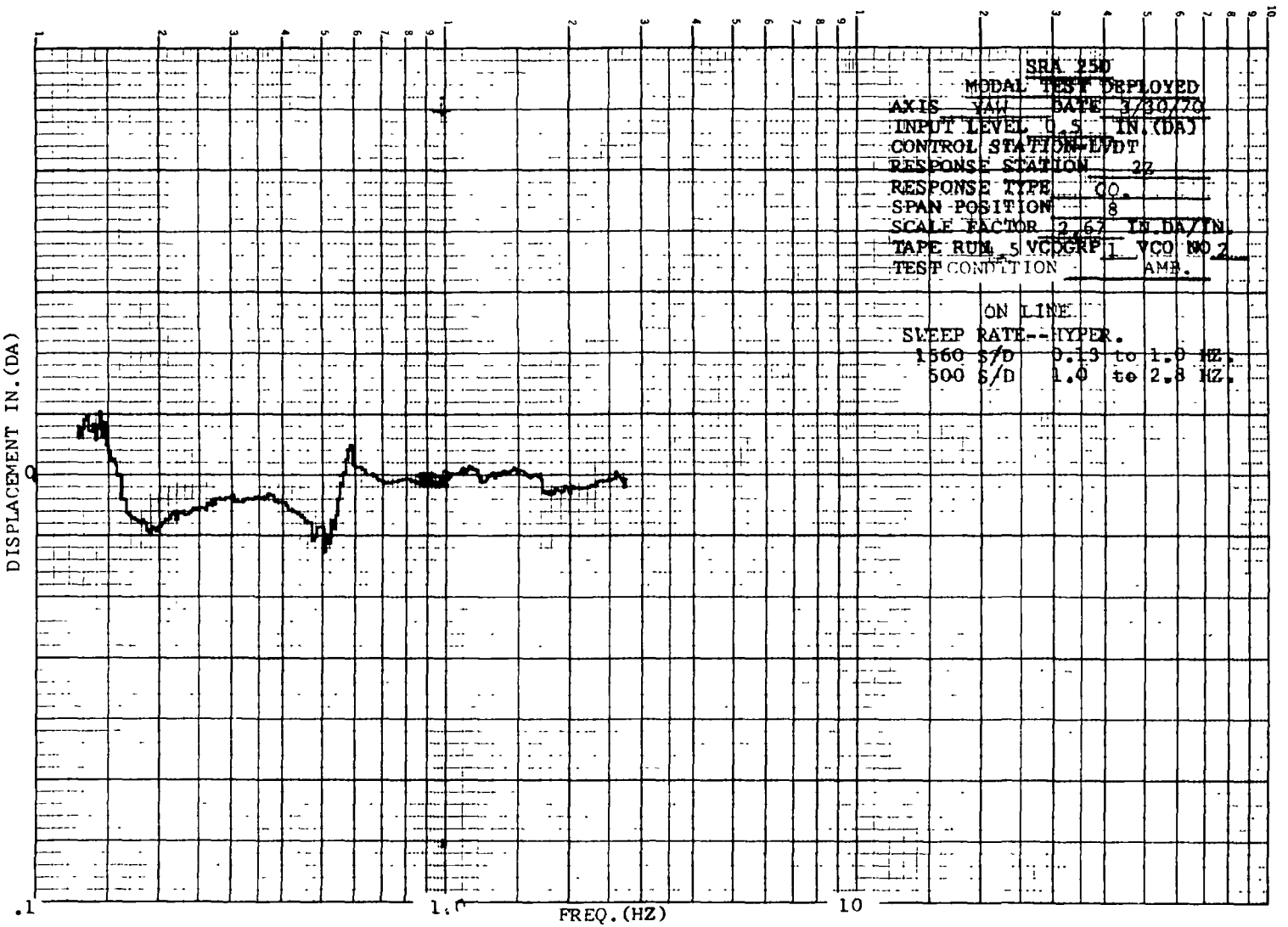

Figure 4.3-10. Frequency Sweep - Out-of-Plane Symmetric Excitation

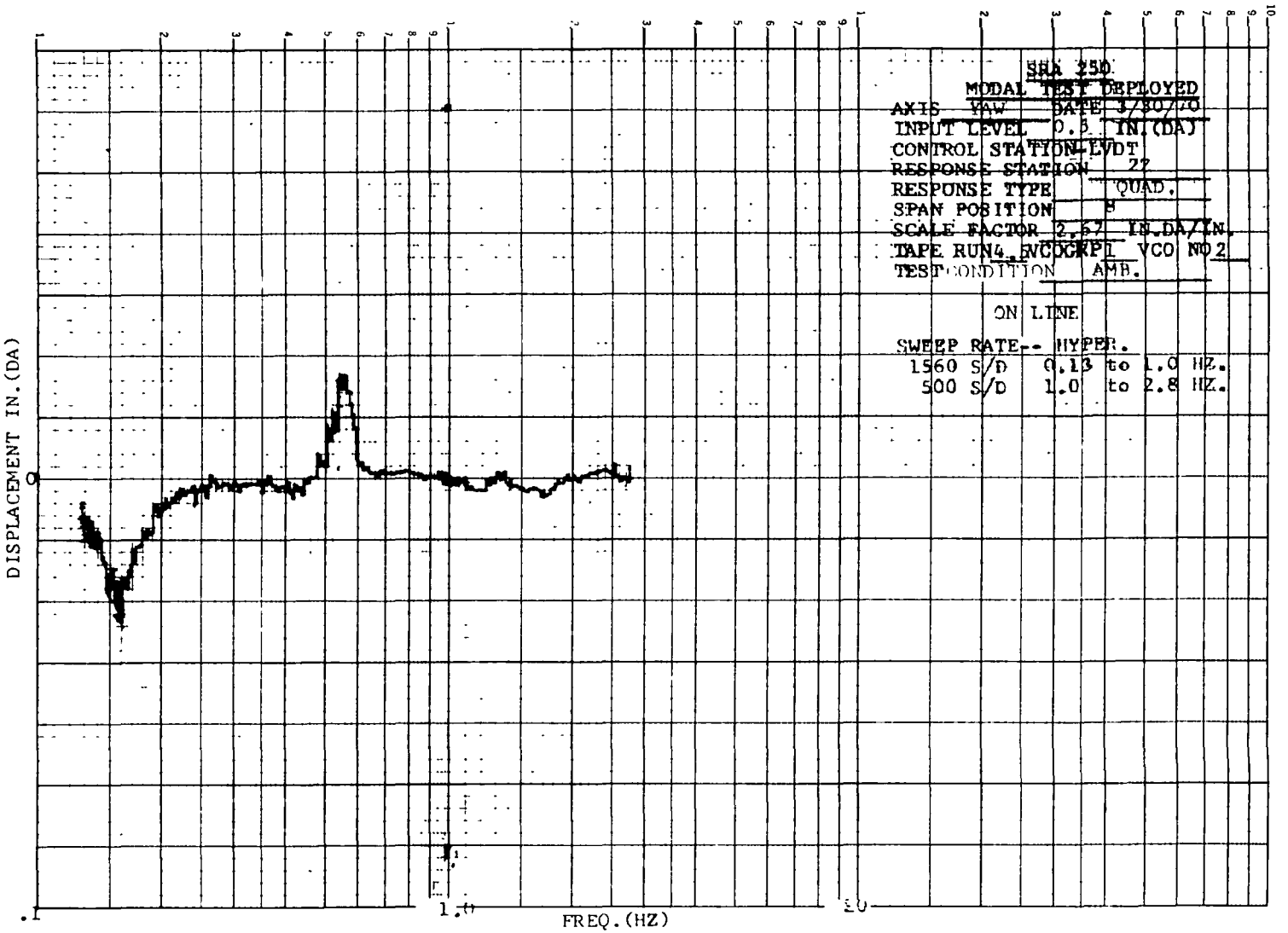

Figure 4.3-11. Frequency Sweep - Out-of-Plane Symmetric Excitation

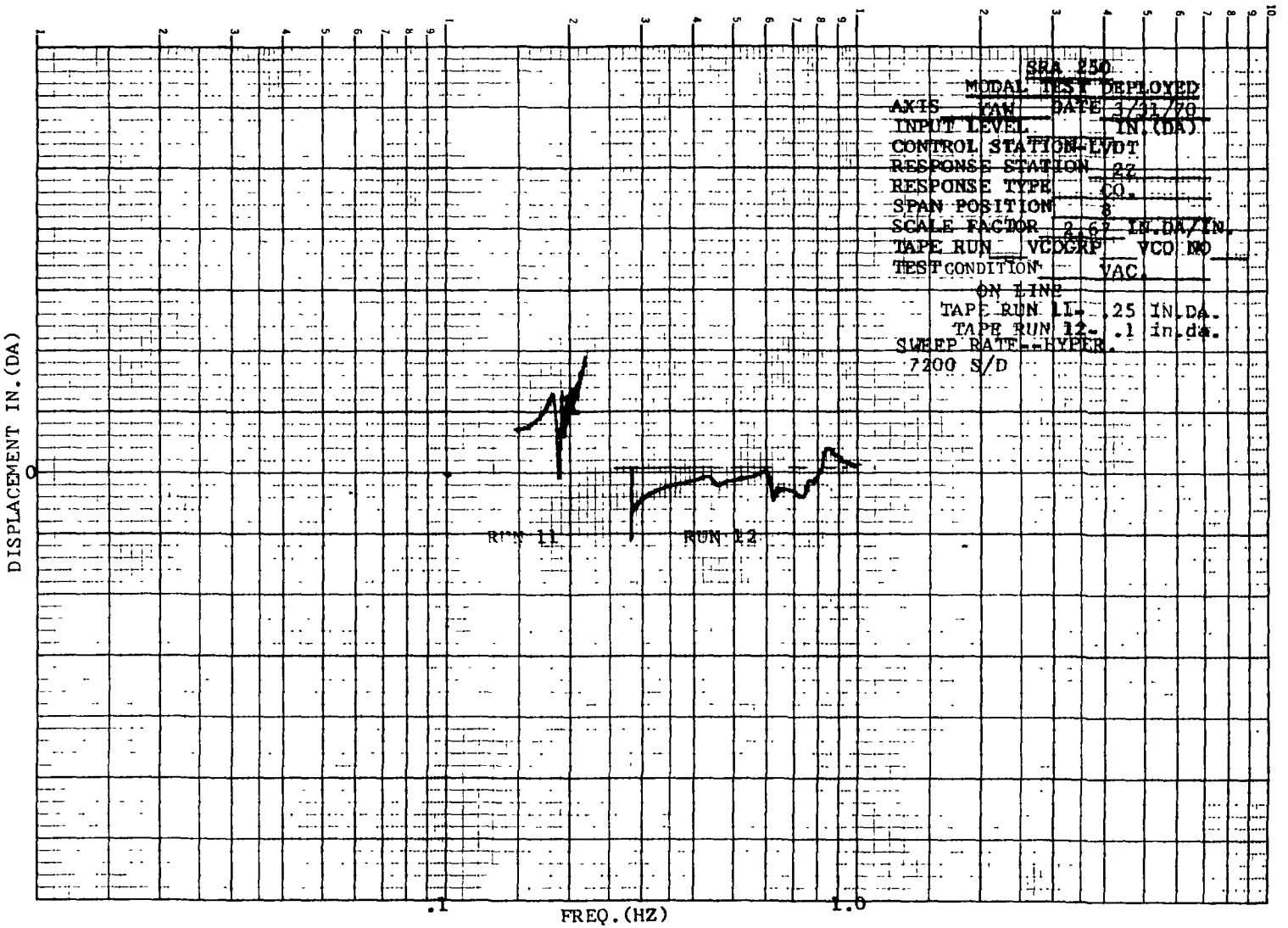

Figure 4.3-12. Frequency Sweep - Out-of-Plane Symmetric Excitation

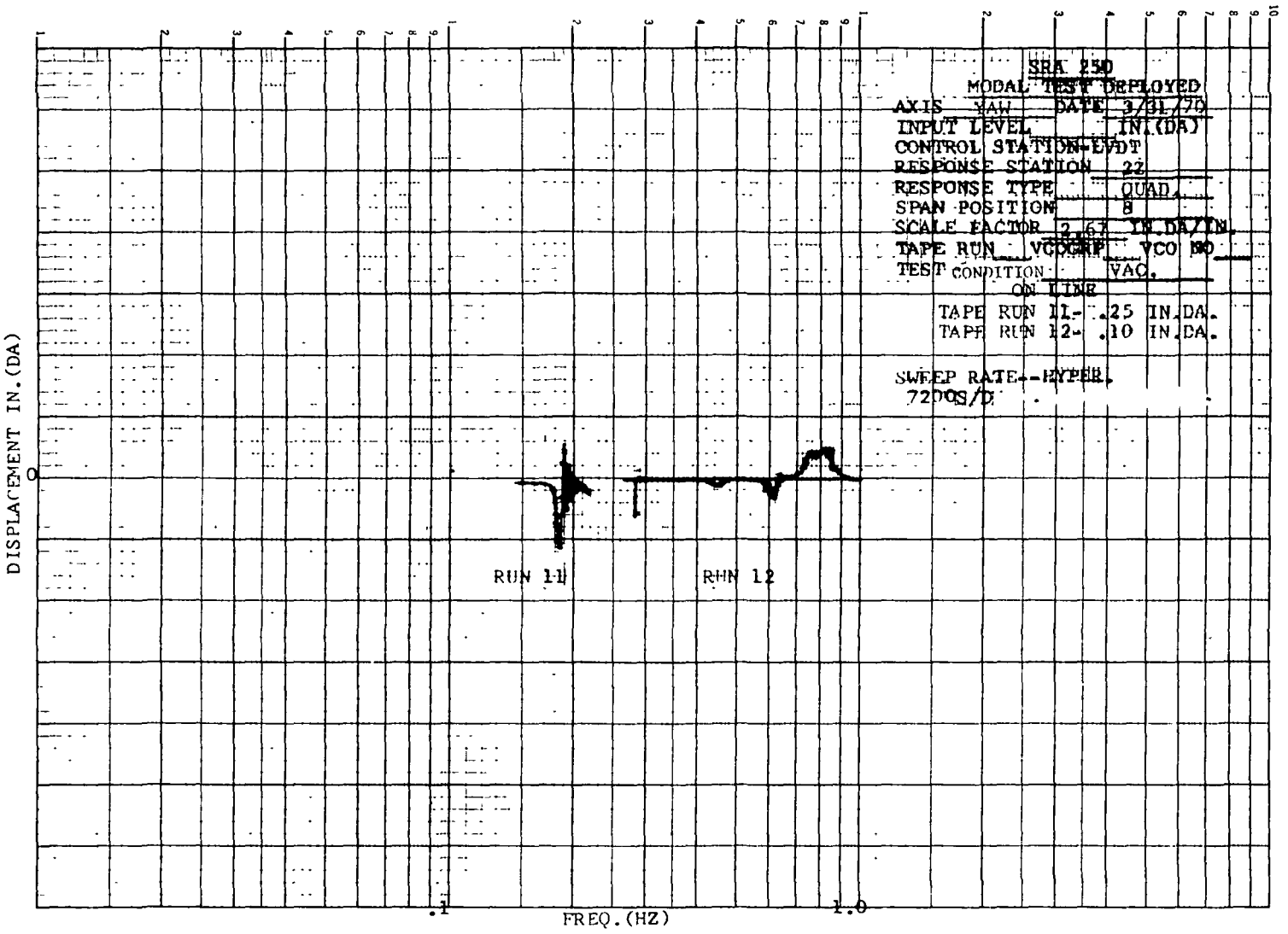

Figure 4.3-13. Frequency Sweep - Out-of-Plane Symmetric Excitation

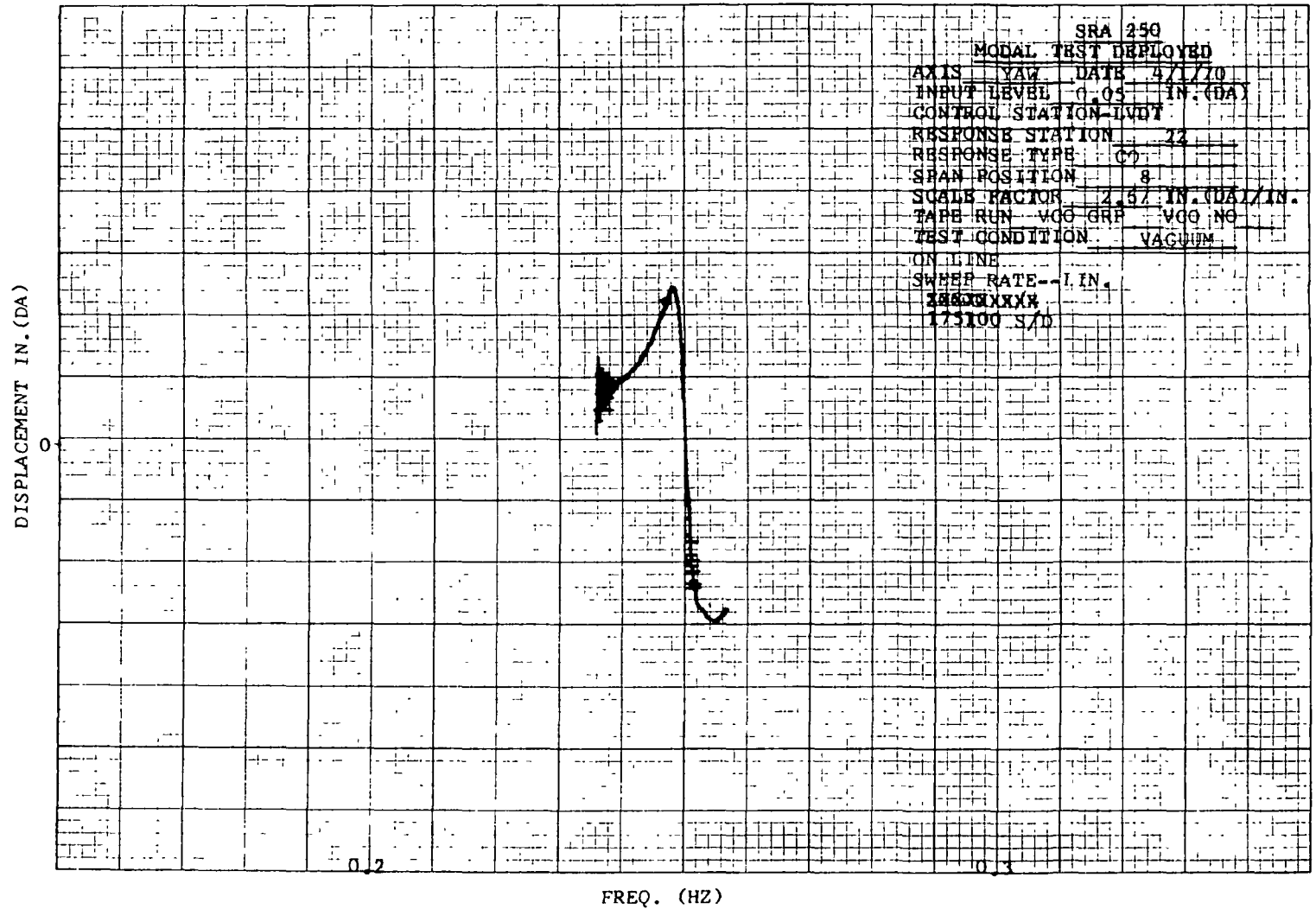

Figure 4.3-14. Frequency Sweep - Out-of-Plane Symmetric Excitation

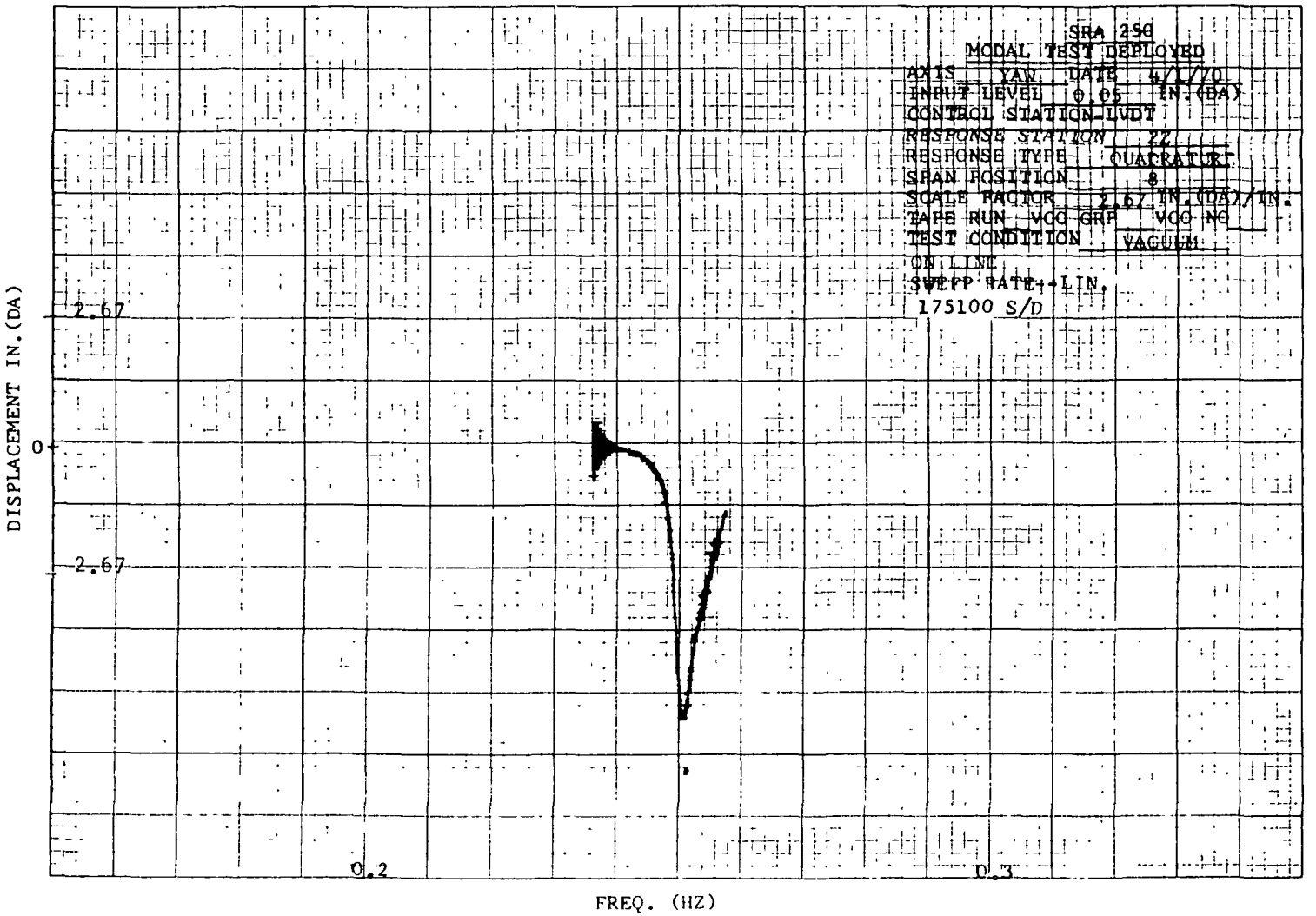

Figure 4.3-15. Frequency Sweep - Out-of-Plane Symmetric Excitation

TABLE 4.3-5

SUMMARIZED TEST RESULTS

Z-AXIS SWEEP TESTS IN VACUO

Analytical Mode No.	Predicted Frequency (Hz)	Measured Frequency (Hz)
		0.19 **
1	0.248	0.252
2/3 *	0.39	
4	0.55	0.632
5/6 *	0.81	----
7	0.94	0.781

* Analytical predictions show two modes at each membrane resonance and that these modes would not be excited by base motion.

** Shown later (Section 5.3.2) to be first torsional resonance.

TABLE 4.3-6

PARAMETERS INFLUENCING WAVE-FORM DISTORTION

(FUNDAMENTAL MODE)

Identification	Assumed Damping Ratio $\zeta = c/c_c$	Number of Cycles Between Half-Power Points **	φ *	Degree of Distortion
Ambient	0.10	46.7	2.68	None
Sweep 9	0.01	4.5	0.27	
10	0.01	4.5	0.25	Severe
11	0.01	15.8	0.50	Moderate
13	0.01	33.3	0.72	None
14	0.01	248	1.98	None

* Per theory $\varphi \geq 2.0$ is criteria for no distortion.

** The number of cycles between half power points, N, is related to Hok's sweep parameter, ζ, by the formula $\zeta = (\frac{\pi}{2} N)^2$. Note that the damping ratio and the half power points are related by the formula used for the determination of damping by method 2.

4.3.3.2.3 Resonance Dwells for Out-of-Plane Symmetric Excitation

Mode shape data was obtained at the three resonant frequencies determined from the sweep tests (0.251 Hz, 0.632 Hz and 0.781 Hz). The data is tabulated in Tables 4.3-7 through 4.3-9 and plotted in Figures 4.3-16 through 4.3-18. The plots have been smoothed to eliminate anomalies in the tabulated data.

Observation of the results shows there is considerable scatter in the data. In particular the displacement measurements on the BI-STEM deviate from what would be anticipated. A problem with the targets is indicated. The outboard edge of the -Y blanket had slack regions which allowed increased out-of-plane displacements. This condition shows in Figure 4.3-16. The experimental shape of the first mode is similar to the analytical mode shape. The experimental mode shapes for the two higher modes differ from the analytical mode shapes. They are not symmetric in that the leading edge member undergoes a rotation. One blanket tends to twist while the other billows or bends. The two modes are complementary or appear to be mirror images of the other. In contrast the analytical modes are symmetric with both blankets billowing and not twisting. (See Section 4.3.4 for a further discussion.)

4.3.3.2.4 Damping ratios (ξ) for Out-of-Plane Symmetric Modes

Damping ratios (ξ) were determined by three methods and are summarized in Table 4.3-10.

(1) From the decay of free oscillations via the formula

$$\xi = \frac{1}{2\pi N} \ell n \quad \frac{Ao}{A_N}$$

Table 4.3-7. Mode Shape Data Summary - First Out-of-Plane Symmetric Excitation

Analysis Results							
Span Position		% Chord On - Y				Frequency: 0.248 Hz	
%	In.	100%	75%	50%	25%	Bi Stem	+Y 100%
0	0	0	0	0	0	0	0
10	31.2	0.089	0.089	0.089	0.089	0.014	0.089
20	62.4	0.185	0.185	0.185	0.185	0.055	0.185
30	93.6	0.289	0.289	0.289	0.289	0.119	0.289
40	124.8	0.399	0.399	0.399	0.399	0.205	0.399
50	156.0	0.514	0.514	0.514	0.514	0.310	0.514
60	187.2	0.634	0.634	0.634	0.634	0.430	0.634
70	218.4	0.752	0.752	0.752	0.752	0.562	0.752
80	249.6	0.865	0.865	0.865	0.865	0.703	0.865
90	280.8	0.959	0.959	0.959	0.959	0.850	0.959
100	312.0	1.0	1.0	1.0	1.0	1.0	1.000

		Test Results							
Span Position		-Y	% Chord On - Y				Frequency: 0.251 Hz		
%	In	LEM	100%	75%	50%	25%	Bi Stem	+Y 100%	+Y LEM
0	0		-	-	-	-	-	-	
10	31.2		0.138	0.076	0.138	0.114	0.046	0.107	
20	62.4		0.077	0.192	0.296	0.238	0.098	0.208	
30	93.6		0.469	0.320	0.367	0.308	0.118	0.322	
40	124.8		0.655	0.350	0.462	0.387	0.158	0.457	
50	156.0		0.915	0.447	0.575	0.520	0.339	0.615	
60	187.2		0.965	0.545	0.685	0.695	0.441	0.765	
70	218.4		1.06	0.650	0.820	0.792	0.580	0.875	
80	249.6		1.06	0.720	0.910	0.850	0.580	1.02	
90	280.8		0.980	0.855	0.900	0.950	0.850	1.09	
100	312.0	1.0	1.35	0.995	1.02	1.07	0.690	1.22	0.885

Note: Test measurement points were nominally 5 inches (11%) inboard from listed % chord locations.

Table 4.3-8. Mode Shape Data Summary - Second Out-of-Plane Symmetric Excitation

Analysis Results							
Span Position		% Chord On - Y				Frequency: 5611 Hz	
%	In.	100%	75%	50%	25%	Bi Stem	+Y 100%
0	0	0	0	0	0	0	0
10	31.2	-0.177	-0.177	-0.177	-0.177	0.016	-0.177
20	62.4	-0.354	-0.354	-0.354	-0.354	0.062	-0.354
30	93.6	-0.513	-0.513	-0.513	-0.513	0.134	-0.513
40	124.8	-0.629	-0.629	-0.629	-0.629	0.227	-0.629
50	156.0	-0.673	-0.673	-0.673	-0.673	0.336	-0.673
60	187.2	-0.611	-0.611	-0.611	-0.611	0.458	-0.611
70	218.4	-0.413	-0.413	-0.413	-0.413	0.589	-0.413
80	249.6	-0.564	-0.564	-0.564	-0.564	0.724	-0.564
90	280.8	0.450	0.450	0.450	0.450	0.862	0.450
100	312.0	1.0	1.0	1.0	1.0	1.0	1.0

Test Results									
Span Position		-Y	Chord On - Y				Frequency: 0.632 Hz		
%	In.	LEM	100%	75%	50%	25%	Bi Stem	+Y 100%	+Y LEM
0	0		-	-	-	-	-	-	
10	31.2		-0.140	0.053	0.045	0.158	0	-0.582	
20	62.4		-0.305	0.058	0.167	0.376	0.009	-1.04	
30	93.6		-0.117	-0.019	0.307	0.587	0.107	-1.34	
40	124.8		-0.823	-0.144	0.391	0.742	0.147	-1.12	
50	156.0		-0.417	-0.024	0.577	0.828	-0.356	-0.835	
60	187.2		-0.306	0.029	0.614	0.867	0.224	-0.358	
70	218.4		-0.492	0.081	0.596	0.865	0.033	0.117	
80	249.6		-0.393	0.126	0.482	0.826	0.217	0.659	
90	280.8		-0.026	0.091	0.364	0.735	0.468	1.21	
100	312.0	-0.310	-0.009	0.020	0.295	0.526	0.004	1.62	1.0

Note: Test measurement points were nominally [illegible] inches (11%) inboard from listed % chord locations.

Table 4.3-9. Mode Shape Data Summary - Third, Out-of-Plane Symmetric Excitation

Analysis Results							
Span Position		Chord On - Y				Frequency: 0.810 Hz	
%	In.	100%	75%	50%	25%	Bi Stem	+Y 100%
0	0	0	0	0	0	0	0
10	31.2	0.360	0.360	0.360	0.360	0.022	0.360
20	62.4	0.664	0.664	0.664	0.665	0.081	0.664
30	93.6	0.812	0.813	0.814	0.814	0.171	0.812
40	124.8	0.720	0.720	0.721	0.721	0.280	0.720
50	156.0	0.351	0.351	0.351	0.351	0.402	0.351
60	187.2	-0.229	-0.299	-0.230	-0.230	0.529	-0.229
70	218.4	-0.808	-0.808	-0.809	-0.810	0.655	-0.808
80	249.6	-1.01	-1.01	-1.02	-1.02	0.776	-1.01
90	280.8	-0.425	-0.425	-0.426	-0.426	0.891	-0.425
100	312.0	1.00	1.00	1.00	1.00	1.00	1.00

Test Results									
Span Position		-Y	Chord On - Y				Frequency: 0.781 Hz		
%	In.	LEM	100%	75%	50%	25%	Bi Stem	+Y 100%	+Y LEM
0	0		-	-	-	-	-	-	
10	31.2		-0.393	-0.161	-0.300	-0.138	0	-0.030	
20	62.4		-0.302	-0.66	-0.83	-0.299	0.055	0.010	
30	93.6		-0.94	-0.99	-1.03	-0.377	0.008	0.023	
40	124.8		-0.69	-0.85	-1.13	-0.474	-	0.031	
50	156.0		0.114	-0.60	-1.11	-0.54	0.335	0.034	
60	187.2		0.212	-0.478	-0.95	-0.480	-0.92	0.037	
70	218.4		1.04	-0.332	-0.64	-0.378	0.188	0.031	
80	249.6		0.84	-0.100	-0.177	-0.314	0.427	0.029	
90	280.8		0.032	0.282	0.190	0.244	-1.00	0.064	
100	312.0	1.0	0.83	0.76	0.91	0.67	0.320	0.099	0.082

Note: Test Measurement points were nominally 5 inches (11%) inboard from listed % chord locations.

Table 4.3-10 Damping Factors (ξ) for Out of Plane Modes - Symmetric Excitation

Mode Frequency (Hz)	Damping Coefficients				
	Method 1		Method 2		Method 3
	ξ_a	ξ_b	Input Level (in. DA)	ξ	ξ
0.251	.003	.0042	.025	.003	.0055
		.0053	.050	.0055	
0.632	--	--		--	--
0.781	--	--	0.10	.0275	--
			0.20	.0226	

Notes: Method 1 is based on the rate of decay of motion. Column a values are for a step input and Column b for decay from dwells at a natural frequency.

Method 2 is based on the frequencies of peak in-phase response when sweeping slowly through a resonance.

Method 3 is based on a comparison of the measured response with the analytically predicted response where the analysis included viscous damping.

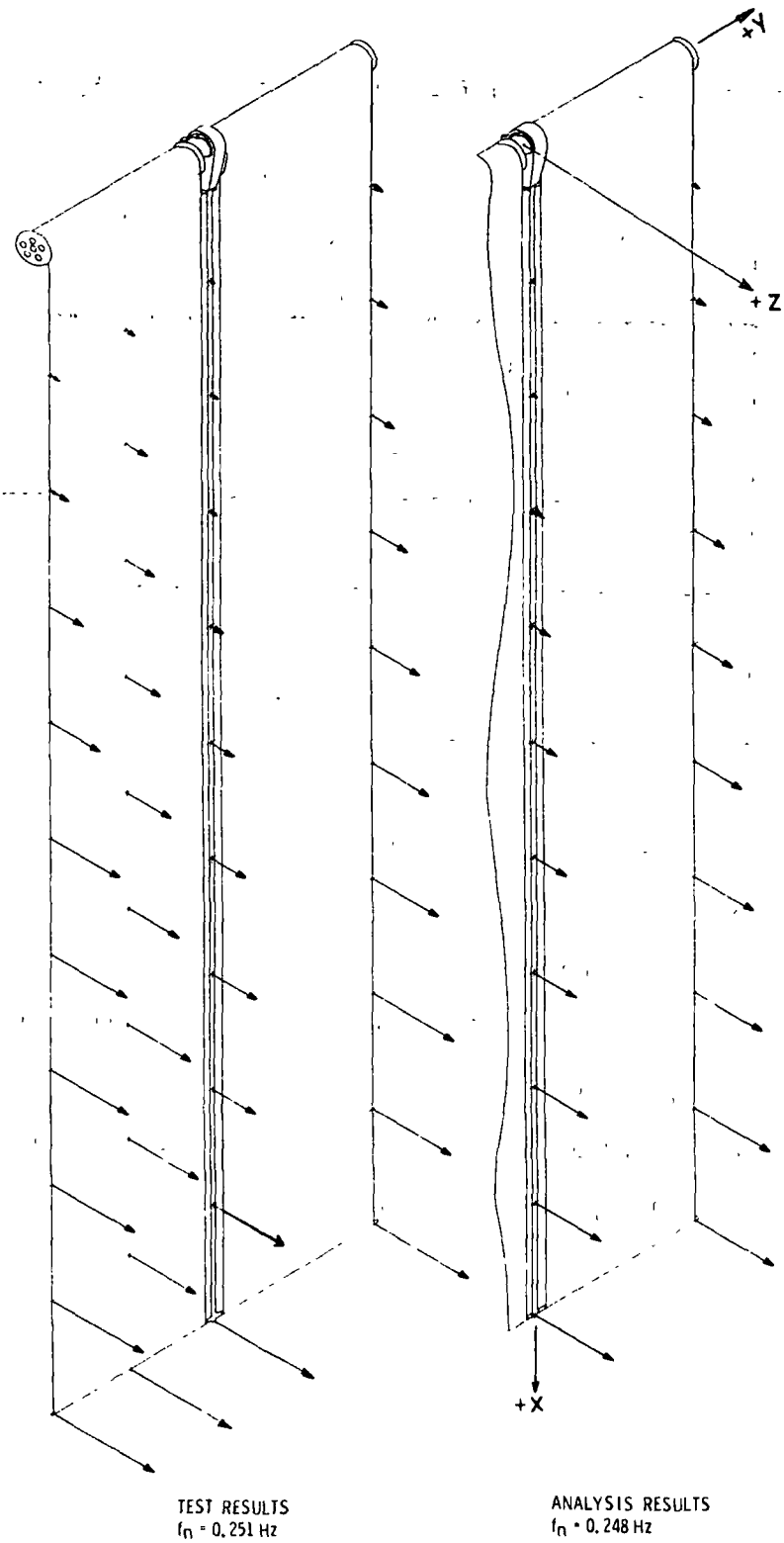

Figure 4.3-16. Mode Shape - First Mode-Out-of-Plane Symmetric Excitation

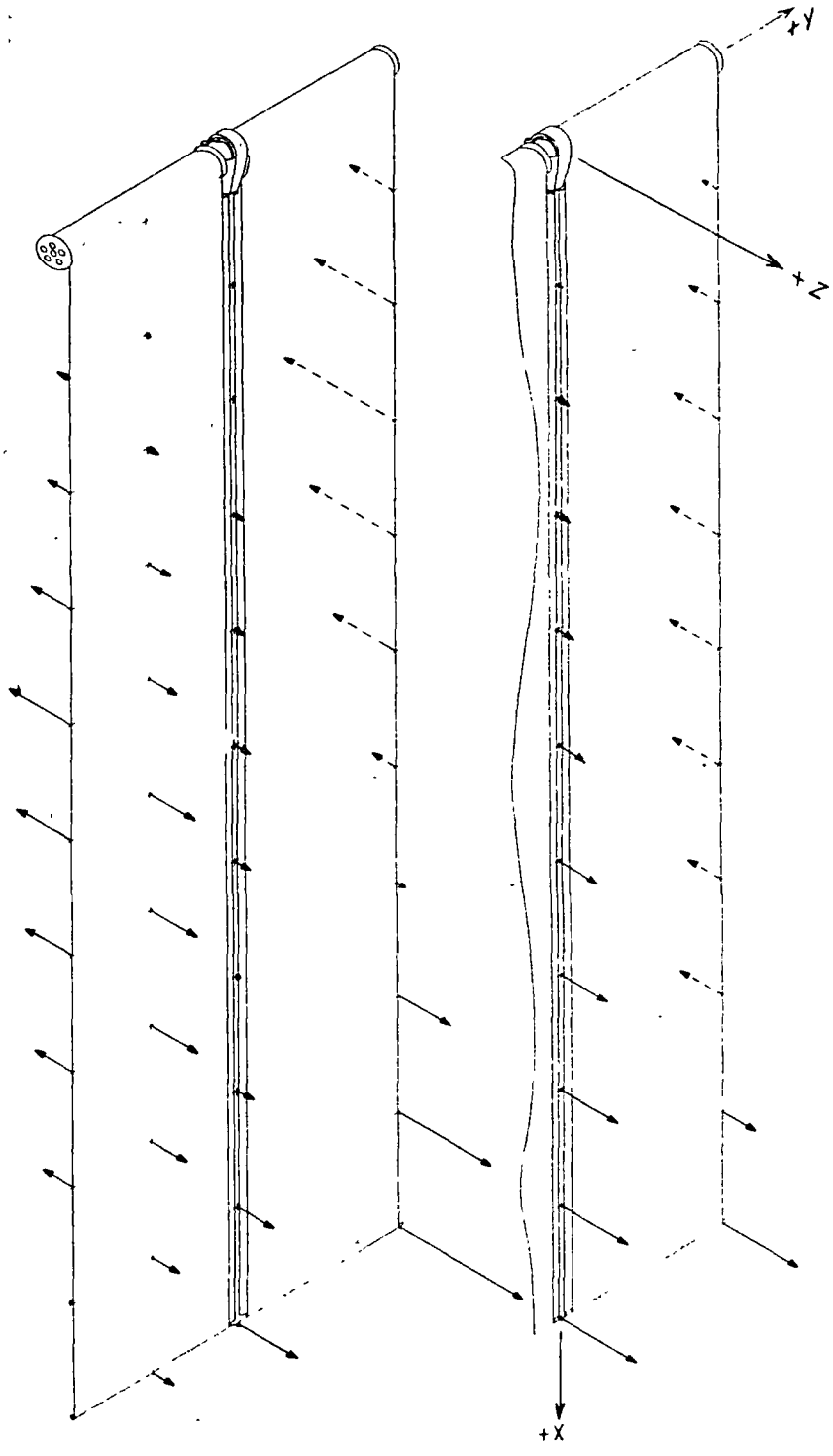

Figure 4.3-17. Mode Shape-Second Mode-Out-of-Plane Symmetric Excitation

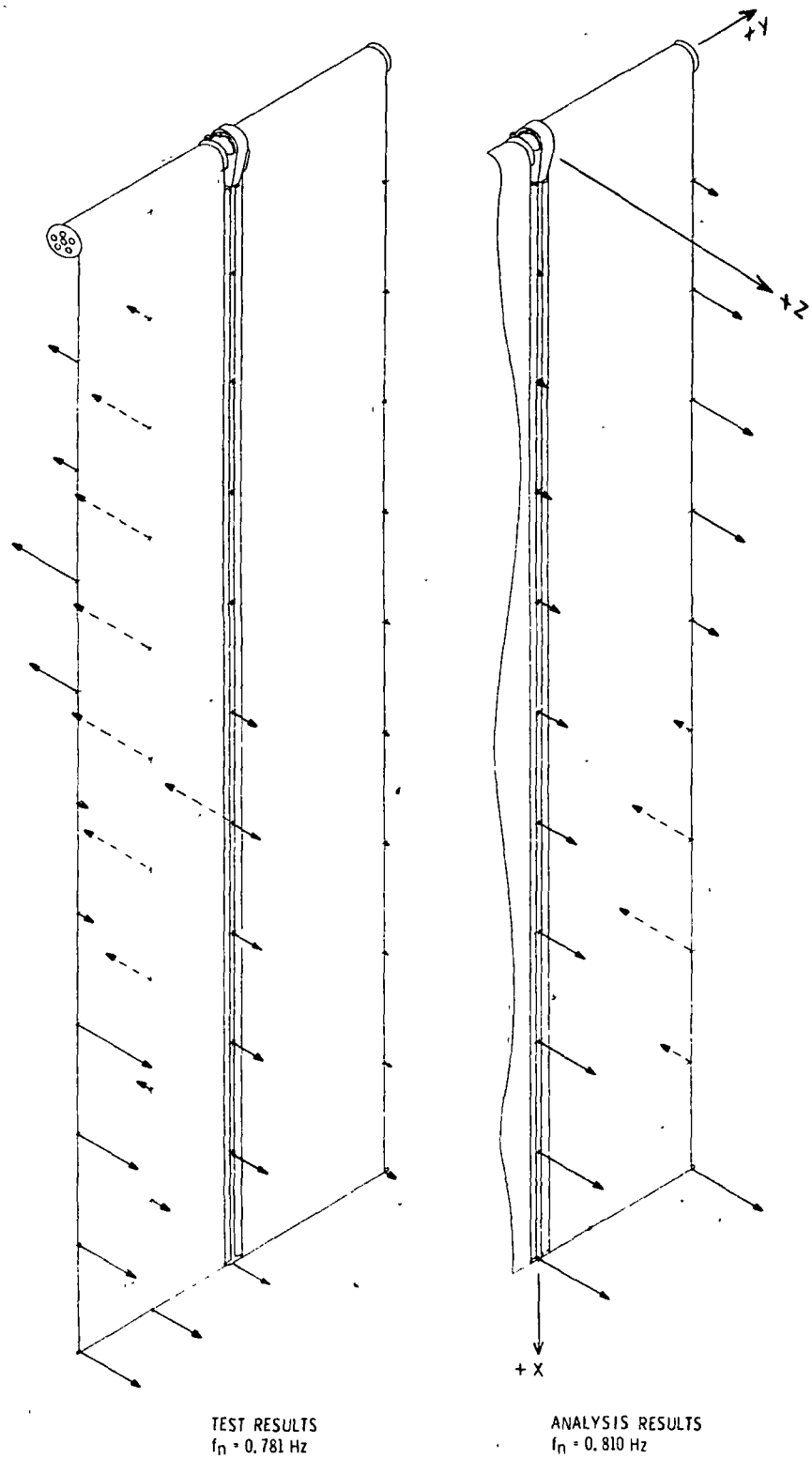

Figure 4.3-18 Mode Shape - Third Mode-Out-of-Plane Symmetric Excitation

where ξ = Damping Ratio = Fraction of critical damping coefficient

A_O = Initial Amplitude

A_N = Amplitude After N Cycles

N = Number of Cycles

(2) From the peak in-phase responses on either side of a resonance via the formula

$$\xi = \frac{1}{2}\left[\frac{(F_B/F_A)^2-1}{(F_B/F_A)^2+1}\right]$$

where: ξ = Damping Ratio

F_A, F_B = Frequencies of in-phase peak response on either side of a resonance

(3) The measured response with respect to the input excitation was compared with the analytically predicted response and the experimental damping ratios determined. This procedure assumes the calculated and experimental mode shapes are similar.

The method or methods appropriate to the available data were used. For example, the in-phase response plots for the second mode showed very ill-defined peaks and no attempt was made to determine damping by method 2. Method 1 was not used for either higher mode because oscillographs of the decay showed the waveform was complex and converged to the fundamental after several cycles.

4.3.3.2.5 Waveforms of Motion

Traces of oscillograph recordings are shown in Figure 4.3-19 thru 4.3-23.

Figure 4.3-19 shows the input excitation waveform as measured by the LVDT

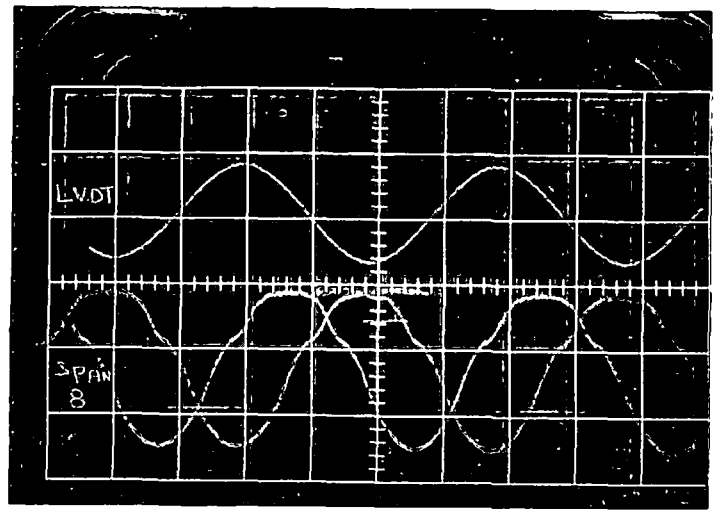

(a) Input = .025 In. D.A. 80% Span Tracker 2Z
Frequency = .252 Hz. 1 sec./cm.

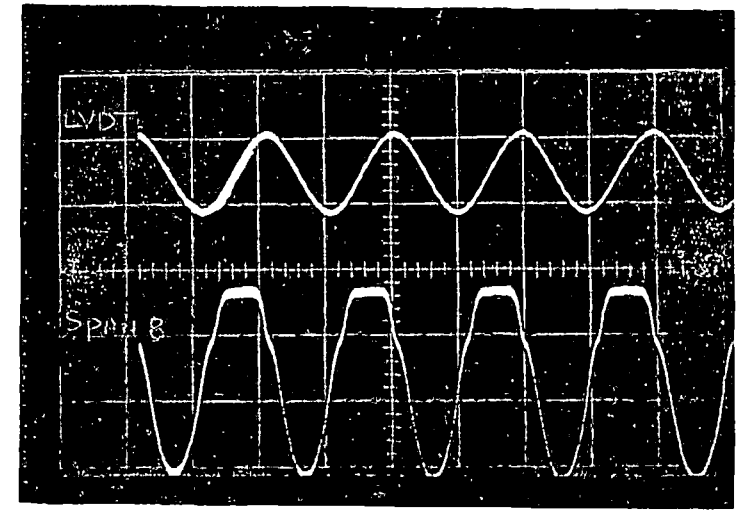

(b) Input = .05 In. D.A. 80% Span Tracker 2Z
Frequency = .252 Hz. 2 sec./cm.

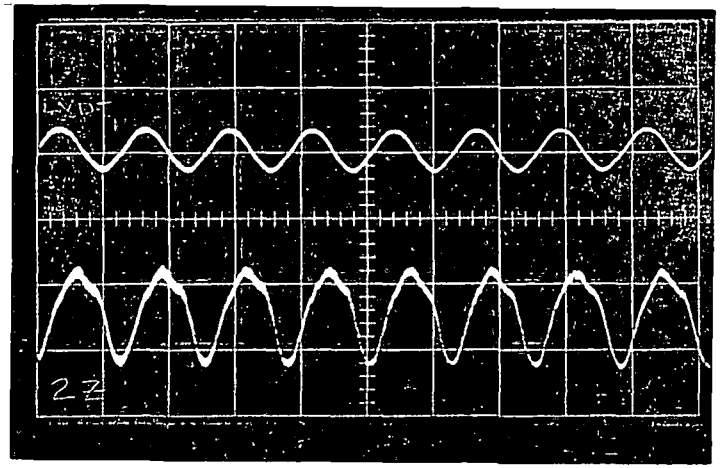

(c) Input = .10 In. D.A. 100% Span Tracker 2Z
Frequency = .781 Hz. 1 sec./cm.

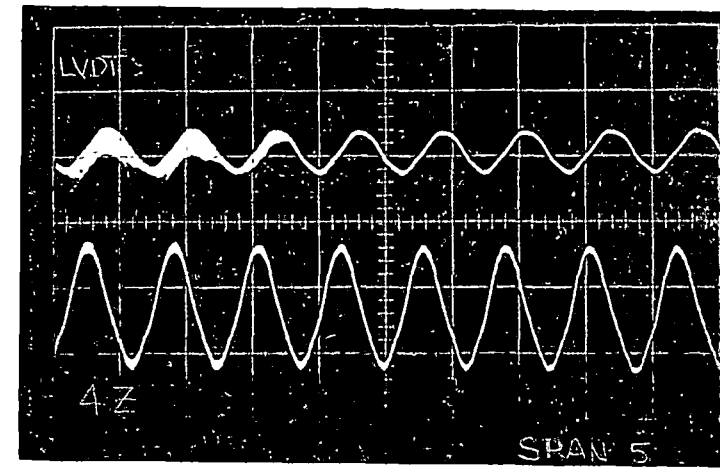

(d) Input = .10 In. D.A. 50% Span Tracker 4Z
Frequency = .781 Hz. 1 sec./cm.

Figure 4.3-19. Oscilloscope Records of Input and Response for Symmetric Excitation

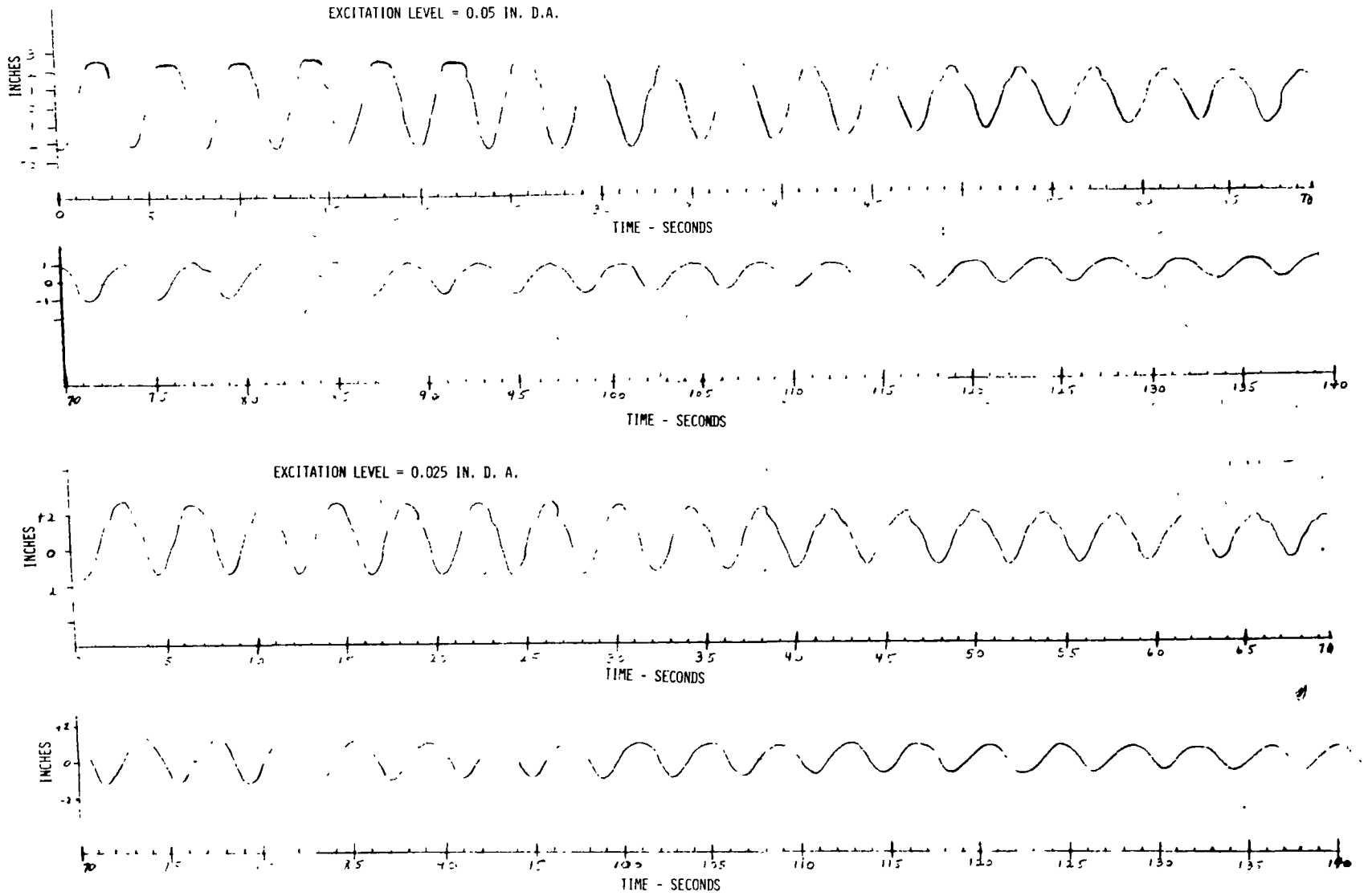

Figure 4.3-20. Decay of Vibration in First Symmetric Mode at 0.251 Hz., 80% Span, Tracker 2z

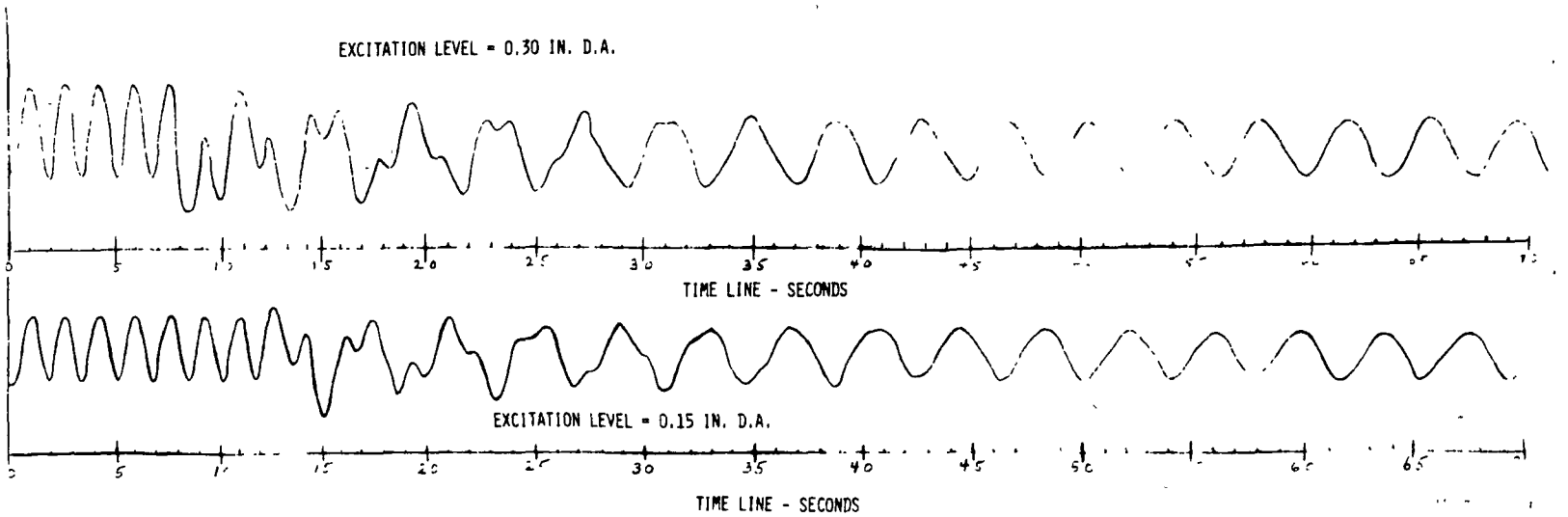

Figure 4.3-21. Decay of Vibration Mode at 0.6325 Hz. Excited by Symmetric Excitation 80% Span, Tracker 5Z

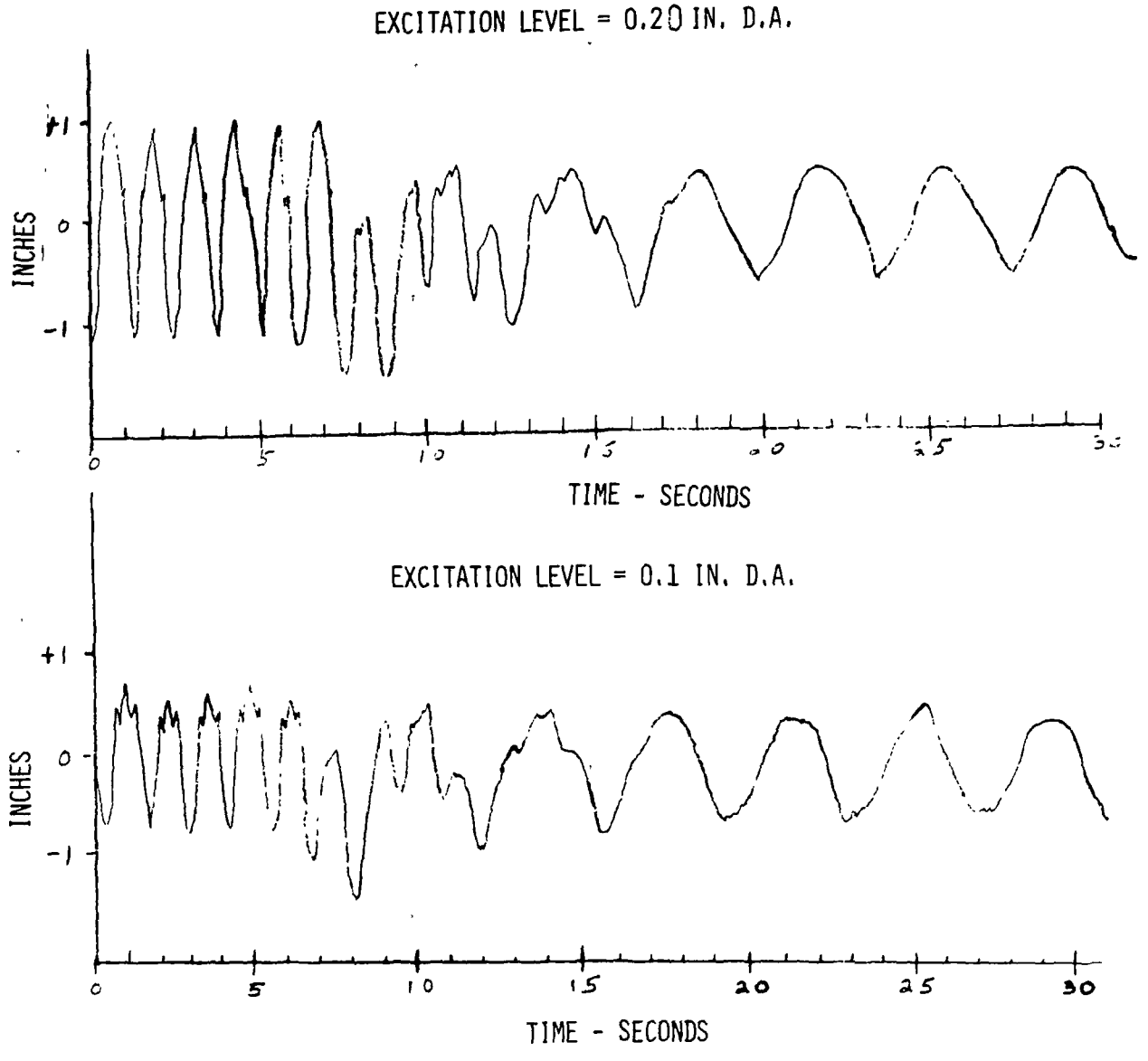

Figure 4.3-22. Decay of Vibration in Mode at 0.781 Hz. Excited by Symmetric Excitation, 80% Span, Tracker 2Z

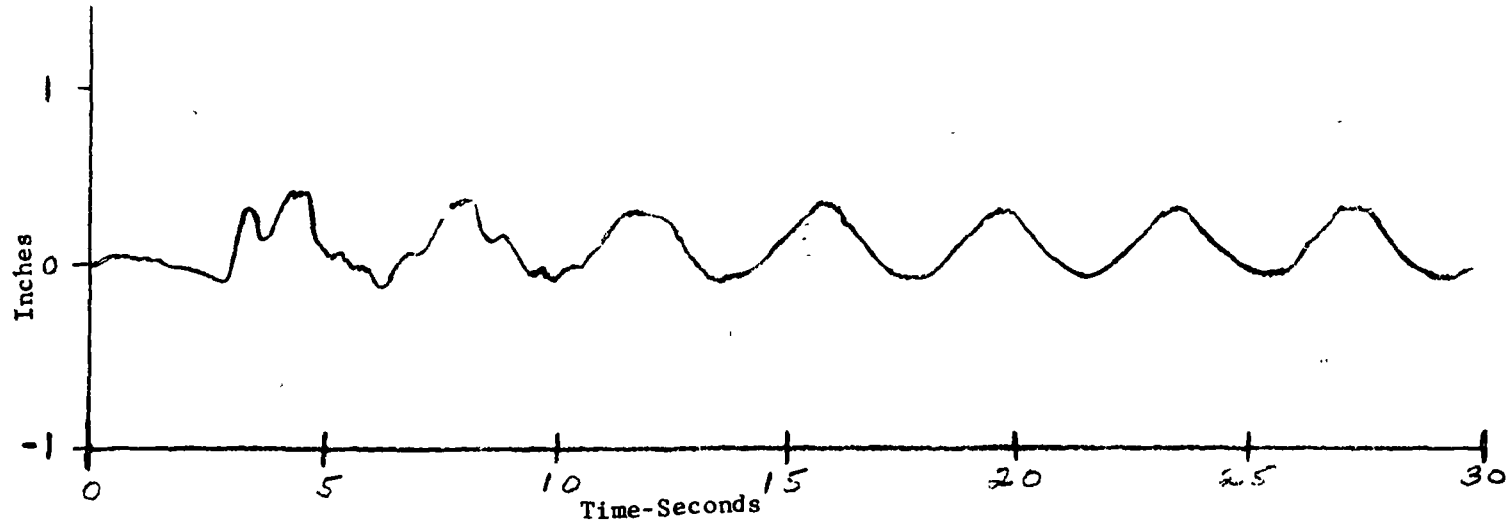

Figure 4.3-23. Response to Step Input Symmetric Excitation, Tracker 1Z

at two resonant frequencies and the response waveform at selected locations. Note the clean sinusoidal waveform of the input. At 0.252 Hz the response waveform is not symmetric but is flat topped on one side for an input level of 0.05 in. D.A. There is a double exposure of the response in the upper left photo.

Figures 4.3-20, 4.3-21 and 4.3-22 show the decay of motion in the first three modes excited with symmetric excitation. Data is shown for two levels of excitation. The rapid breakup of the higher modes into the first mode when excitation is removed is shown. The mode at 0.781 Hz is not a sinusoid while the mode at 0.632 Hz has significantly less higher harmonic content.

The response of the system to a suddenly applied input is shown in Figure 4.3-22. The input was produced by suddenly applying DC current to the exciter. This caused the moving element to seek "magnetic center." If the exciter was off magnetic center when the current was applied, the excitation approached a step input of the magnitude of the distance off magnetic center.

4.3.3.2.6 Linearity Checks for Out of Plane Symmetric Excitation

Linearity checks were performed by changing the input excitation level and determining the effect on resonant frequency. Results are given in Table 4.3-11. Input level has a very small effect on resonant frequency for these modes.

4.3.3.2.7 Other Investigations

Narrow band sweeps were made to investigate: (1) a mode at 0.19 Hz; and (2) a mode at 0.45 Hz (a blanket membrane mode). The possible existence of these modes was detected by the on-line data plots of the initial sweep. No modes could be found in these frequency regions.

Table 4.3-11 Results of Linearity Checks - Out of Plane Symmetric Excitation

Mode	Excitation Level in D.A	Resonant Frequency Hz
1	0.050	0.25
	0.025	0.252
2	0.50	0.634
	0.25	0.631
	0.10	0.631
3	0.20	0.767
	0.10	0.781

Table 4.3-12 Sweep Characteristics

Sweep No.	Input Level	Expected Resonance(Hz) from Earlier Sweep	Sweep Freq. Band-width (Hz) Start	End	Linear Sweep Rate Const. (Hz/Sec)	No. of Cycles Bet.1/2 Power Points	α	Time(Sec) to Sweep Decade
a	0.25"	0.19	.17	.22	$2.26(10^{-5})$	32	.71	40,000
b	0.25"	0.45	.40	.50	$1.01(10^{-4})$	40	.79	8,800
c1,c2	0.50"	0.45	.40	.50	$1.01(10^{-4})$	40	.79	8,800

Resonances were neither visually seen (via the vacuum chamber port/mirror arrangement set up to observe motion during vacuum tests) nor monitored on-line (via either on-line plots or tracker voltage meters). In addition, the 0.45 Hz resonance was: (a) scanned both at the 50% span and at the 80% span (tests c1 and c2); and (b) subjected to a .45 Hz dwell. These efforts were in vain.

It was observed that input levels on the order of 0.50" D.A. caused significant distortion in the input signal waveform. Consequently, no effort was made to force the modes by increasing input levels.

4.3.3.3 Out of Plane Anti-Symmetric (Torsional) Excitation

4.3.3.3.1 Ambient Sweep Test

The torsional (about X-axis) segment of the deployed modal test was initiated using procedures and data acquisition provisions identical to those used for the Z-axis ambient sweep (Section 4.3.3.2.1).

This test run consisted of two frequency sweeps with a hyperbolic sweep rate:

Sweep	Duration	Lower Freq.	Upper Freq.	φ	Time to Sweep Decade
1	26 min.	.05	.10	2.21	14,000 sec.
2	26 min.	.10	1.00	2.35	1,560 sec.

The above values of φ were computed using a value of $\xi = c/c_c = 0.10$ (as for the Z-axis ambient sweep).

Input levels were based on the fact that the shaker input is 1 foot away from the center of rotation. For a peak response of 4.0" double amplitude (D.A.) at the LEM tips with an assumed transmissibility of 8, 0.5" D.A. of motion would occur at the outboard drum extremity, which is approximately 4 feet from the pivot point. Consequently, the displacement at the shaker location was set at 0.10" D.A. input level. This input was employed up to 0.40 Hz. Above this frequency, the input was increased to 0.25" D.A. to allow for better resolution of the higher modes.

Test results are summarized in Table 4.3-13. The fundamental ambient torsional resonance is at 0.12 Hz. Problems in resolving higher frequency resonances were

identical to those cited in describing Z-axis results.

On-line in-phase and quadrature response plots (outboard edge of -Y blanket at 80% span) are given in Figures 4.3-24 and 4.3-25.

Table 4.3-13 Torsional Ambient Sweep Test Summary

Analytical Mode Number	Analytical Frequency (Hz)	Apparent Resonant Frequency (Hz)	Phenomena Exhibited
1	.232**	.12	1st array torsion
2/3*	0.39	.42	Blanket Membrane Modes
4	0.58	.50	2nd array torsion
5/6*	0.81	---	Blanket Membrane Modes
7	0.96	0.99	3rd array torsion

* Analytical predictions show two modes at each membrane resonance and that they would not respond to base excitation.

** Analytical value (.232 Hz) is not corrected for apparent air mass effects.

4.3.3.3.2 Vacuum Sweep Tests

Sweeps were performed under vacuum conditions as listed in Table 4.3-14 to identify natural frequencies. Sweep rates were based on experience from the out of plane symmetric excitation tests. Severe beating occurred in Sweep No. 1 around .18 Hz indicating the sweep rate was too high. Successively slower sweeps were performed (Nos. 4, 5, and 7) in an attempt to sweep through the natural frequency without beating. For the final sweep the input was halved and 40

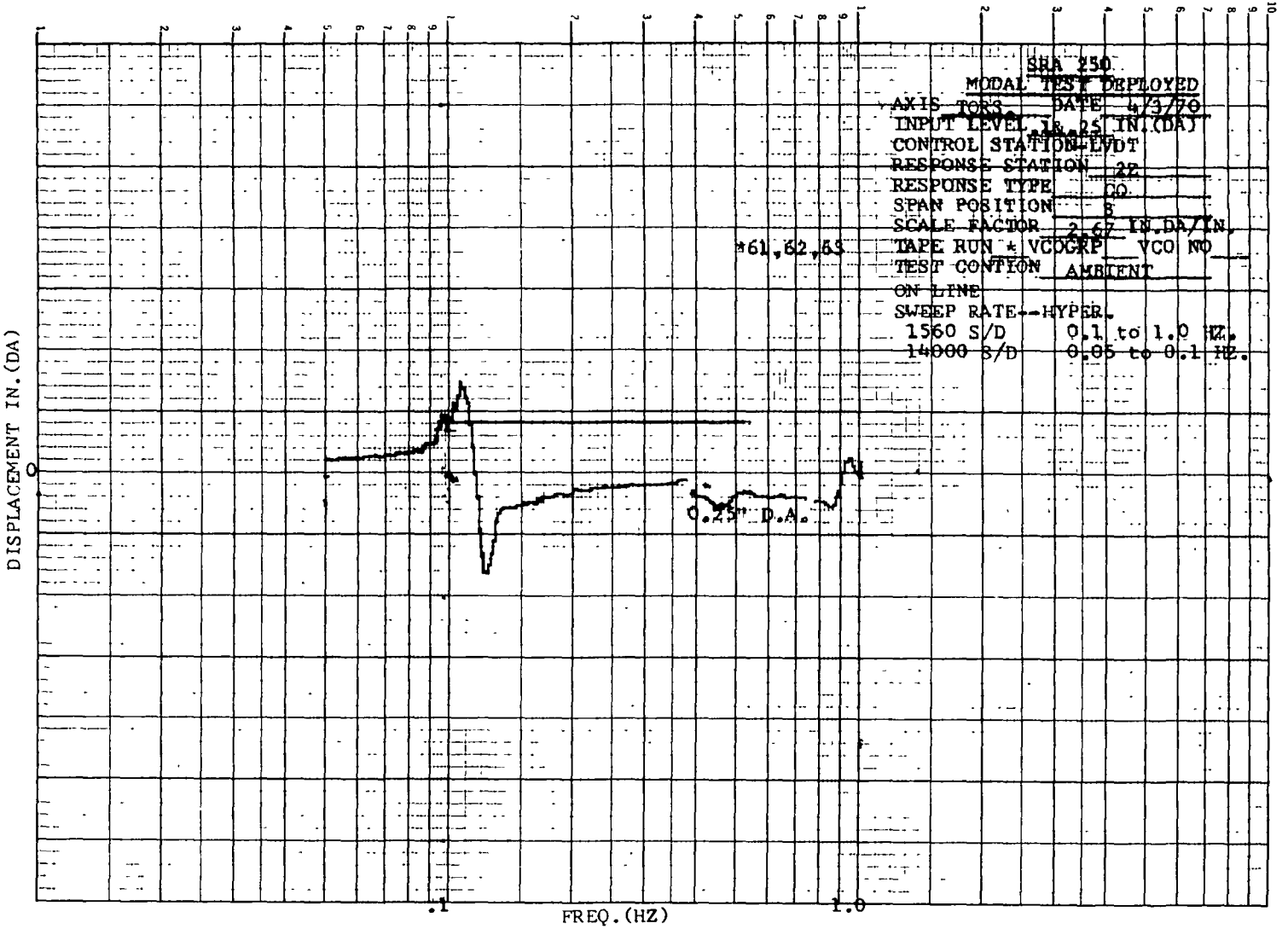

Figure 4.3-24. Frequency Sweep - Out-of-Plane Antisymmetric Excitation

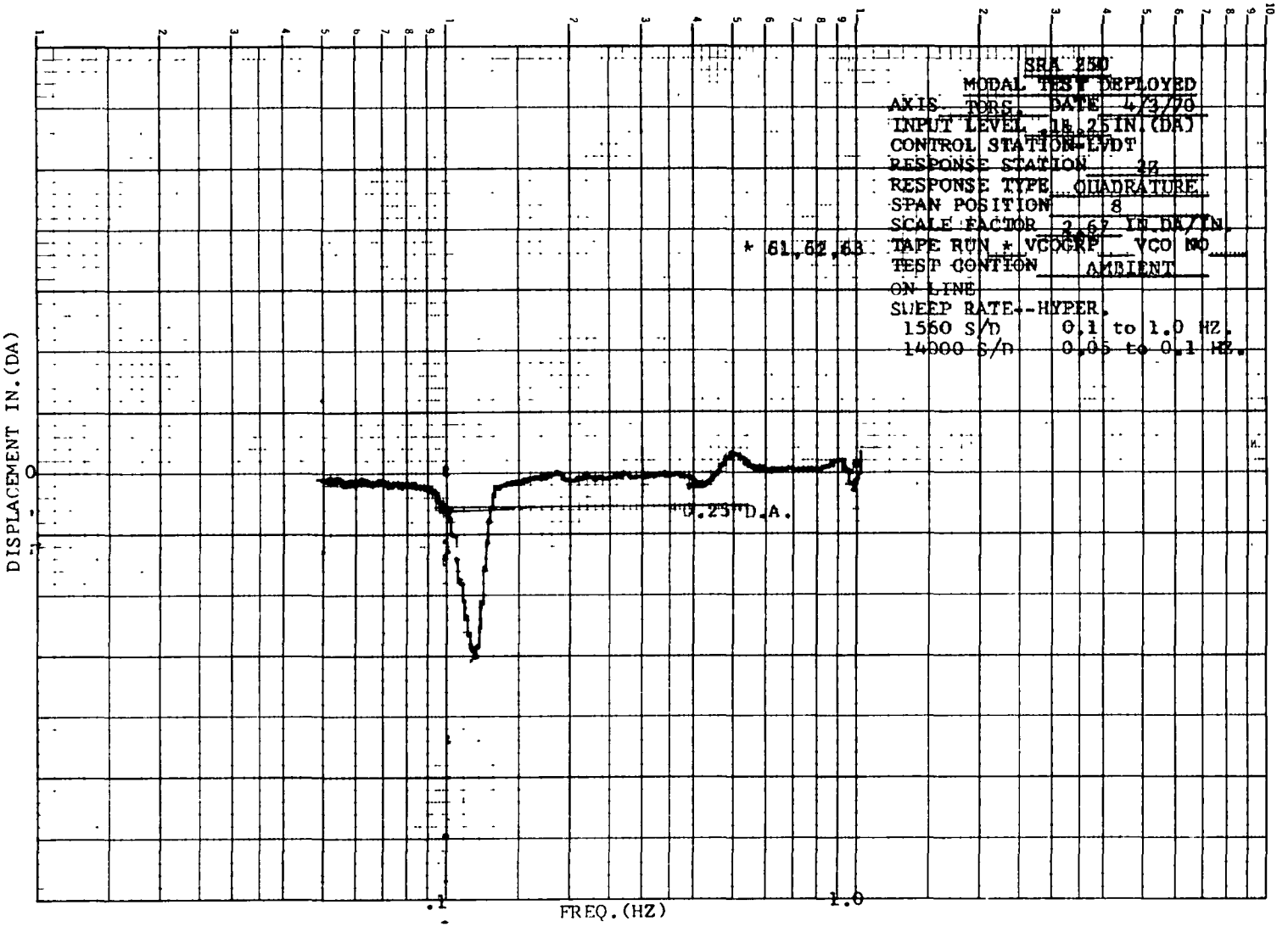

Figure 4.3-25. Frequency Sweep - Out-of-Plane Antisymmetric Excitation

Table 4.3-14. Summary of Vacuum Sweeps Out of Plane Anti-Symmetric (Torsional) Excitation

Sweep No. *	Frequency Range (Hz)	Time to Sweep Decade (Seconds)	Sweep Rate Mode	Input Level in. D.A.	Comments
1	.15 to .20	9,000	Hyperbolic	0.01	Terminated at .19 Hz Severe beating.
2	.20 to .425	7,200	Hyperbolic	0.10	
3	.425 to 1.0	8,000	Hyperbolic	0.10	
4	.165 to .182	17,800	Hyperbolic	0.01	Beating f_n = .178
5	.165 to .182	140,000	Linear	0.01	Beating f_n = .178
6	.182 to 2.14	14,000	Linear	0.01	
7	.170 to .176	360,000	Linear	0.005	f_n = .174
8	.60 to .72	10,000	Linear	0.25	Two Modes - .64 Hz & .67 Hz
9	.60 to .75	10,000	Linear	0.10	Resonances at .645 Hz & .715 Hz
10	.60 to .765	10,000	Linear	0.05	Resonances at .66 Hz & .74 Hz
11	.60 to .80	10,000	Linear	0.01	Input too low to give definitive results.
12	.85 to 1.0	5,600	Linear	0.10	No resonances.
13	.40 to .45	36,000	Linear	0.10	No resonances.
14	.30 to .40	29,600	Linear	0.10	No resonances.

* Sweep Numbers are assigned in the order that sweeps were run.

minutes used to sweep from .170 Hz to .176 Hz. Only slight beating occurred and the frequency was considered defined at 0.174 Hz.

The frequency range above the first mode was swept with the results shown in Figures 4.3-26 and 4.3-27. There is beating at .26 Hz near the frequency of the first mode for symmetric excitation. The quadrature plot (Figure 4.3-27) shows an indication of resonances at .52 Hz and at .72 Hz. Stronger resonances are at .65 Hz and .78 Hz.

Narrow band sweeps were carried out to investigate the higher modes. No resonances were detected in the frequency regions .30 to .45 and .85 to 1.0. (Sweeps 12, 13, and 14). A distorted response was observed near 1.0 Hz. This was later found to be a mode involving in-plane motion.

The frequency range from 0.63 to 0.75 Hz was investigated with Sweep Nos. 8, 9, 10 and 11. The results are tabulated in Table 4.3-15. Examples of the response analysis are shown in Figures 4.3-28 and 4.3-29.

Table 4.3-15 Results of Vacuum Sweeps in .63 Hz to .75 Hz Band-Out of Plane Anti-Symmetric Excitation

LVDT Input (In., D.A.)	Frequency (hz) of Lower Mode	Frequency (Hz) of Higher Mode
.01	.678	.755
.05	.658	.742
.10	.643	.715
.25	.638	.670

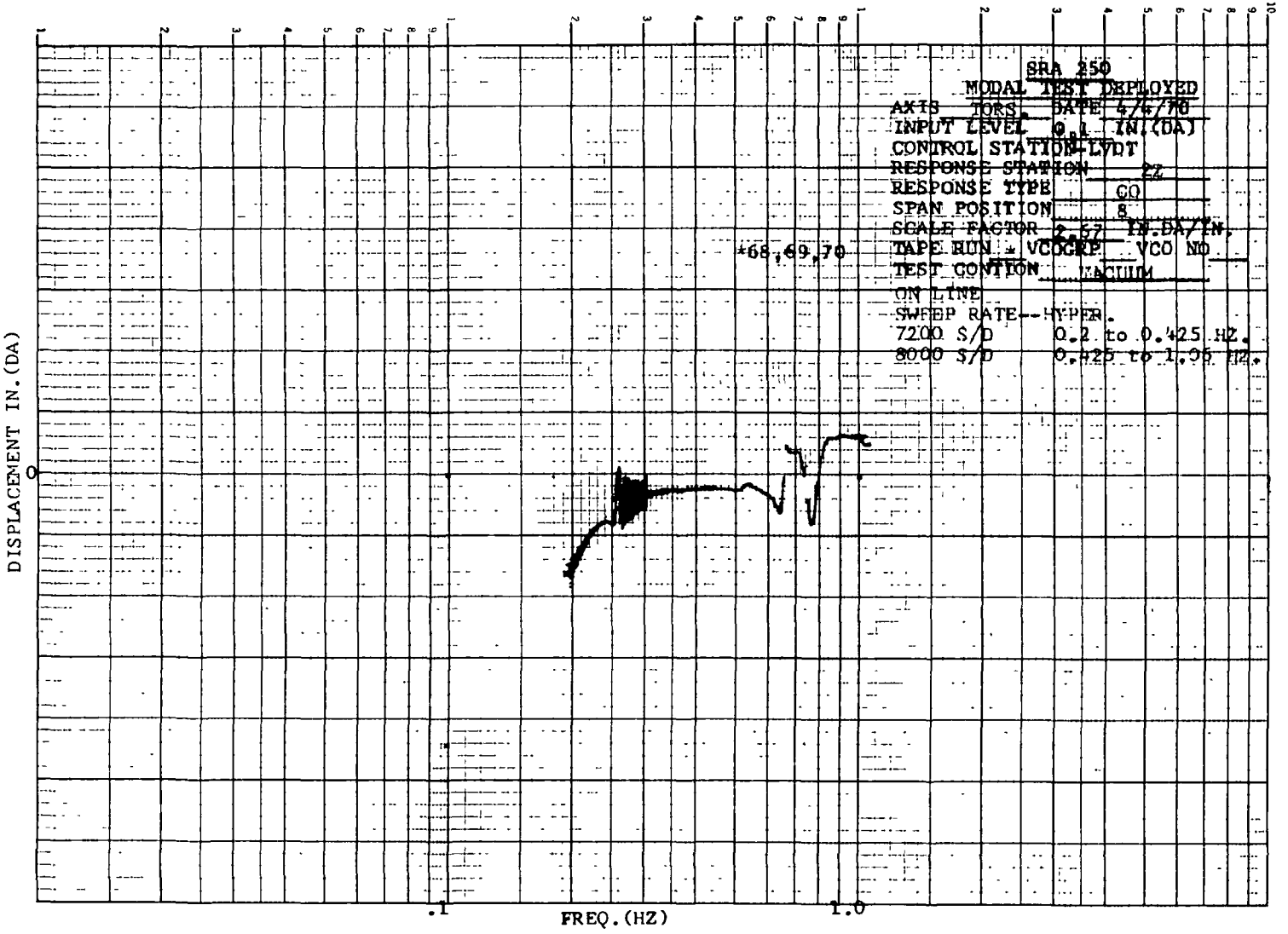

Figure 4.3-26. Frequency Sweep - Out-of-Plane Antisymmetric Excitation

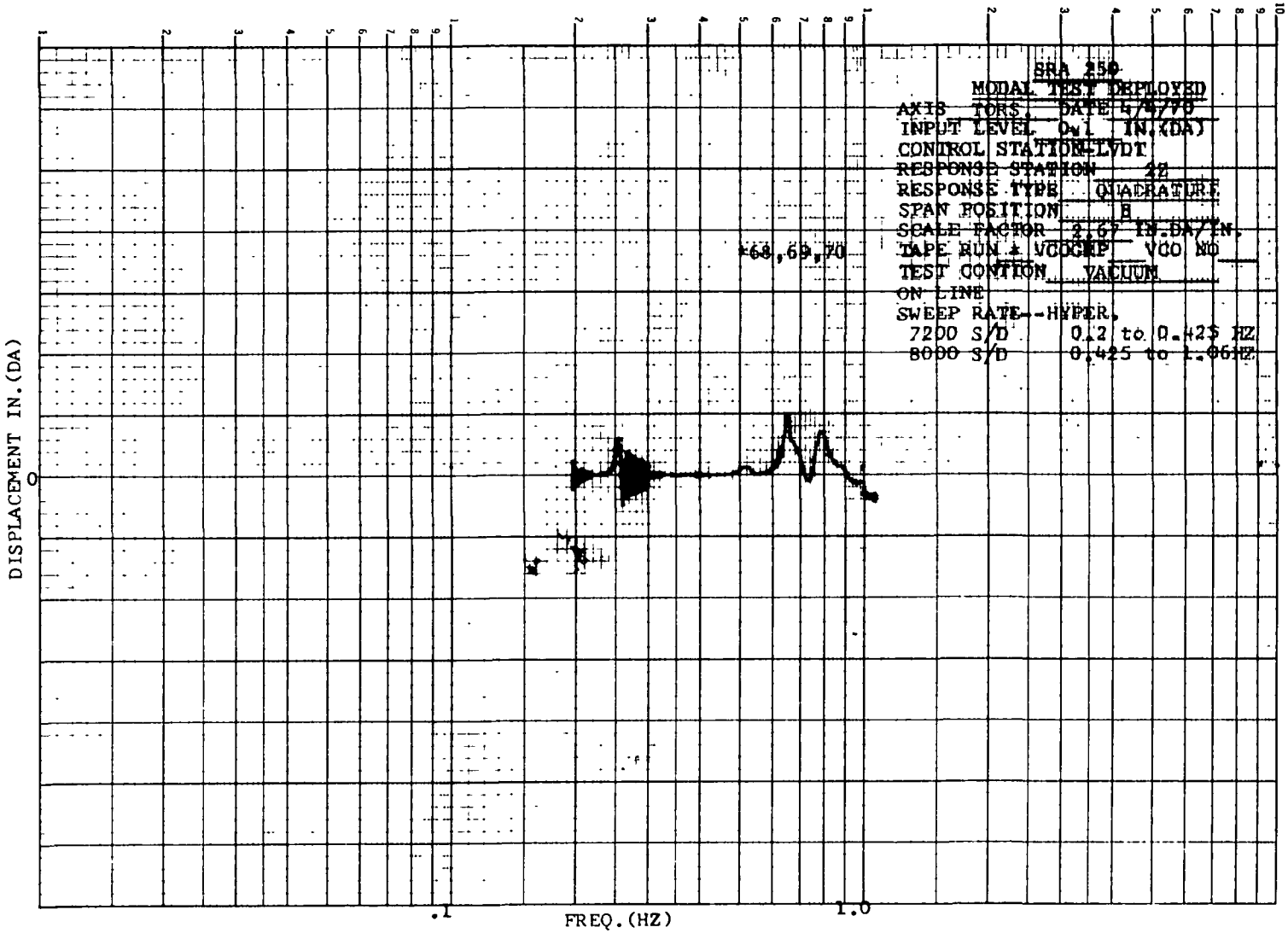

Figure 4.3-2 7 Frequency Sweep - Out-of-Plane Antisymmetric Excitation

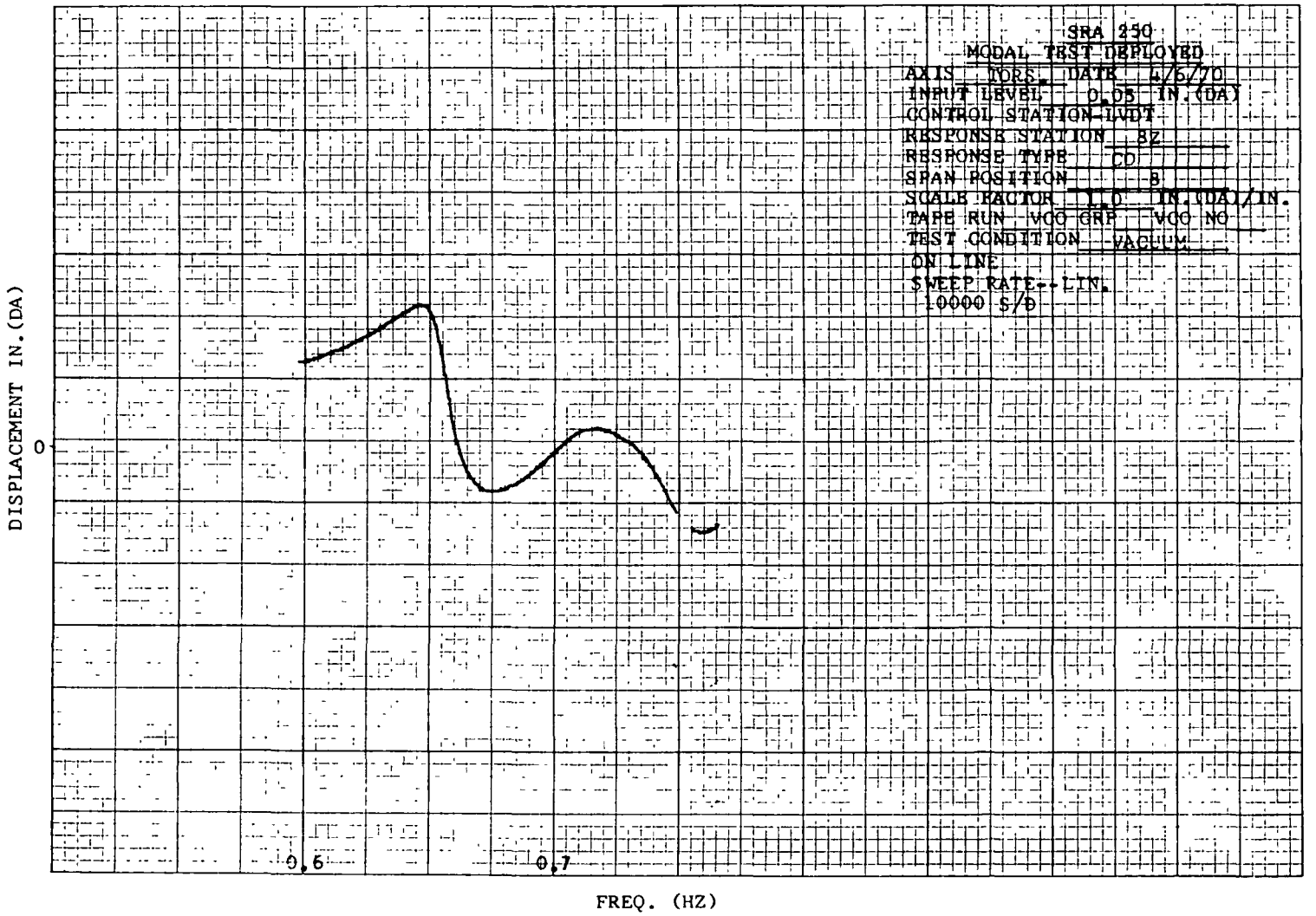

Figure 4.3-28. Frequency Sweep - Out-of-Plane Antisymmetric Excitation

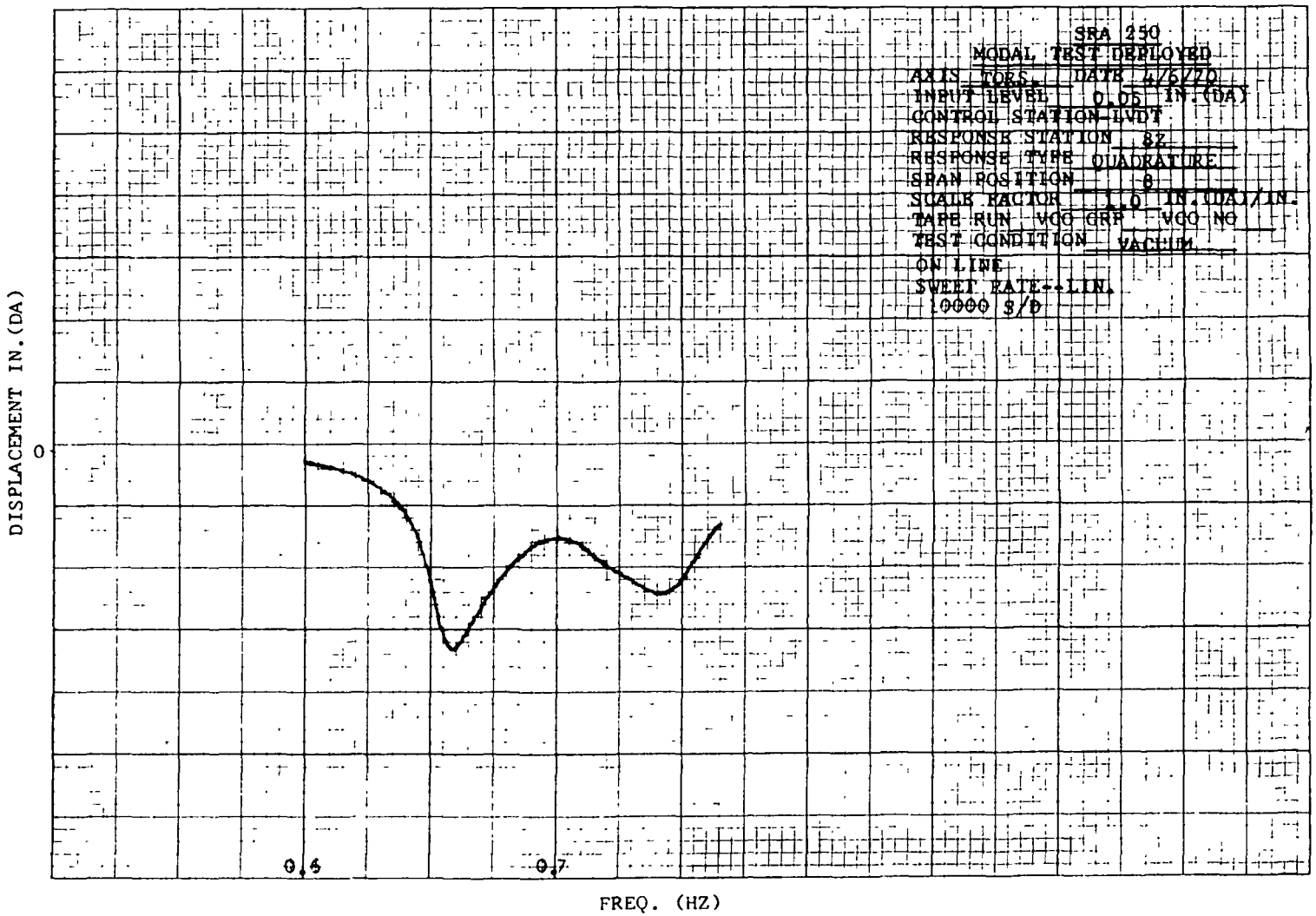

Figure 4.3-29 Frequency Sweep - Out-of-Plane Antisymmetric Excitation

The frequencies are affected by input level and a comparison with Figure 4.3-13 shows they are close to the frequencies obtained with symmetric excitation.

4.3.3.3.3 Resonance Dwells

4.3.3.3.3.1 Fundamental Resonance (0.174 Hz). Based on the narrow band sweep test results the dwell test was performed at 0.1737 Hz, using an 0.05" D.A. excitation level. This dwell proved to be a difficult undertaking.

The fixed tracker (Scanners 1 and 8) peak readings varied indicating a changing amplitude, though the excitation remained constant. Despite all efforts, no way was found to eliminate the variations. The resonance dwells started at the 100% span station and proceeded up the array at 10% span intervals. Upon reaching the 20% span location, the array response was 180 degrees out-of-phase with the LVDT input signal rather than the desired 90 degrees. The procedure was reviewed and it was concluded that better data could not be obtained within the test schedule and that data for the 10% and 20% span locations was not essential to the determination of the mode shape. The data is tabulated in Table 4.3-16 and plotted in Figure 4.3-30. The plot was smoothed to agree with visual observations and to eliminate apparent anomalies in the data.

4.3.3.3.3.2 Higher Modes. The variation in natural frequency with input level for the higher modes caused uncertainty with respect to dwell frequencies. Visual observations of the modes through the vacuum chamber port showed their shape was similar to the 0.78 Hz mode investigated with symmetric excitation. At this point a malfunction occurred in the tracker support system and it was necessary to vent the chamber for repairs. The test setup was modified for in-plane excitation and no further modal testing was done with anti-symmetric excitation.

Table 4.3-16. Mode Shape Data Summary - First Out-of-Plane Antisymmetric Excitation

Analysis Results							
Span Position		Chord On - Y				Frequency: 0.232 Hz	
%	In.	100%	75%	50%	25%	Bi Stem	+Y 100%
0	0	0	-	0	0	0	0
10	31.2	-0.079	-	-0.040	-0.020		0.079
20	62.4	-0.165	-	-0.083	-0.041		0.165
30	93.6	-0.258	-	-0.129	-0.064		0.258
40	124.8	-0.358	-	-0.179	-0.089		0.358
50	156.0	-0.464	-	-0.232	-0.116		0.464
60	187.2	-0.575	-	-0.288	-0.144		0.575
70	218.4	-0.690	-	-0.345	-0.172		0.690
80	249.6	-0.806	-	-0.403	-0.201		0.806
90	280.8	-0.915	-	-0.457	-0.228		0.915
100	312.0	-1.00	-	-0.500	-0.250	0	1.00

Test Results									
Span Position		-Y	Chord On - Y				Frequency: 0.1737 Hz		
%	In.	LEM	100%	75%	50%	25%	Bi Stem	+Y 100%	+Y LEM
0	0		-0.2	-0.15	-0.10	-0.017	0	0.2	
10	31.2		-	-	-	-	-	-	
20	62.4		-	-	-	-	-	-	
30	93.6		-0.089	-0.124	-0.156	-0.019	0.027	0.235	
40	124.8		-0.439	-0.174	-0.211	0	0.028	0.300	
50	156.0		-0.637	-0.248	-0.173	-0.032	0	0.401	
60	187.2		-0.565	-0.289	-0.200	-0.034	0	0.580	
70	218.4		-0.739	-0.335	-0.251	-0.082	0	0.538	
80	249.6		-0.949	-0.435	-0.285	-0.113	0.015	0.590	
90	280.8		-0.079	-0.368	-0.286	-0.158	0.032	0.715	
100	312.0	-0.246	-0.636	-0.547	-0.312	-0.050	0.056	0.581	1.0

Note: Test Measurement points were nominally 5 inches (11%) inboard from listed % chord locations.

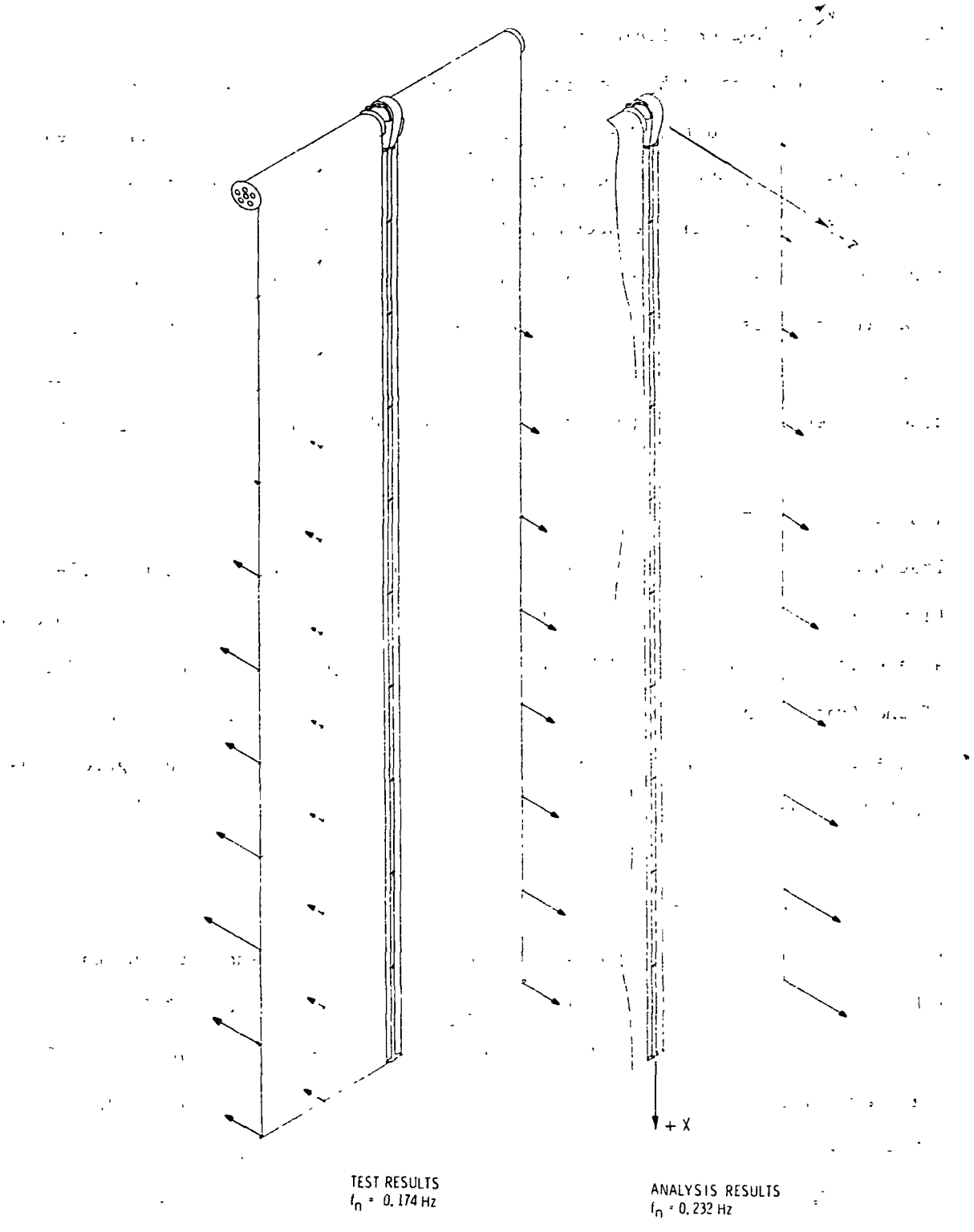

Figure 4.3-30. Mode Shape- First Mode-Out-of-Plane Antisymmetric Excitation

4.3.3.3.4 Damping Coefficients

Damping was determined by the methods described in Section 4.3.3.2 as appropriate with the available data. Method 3 was not used. The results are tabulated in Table 4.3-17. Slight beating on the data prevented the use of Method 2 for the lowest mode. Data for the second mode is given in the table for two excitation amplitudes and is based on the number of cycles required for the response to decay to half its initial value. This data as plotted as a function of the number of cycles of decay in Figure 4.3-31. Decay traces for the third mode rapidly deteriorated into the fundamental mode and could not be used for damping data.

4.3.3.3.5 Wave Forms

Traces of oscillograph recordings are shown in Figures 4.3-32 through 4.3-35. Figure 4.3-32 shows oscilloscope traces of the input (LVDT) and the response at a selected location at 0.642 Hz and 0.715 Hz. Figure 4.3-33 shows the decay of the free vibration after excitation at two input levels at two resonant frequencies. The response to suddenly applied inputs is shown in Figures 4.3-34 and 4.3-35 for two locations on the test unit.

4.3.3.3.6 Linearity Checks

The effect of excitation amplitude on the lowest mode is shown by the data in Table 4.3-14. Reducing the input level from 0.01 in. D.A. to 0.005 in. D.A. (Sweep Nos. 5 and 7) changed the frequency from 0.178 Hz to 0.174 Hz or 2.3%. A larger effect was found for the higher two modes. The data is tabulated in Table 4.3-15. When the excitation levels decreased from 0.25 in. D.A. to .01 in. D.A. the second mode frequency increases from .63 Hz to .678 Hz or 5.9% and the third mode frequency increases from .670 Hz to .755 Hz or 11.2%. Note that the frequency ranges of these modes are near the frequencies of modes excited by symmetric excitation.

Table 4.3-16. Damping Coefficients (ξ) For Out-Of-Plane Modes - Anti Symmetric Excitation

Mode Frequency (Hz)	Damping Coefficients			
	Method 1		Input Level (in. D.A.)	Method 2
	ξ_a	ξ_b		ξ
.178		.0060	0.0025	
.178	.0069	.0054	0.0050	
.65			0.01	.010
		.037	0.05	.010
		.043	0.10	.011
			0.25	.012
.74			0.01	.015
			0.05	.015
			0.10	.018
			0.25	.019

NOTES: Method 1 is based on the rate of decay of motion. ξ_a values are for motion resulting from a step input and ξ_b for decays from dwells at a natural frequency. Method 2 is based on the frequencies of peak in-phase response when sweeping slowly through a resonance.

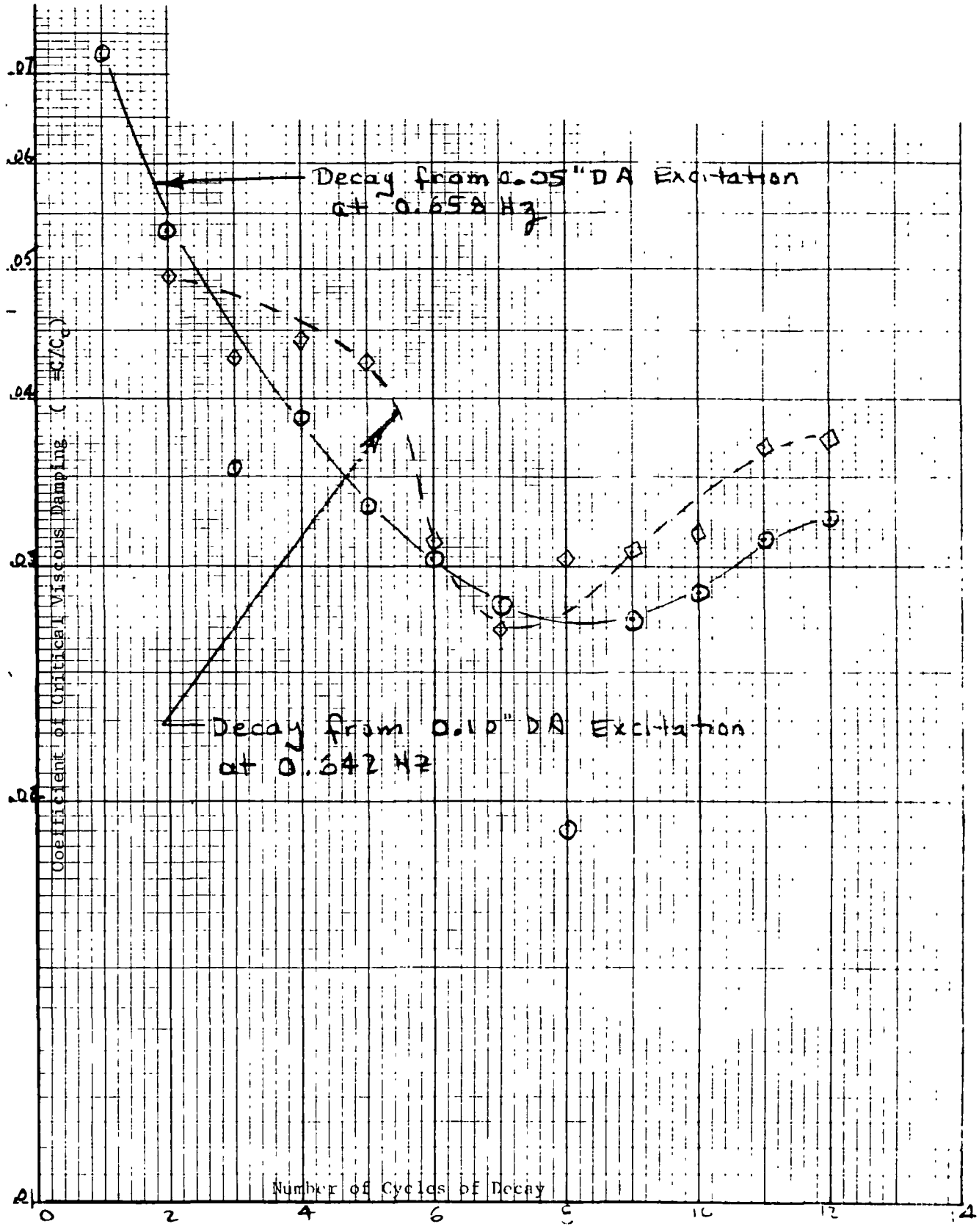

Figure 4.3-31. Damping Coeff cients for Lower Nested Torsional Resonance, Based on Exponential Decay from Suddenly Removed Shaker Excitation

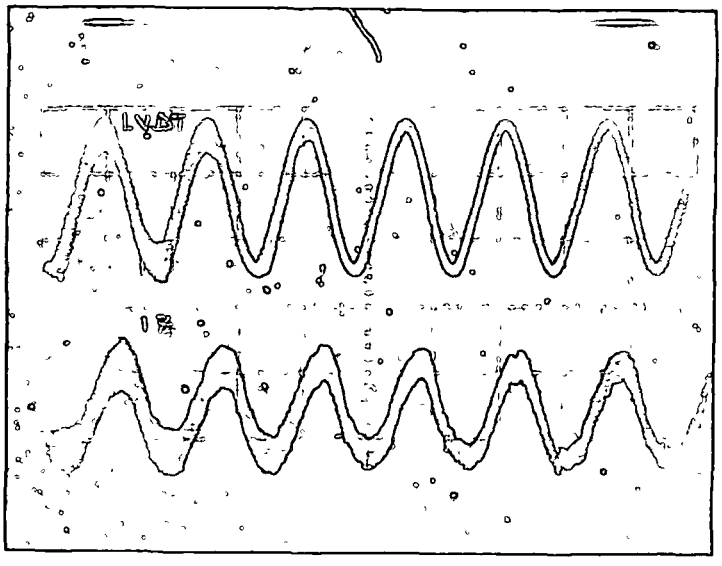

(a) Tracker 1Z Frequency .642 Hz.
1 Sec./Cm.

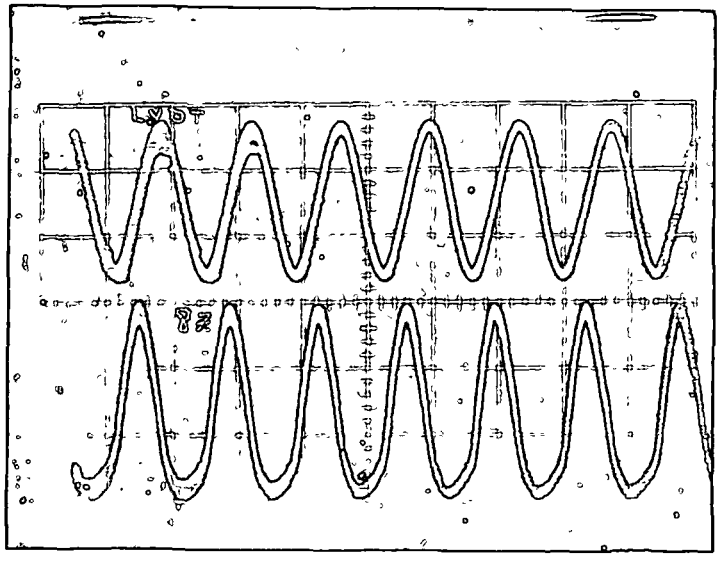

(b) Tracker 8Z Frequency .715 Hz.
1 Sec./Cm.

Figure 4.3-32 Oscilloscope Records of Input (LVDT) and Response for Antisymmetric Excitation

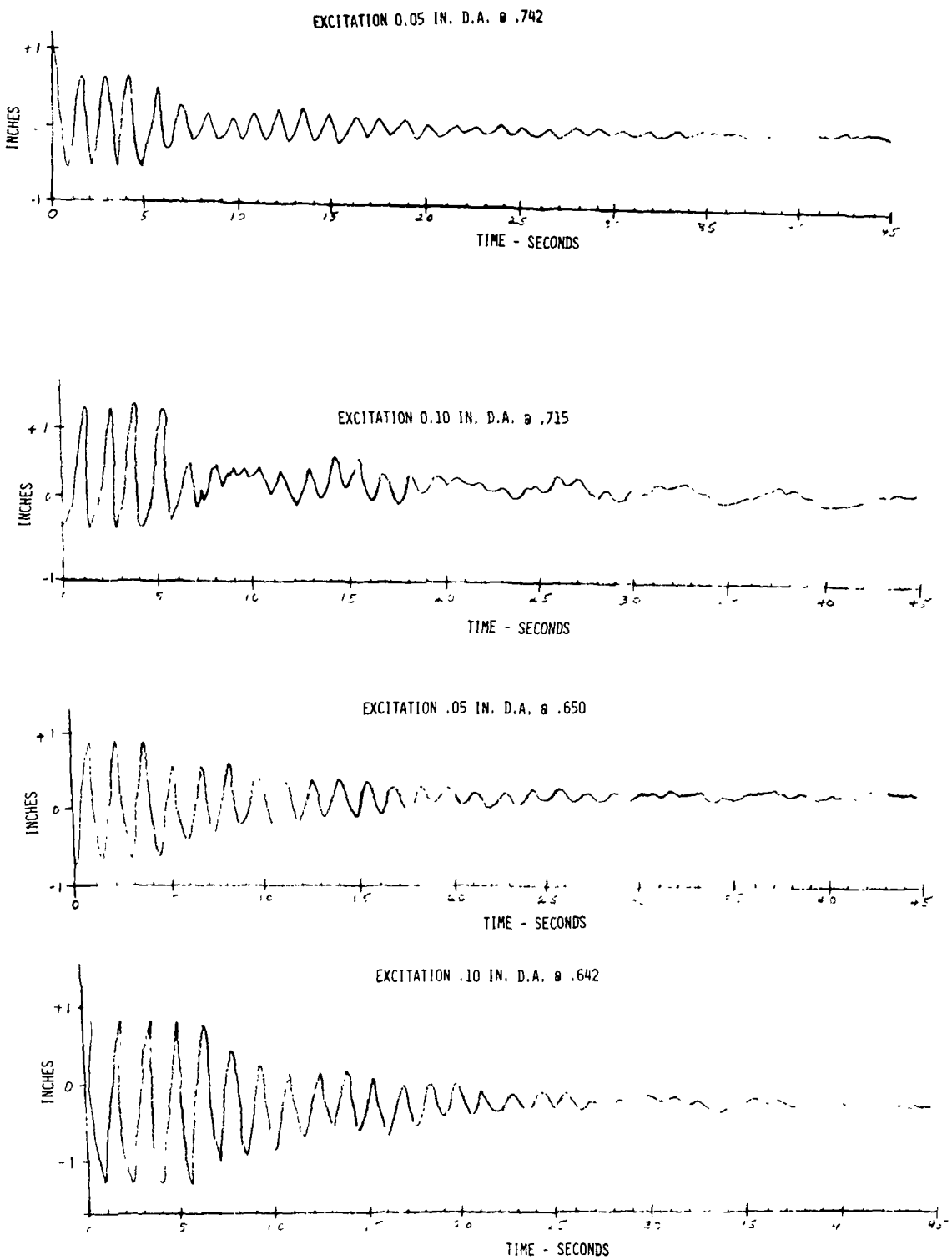

Figure 4.3-33. Decay of Vibration from Higher Modes Excited by Antisymmetric Excitation, 80% Span, Tracker 8Z

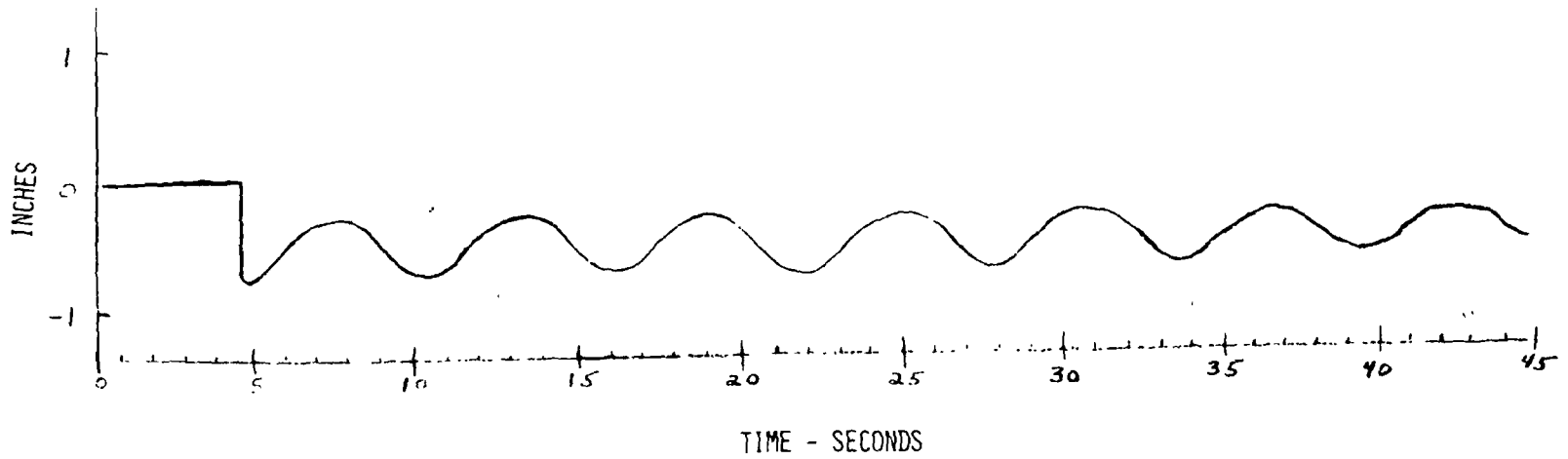

Figure 4.3-34. Response of System to Step Input (Symmetric Excitation) 80% Span, Tracker 2Z

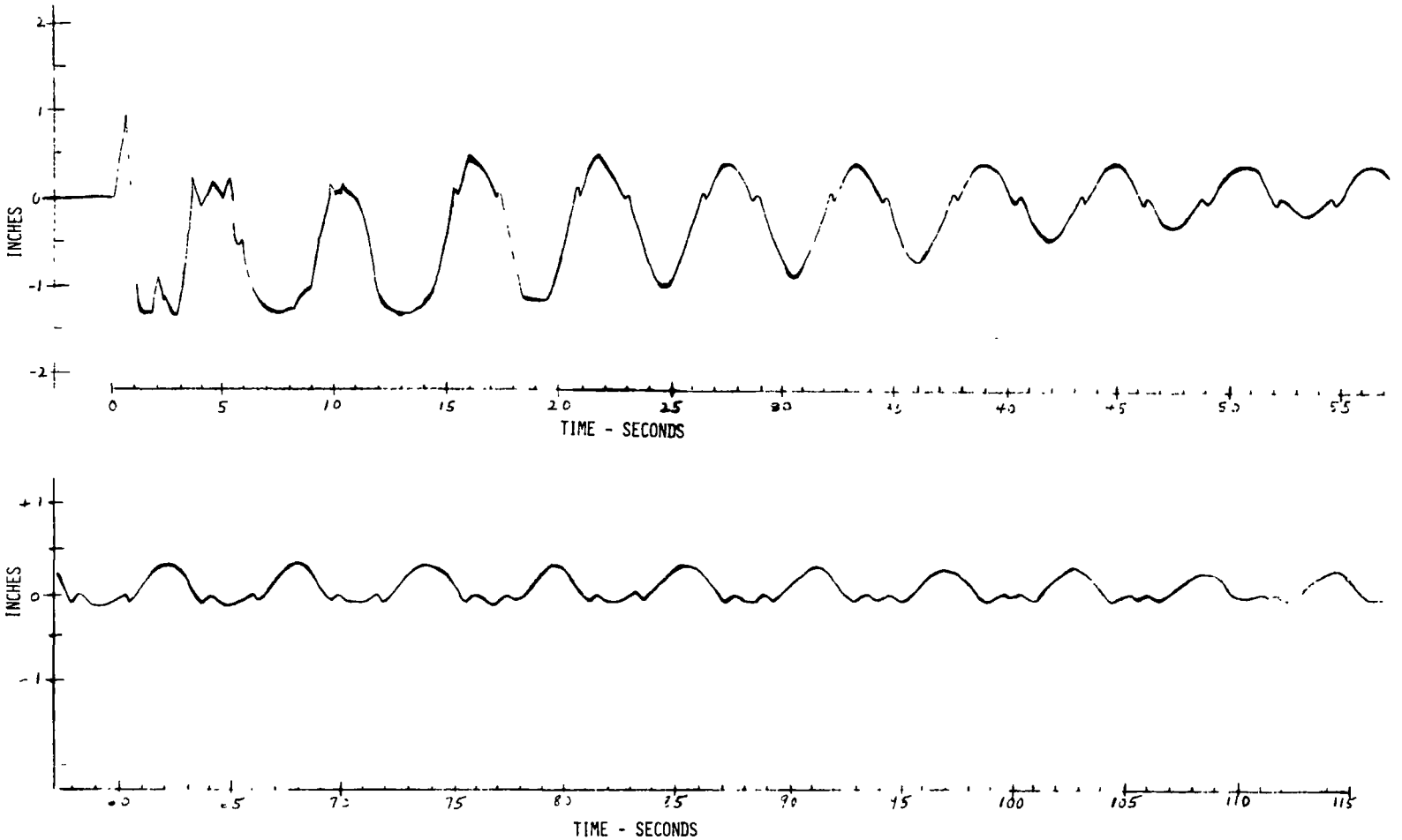

Figure 4.3-35. Response of System to Step Input, Antisymmetric (Torsion) Excitation, 80% Span, Tracker 8Z

4.3.3.4 In-Plane Excitation (Y-Axis)

4.3.3.4.1 Ambient Sweep Test

The spectrum from 0.10 Hz to 2.3 Hz was hyperbolically swept at an input level of 0.20" D.A., in two sweeps:

Sweep	Frequency Band (Hz)	Time (Sec) to Sweep Decade
1	0.1 - 1.0	1560
2	1.0 - 2.3	500

The in-phase and quadrature response acquired on-line (outboard edge of the -Y blanket at the 70% span) are included here as Figures 4.3-36 and 4.3-37.

While the on-line data plots show indications of some minor (out-of-plane) resonances at lower frequencies, the principal "pendulum" resonance occurred at about 1.0 Hz. In this mode the array moved like a planar rigid body about the Z-axis, but with a very "stiff legged", highly damped motion. In addition, the drums were observed to roll approximately 1/8" at their circumference and to bend downward approximately 1/16" at their outer ends.

4.3.3.4.2 Vacuum Sweep Tests

Because some reduction in damping was expected in vacuum, the first sweep was made at an input level of 0.05" D.A., one quarter of that used in the ambient sweep. The results of this sweep were very surprising in that no resonances were found. The sweep was rerun in the same 0.8 to 1.5 Hz region but at an input level of 0.1" D.A. With this higher input level the mode appeared at 1.015 Hz, as expected, except that the amplitude increased out of proportion to the increase in excitation

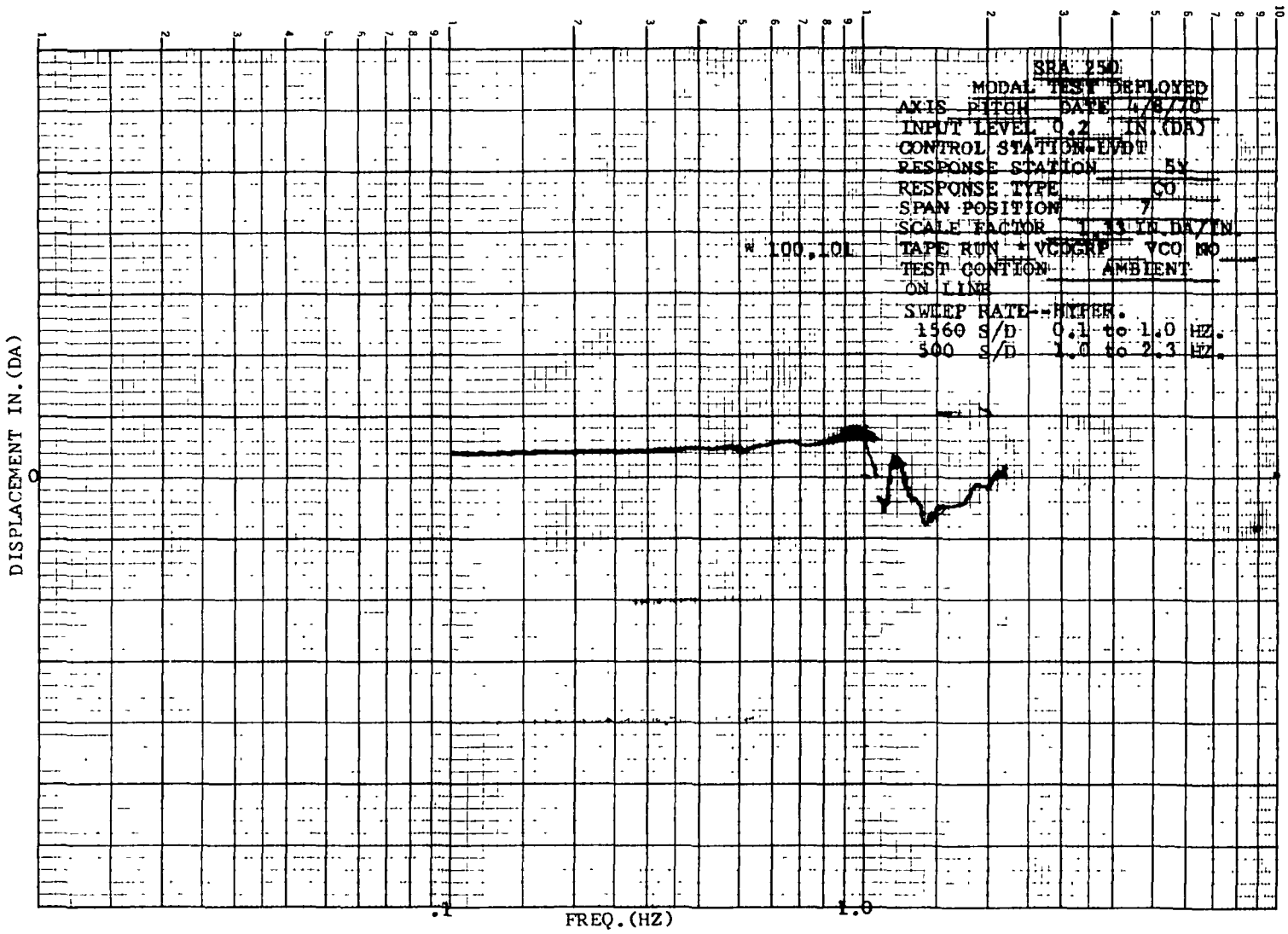

Figure 4.3-36. Frequency Sweep - In-Plane Excitation

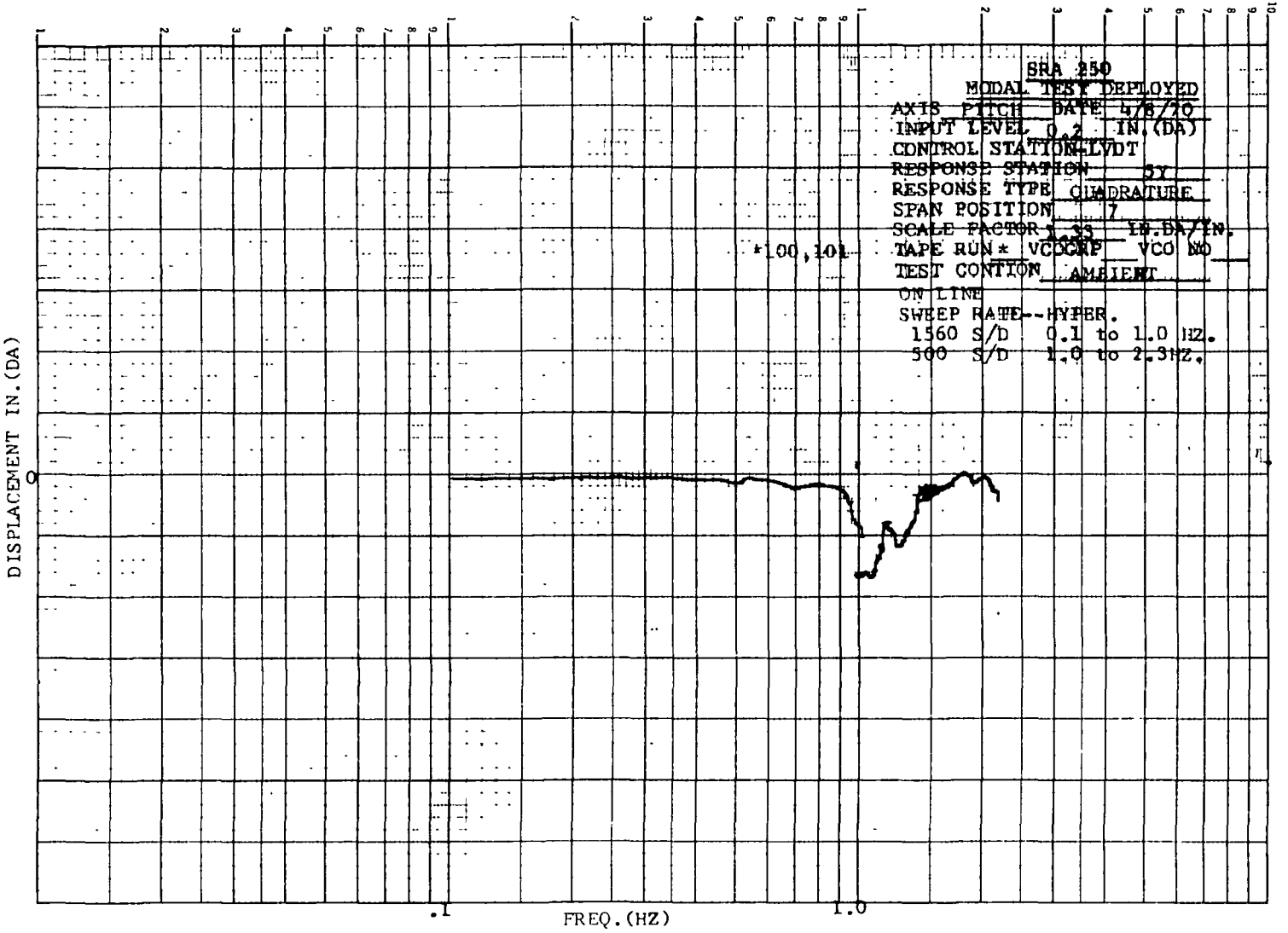

Figure 4.3-37. Frequency Sweep - In-Plane Excitation

level. The extent of this non-linear behavior is shown in Table 4.3-18.

Table 4.3-18. Variation of First In-Plane Mode Amplification Factor With Input Level

Input Level	Amplification Factor*	
	Ambient	Vacuum
0.05" D.A.	---	1.0
0.10" D.A.	---	8.0
0.20" D.A.	5.5	---

* Quadrature response of outboard edge of -Y blanket at 70% span relative to input level.

Figures 4.3-38 and 4.3-39 describe the in-phase and quadrature response obtained for the outboard edge of the -Y blanket at the 70% span. During the vacuum tests the array exhibited the same stiff-legged pendulum motion observed during the ambient test except for an increased amount of out-of-plane blanket billowing. Potentiometer readings indicated that the drums rotated $\pm$3.6 degrees which corresponds to a $\pm$ 1/4" change in blanket length.

Further sweeps in the 0.60 to 0.80 Hz bandwidth verified that the lower resonances were indeed the previously observed out-of-plane modes. It was observed that aerodynamic effects on the in-plane motion are small but that there was more out-of-plane motion in the vacuum tests.

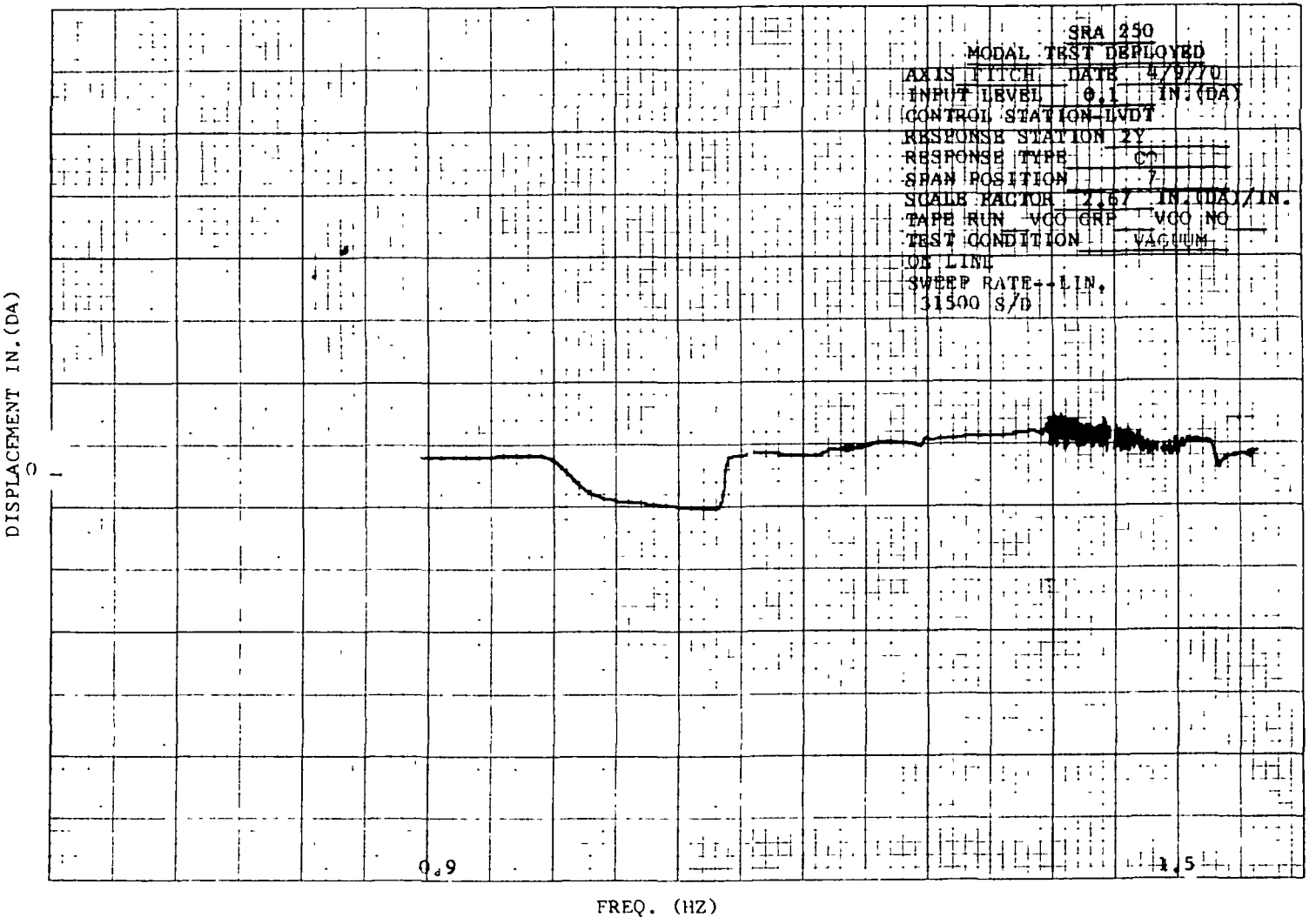

Figure 4.3-38. Frequency Sweep - In-Plane Excitation

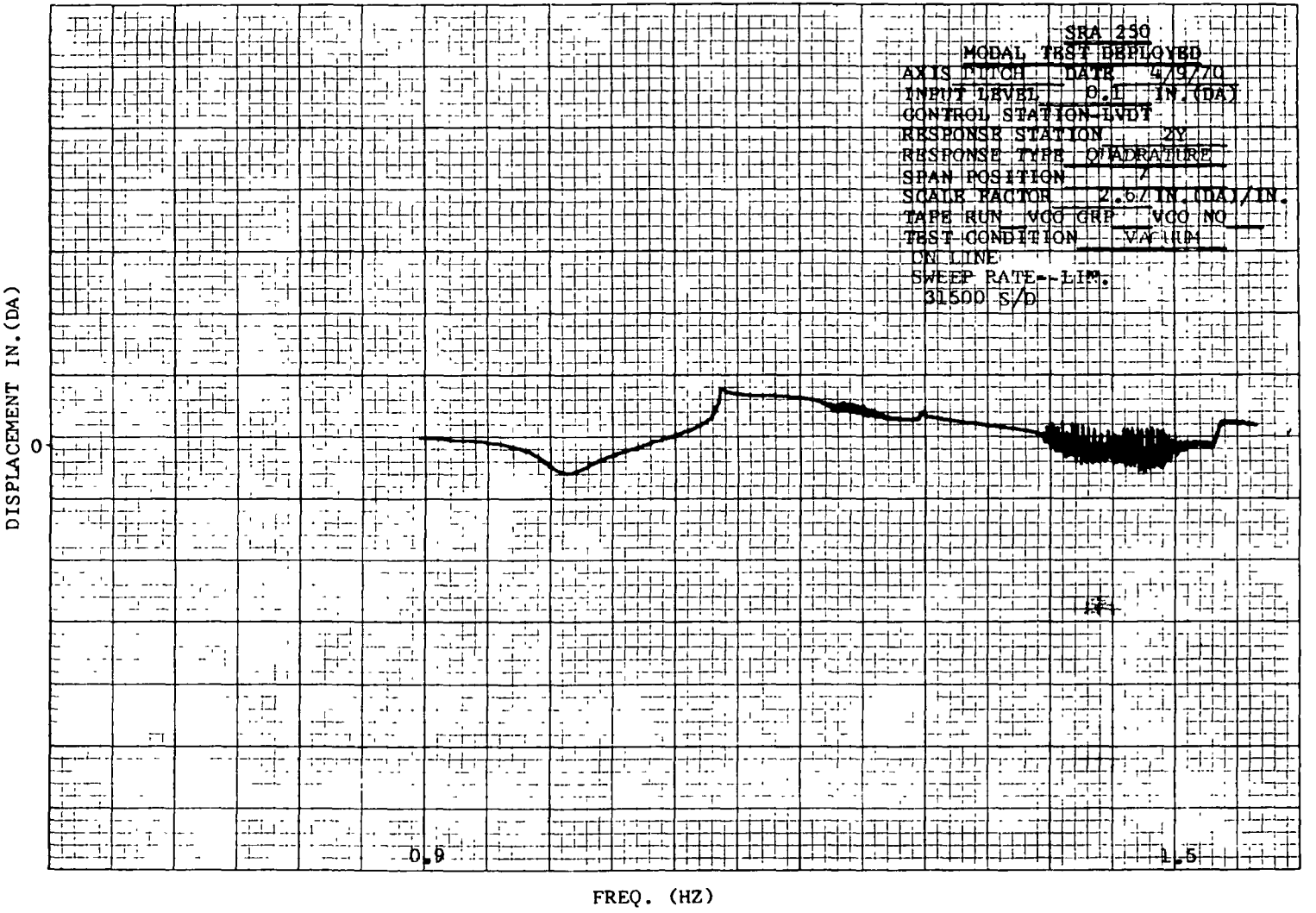

Figure 4.3-39. Frequency Sweep - In-Plane Excitation

4.3.3.4.3 Damping Coefficients

Since the damping of the in-plane mode appears to be associated with a non-linear spring rate and hysteresis, the effective damping coefficient is not strictly meaningful in that it is probably amplitude dependent. However, two decay tests were performed to determine damping from resonant excitations of 0.20 in. D.A. and 0.10 in. D.A. Both responses decayed rapidly with distortion of the waveform and beating. The response damped out too quickly to provide a measure of the damping coefficient. However, assuming a modal participation factor of unity, the transmissibilities shown in Table 4.3-18 imply a damping coefficient (c/c_c) of around 0.1. In any case the damping is high compared to the out-of-plane modes.

4.3.3.4.4 Comparison with Predicted In-Plane Modes

Although no resonance dwells to measure the mode shapes were performed, the mode at 1.015 Hz was visually observed to be the in-plane plane rigid body mode as predicted by the preliminary analysis. However, the natural frequency was much higher than the predicted value of 0.38 Hz. The source of this discrepancy appears to lie in modeling the stiffness of the drum assembly and particularly the effect of the tension redistribution which accompanies the observed drum rotation. A discussion of the modeling problem is included as Section 4.3.5.

4.3.3.5 Exploratory Tests

4.3.3.5.1 Blanket Preload Distribution Tests

The tension distribution in both blankets was of concern throughout the test program because of its possible effect on the dynamic characteristics. The tension distribution along the leading edge member was visibly quite non-uniform and drum

droop resulting from the large downward pull of the blankets was expected to have created slack in the top outside corners and outer edges of the blankets.

To determine the extent of the drum droop, preparations were made to rerun the ambient torsional and in-plane sweep tests with the drums caged, i.e., with the outboard end supports supporting the drums. However, when the drums were caged, it was noted that: 1) the drums only had to be lifted about 0.03" to affect the caging and 2) the caging did not visibly effect the blanket tension distribution. As a result of the lack of visible changes, the sweep tests were not conducted.

As an alternative, an attempt was made to improve the tension distribution in the blankets at the Leading Edge Member (LEM) by stuffing the loop in the blanket with paper towels. This improved the tension distribution and the blanket appearance over the lower 20% of its span.

The torsional (about X-axis) and in-plane (Y-axis) ambient sweep tests were repeated with this improved distribution. However, there was relatively little change in the array's modal response, thus indicating that the tension uniformity at the leading edge was not a significant factor.

4.3.3.5.2 Blanket Vibration Tests (Out-of-Plane Symmetric Excitation)

4.3.3.5.2.1 Ambient Tests. Vibration testing was initiated under ambient conditions to determine blanket characteristics. The LEM was removed from the array leaving the blankets and BI-STEM suspended from the drums and center support, respectively. The drums were locked. This configuration has the blanket elements

under fixed-free boundary conditions. In this state, data could be obtained to verify concepts employed for the analytical modeling of these blankets.

An ambient hyperbolic sweep was performed with excitation along the Z-axis (normal to the blanket plane) from 0.1 Hz to 0.2 Hz. The input level was .1" D.A. and the rate was 1560 seconds per decade. (This was the same rate used for the array Z-axis ambient sweep test, Section 4.3.3.2).

This sweep disclosed the -Y blanket fundamental resonance at 0.140 Hz in air. These results can be compared with the results of the array Z-axis ambient testing:

Configuration	Frequency (Hz) in Air	Frequency (Hz) in Vacuum
Total Array	.16	.251
-Y Blanket Alone	.14	.213

The small difference in natural frequencies of the blanket alore and the system show that the stiffness provided by the boom is small compared to the gravity forces for out-of-plane motion.

4.3.3.5.2.2 Sweep Tests in Vacuum. Sweep tests were performed in vacuum to detect blanket Z-axis resonances. Two hyperbolic sweeps were performed over the 0.2 - 0.3 Hz frequency bands.

Sweep	Input Level (In. D.A.)	Time (Sec) to Sweep Decade	Purpose of Sweep
a	0.01	1,560	Fast sweep to locate resonance region
b	0.01	10,000	Slow sweep to identify resonance.

Another hyperbolic sweep at the same input level was performed over the 0.28-1.00 Hz bandwidth; the sweep rate used was such that 7200 seconds would have been required to sweep this decade. Resonances were found at .213 Hz and .89 Hz.

4.3.3.5.2.3 Damping Measurements in Vacuum

The damping of the fundamental blanket resonance in vacuum was determined by the instantaneous shutdown of shaker resonant inputs (0.01" D.A. excitation at 0.2136 Hz). This procedure was done twice; the first time using the center of the -Y blanket at midspan as a reference and the second time using the outboard edge of the +Y blanket at midspan. Both decay traces were recorded on oscillograph paper.

These results are summarized as follows:

Parameter	+Y Blanket	-Y Blanket
Number of cycles required for Vibration to Decay to 50% of Initial Value	112	58
Damping Coefficient ($\xi = c/c_c$)	.0011	.0023
Natural Frequency of Decay (Hz)*	.2180	.2185

These results show there is a difference between the blankets in that the damping in the -Y blanket is double that of its mate. These results also indicate that the blankets contribute relatively little to the array damping. The oscillograph waveforms appear to be sinusoids.

---

* As determined from measuring the time for 100 cycles on the oscillograph record. The excitation frequency was 0.2136 Hz.

4.3.3.5.3 Analysis of Blanket Dynamics

For out-of-plane chordwise uniform motion an appropriate mathematical model for the blankets alone should be the classical problem of the transverse vibrations of a vertical chain in the gravity field. Using the coordinates shown below,

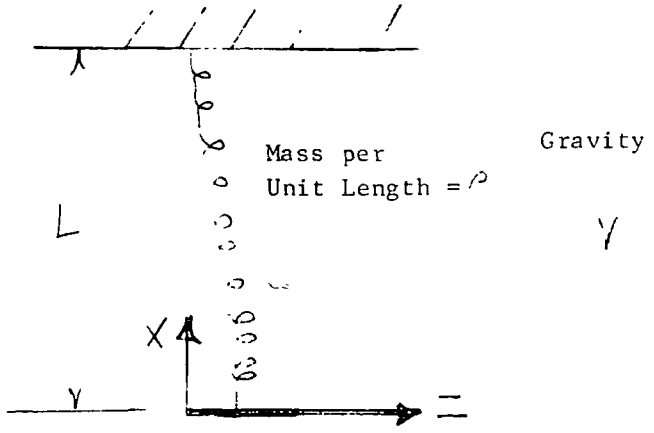

the equation of motion is:

$$\frac{\partial}{\partial x}\left(\rho g x \frac{\partial z}{\partial x}\right) = \rho \frac{\partial^2 z}{\partial t^2}$$

For product solutions of the form

$$z = \phi(x) \sin wt$$

the function ϕ (x) is given by

$$\frac{d^2\ \phi}{d\ x^2} + \frac{1}{x}\ \frac{d\ \phi}{d\ x} + \frac{1}{x}\ \frac{w^2}{g}\ \phi = 0$$

which has solutions of

$$\phi(x) = A\ J_o\ (2\ w_n\sqrt{\frac{x}{g}}\ ) + B\ Y_o\ (\ 2\ w_n\ \sqrt{\frac{x}{g}}\ )$$

J_o and Y_o are zero order Bessel functions of the first and second kinds. Applying the boundary conditions leads to the transcendental equation to be solved for the eigenvalues.

$$0 = J_o\ (2\ w_n\sqrt{\frac{L}{g}}\ )$$

Solutions of the equation for a length of 26 feet provide the following values for natural frequencies:

$$w_1 = 1.202\ \sqrt{g/L} = 1.34 \text{ rad/sec};\quad f_1 = 0.2135 \text{ Hz}$$
$$w_2 = 2.660\ \sqrt{g/L} = 2.96 \text{ rad/sec};\quad f_2 = 0.472 \text{ Hz}$$
$$w_3 = 4.327\ \sqrt{g/L} = 4.82 \text{ rad/sec};\quad f_3 = 0.768 \text{ Hz}$$

The first natural frequency of the mathematical model agrees very well with the test results. However, the second test mode frequency (.89 Hz) correlates with the third mode of the mathematical model. The reason for the absence of the second mode from the test results has not been determined.

4.3.4 POST TEST ANALYSIS OF OUT OF PLANE MODES USING REVISED MATHEMATICAL MODELS*

4.3.4.1 Introduction

Before conducting the deployed modal tests, the natural frequencies and mode shapes were predicted for the array deployed vertically downward 26 feet in one-g field test environment. As described in Section 4.3.3, the first symmetric resonance agreed very well with the experimental one, the first torsion resonance occurred at a frequency 30% lower than the calculated value, and the higher order resonances include both symmetric and anti-symmetric components.

The dynamic model used in the preliminary analysis utilized finite element techniques to describe the bending stiffness of the boom and leading edge member (LEM) and the effective stiffness of the blankets due to the imposed tension (Reference 1-4). However, in order to reduce the problem to a manageable size, the analysis assumed the array to be symmetric about its centerline and assumed the tension to be evenly distributed across the blanket's width. In addition, it assumed the bending stiffness of the blanket material to be negligible compared to the stiffness due to the imposed tension.

These assumptions represent an ideal array, and were not exactly satisfied by the array in its test configuration. The differences could contribute significantly to the difference between the analytical and experimentally measured modes. The symmetry and uniformity assumptions were made particularly inappropriate by the following factors:

---

* This section written by Dr. R. Ross, Jet Propulsion Laboratory

1) Different weights for the two blankets and uncertain amounts of friction in the blanket tensioning mechanisms is expected to have led to unequal tensions in the two blankets. Figures 4.3-40 and 4.3-41 describe the hysteresis in the blanket tensioning mechanisms.

2) Downward bending, or drooping, of the blanket storage drums under the weight of the blankets is considered to have resulted in a non-uniform tension distribution at the attachment between the blankets and the drums.

3) Misalignment between the leading edge member and the blankets is known to have resulted in a non-uniform tension distribution along the blanket's attachment to the LEM.

4) Because of the inelastic nature of the blankets relative to in-plane displacements, the non-uniform boundary tensions are expected to have resulted in significant tension non-uniformities throughout the blankets.

In order to explore the significance of the non-uniform tension distributions and the effect of the blanket's bending stiffness, a more detailed analysis of the array was conducted using an expanded dynamic model. The following sections describe the revised mathematical model and explore the effects of various blanket stiffnesses and tension distributions on the modal characteristics of the deployed array.

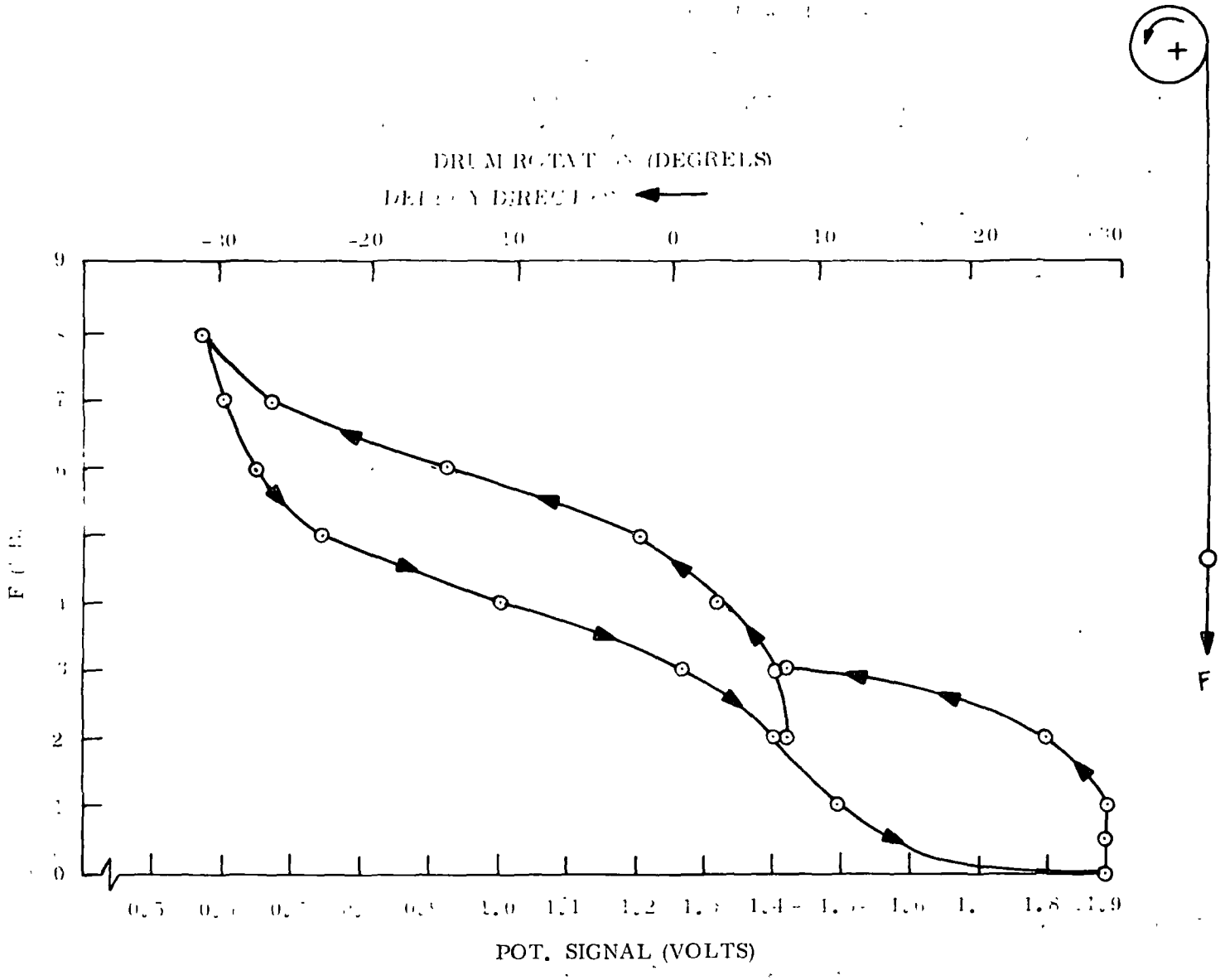

Figure 4.3-40. Characteristics of -Y Blanket Support

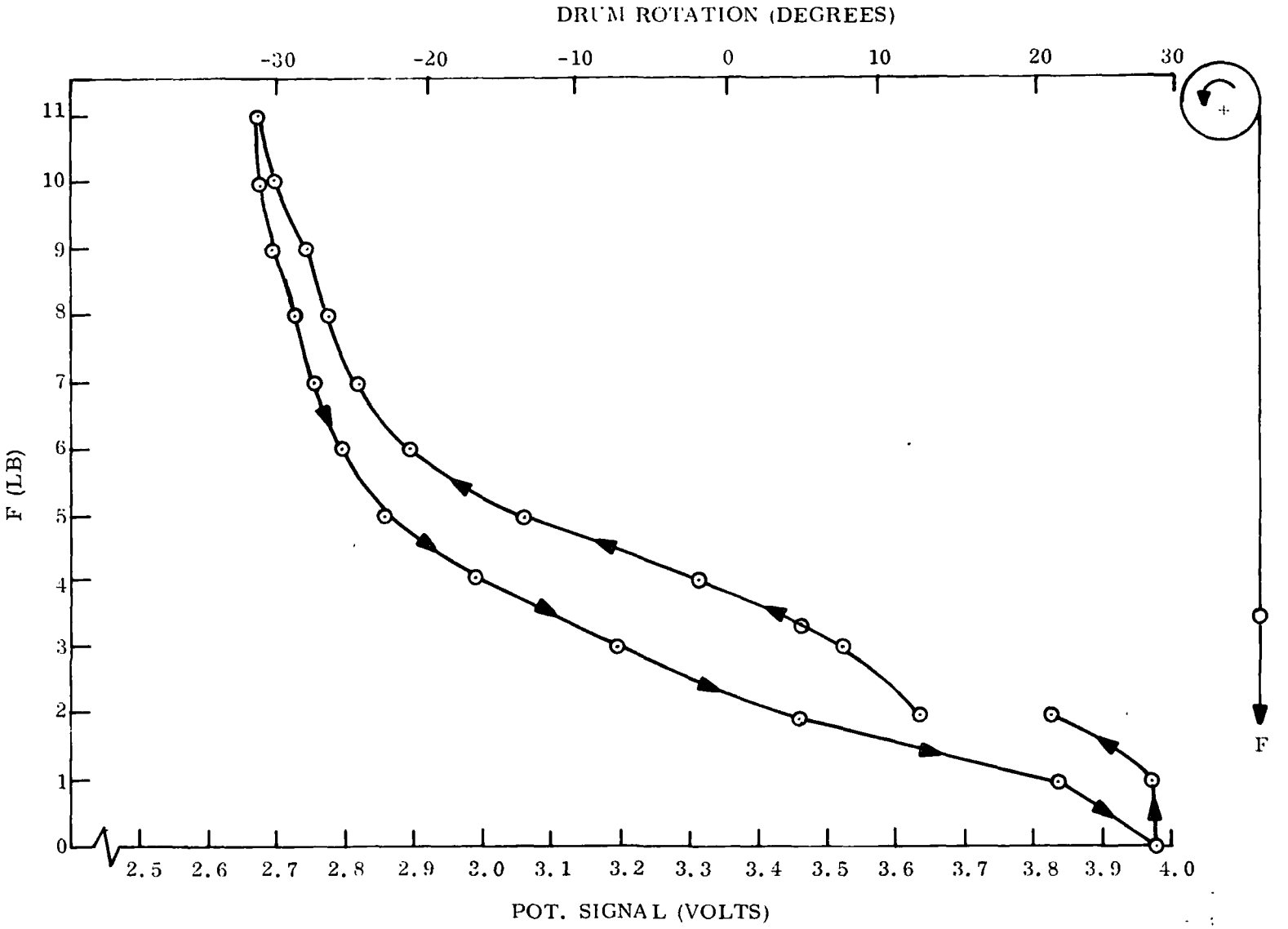

Figure 4.3-41 Characteristics of +Y Blanket Support

4.3.4.2 Modification of the Model

As described above the preliminary analysis used finite element techniques to model the mass and stiffness properties of the boom, LEM, and blankets which make up the deployed array. By taking advantage of symmetry and by neglecting the blanket's bending stiffness, it was possible to reduce the problem to around 50 degrees of freedom with a 20 element blanket.

In order to provide for arbitrary tension distributions in the two blankets, the symmetry condition was dropped in the present analysis and each blanket was discretized using thirty rectangular finite elements. Each blanket element included a rectangular plate bending element in addition to the geometric stiffness element used previously to describe the tension induced stiffness. Although the boom was modeled with standard beam-column elements as before, the LEM was considered a rigid member in the revised analysis. Removing the degrees of freedom associated with the LEM has a negligible impact on the array's behavior, but serves both to reduce the problem size and to improve the conditioning of the computational problem. In order to further reduce the remaining 250 degrees of freedom to a manageable level, each of the blankets was considered as a substructure as shown in Figure 4.3-42. By neglecting the inertia associated with the rotational degrees of freedom, it was possible to remove these coordinates and obtain a reduced stiffness matrix for each blanket with only 41 degrees of freedom. The mass associated with the remaining coordinates was modeled with the rectangular consistent mass element used in the preliminary analysis.

Figure 4.3-43 shows the complete finite element model obtained by combining the two blanket models with the boom model and applying the constraints associated with the rigid leading edge member. Since the substructure coordinates 37 through

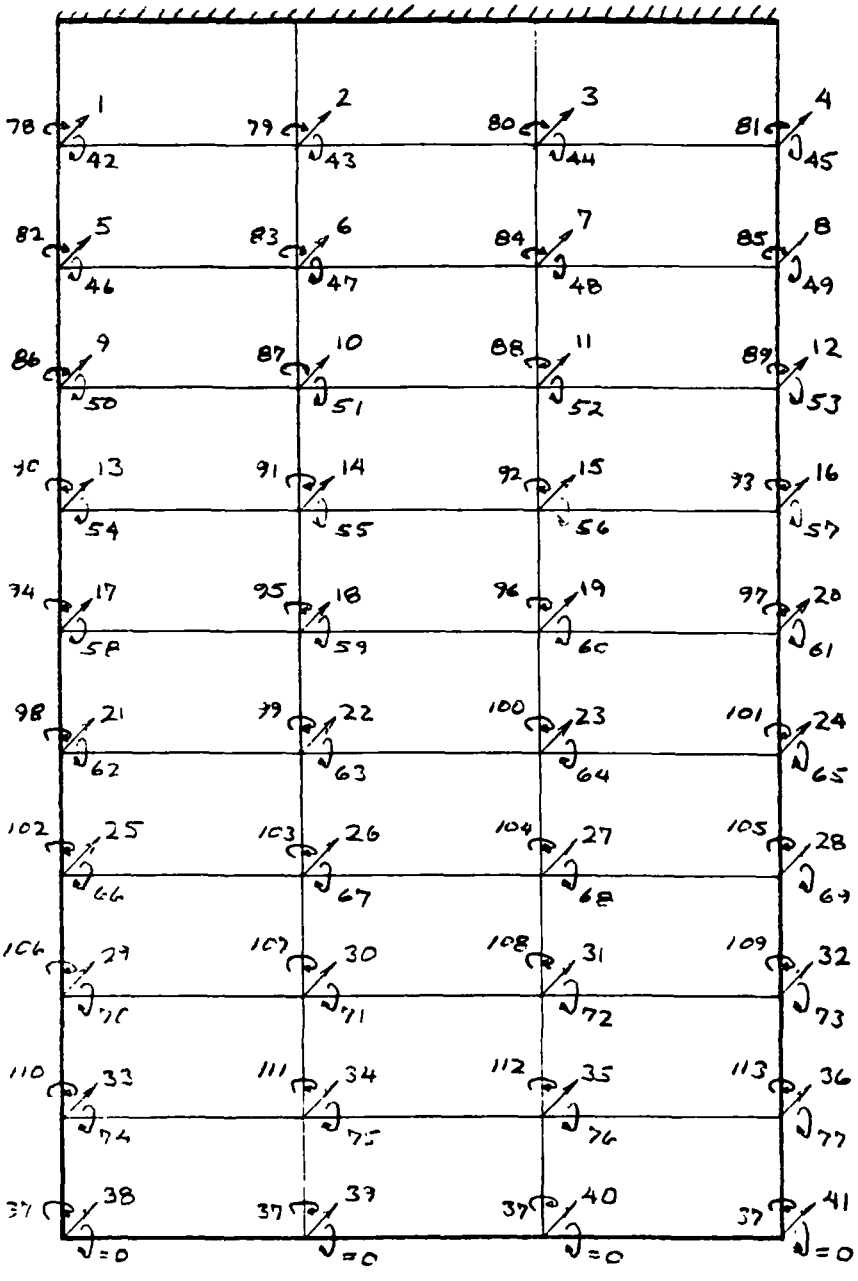

Figure 4.3-42. Blanket Substructure Discretization

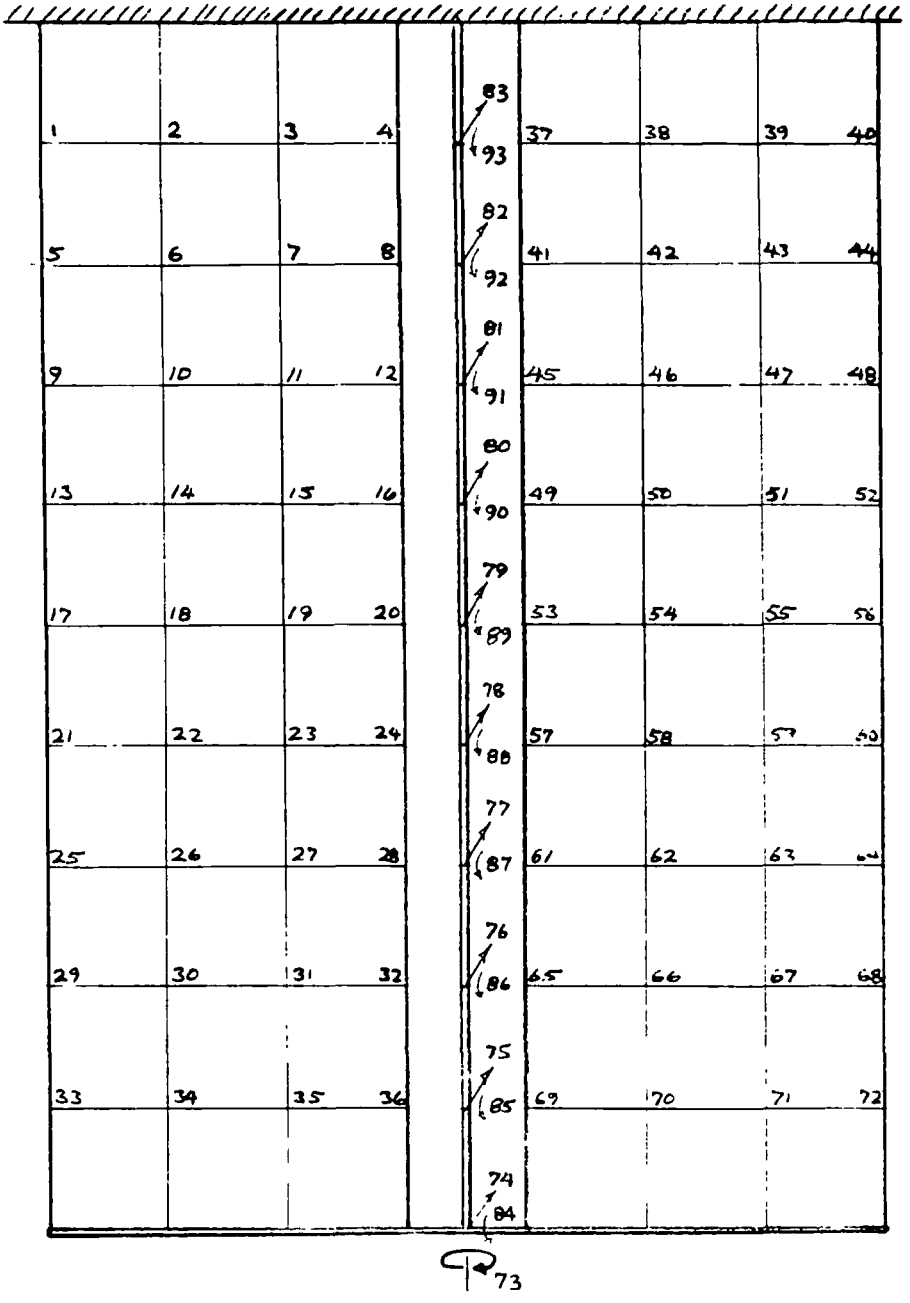

Figure 4.3-43. Complete Finite Element Discretization of the Deployed Roll Up Array

41 of each blanket and the boom tip deflection are interrelated by the rigid LEM assumption, all but two of these coordinates were removed by applying the appropriate multi-point constraints. The final model thus contains 60 blanket elements, 10 beam-column (boom) elements and a total of 93 degrees of freedom.

To provide for arbitrary tension distributions, the tension in each of the 60 blanket elements was made individually prescribable and the tension (compression) in the boom was allowed to vary linearly from one end to the other. However, only longitudinal tensions were included in the blanket stiffness element, and thus the model neglected the effects of local tensions running perpendicular to the blankets length and the effects of in-plane shear stresses resulting from non-uniform tension distributions.

4.3.4.3 Results

4.3.4.3.1 Parametric Study Definition

Once the expanded model was completed and its solutions for even tension distributions checked against earlier solutions, a parametric study was conducted in an attempt to improve correlation with the experimental results. The direction of the study was focused at the following four general areas:

1) The effect of the bending stiffness of the blanket material.

2) The effect of the magnitude and symmetry of the blanket tension at the LEM attachment.

3) The effect of non-uniform tensions within the blankets

   a) Top outside corners slack

   b) Bottom outside corners slack

   c) Top outside corners and sides slack

   d) Top and bottom corners and sides slack

4) Effect of increased blanket bending rigidity due to edge curl. The results of each of these areas of study are summarized in the following subsections.

4.3.4.3.2 Effect of Blanket Bending Stiffness

To determine the effect of the stiffness of the blanket material, modal analyses were conducted using no flexural rigidity and several values of flexural rigidity bracketing the approximate value of 0.1 in-lb determined from load deflection tests on the cell blanket (Reference 1-4). Figure 4.3-44 describes the change in the natural frequencies as a function of increased flexural rigidity. When the blanket is modeled with no bending stiffness the frequency spectrum consists of an alternating series of symmetric and antisymmetric structural modes with a set of pure blanket resonances following each pair of structural modes. Each set of blanket resonances consists of a number of self-equilibrating modes, all at the same frequency. In these modes the boom and LEM remain fixed while the blankets flap with a given longitudinal wavelength, but with varying wavelengths perpendicular to the boom. The number of blanket modes obtained for each such frequency equals the number of finite elements used across the width of the array, and thus 6 were obtained in the current study.

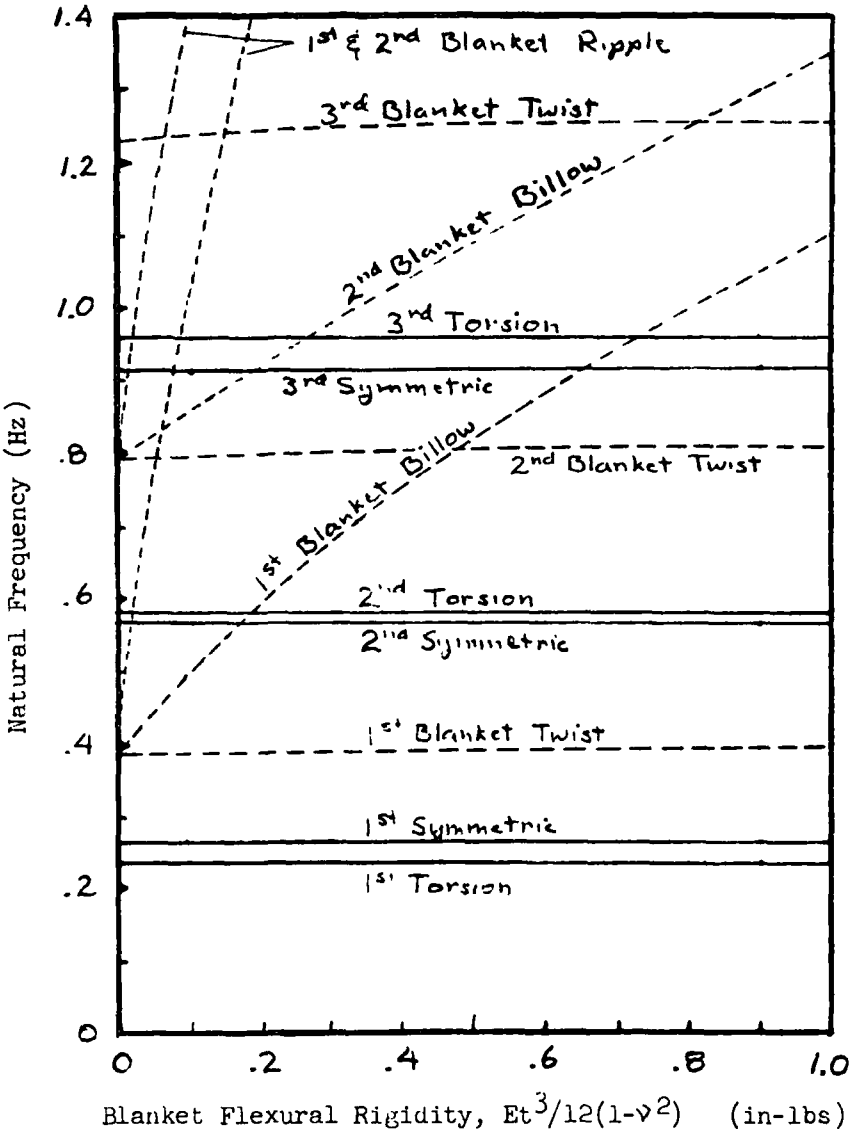

Figure 4.3-44. Effect of Blanket Rigidity on Deployed Natural Frequencies (LEM Tension = 2 lbs./Blanket)

When the blanket's flexural rigidity is added to the model the higher order members of each blanket resonance set (those with shorter transverse wavelengths) separate and become higher order modes. However, the fundamental blanket resonances and the symmetric and antisymmetric structural resonances are essentially unaffected by the blanket's rigidity. As a result, the overall ordering of the modes is sensitive to the amount of rigidity assumed for the blankets, and to the number of blanket modes included in the analysis.

When the symmetry or tension distribution of the array is altered, the effect is even more complex because the distinction between blanket modes and structural modes disappears. Thus, as the descendants of the higher order blanket modes increase in frequency with increasing rigidity, they combine with various structural modes and form hybrid modes with widely varying mode shapes.

4.3.4.3.2 Effect of Blanket Tension at LEM

Because the blanket tension at the leading edge member was determined by the difference between the blanket's weight and the tension of a device with some inherent friction, the precise tension applied during the test contained some uncertainty. As a result, the sensitivity of the array's modes was explored using various equal LEM tensions between 0 and 2.5 pounds per blanket and a nominal blanket rigidity of 0.1 in-lbs. As shown in Figure 4.3-45, similar variations in both blanket tensions resulted in only minor changes in the array's frequencies. The mode shapes were similarly uneffected by the tension variations.

As a second step, unequal tensions such as 1.5 pounds in the left blanket and 2.0 pounds in the right blanket were explored. Although the natural frequencies were only slightly affected, the unequal tensions had a significant effect on all of

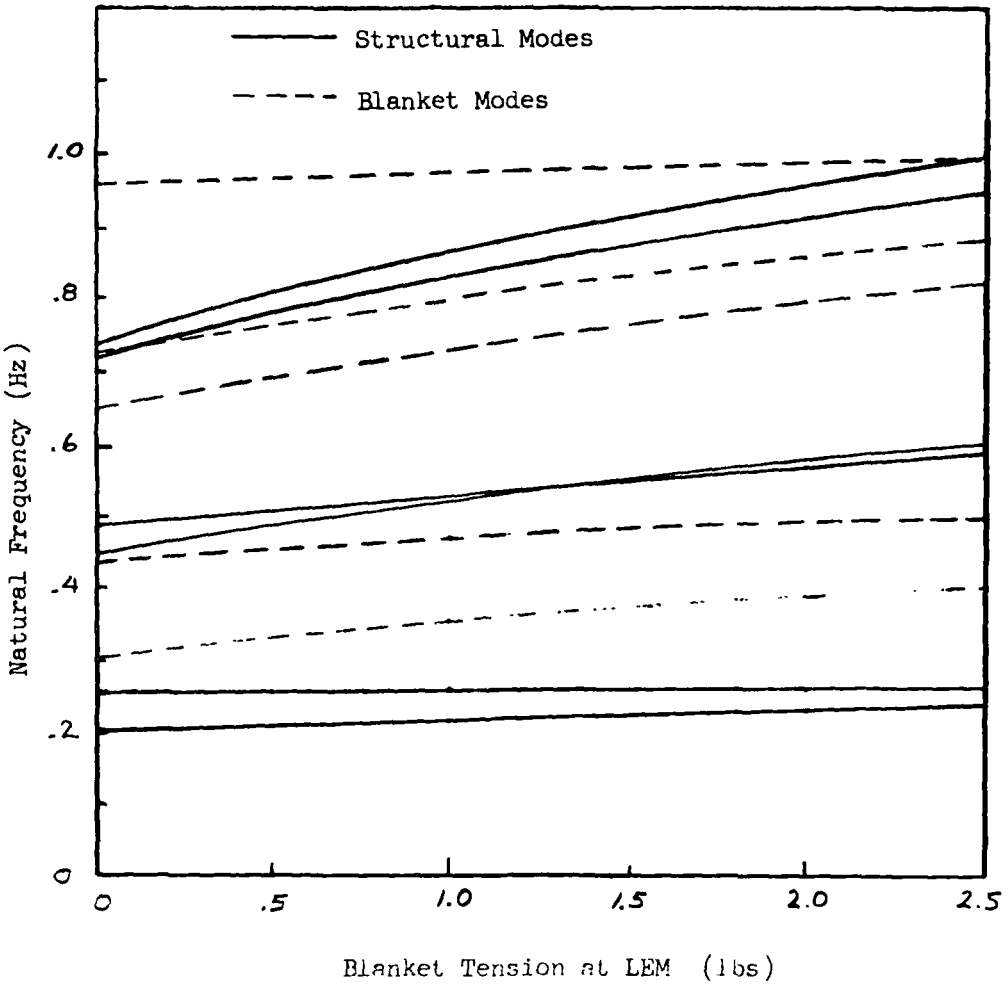

Figure 4.3-45. Effect of Blanket LEM Attachment Tension on Deployed Natural Frequencies (Blanket Rigidity = 0.1 in./lbs.)

the array's mode shapes except the first symmetric and first antisymmetric structural modes. The dominant effect on the blanket modes was to split each symmetric/anti-symmetric pair into two modes -- one with only the left blanket vibrating with a characteristic blanket mode shape and the right blanket motionless, and the second mode at a slightly higher frequency with the blanket roles reversed.

The structural modes, except the first two, were also affected, but in a different way. Here the symmetric and antisymmetric modes with similar frequencies combined and formed hybrid modes with, for example, the top of the blanket's twisting and the bottoms billowing in a manner reminiscent of higher order modes observed during the modal testing. Figure 4.3-46 describes a typical composite mode obtained when the second symmetric and antisymmetric structural modes are altered by unequal LEM tensions.

4.3.4.3.3 Effect of Non-Uniform Blanket Tensions

Because of the non-uniform tension distribution observed along the blanket's LEM attachment and expected at the drum attachment, the improved model was also used to determine the effects of various non-uniform tension distributions within the blankets. The distributions studied can be roughly divided into four categories:

1) Top outside corners slack
2) Bottom outside corners slack
3) Top outside corners and sides slack
4) Top and bottom outside corners and sides slack

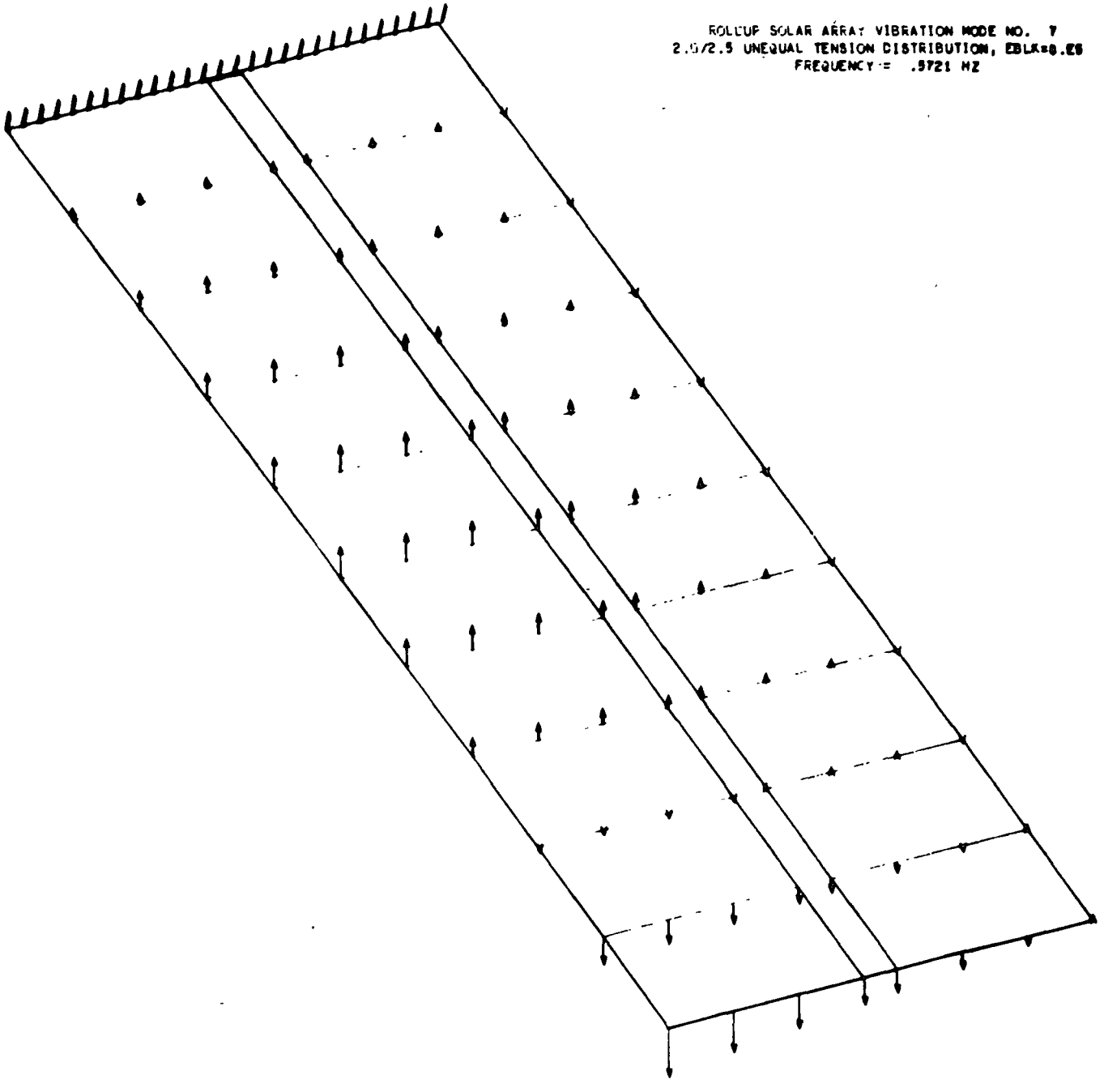

Figure 4.3-46. Composite Structural Mode Resulting From Unequal LEM Tensions

Figure 4.3-47 describes the element tension fractions used to define four of the tension distributions studied. These element tension fractions indicate the fraction of the total tension applied to each element row which was assigned to the particular element. Thus, the total tension in a particular element equals the element's tension fraction times the total tension applied to the bottom of that row of elements, plus one half the weight of the element. The tension applied to the bottom of each row of elements is calculated as the tension applied by the LEM plus the sum of the weights of the elements below the row.

The changes in the array's frequency spectrum caused by these tension distributions is shown in Figure 4.3-48. Except for some scrambling of the higher order modes by the more radical distributions, the array's natural frequencies are relatively insensitive to considerable loosening in the outer corners and edges of the blankets. As a result, the more extreme non-uniformities were required to bring the first torsion frequency into agreement with the experimentally measured value. At the same time, however, the mode shapes experienced considerable change in at least two ways.

The most significant change was the disappearance of the distinction between blanket modes and structural modes. As soon as any appreciable non-uniformity was added to the tension distribution, the pure blanket modes acquired the same amount of boom and LEM participation exhibited by the structural modes. On the other hand, the participation of the LEM and boom in the structural mode essentially became a blanket mode. Figure 4.3-49 describes this behavior for what is the first blanket resonance when the tension is uniform.

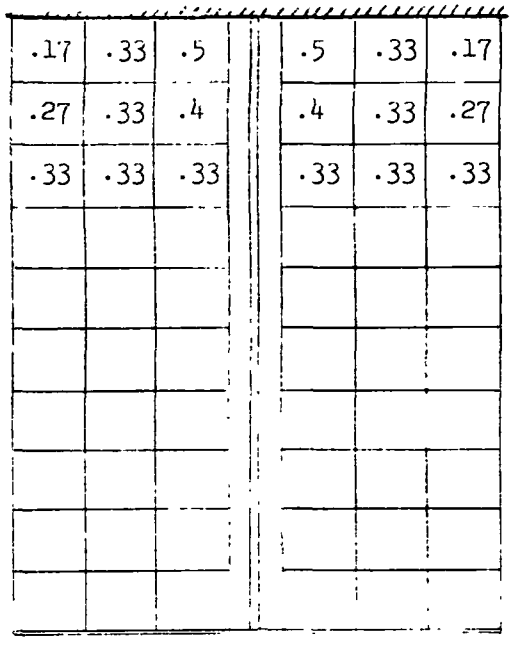

Upper Corners Slack

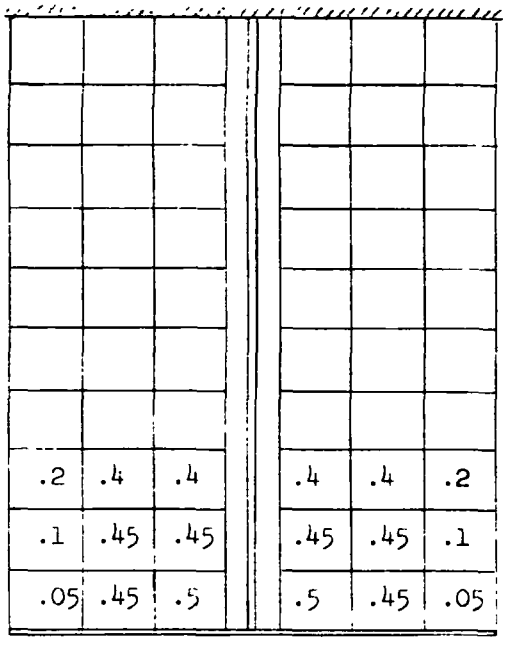

Lower Corners Slack

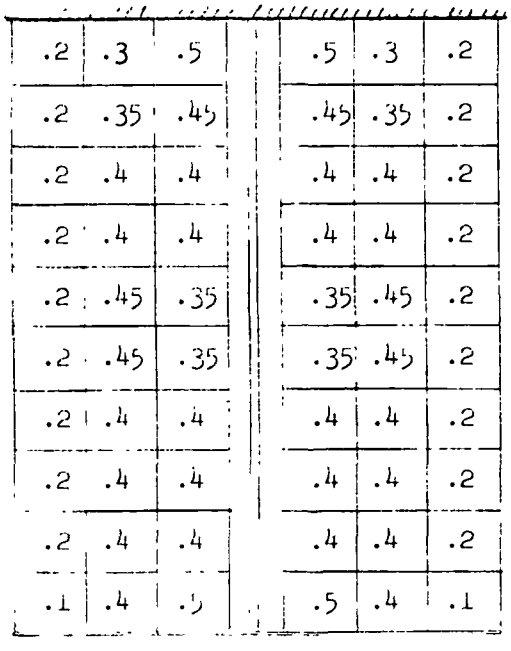

Overall Slack (.2/.4/.4)

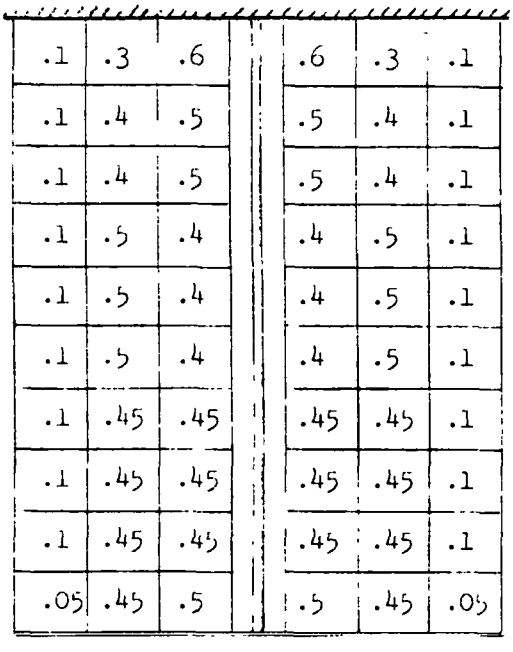

Overall Slack (.1/.5/.4)

Values Not Shown Are Equal to 0.333 (Uniform Distribution)

Figure 4.3-47. Four Tension Distributions Used to Analyze the Effect of Non-Uniform Blanket Tensions

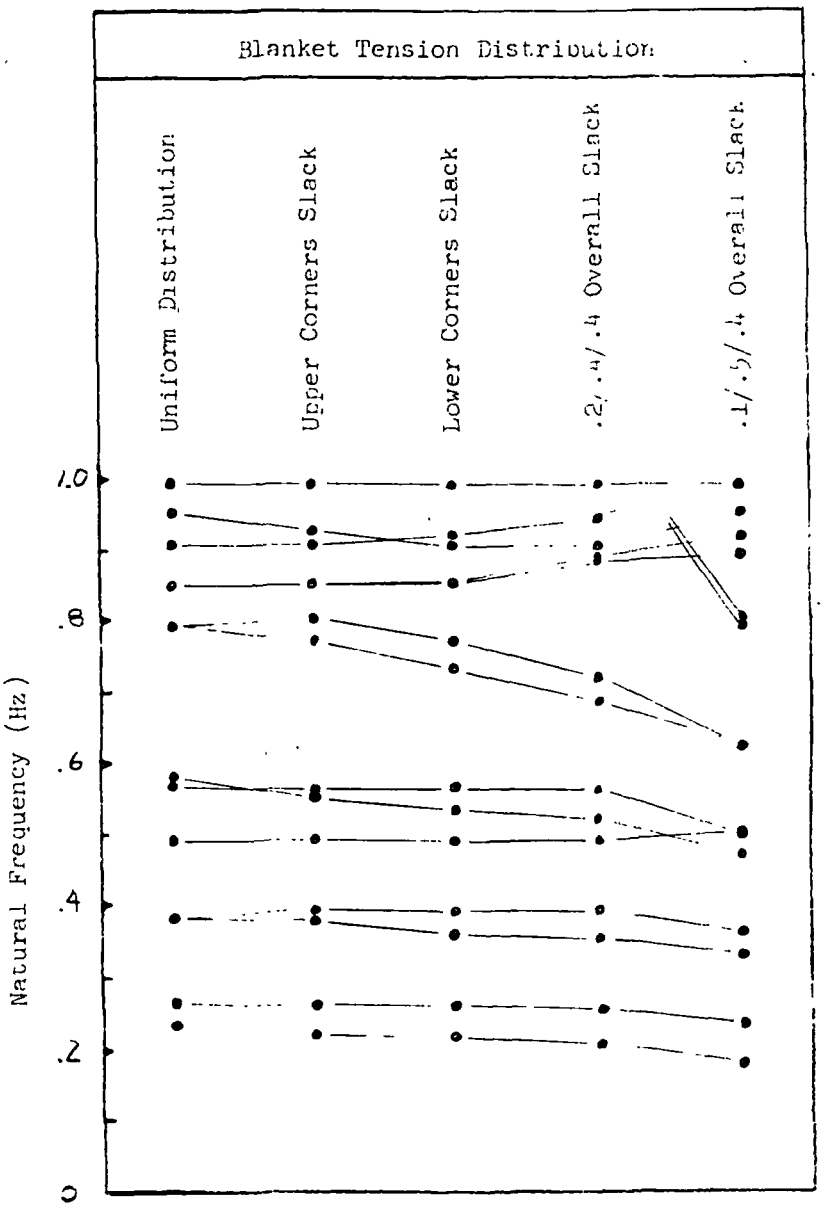

Figure 4.3-48. Effect of Non-Uniform Blanket Tensions on Deployed Natural Frequencies

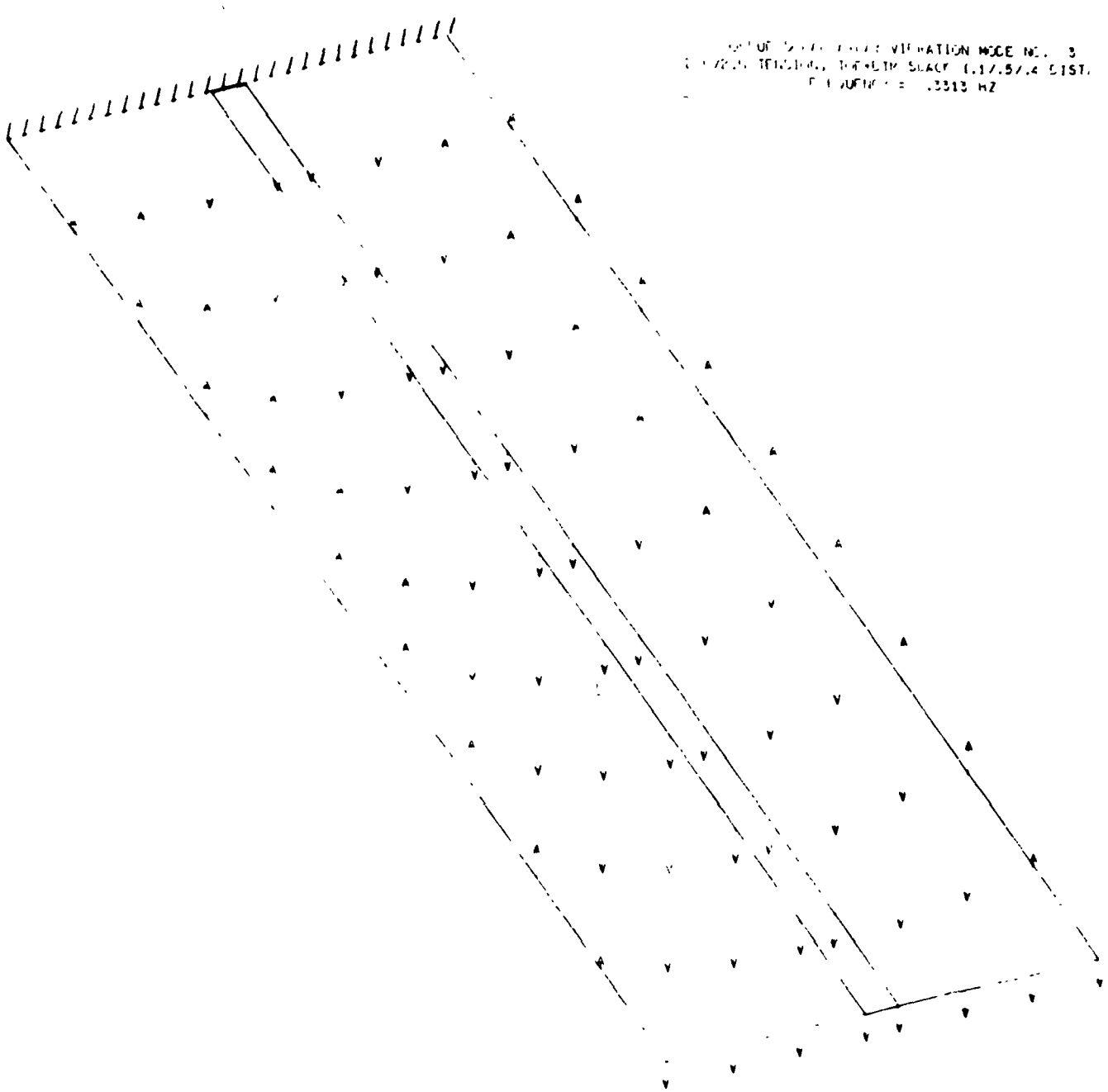

Figure 4.3-49. First Blanket Resonance with Non-Uniform Tension Distribution

A second change brought about by loosening the outer edges was an increased amount of edge flapping. All modes, and particularly the first symmetric mode, acquired a significant increase in motion along the outer third of the blankets. Related with this was an increase in the number of vibration nodes along the blanket's outer edge. Because of the lower tension in the outer edges these areas tended to vibrate in a mode one order higher than the rest of the blanket, and thus, contained an extra node line. The first blanket mode shown in Figure 4.3-49 exhibits this behavior.

When unequal LEM tensions and various blanket stiffnesses were superimposed on the non-uniform tension distributions, it was possible to generate a wide variety of mode shapes and some variation in the frequency spectrum. Although many modes were reminiscent of the measured mode shapes, none could compare point by point with the empirical modes. The primary discrepancy was the presence of the increased edge flapping which was not observed in the experimental modes. Figure 4.3-50 describes a typical higher order mode obtained using a non-uniform tension distribution with unequal LEM tensions and a nominal blanket rigidity.

4.3.4.3.4 Effect of Increased Rigidity Due to Edge Curl

In an attempt to remove the excessive edge flapping noted above, the dynamic model was further extended to allow for increased bending rigidity due to initial blanket curvature. Calculations based on observed edge curl indicate that the blanket's effective stiffness could easily have been 50 times greater than that calculated from the rigidity of the blanket's material. Since this increased rigidity does not effect the bending about a longitudinal axis, the model allowed for different rigidities with respect to the two bending axes.

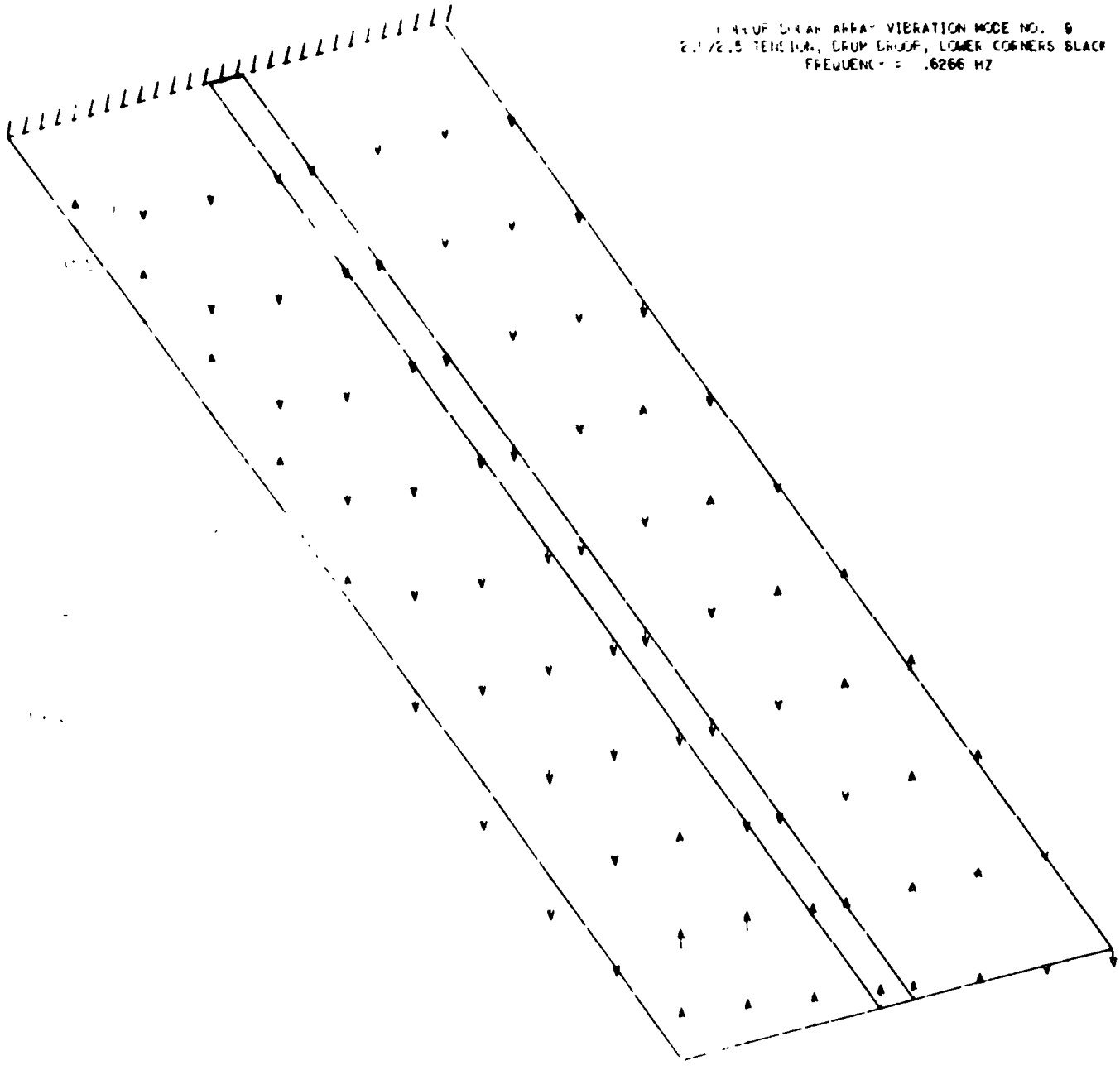

Figure 4.3-50. Typical Higher Order Mode with Non-Uniform Unequal Tension Distribution

Tests conducted with a factor of fifty increase in the bending rigidity about the transverse (Y) axis showed some decrease in the amount of edge flapping. However, addition of increased rigidity did not lead to modal responses which correlated significantly better with the experimental modes.

4.3.4.4 Conclusions

At least two major conclusions can be drawn from the above analysis. One is concerned with the sensitivity of the deployed modes to the blanket's stiffness and tension distribution, and the other is related to the current modal prediction capability.

The first conclusion to be drawn is that the array's lowest symmetric and antisymmetric resonant frequencies are rather insensitive to large variations in the blanket's bending rigidity and tension uniformity, whereas the higher order modes are very sensitive to both the bending rigidity and the tension uniformity. This indicates that, although the primary resonances should be quite predictable, the higher order resonances will be generally dependent on a number of unknown and uncertain parameters such as the blanket's tension distribution, the NEGATOR spring torque, and the blanket's bending rigidity. Since all of these parameters may vary with both time and temperature, it is doubtful whether the higher order modes can be predicted with confidence, even with an exact mathematical model. It is difficult to predict the state of the structure with confidence.

Adding to the problem, of course, is the accuracy of the mathematical representation of the structural properties of the array. Although the finite element model used in this analysis appears to accurately predict the primary resonances, certain inconsistencies arise when comparing the high order modes with the

experimentally measured ones. The primary difference is the edge flapping which appears in the analytical modes when the outer edges of the blankets are loosened as required to match the first torsion frequency. Intuitively the edge flapping behavior is expected, and it is the experimentally observed behavior which seems inconsistent.

As a manner of checking the accuracy of the finite element analysis, the blanket substructure model was used to predict the first mode resonance of a single blanket hanging vertically with the lower end free. Since this represents blanket pendulum motion with no tension at the LEM attachment, its frequency should provide a lower bound for the first torsion mode, which exhibits the same pendulum motion, but has an additional tension applied to the lower edge.

As expected, the free blanket frequency predicted by the analysis agreed with the array's first torsion frequency obtained using zero LEM tension. In addition, it agreed within 2% with the free blanket frequency determined experimentally during the modal testing. Since the experimentally measured torsion frequency was nearly 20% lower than the free blanket frequency, there is considerable justification for assuming the presence of a non-uniform tension distribution. Small errors in representing the array's mass properties, for example, could not lead to the 30% lower frequency obtained experimentally for the first torsion mode.

Considering the above, one must thus conclude that although certain inconsistencies exist, the current finite element model appears to provide adequate prediction capability for the array's primary resonances. However, the capability and desirability of predicting the higher order modes is uncertain at this time.

Increased accuracy might be obtained in future analyses by including complete in-plane stress information in the blanket stiffness element and by using an in-plane equilibrium analysis to determine the initial stress distribution.

4.3.5 IN-PLANE RESULTS DISCUSSION*

4.3.5.1 Introduction

The rollup array modal testing program determined the existence of a first in plane resonant mode at a frequency of about 1.0 Hz with the array deployed vertically downward 26 feet in the one-g field test environment. In this mode the array appeared to swing about the root of the boom with essentially rigid body motion. Observations made during the test also indicated that the drums participate in the mode by rolling in and out and by flexing about the center support structure. Although the significance of this participation is not known, tests under ambient conditions (which resulted in the same resonant frequency) indicated that the drums roll approximately 1/8" (zero to peak) and bend downward approximately 1/16" (peak to peak) when the array has a 1.3" (peak to peak) displacement at span position 7 (18 feet down).

The following section describes the results of an attempt to correlate this data with the array's known mass and stiffness properties. Although a reasonable correlation was found, the analysis primarily serves to define an area requiring future work.

---

* This section written by Dr. R. Ross, Jet Propulsion Laboratory.

4.3.5.2 In-Plane Stiffness Analysis

As a first attempt to understand the in-plane stiffness of the array, a small 2 foot high model was constructed with the general features of the actual rollup array. Although the model made no attempt to match the stiffnesses of the array, its correct geometry and moveable drums allowed the characteristics of the in-plane motion to be observed.

The highly non-linear motion indicated by the model is shown in Figure 4.3-51. When the array swings to the right as shown, the high longitudinal rigidity of the boom, the rolling capability of the left drum, and the inability of the blankets to resist compression loads causes the array to pivot about the root of the boom with essentially rigid body motion.

Although the left drum rolls out as expected, the right drum does not move because the length determining part of the right blanket moves parallel to the drum axis. As a result the tension distribution at the left drum shifts to the outside edge and that at the right drum shifts to its inside edge. Since the drums supply a constant force to each blanket, this tension shift applied a constant restoring torque to the array once it has fully developed.

The motion required to reach the shifted tension state is dependent on the stiffness of the blanket and drum assemblies. If all structural elements are rigid, it is reached immediately, but with a typical array it is reached only after the drums have flexed with the changing moments and after the blankets have adjusted to the new tension distribution. If we consider the blankets of the RA250 as rigid, then the 0.65" peak displacement measured at the 18' span position implies a total drum

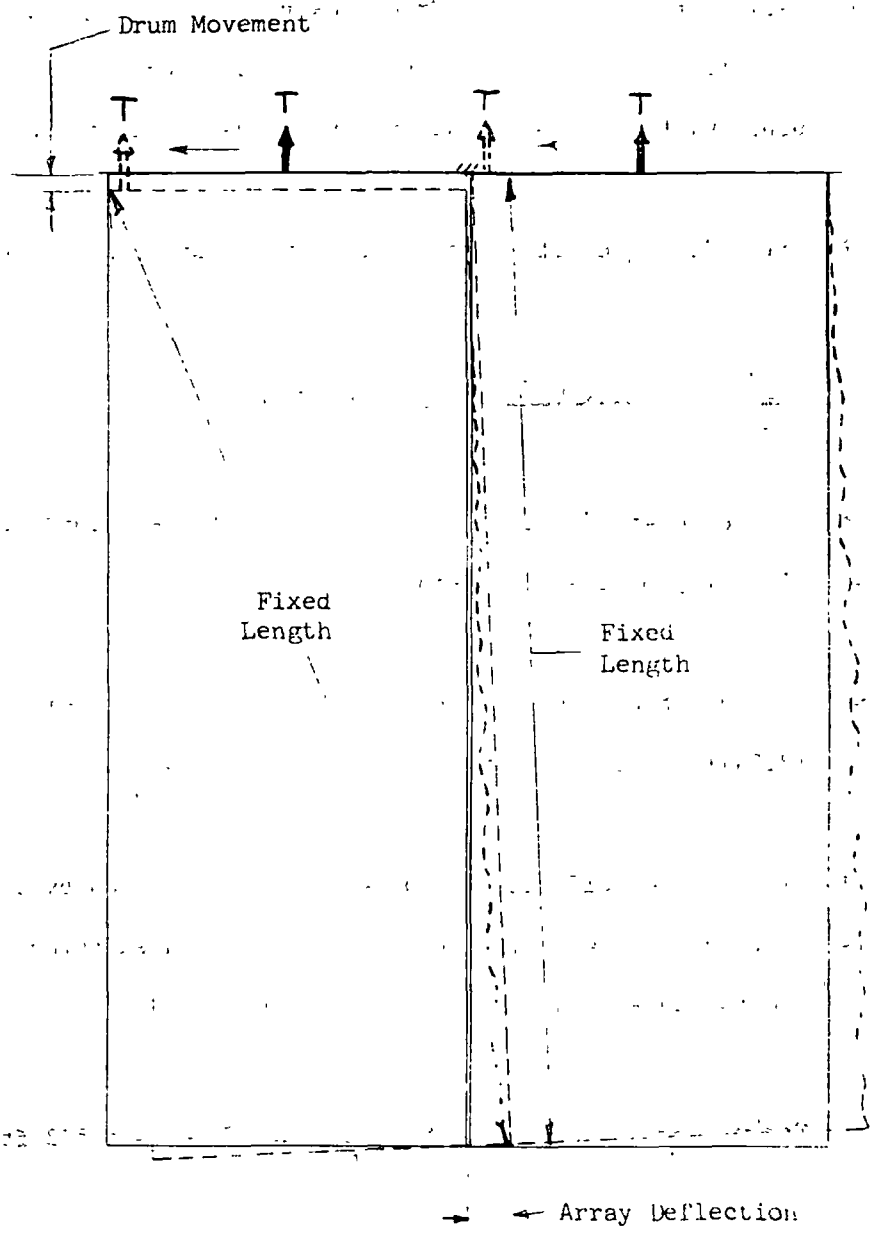

Figure 4.3-51. In-Plane Deflection Mode

tip movement of 0.65" (4.0/18.0) = .145". Since this correlates well with the observed drum motion, it appears the blanket elongation probably played a limited role in the observed mode, while the drum flexing and rolling probably played the dominant role. With this assumption, an attempt was made to correlate the observed resonant frequency with the known mass and stiffness properties of the array.

Assuming the array is rigid, its first mode inertia can be approximated by

$$I = \frac{Wl^2}{3g} = \frac{44\ (26)^2}{3 \times 32.2} = 308\ \text{ft-lb/sec}^2$$

where the effective weight (W) is defined in terms of the array's deployed length (l) and half width (w) by the expression

$$W = 2wl\ (\text{Blanket Density}) + 1\ (\text{Boom Density}) + 3\ (\text{LEM Weight})$$
$$= 2\ (3.84)(26)(.1785) + 26\ (.195) + 3(1.0) = 44\ \text{lbs.}$$

The effective first mode stiffness of the array is determined by a combination of mechanisms acting in parallel. With the rigid body assumption the effective stiffness due to the one-g gravity force can be described as

$$K_g = \frac{\text{Restoring Torque}}{\text{Angle}\ (\theta)} = \frac{W\ l \sin}{2\ \theta} = \frac{W\ l}{2} = 572\ \text{ft-lb/rad}$$

Added to this is the bending stiffness (K_b) of the boom. Since the effect of the gravity induced tension load is included in K_g only the reduced stiffness due to the 4 pound compression is included. Thus

$$K_b = \frac{\text{Restoring Torque}}{\text{Deflection Angle}}$$

$$= \frac{Fl}{\delta/l} = \frac{Fl^2}{\delta}$$

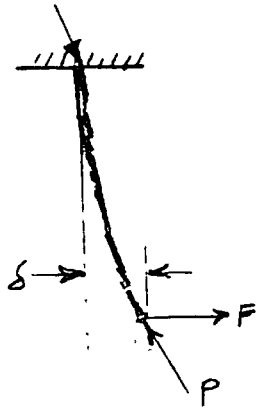

But for a cantilevered column loaded as shown

$$F/\delta \approx \frac{3EI}{l^3} - \frac{3P}{10}$$

Thus

$$K_b = \frac{3EI}{l} - \frac{3Pl}{10} = \left[\frac{3(2390)}{26} - \frac{3(4)(26)}{10}\right] = 245 \ \frac{\text{ft/lb}}{\text{rad}}$$

Before analyzing the stiffness due to drum flexing, consider the stiffness required for the 1.0 Hz measured first mode frequency. Assuming the inertia calculated above, the required stiffness (K_R) is obtained by noting that

$$2\pi f = \sqrt{\frac{K_R}{I}}$$

and thus

$$K_R = 4\pi^2 f^2 I = 4\pi^2(1.0)^2(308) = 12000 \ \frac{\text{ft-lb}}{\text{rad}}$$

As expected, this value is significantly higher than the previously calculated stiffnesses which correspond to natural frequencies approximating the first out of plane resonances with frequencies around 0.2 Hz. The additional stiffness of over 11,000 ft-lb/rad must be provided by the drum assembly.

Referring to Figure 4.3-52, the effective stiffness (K_d) due to the shifting tension distribution combined with the drum bending can be approximated by

$$K_d = \frac{\Delta \text{ Moment}}{\Delta \text{ Angle}} = \frac{TW}{\theta}$$

where

$$\theta = \frac{\text{Change in drum moment}}{\text{Stiffness of drum Assembly}} = \frac{T\ (R-r)}{K}$$

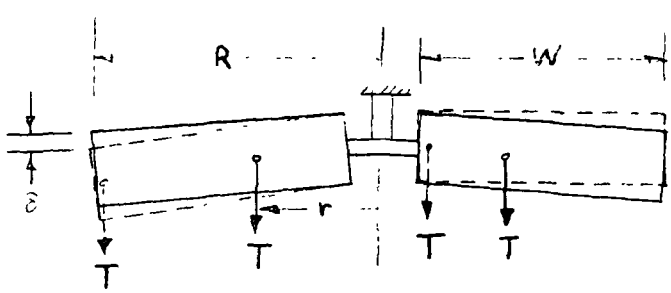

Figure 4.3-52. Drum Flexing Caused by In-Plane Displacement

The parameter K ≈ 33,000 ft-lb/radian is the measured stiffness of the drum cantilevered from the center support. (See Reference 1-6) Thus

$$K_d = \frac{TWK}{T\,(R-r)} = \frac{WK}{(R-r)}$$

If there was no drum droop so that the original tension distribution was uniform, then (R-r) = w/2 and

$$K_d = 2K = 66{,}000 \ \frac{\text{ft-lb}}{\text{rad}}$$

However, if drum droop resulted in (R-r) = 3w/4, then

$$K_d = 4/3K = 44{,}000 \ \frac{\text{ft-lb}}{\text{rad}}$$

Although both of these figures are significantly higher than the required stiffness of about 11,000 ft-lb/radian, recall that no drum rotation was assumed to occur during the tension redistribution. If the observed 4 to 1 ratio of rolling to bending is typical, then the effective stiffness is actually a quarter of the above values because the array rotates through an angle four times that of the drum flexure. Thus, with the observed rolling to bending ratio, the effective stiffness of the drum assembly correlates reasonably well with the required stiffness for the measured first mode response.

4.3.5.3 Conclusions

In the light of the above study, it is clear that the in-plane properties of the array are considerably more complex than the out-of-plane properties. For example,

the in-plane stiffness appears to be a non-linear function of the stiffness of the drums, of the original tension distribution, and of the manner in which the distribution changes with increasing deflections. Added to this is the unknown correlation between drum roll and drum flexing which is probably dependent on the amount of blanket tension and on the uniformity of its distribution.

Thus, although a reasonable correlation was found between the observed frequency, the observed array motion, and known stiffness properties, the mathematical model does not exist at this time for making general predictions about the in-plane behavior of the array under conditions different from those present during the modal tests. Therefore, the above analysis serves primarily to define an area requiring further work.

4.3.6 SUMMARY OF PRETEST ANALYSIS

Prior to the tests the mathematical models of the deployed rollup array were exercised to predict test results, generate data for test planning, and provide a basis for comparison with test results. Predicted frequency and mode shapes have been incorporated in the presentation of test results in this section. Response plots such as are shown in Figures 4.3-53 and 4.3-54 were generated. Figure 4.3-55 is a tracing of the measured response in a sweep through the first bending mode. Note the good agreement between experimental and analytical results. Both the excitation level and the damping values are different for the two types of data.

Because the damping levels were not known in advance two values were used in the analyses. An example of the results is shown in Figure 4.3-56. The mathematical

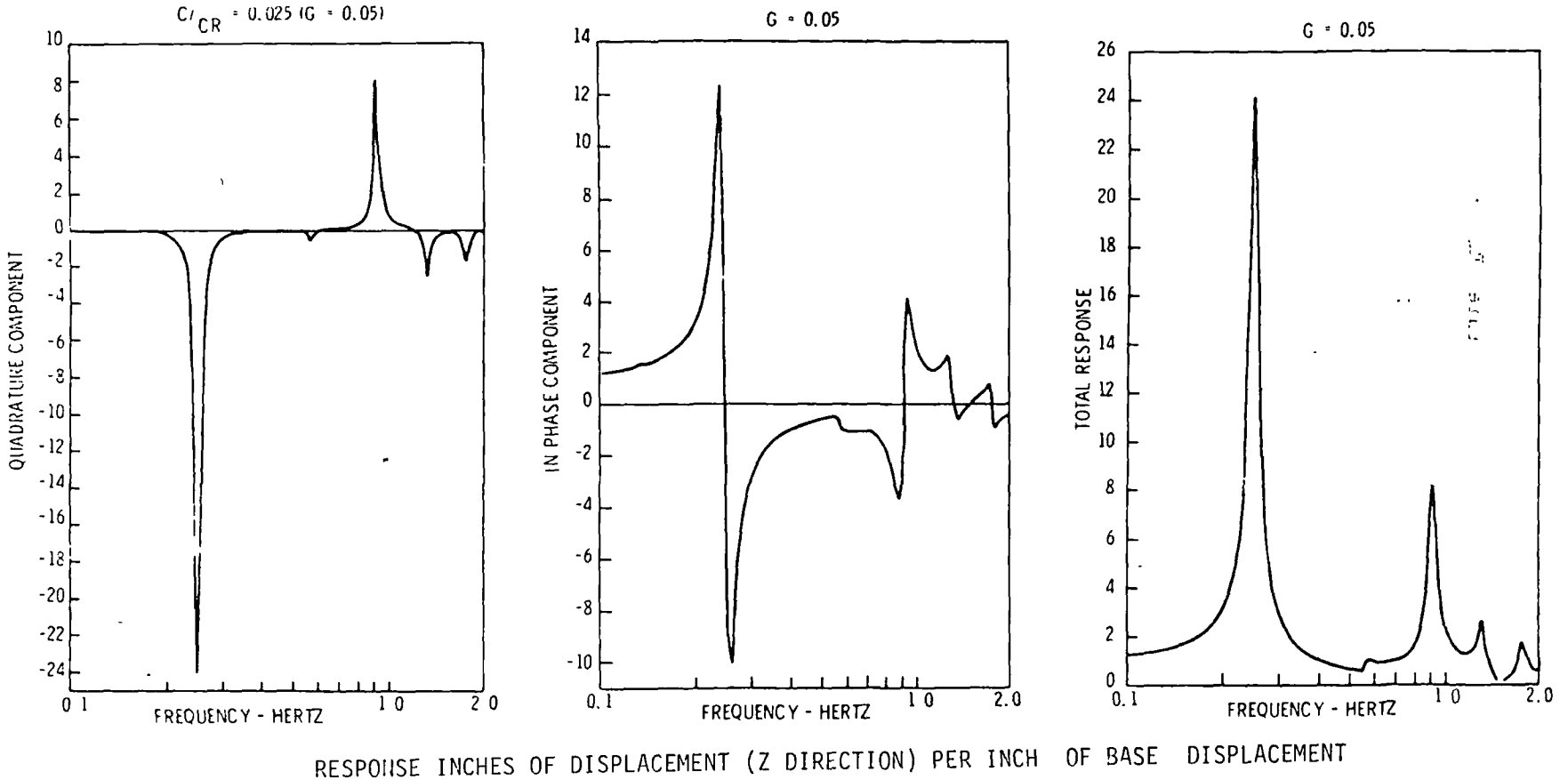

Figure 4.3.53. Predicted Response at Outboard Edge of Blanket (80% Span) Out-of-Plane Symmetric Excitation

Quadrature Response

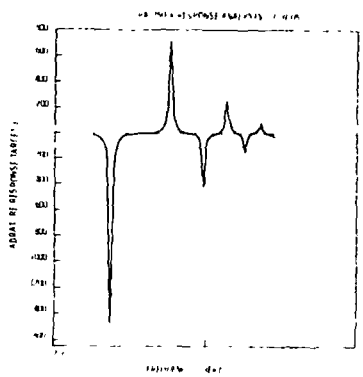

Total Response

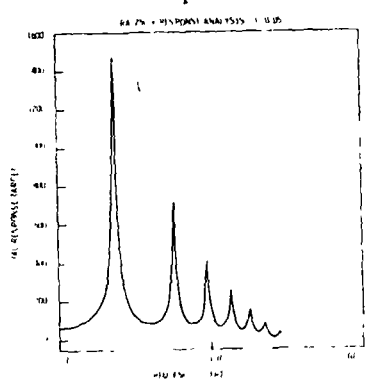

In-Phase Res ponse

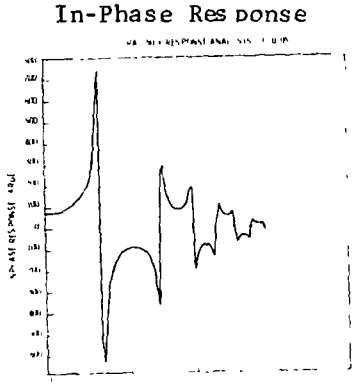

Response - Inches of Target Displacement (Z Direction)
Per Unit Radian Rotation at Base

Figure 4.3-54. Predicted Response at Outboard End Of Leading Edge Member (Torsional Excitation)

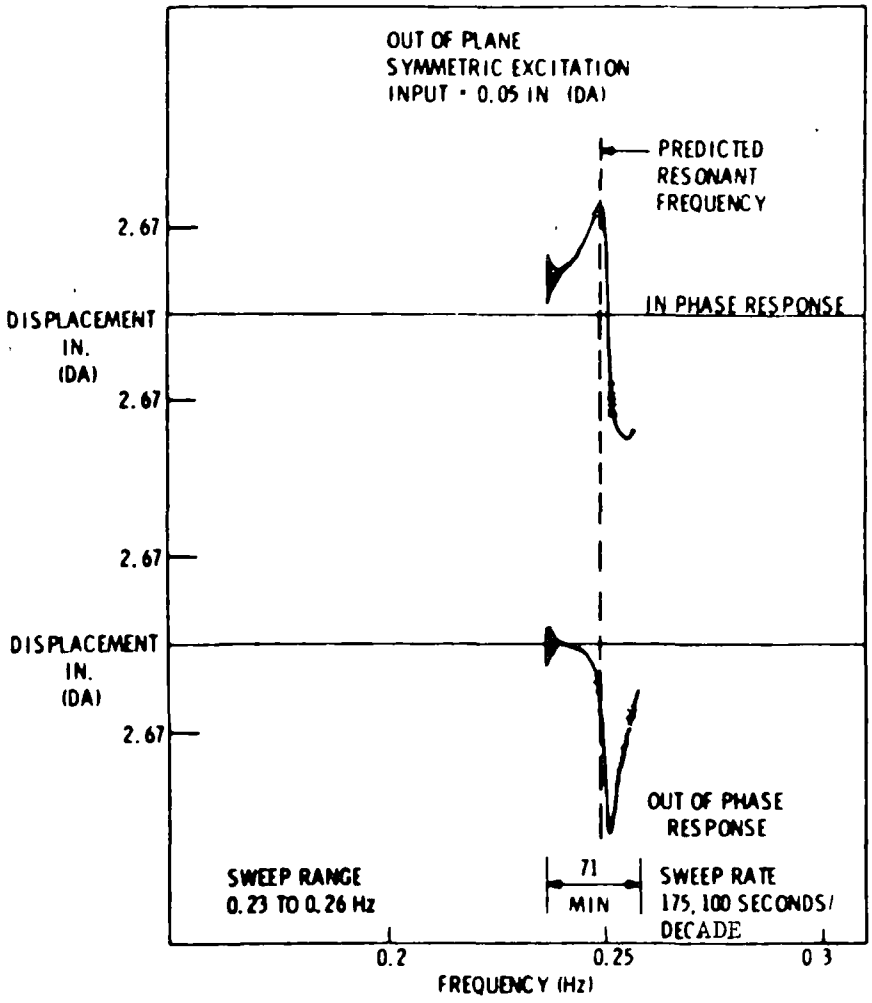

Figure 4.3.55. Results of Narrow Band Frequency Sweep

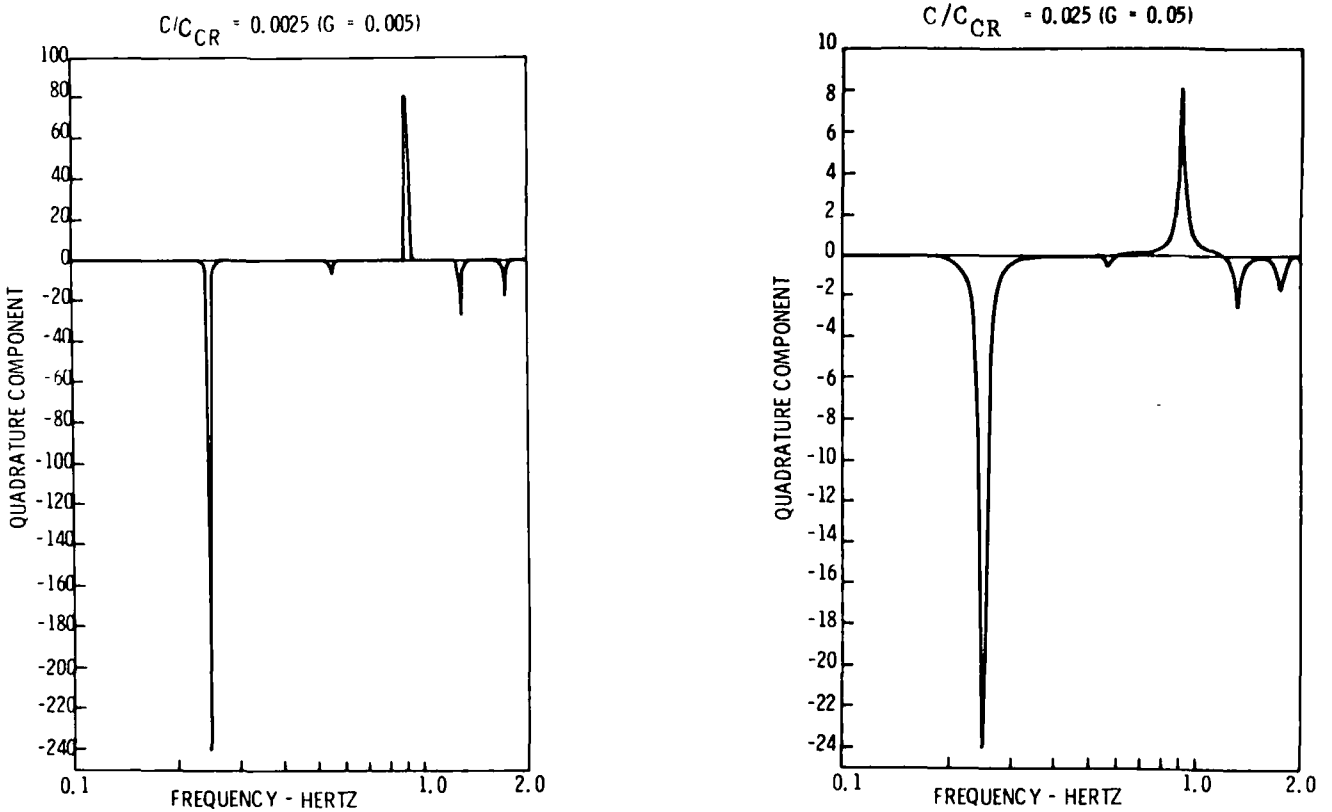

Predicted Response at Outboard Edge of Blanket
80% Span
Out- of - Plane Symmetric Excitation

Figure 4.3-56. Effect of Damping on Response

model is linear and so the peak amplitudes vary as the inverse of the damping ratio. Note how narrow in frequency the response peaks are, particularly for the lower damping value. Excitation of these modes occurs in a very narrow frequency band. This characteristic may be important in avoiding problems with the interaction of large solar arrays with attitude control system.

4.4 PYROTECHNIC SHOCK TEST

4.4.1 INTRODUCTION

The Pyrotechnic Shock Test was conducted in the Structural Dynamics Laboratory where the stowed configuration array was subjected to three shocks resulting from actuation of explosive nut assemblies. In each case of pyro uncaging, the array suffered no visible or operational damage and post test inspection (Health Check #3, Ref. Section 4.2) disclosed no gross system degradation.

4.4.2 TEST OBJECTIVES

The prime objective of this test was to demonstrate array structural and functional integrity following exposure to shock loads induced by firing the array uncaging pyrotechnic nut assemblies, P/N 47C218327.

Secondary objectives were:

1. To define shock spectra at array mounting interface surfaces due to array pyrotechnics.
2. To determine the necessity for pyroshock and shaped pulse, or spectra shock testing, of the array subsystem or components and appropriate levels for such tests.

4.4.3 RESULTS AND CONCLUSIONS

4.4.3.1 Results

Table 4.4-1 presents a tabulation of peak acceleration of G loads experienced by the array and array components due to firing of separation (uncaging) nuts. Figure 4.4-1 portrays the coordinate system used. The highest accelerations were

Table 4.4-1 Instrumentation Locations & Tabulated Response

Accel. No. & Sensitivity Direction	Location ***	Coordinates X Inches	Y Inches	Z Inches	Gs (o-p) Firing No. 1	2	3
	Pyro Nut	-4.75	+51	+3.75	*	*	*
330X	Fixture I.F. with Caging Arm, -Y	-8.50	-51	+2.50	1880	*	*
331Y	Fixture I.F. with Caging Arm, -Y				3420	5850	5000
332Z	Fixture I.F. with Caging Arm, -Y				2000	*	*
333X	Caging Arm Rotary Lock Pin, -Y	-2.50	-51	+2.50	Sat.	*	2500
334Y	Caging Arm Rotary Lock Pin, -Y				4040	*	*
335Z	Caging Arm Rotary Lock Pin, -Y				3000	*	*
308Z	Caging Arm LEM Plug, -Y	+7	-47	+4	1710	*	*
310Z	Drum, 100% Span, = 90°, -Y	0	-50	-4	*	1350	1380
311Z	Blanket 100% Span, = 90°, -Y	0	-49	-4	*	60	*
322X	Bearing Support, -Y	-1.25	- 8	0	*	in Noise	86
322Y	Bearing Support, -Y				*	93	*
322Z	Bearing Support, -Y				*	115	*
323X	Drum, Zero Span, = 90°, -Y	+4	- 3	0	*	*	128
323Z	Drum, Zero Span, = 0°, -Y	0	- 3	-4	*	120	*
306Z	LEM At BiStem Attachment	+7	- 2	+4.50	*	*	817
304X	BiStem Motor	+4	0	+6	*	62	*
304Z	BiStem Motor				*	60	*
341Y	Fixture I.F. Center Support				*	*	150
303Z	Fixture I.F. Center Support				*	119	*
336X	Fixture I.F. Caging Arm, +Y	-8.50	-48	+4	2060	*	*
337Y	Fixture I.F. Caging Arm, +Y				1880	*	*
338X	Caging Arm Rotary Lock Pin,+Y	-2.50	+51	+2.50	Sat	*	6000

Table 4.4-1 Instrumentation Locations & Tabulated Response (Cont.)

Accel. No. & Sensitivity Direction	Location ***	Coordinates X Inches	Y Inches	Z Inches	Gs o-p Firing No. 1	2	3
339Y	Caging Arm Rotary Lock Pin, +Y				Sat	*	4880

* Date not recorded during this run because of limited number of channels in data system.

** Coordinate origin is on drum rotational axis and intersects center of stowed BiStem tip. See Figure 4.4-1.

Abbreviations & Notations

IF - Interface

Sat - Recording setting low, charge amplifier output

In Noise - Low Signal Level - No Useable Data

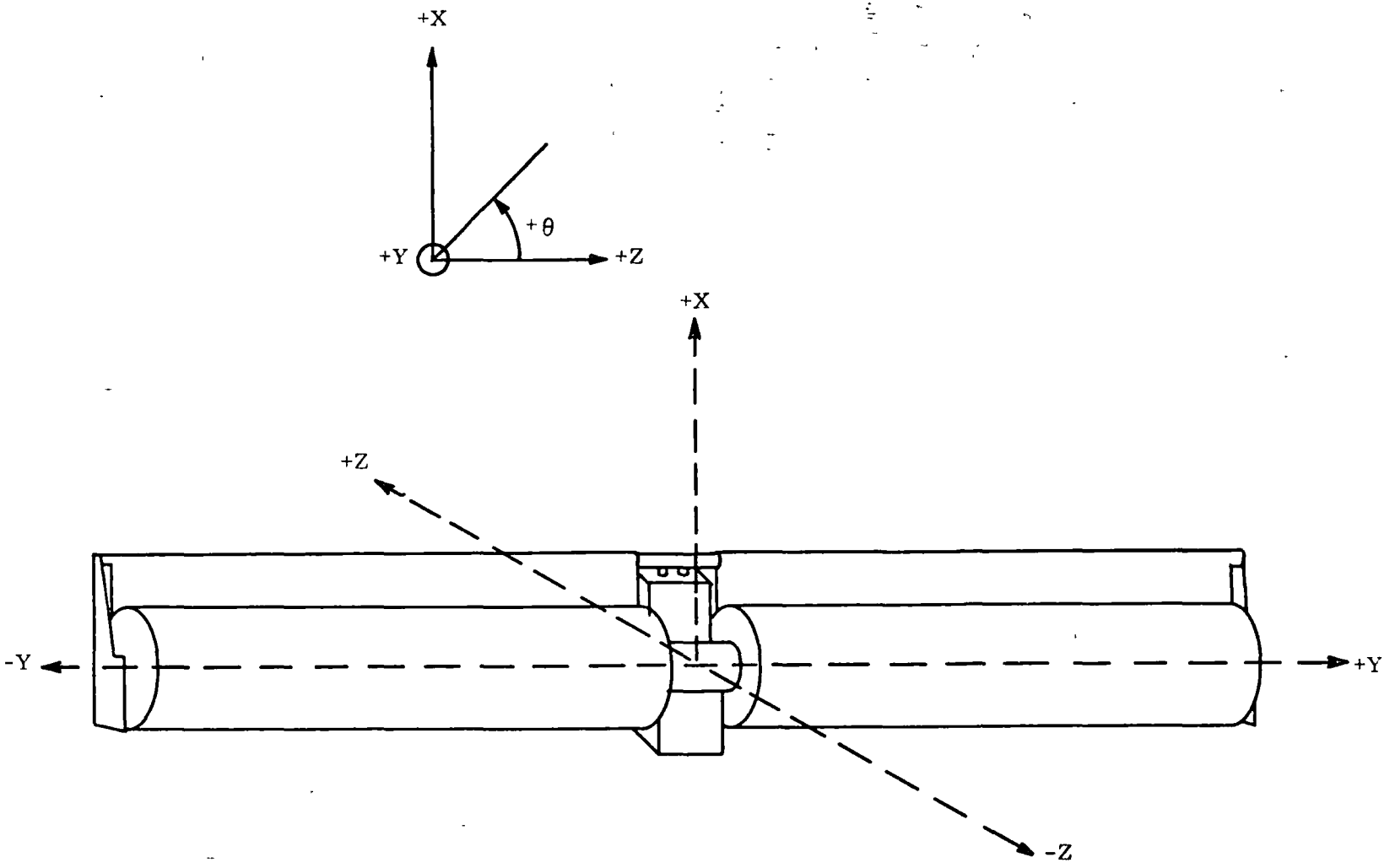

Figure 4.4-1. Coordinate System for Use in Shock Data Discussion

measured at accelerometers on the caging arms four inches from a pyrotechnic nut assembly. Here acceleration levels of 6,000 and 2,500 G (o-p) were noted. These levels were approximately equal to shock levels measured on the array handling frame at its interface with the outboard end supports.

The shock level rapidly decreased in magnitude with distance from the shock source. Shock levels in the drums at 100% span (near pyrotechnics) were 1365 G (o-p); and at 0% span, near the center support, dropped to 124 G (o-p). The blanket outer wrap, (about 4 in. from the caging arm interface), the center support structure and drum bearing support shaft (approximately 50 inches from the caging arms) experienced acceleration levels of 125 G (o-p) or less. This attenuation results from the flexibility across the blanket wraps and the distance between the shock source and the response points monitored in the array center structure.

Inspection of the array disclosed no damage, and no anomalies occurred in subsequent operations.

This test has demonstrated the following:

The RA250 Solar Array shock loads induced by firing of pyrotechnic uncaging nuts had no deleterious effects upon the array assembly.

The shock loads resulting from firing of array pyrotechnic nut assemblies results in acceleration loads comparable to those induced in spacecraft structures by firing of spacecraft separation band pyrotechnic release devices (Reference Figure 4.4-2).

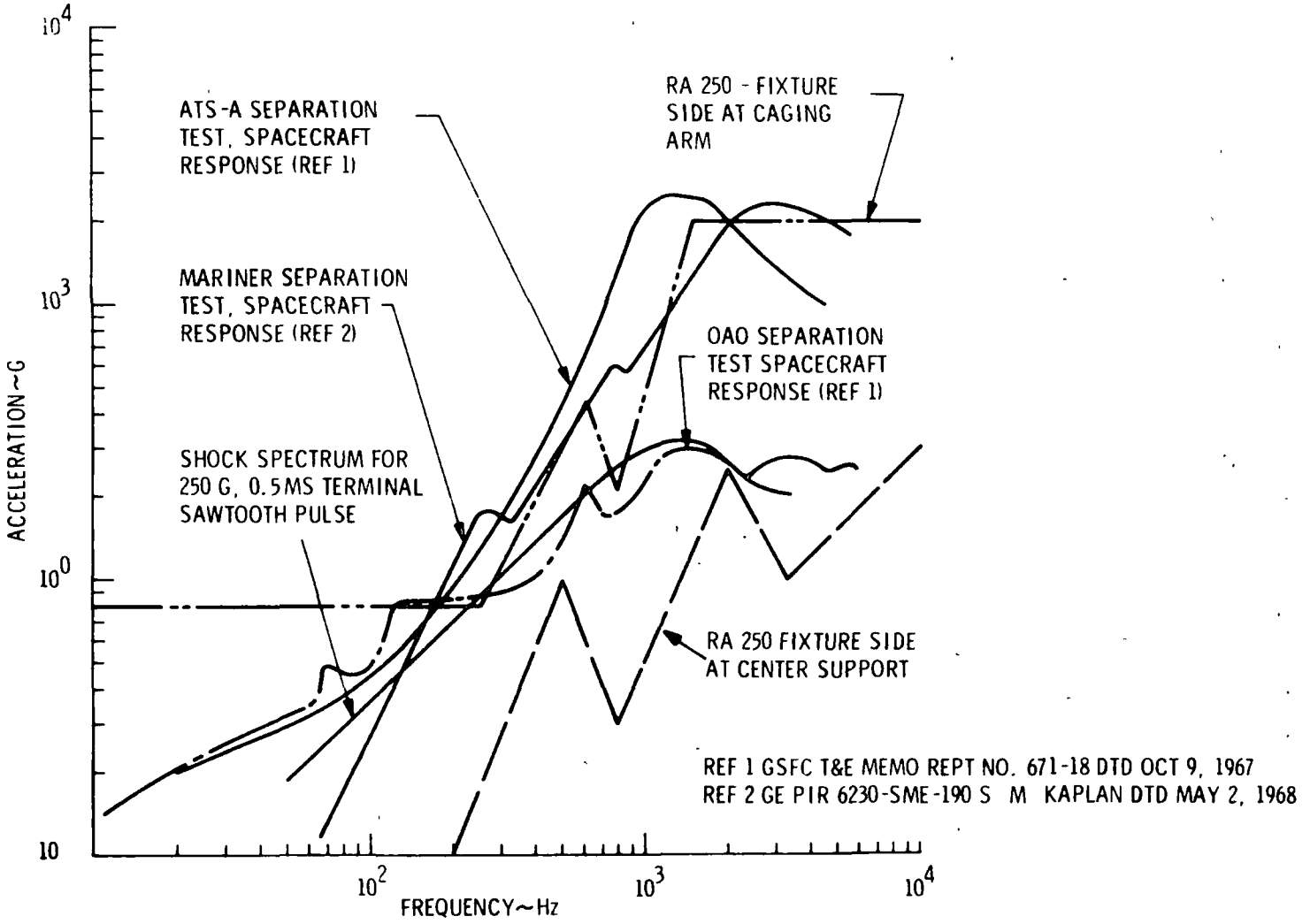

Figure 4.4-2 Comparison of Various Spacecraft Separation Shock Spectra with the RA250 Specification and Realized Shock Spectra

At the outboard end supports, the shock spectra of array uncaging pyros is higher than that resulting from the 250 G, 0.5 msec saw tooth shock defined in Reference 1-2 for array shock testing. (see Figure 4.4-3) (Reference Figures 4.4-4, 4.4-5, 4.4-6 & 4.4-7) In the center support region the shock spectra from the uncaging pyros is equivalent to the spectrum of the sawtooth shock above 2000 Hz and approximately 50% of the sawtooth shock spectrum below 2000 Hz.

The use of Teflon pipe tape improves the squib installation. See paragraph 4.4.4.3.

4.4.3.2 Conclusions

Mechanical shock testing (250 G, .5 msec saw tooth pulse input) and pyro shock testing are not needed in a flight qualification program or for acceptance testing of rollup solar arrays of this configuration. The shock levels transmitted to the solar array blankets are low and this type of testing is not necessary in development programs for blankets.

Shock testing of array components is not required because the transmitted shock levels are low.

A spacecraft pyro shock test, (firing array uncaging pyrotechnics) should be required in the system tests of any vehicle incorporating a light weight array.

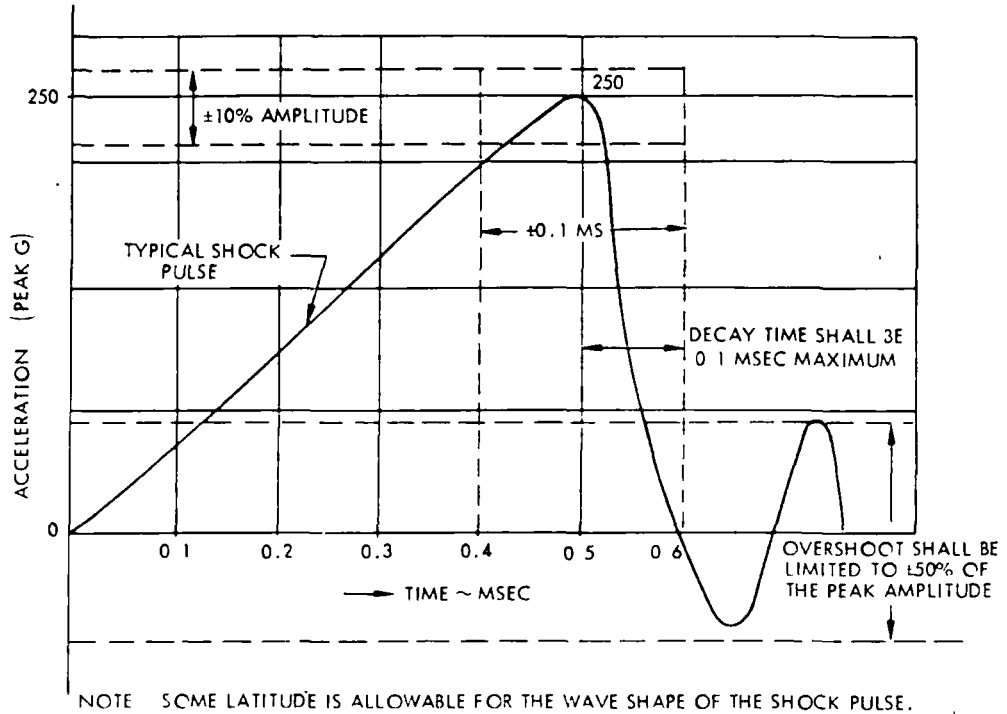

NOTE SOME LATITUDE IS ALLOWABLE FOR THE WAVE SHAPE OF THE SHOCK PULSE. HOWEVER, IT IS DESIRABLE THAT THE SHAPE CONFORM TO THAT OF A TERMINAL PEAK SAWTOOTH AS NEAR AS PRACTICAL.

Figure 4.4-3 Shock Pulse

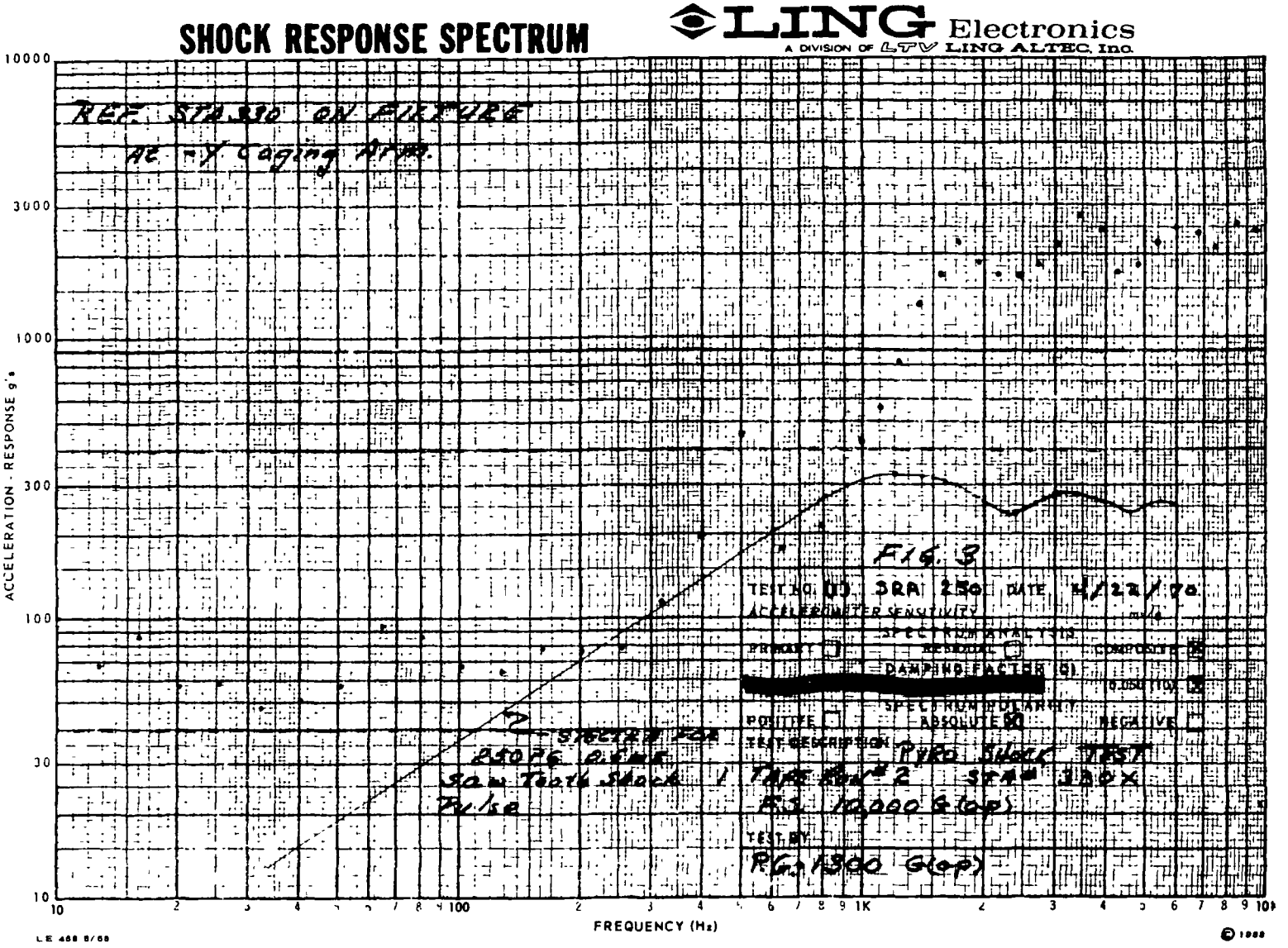

Figure 4.4-4. Comparison of Response Spectrum at Fixture With Sawtooth Shock Pulse

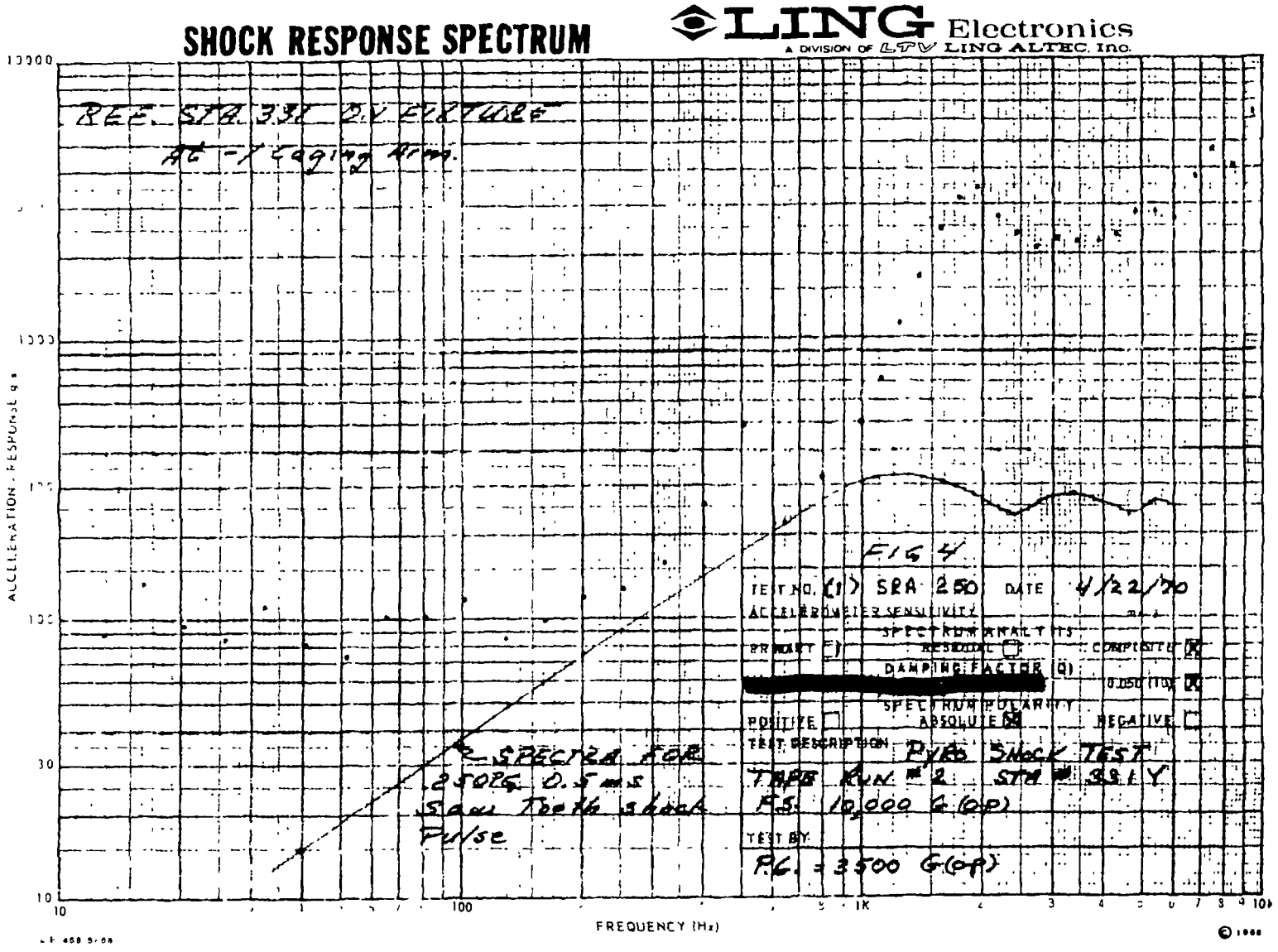

Figure 4. 1-5. Comparison of Response Spectrum at Fixture With Sawtooth Shock Pulse

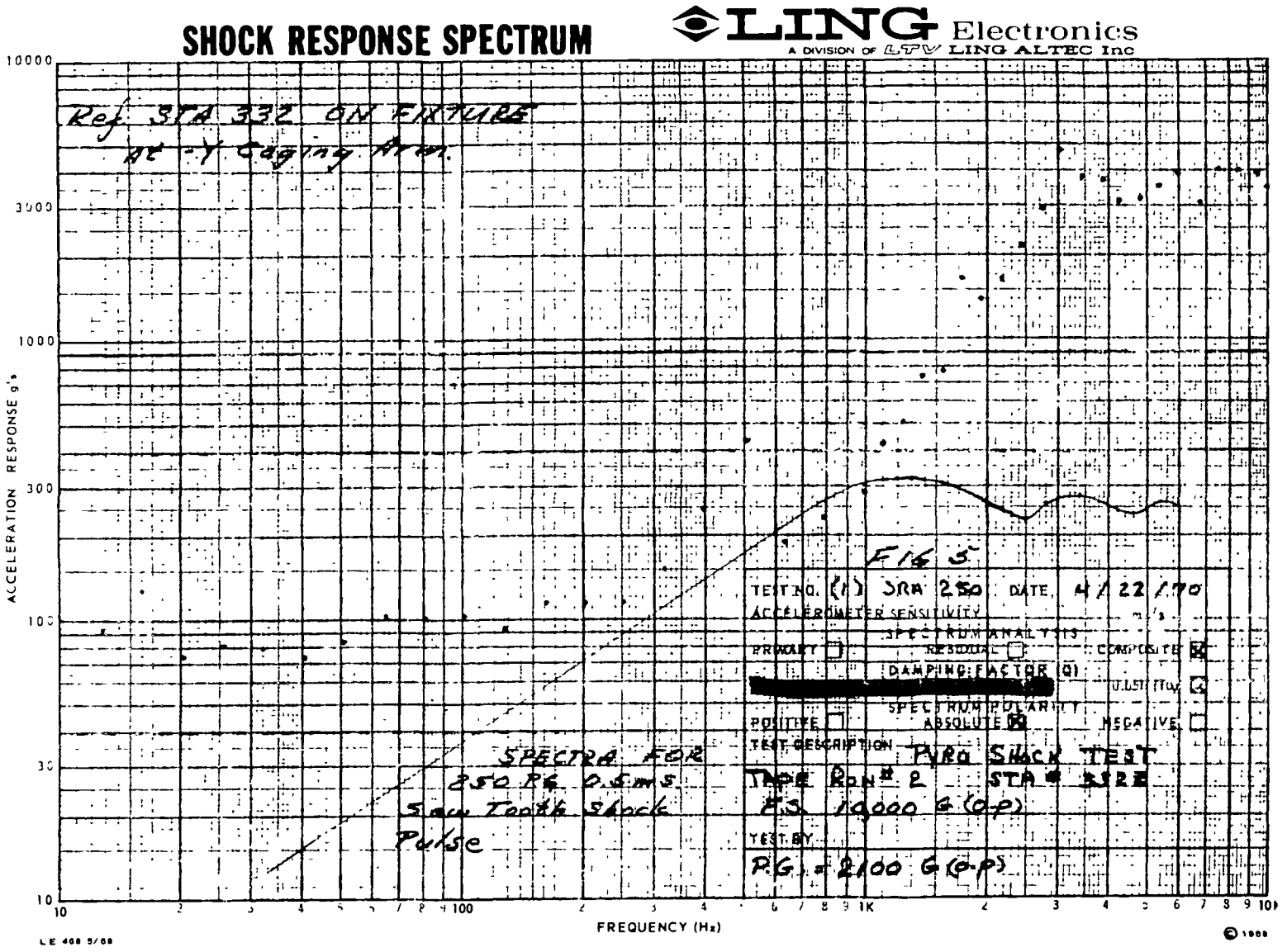

Figure 4.4-6. Comparison of Response Spectrum at Fixture With Sawtooth Shock Pulse

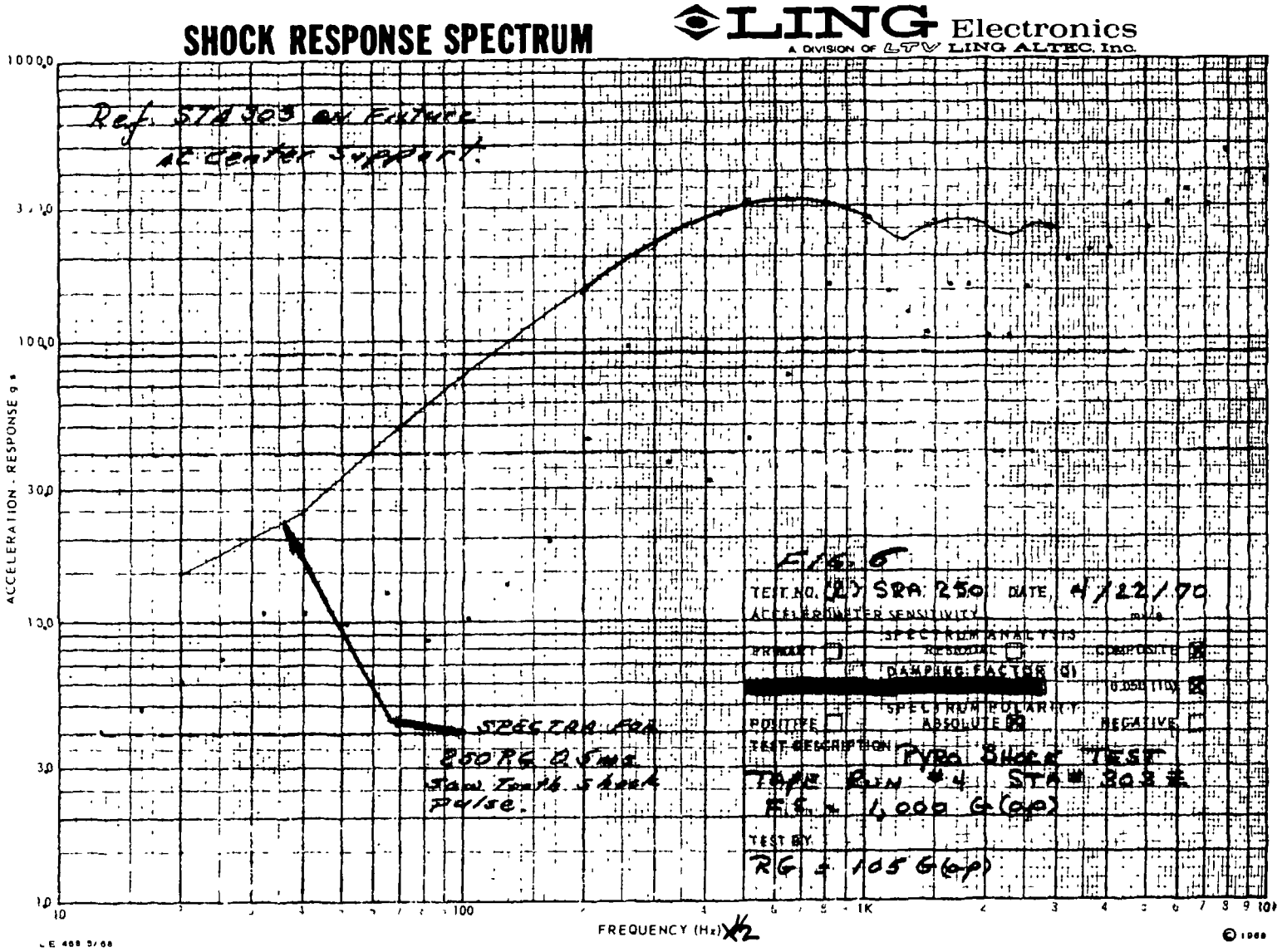

Figure 4.4-7. Comparison of Response Spectrum at Center Support With Sawtooth Shock Pulse

4.4.4 DISCUSSION OF TESTING

4.4.4.1 Instrumentation, Data Recording and Analysis

The array and handling frame were instrumented with 24 shock accelerometers. All accelerometers were piezoelectric type having linear frequency response out to at least 20 KHz. Depending upon installation area, geometry or expected response considerations, one of the following types of accelerometers was installed:

1. CRL Mod. 352-A
2. CRL Mod. 606
3. CEC Mod. 2213
4. CEC Mod. 2224

A block diagram of data recording and playback analysis setups is presented in Figure 4.4-8.

4.4.4.2 Test Setup

The stowed configuration array assembly was bolted to its handling frame which in turn was clamped to the laboratory seismic floor plate. Figure 4.4-9 presents an overall view of the test installation and closeup views of instrumented areas.

4.4.4.3 Operations

The test consisted of three pyro uncaging events with a different patch of 10 accelerometer responses recorded during each firing. Each patch group included station 331Y, Fixture Interface (IF) with -Y caging arm, as a data control signal. Each uncaging was produced by simultaneous actuation of the two separation nut assemblies, each armed with two active squibs. Squib installation procedure in each firing was varied and results are presented in Table 4.4-2.

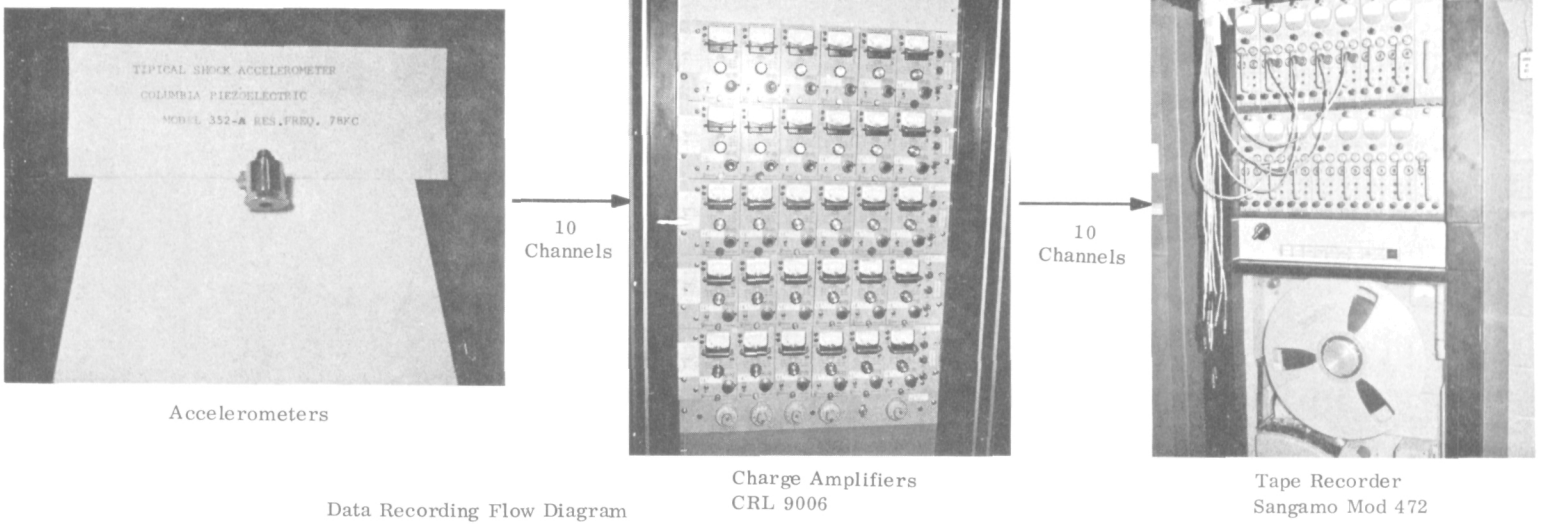

Data Recording Flow Diagram

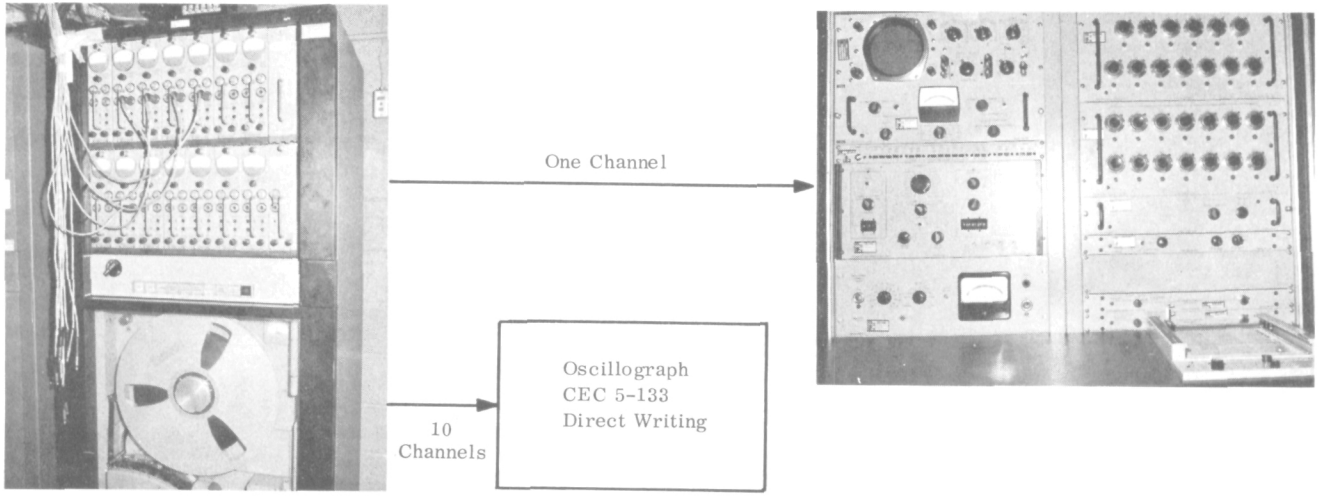

Data Playback Flow Diagram

Figure 4.4-8 Shock Test Data System

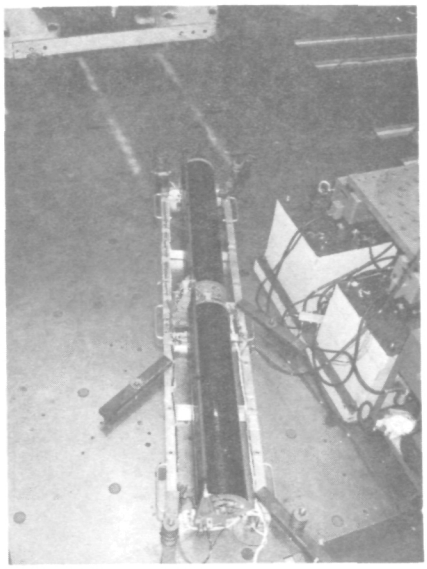

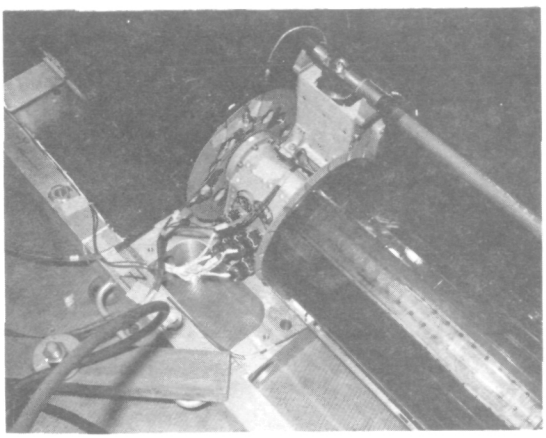

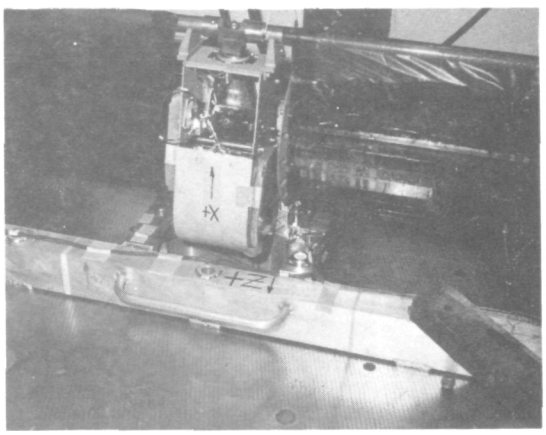

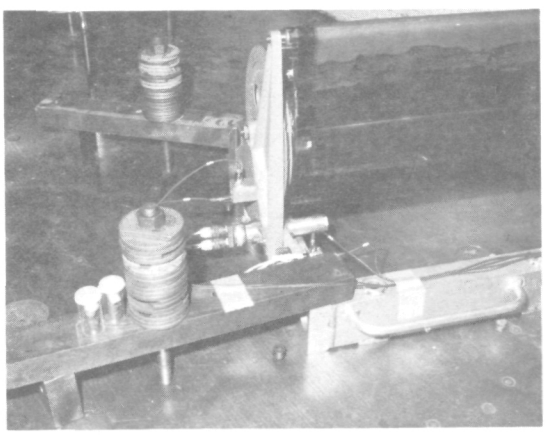

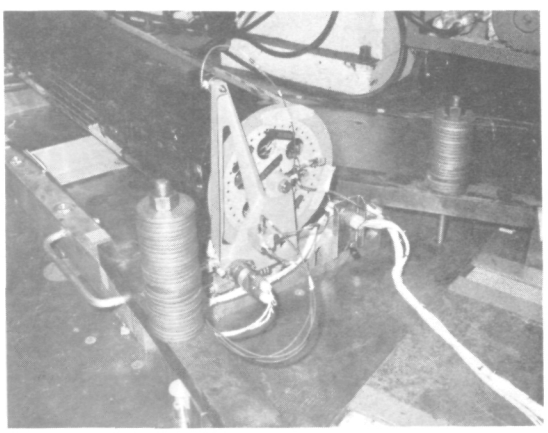

+Y End

-Y End

Figure 4.4-9. Test Set Up

Table 4.4-2 Squib Installation and Results

Firing No.	Installation Method	Results
1	"O" Ring Seal; Squibs Torqued 80 lb-ins.	Heavy contamination of squib port threads by combustion products. "O" Ring deformed, not reuseable.
2	"O" Ring Seal; Teflon pipe tape over last two squib threads; squib torqued 30 lb-ins.	Light combustion products contamination of squib port threads under teflon tape; "O" Ring reuseable.
3	No "O" Ring; Teflon pipe tape over all squib threads; squibs torqued 80 lb-ins.	Minimal contamination of squib port threads. Nut cleaning simplified if to be reused.

Inspection of tabulated results of Table 4.4-1 indicate the following:

a. Shock accelerations induced by the plus and minus pitch pyro-nut assemblies were of the same intensity in the X and Z axes. (1,900G ± 200G stations 330X, 331Y, 336X, 337Y)

b. Shock responses between successive firings were similar.

c. The two firings employing teflon pipe tape to seal squibs in the nut assemblies yielded a higher shock input. (Station 331Y firings 1, 2, 3).

Data was reduced to shock spectrum plots and oscillograph time traces. Levels listed in Table 4.4-1 were taken from oscillographs, not included in this report, while peak responses listed on spectra plots were read from the analyzer peak g meter. Oscillograph shock traces indicate that the peak response occured at approximately 18,000 Hz.

4.4.4.4 Detailed Results

Shock spectra for selected data channels are given in Figures 4.4-10 and 4.4-11. These data are typical for transducers with high responses.

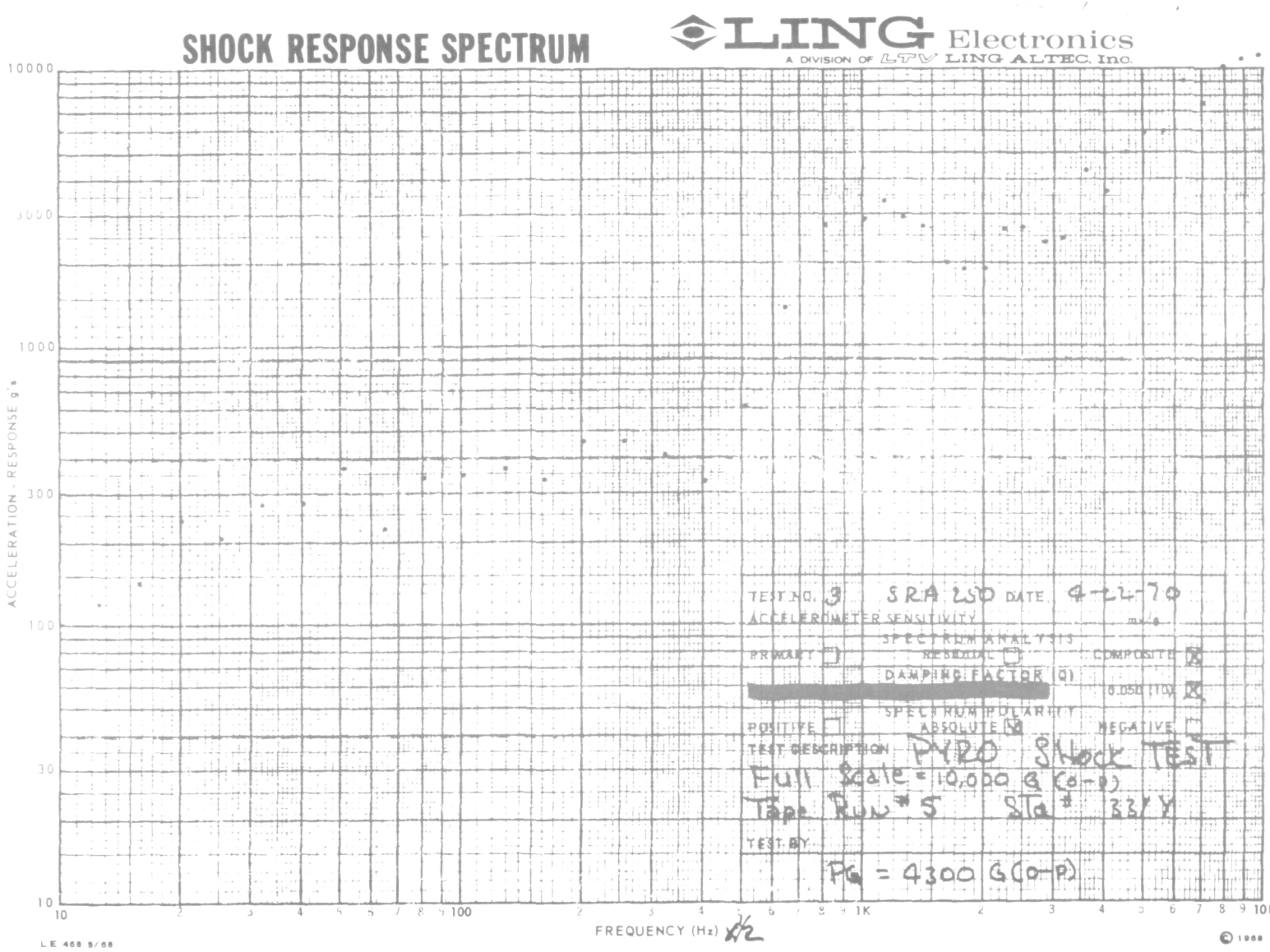

Figure 4.4-10. Shock Response Spectrum at Fixture (331Y)

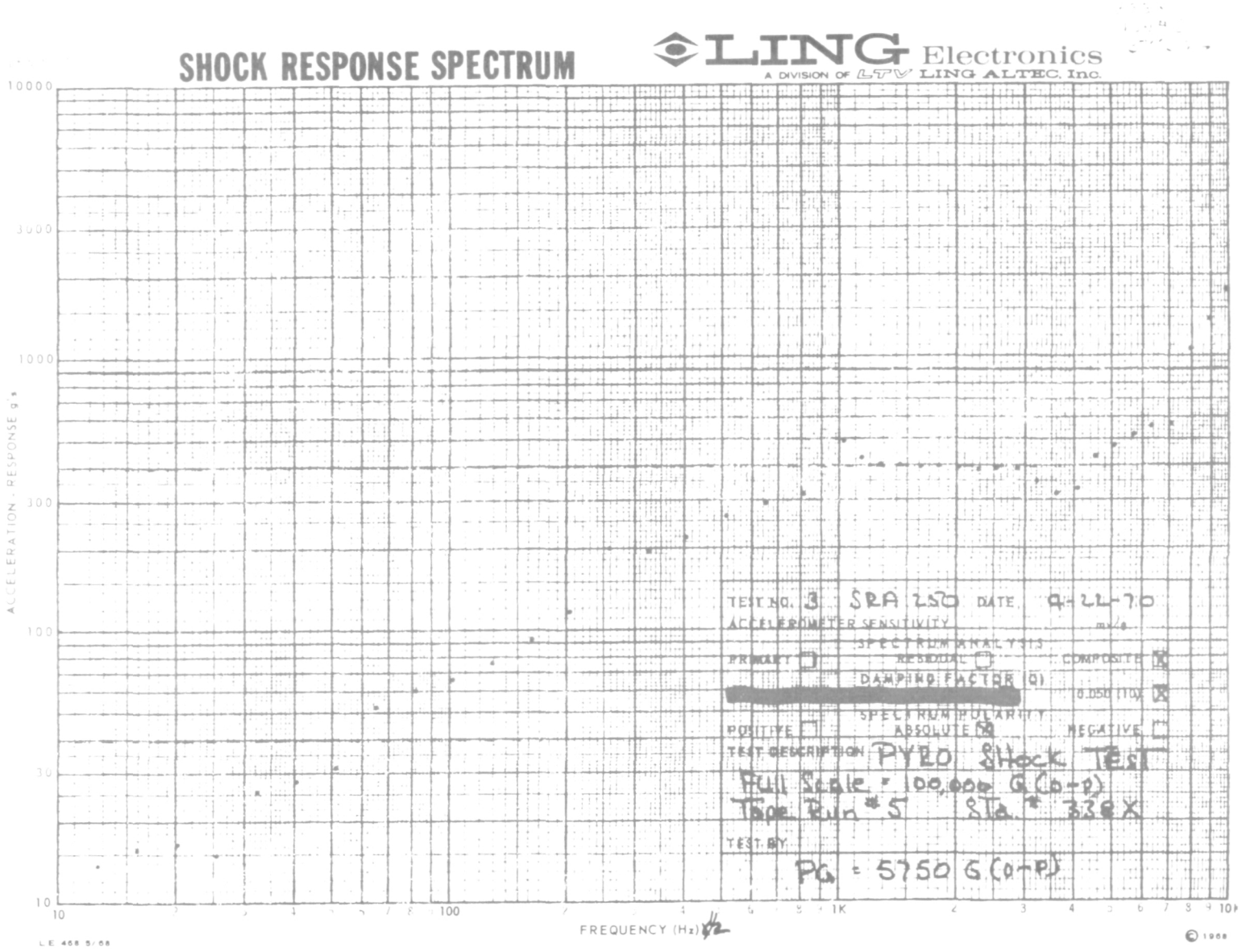

Figure 4.4-11. Shock Response Spectrum on Caging Arm (338X)

4.5 THERMAL VACUUM TEST

4.5.1 INTRODUCTION

The engineering prototype model RA250 was subjected to a series of thermal vacuum tests in accordance with the requirements delineated in Reference 1-2. These tests were performed in the 32 ft. diameter by 54 ft. high thermal vacuum chamber located in Building 200 at the General Electric Valley Forge Space Center.

This test series consisted of the following test segments

Test Segment No.	Description	Reference 1-2 Paragraph No.
1	Deployed Transient	3.10.8.2.3
2	Low Temperature Stowed	3.10.8.1.2.2
3	Low Temperature Deploy and Retract	3.10.6 (a)
4	Stowed Transient and High Temperature Soak	3.10.8.1.3 3.10.8.1.2.1
5	High Temperature Deploy and Retract	3.10.6(b)

4.5.2 DESCRIPTION OF TEST SETUP

The heat input to the RA250 test specimen was supplied by an array of Quartzline lamps mounted on a scaffold structure. Figure 4.5-1 shows this lamp array during its assembly on the preparation area floor adjacent to the chamber. The lamps were located to enable the illumination of all active solar cell modules, the BI-STEM boom, the leading edge member and the storage drum and BI-STEM actuator housing. The spacing of these lamps was determined based on the requirement to drive these areas to $+284^{o}F$ ($+140^{o}C$). These areas were divided into 42 individually

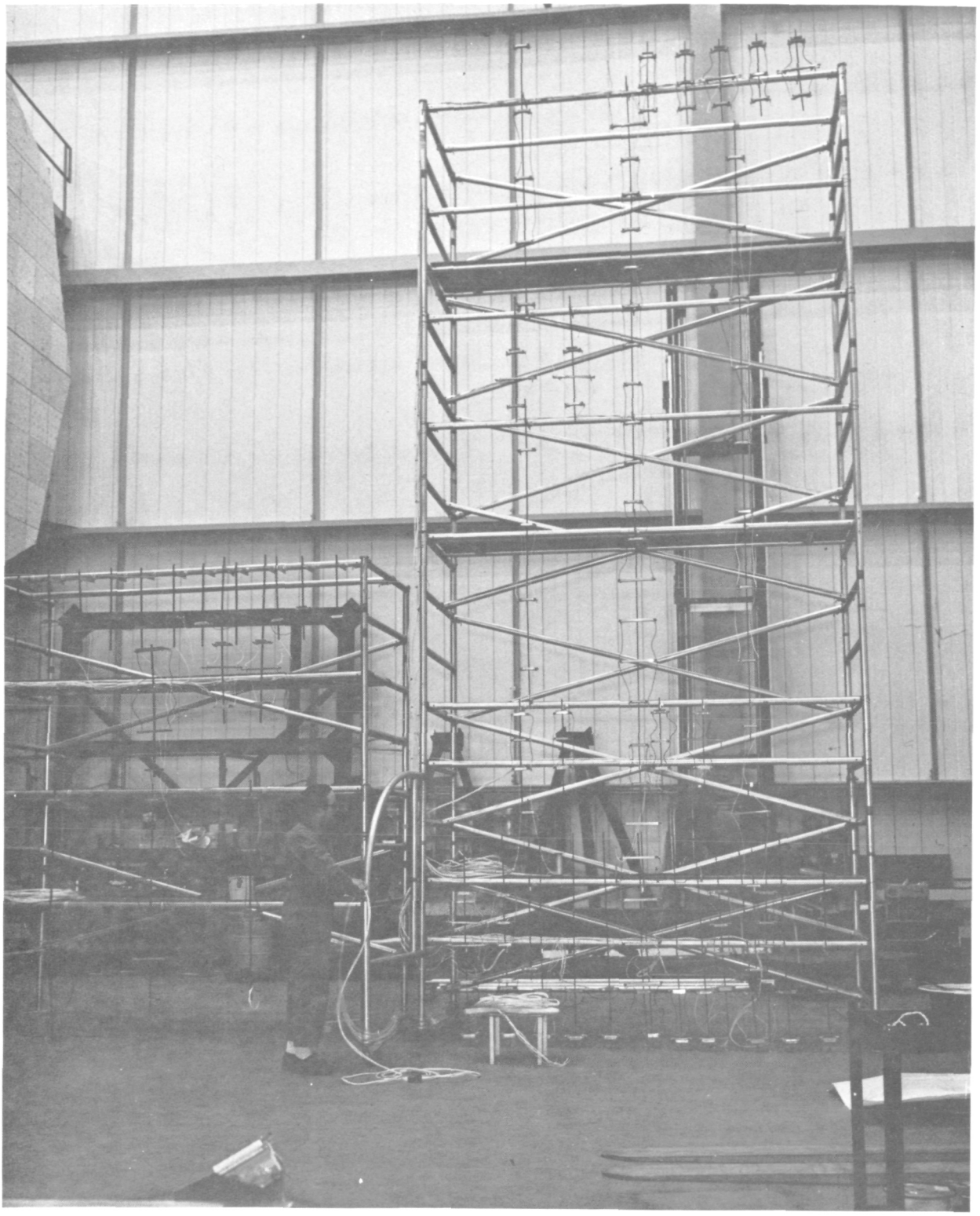

Figure 4.5-1. IR Lamp Array Under Construction (VF 70 208C)

controlled heater zones as shown in Figure 4.5-2. Each of these zones was automatically controlled by a THERMAC proportional controller based on the signal from a monitor thermocouple placed on the deployed array directly under the three lamps in each zone. Each THERMAC control unit supplies a signal to a LABAC power unit which, in turn delivers the required output voltage to the lamp zone.* The dummy glass module areas of the deployed blankets were illuminated by guard heater lamps which were spaced to maintain these areas at a temperature of greater than -202°F (-130°C) at all times (Zones 43 thru 53).

The IR lamp array was positioned in the chamber as shown in Figure 4.5-3. The RA-250 mounted on the holding fixture, was supported from structure at the bottom of the chamber such that the full 33.5 ft. of deployment could be accommodated. The holding fixture was electrically and thermally insulated from the chamber supporting structure.

Figure 4.5-4 shows the leading edge of the fully deployed array. The leading edge member of the array was attached to the strongback of the upward deployment aid which is shown on the left hand side of the photograph. This deployment aid provides a variable counterbalance force which is equal to the weight of the deployed BI-STEM element plus the weight of the deployed array blankets. The fixed weight of the leading edge member and the strongback are also counterbalanced.

To eliminate the possibility of interference with the lamps during deployment or retraction, the tip of the array was constrained to move in a fixed vertical plane

* The LABAC power units can be either operated manually or automatically by the THERMAC controllers.

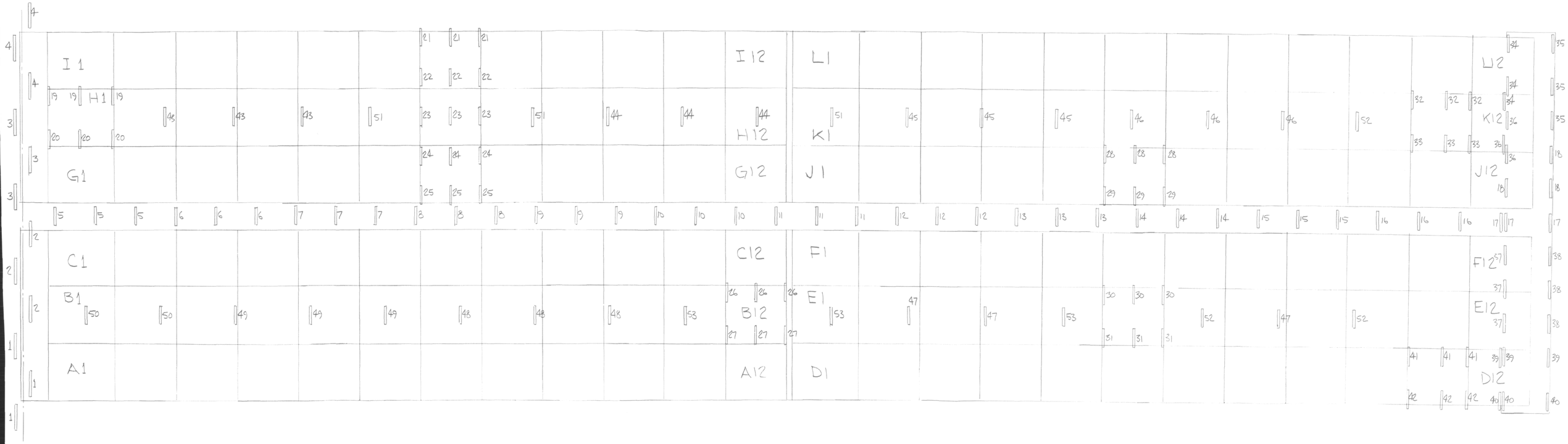

Figure 4.5-2. Lamp Zone Arrangement

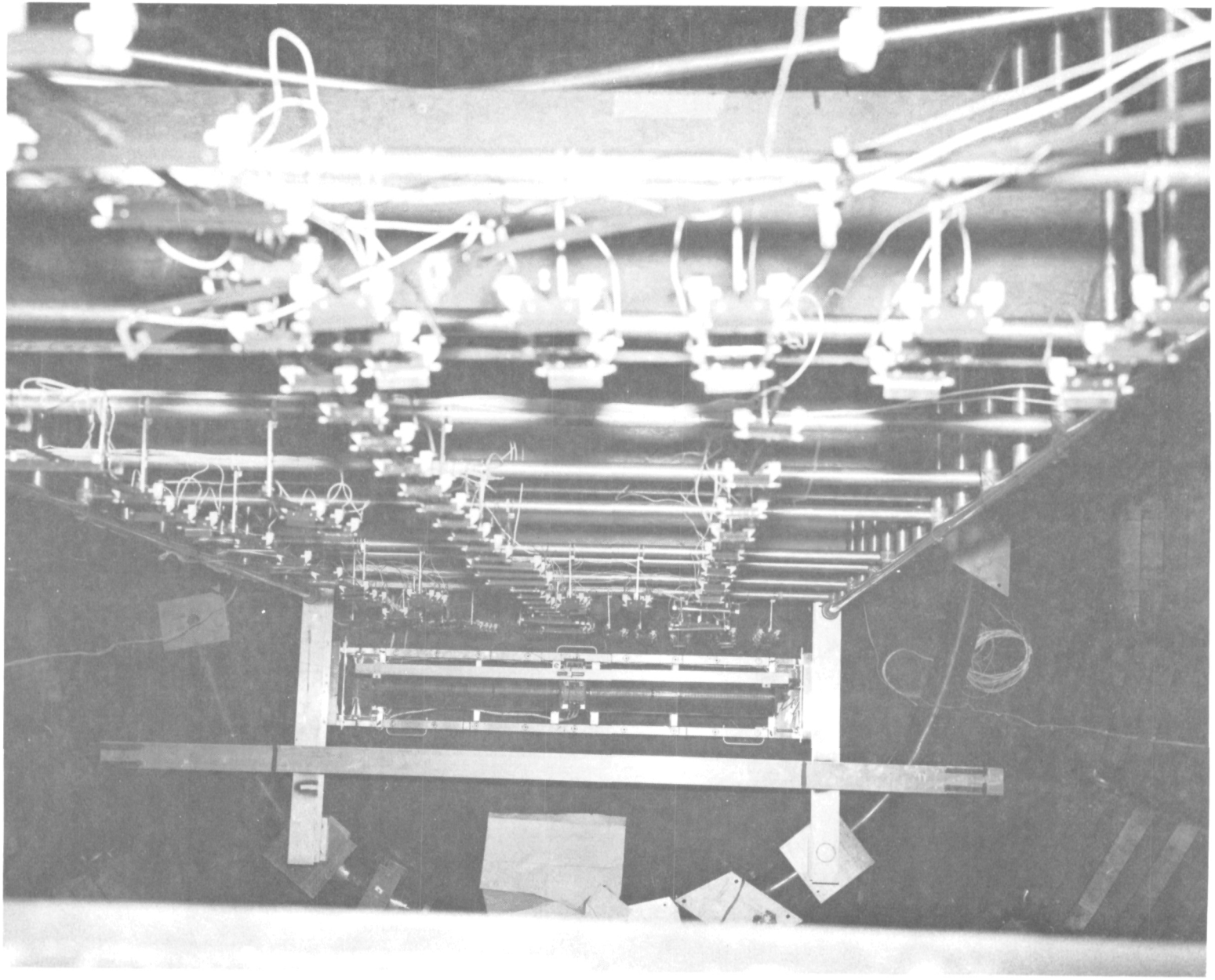

Figure 4.5-3. IR Lamp Array Mounted in Chamber (Viewed From Above) (VF 70 237A)

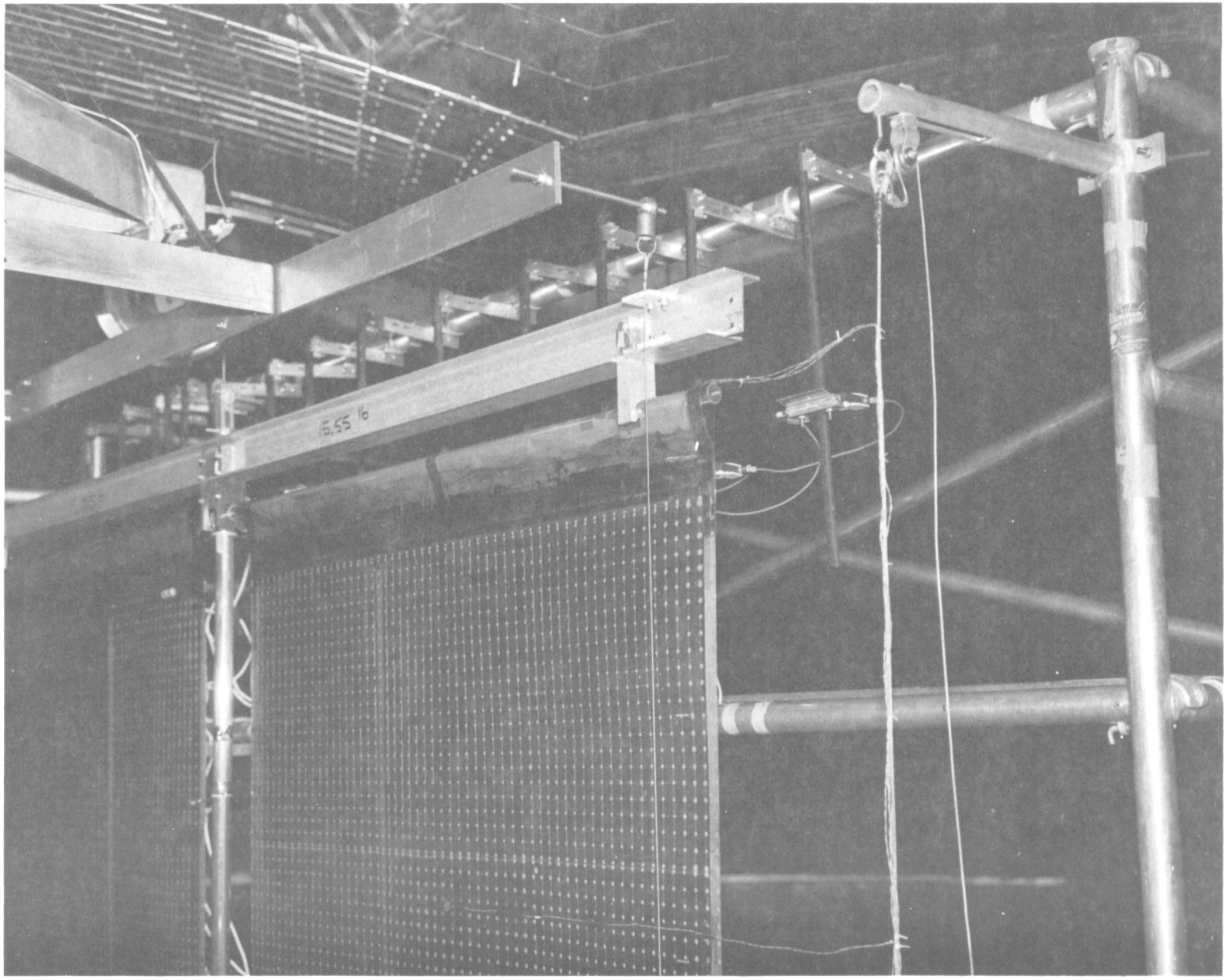

Figure 4.5-4. Leading Edge of Fully Deployed Array (VF 70 240C)

by the guide wire system shown in Figure 4.5-4. A vertical wire at each edge of the array passes through a hole in a Teflon pad on each end of the deployment aid strongback.

For the deployed transient test, the array blanket thermocouples were attached to the rear side of the blanket substrates and routed horizontally to a wire bundle supporting cable on each side of the array. This cable is shown on the right side of Figures 4.5-4 and 4.5-5. Figure 4.5-5 also shows the lamp arrangement for the illumination of the Heliotek, GE No. 2, and Boeing modules on the -Y array blanket. The spacing between the active cell modules and the lamps varied between 4 and 8 in. depending on the deviation of the substrate from a plane.

4.5.3 INSTRUMENTATION

The RA-250 was instrumented with copper-constantan Thermocouples as specified in Table 4.5-1. These thermocouples were used to monitor the temperature of the specimen while additional thermocouples were used as feedback sensors for the automatic controllers for the lamp zones. The readout of this thermocouple data was provided by a 200 channel Keineth K-Logger and a 24 channel Brown recorder during the stowed tests.

Figures 4.5-6 and 4.5-7 show the physical location of the majority of the specimen mounted thermocouples. The array blanket mounted thermocouples consisted of 36 gage wire thermocouples which were installed between the solar cells and the Kapton substrate during the module bonding phase of the assembly. There are two such thermocouples on each active solar cell module as identified by the symbol on Figure 4.5-6. All other blanket mounted thermocouples were made with

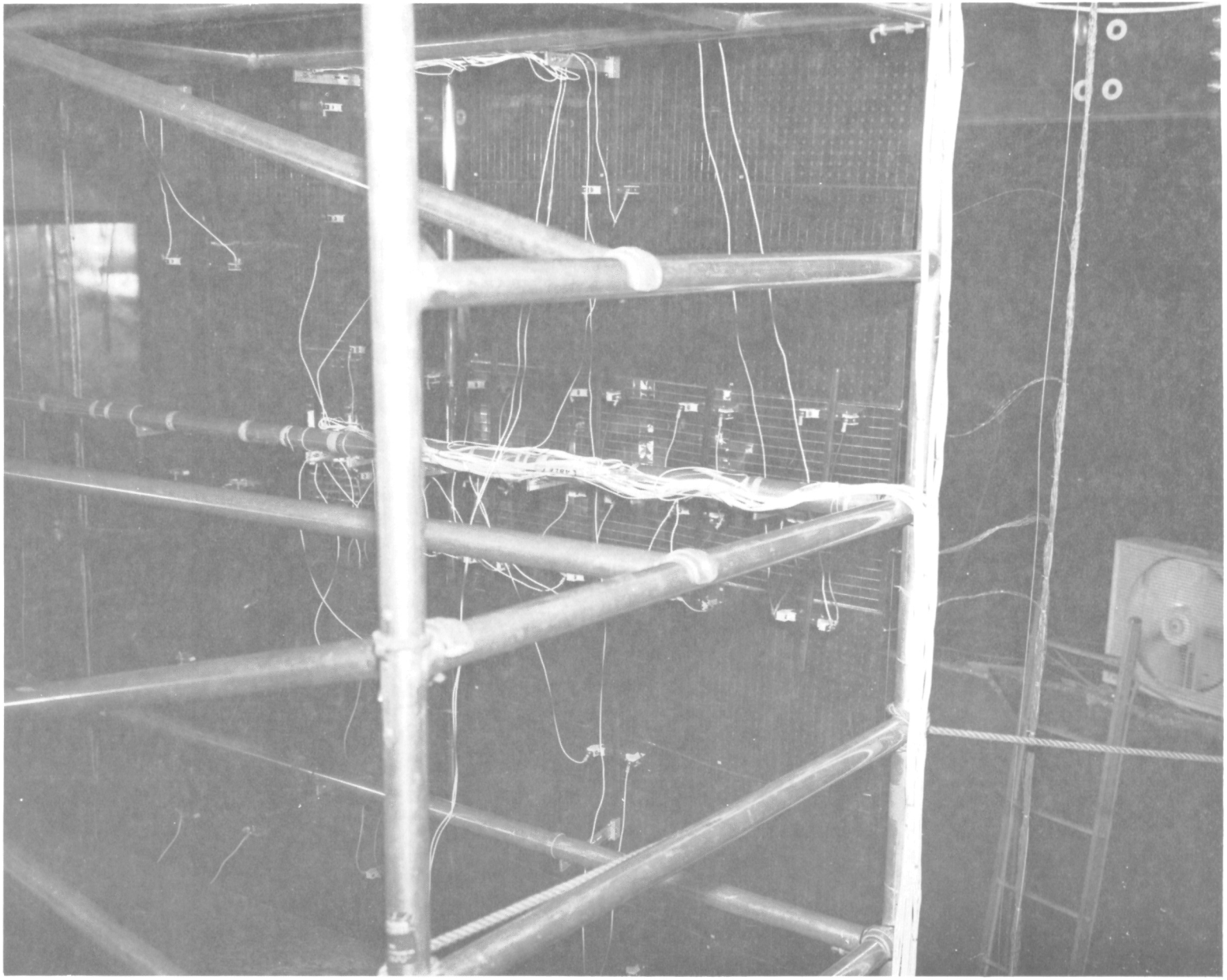

Figure 4.5-5. Lamp Zones for Heliotek, GE No. 2, and Boeing Modules (VF 70 240E)

Table 4.5-1 Thermocouple List

Specimen Thermocouple Number	Location	See Fig. No. 4.5-6 & 4.5-7	Data Channel Deployed Transient Test	Data Channel Stowed Tests
1	Bi-Stem Motor	--	K1(1)	B2
2	Bi-Stem Motor	--	B16(2)	B16
3	Center Support +Z face	--	K3	B3
4	Center Support -Z face	--	K4	B4
5	Support Shaft	--	K5	B5
6	Storage Drum, 1/4 Span	7	K79	
7	Storage Drum, 1/4 Span	7	K80	
8	Storage Drum, 1/4 Span	7	K81	
9	Storage Drum, 1/4 Span	7	K15	
10	Storage Drum, 1/2 Span	7	B14	B14(3)
11	Storage Drum, 1/2 Span	7	B15	B15(3)
12	Storage Drum, 1/2 Span	7	K16	
13	Storage Drum, 1/2 Span	7	K17	
14	Storage Drum, 3/4 Span	7	K18	
15	Storage Drum, 3/4 Span	7	K19	
16	Storage Drum, 3/4 Span	7	K20	
17	Storage Drum, 3/4 Span	7	K21	
18	Inboard End Cap	7	K22	
19	Inboard End Cap	7	K23	
20	Outboard End Cap	7	K24	
21	Outboard End Cap	7	K25	
22	Outboard End Support	--	K8	B6
23	Handling Fixture at Center	6	K9	B7
24	Handling Fixture at +Y End	6	K10	B6
25	Handling Fixture at -Y End	6	K11	B9
26	B12 Module	6	B2	
27	B12 Module	6	K26	
28	E6 Module	6	B3	
29	E6 Module	6	K27	
30	D11 Module	6	B4	
31	D11 Module	6	K28	
32	D12 Module	6	B5	
33	D12 Module	6	K29	
34	H1 Module (Control T/C)	6	B1	B1(4)
35	H1 Module	6	K30	
36	G7 Module	6	B6	
37	G7 Module	6	K31	
38	H7 Module	6	B7	
39	H7 Module	6	K32	
40	I7 Module	6	B8	
41	I7 Module	6	K33	
42	J6 Module	6	B9	
43	J6 Module	6	K34	
44	K11 Module	6	B10	

Table 4.5-1 Thermocouple List (Cont.)

Specimen Thermocouple Number	Location	See Fig. No. 4.5-6 & 4.5-7	Data Channel	
			Deployed Transient Test	Stowed Test
45	K11 Module	6	K35	
46	K12 Module	6	B11	
47	K12 Module	6	K36	
48	+Y Blanket Thermister Location	6	B12	
49	-Y Blanket Thermister Location	6	B13	
50	Bi-Stem Zone 5	6	K37	
51	Bi-Stem Zone 6	6	K38	
52	Bi-Stem Zone 7	6	K39	
53	Bi-Stem Zone 8	6	K40	
54	Bi-Stem Zone 9	6	K41	
55	Bi-Stem Zone 10	6	K42	
56	Bi-Stem Zone 11	6	K43	
57	Bi-Stem Zone 12	6	K44	
58	Bi-Stem Zone 13	6	K45	
59	Bi-Stem Zone 14	6	K46	
60	Bi-Stem Zone 15	6	K47	
61	Bi-Stem Zone 16	6	K48	
62	Bi-Stem Zone 17	6	K49	B10
63	LEM Zone 1	6	K50	
64	LEM Zone 2	6	K51	
65	LEM Zone 3	6	K52	
66	LEM Zone 4	6	K53	
67	Blanket Zone 19	6	K54	
68	Blanket Zone 20	6	K55	
69	Blanket Zone 21	6	K56	
70	Blanket Zone 22	6	K57	
71	Blanket Zone 23	6	K58	
72	Blanket Zone 24	6	K59	
73	Blanket Zone 25	6	K60	
74	Blanket Zone 26	6	K61	
75	Blanket Zone 27	6	K62	
76	Blanket Zone 28	6	K63	
77	Blanket Zone 29	6	K64	
78	Blanket Zone 30	6	K65	
79	Blanket Zone 31	6	K66	
80	Blanket Zone 32	6	K67	
81	Blanket Zone 33	6	K68	
82	Blanket Zone 36	6	K69	
83	Blanket Zone 41	6	K70	
84	Blanket Zone 42	6	K71	
85	Blanket Zone 39	6	K72	
86	Blanket Zone 40	6	K73	

Table 4.5-1 Thermocouple List (Cont.)

Specimen Thermocouple Number	Location	See Fig. No. 4.5-6 & 4.5-7	Data Channel Deployed Transient Test	Data Channel Stowed Tests
87	Storage Drum Zone 37	6	K74	
88	Storage Drum Zone 18	6	K75	
89	Storage Drum Zone 35	6	K76	
90	Storage Drum Zone 34	6	K77	
91	Storage Drum Zone 38	6	K78	
92	Upward Deploy Aid +Y Drum Brg	--	K6	B11
93	Upward Deploy Aid -Y Drum Brg	--	K7	B12
94	Upward Deploy Aid +Y Sheave Brg	--	K12	B13
95	Upward Deploy Aid -Y Sheave Brg	--	K13	B17
96	Upward Deploy Aid Potentiometer	--	K14	B18
97	Guard Heater Zone G1	6	K82	
98	Guard Heater Zone G2	6	K90	
99	Guard Heater Zone G3	6	K83	
100	Guard Heater Zone G4	6	K84	
101	Guard Heater Zone G5	6	K93	
102	Guard Heater Zone G6	6	K85	
103	Guard Heater Zone G7	6	K91	
104	Guard Heater Zone G8	6	K86	
105	Guard Heater Zone GS1	6	K87	
106	Guard Heater Zone GS1	6	K94	
107	Guard Heater Zone GS3	6	K88	
108	Edge +Y Blanket	6	K89	
109	Edge -Y Blanket	6	K92	

NOTES:

(1) K signifies Keinath K-Logger

(2) B signifies 24 point Brown recorder

(3) Thermocouples pull apart upon release of outboard end support

(4) Thermocouple pulls apart upon deployment of BI-STEM

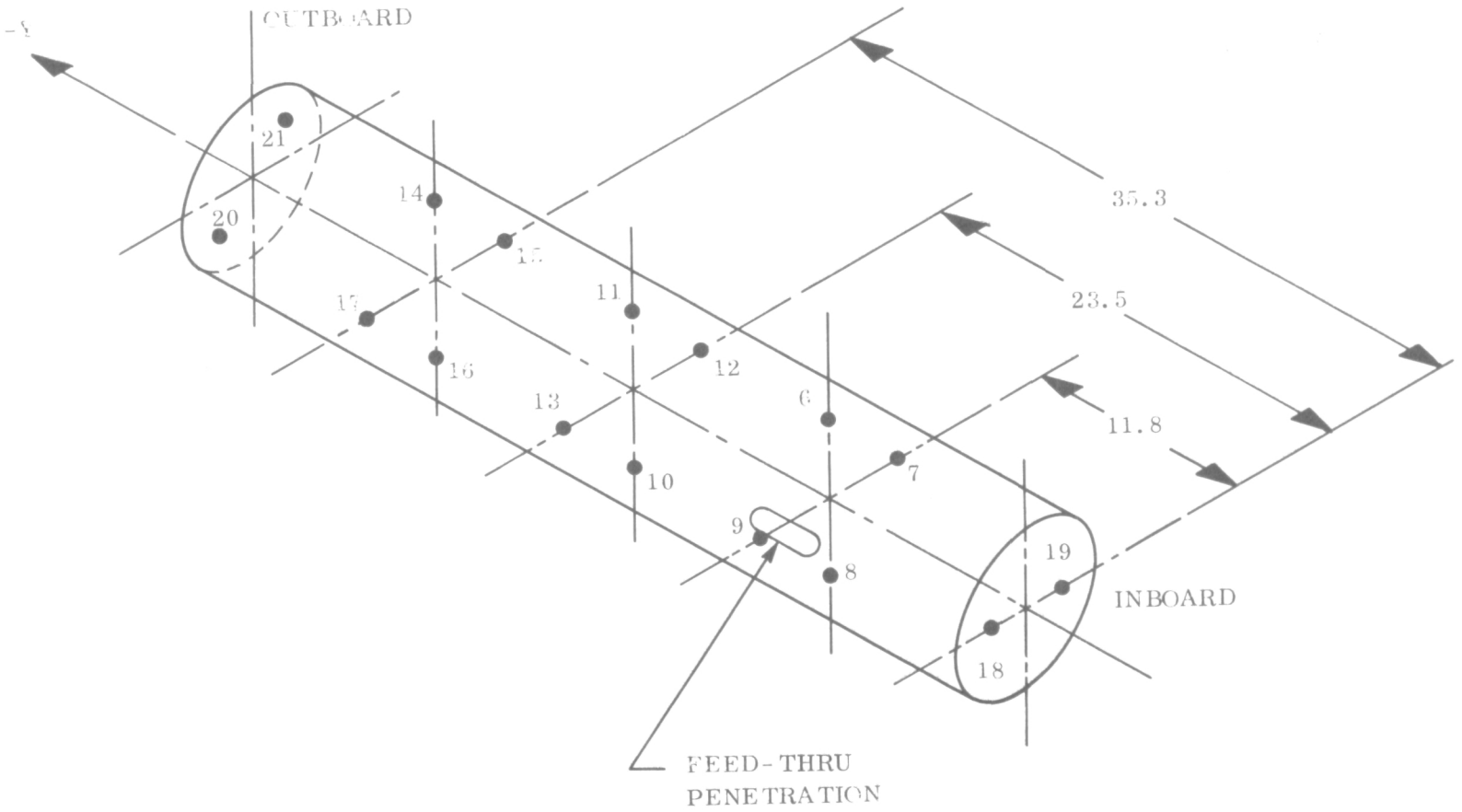

Figure 4.5-7. Storage Drum Thermocouple Locations

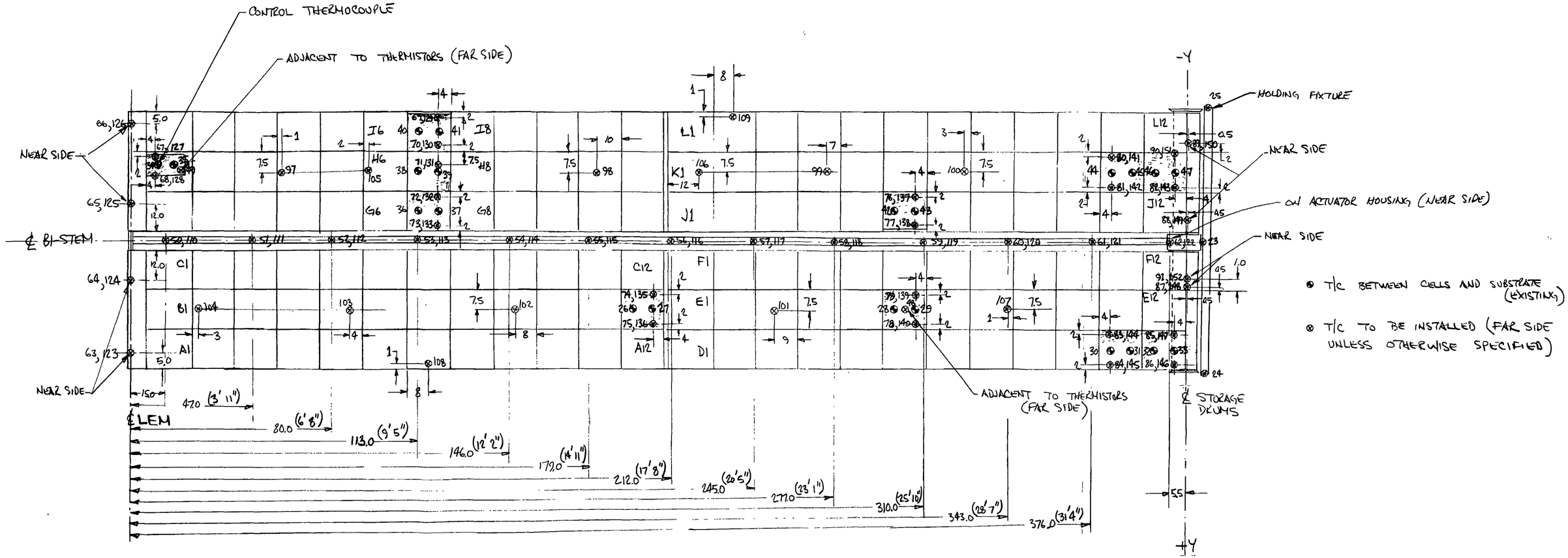

Figure 4.5-6. Specimen Thermocouple Locations

24 gage wire and installed immediately prior to the test. These thermocouples were bonded to the rear of the substrate (except as noted) with ECCOBOND 56C. Where indicated two thermocouples were bonded at one location with one used as a monitor and the other used as the feedback control for the lamp zone. All thermocouples shown in Figure 4.5-7 were bonded on the inside of the drum or end caps. The thermocouples on the BI-STEM element were installed as shown in Figure 4.5-8. ECCOBOND 56C without the catalyst was used around the two beads at each location to provide good thermal contact.

As noted in Table 4.5-1, the thermocouple data was read out differently for the stowed tests. For these stowed thermal tests, all blanket mounted thermocouples were removed (or not connected) except for No. 34 which is defined as the control thermocouple for these tests. In addition, only two of the thermocouples mounted on the storage drum were read out. This was done to minimize the number of thermocouples which had to be separated to permit the deployment of the array.

4.5.4 TEST PROCEDURE

4.5.4.1 Test No. 1 - Deployed Transient

1. The RA250 Test specimen was installed at the bottom of the chamber on its mounting brackets. All electrical circuits which mate to the center support were checked out for continuity thru to the performance test rack located in the control room.

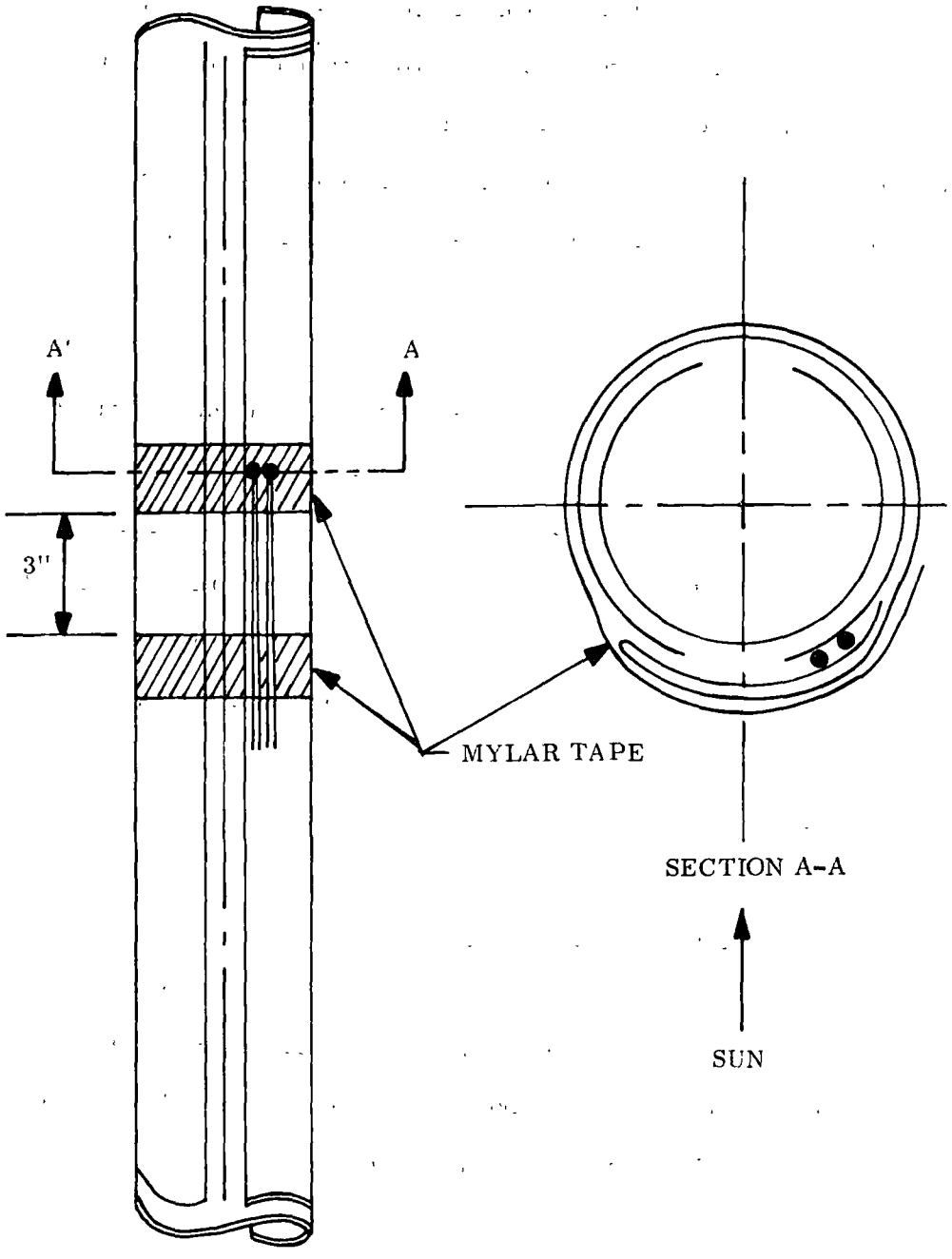

Figure 4.5-8. Thermocouple Installation on Bi-Stem Elements

2. With the IR lamp array fully assembled, the upward deployment aid was installed in its operating position. The strongback of the deployment aid was installed. In the fully stowed position, the deployment aid potentiometer signal was 0.541 VDC.

3. The outboard end supports were released manually and the RA250 was deployed to the fully extended position (4.455 VDC potentiometer signal). The fully deployed array was inspected to determine if the IR lamp array was properly positioned with respect to the active solar cell modules. The lamp positions were adjusted as required.

4. The RA250 was retracted to the orbital retract position (approximately 0.580 VDC potentiometer signal).

5. The upper portion of the IR lamp array was temporarily disassembled to allow for the installation of the chamber dome.

6. Another complete deploy/retract cycle was performed prior to the thermocouple installation.

7. The array was extended in increments during the installation of thermocouples on the blanket substrate and the BI-STEM deployable boom.

8. After all thermocouples had been installed and connected to the heater control system, the K-Logger and the Brown recorders, the IR lamp power controllers were checked out by activating each THERMAC one at a time. At a set point of 150°F, the operation of the lamps, the response of the output voltage meter, and the response of all monitor thermocouples within that zone were observed.

9. The chamber was pumped down while recording all monitor thermocouples on the K-Logger and Brown recorder.

10. When the chamber pressure reached 1×10^{-4} torr, all THERMAC's and guard heater LABAC zones were energized. The set point on all THERMAC's was adjusted for -67°F (-55°C). All guard heater LABAC's were set to maintain at least -202°F (-130°C) in the dummy glass module areas of the blankets.

11. With LN_2 flow to the cryo panels and cryoelbows thermal equilibrium was reached at this flux level. The chamber pressure was 1.5×10^{-5} torr during this period. The LABAC output voltages for each zone were recorded.

12. All THERMAC's were switched to the MANUAL position and the same output voltages were set for each zone to monitor the -67°F, (-55°C) flux level. The temperature level on all thermocouples was verified as being the same as previously recorded while in the set point mode.

13. The set point of each THERMAC was set at +240°F and thermal equilibrium was reached at +240°F. Each controller was gradually increased so that all specimen thermocouples, except those in the dummy glass areas, reached +284 ± 18°F. Thermal equilibrium was reached at this flux level. The LABAC output voltage readings at this flux level were recorded. These lamp voltages were set in the MANUAL mode to ascertain that the temperatures monitored within each zone did not change appreciably.

14. The +284°F flux level was maintained for 2 hours using the THERMAC controllers.

15. After this time, the power to all lamps was turned off and the array was allowed to cool to -202°F (-130°F) by radiating to the chamber cryo panels.

16. When the control thermocouple (No. 34) had attained the desired temperature of -202°F, the IR lamp array was reactivated, in the set point mode, to drive the temperature up to +284°F. This high temperature limit was maintained for 2 hours.

17. Following this 2 hour period, the chamber warmup and vent procedure was initiated.

18. After the chamber had reached ambient temperature and pressure, all thermocouples were removed from the BI-STEM element and from the array substrate (with the exception of the permanently installed thermocouples between the cells and the substrate). This removal was done as the array was retracted in incremental steps. The BI-STEM element was thoroughly cleaned before it entered the actuator.

19. Two complete ambient deploy/retract cycles were performed.

4.5.4.2 Test No. 2 - Low Temperature Stowed

After performing the two ambient deploy/retract cycles, the three pull-apart thermocouple connectors were rigged as follows:

1. The control thermocouple (No. 34) connector was positioned so that it pulled apart as the BI-STEM deployed.

2. Thermocouple Nos. 10 and 11 on the storage drum shell were positioned so that the connectors were pulled apart as the outboard end support pivots during uncaging.

The outboard end supports were recaged and two squibs were installed in each separation nut.

The chamber was pumped down while all monitor thermocouples were read out on the Brown recorder. LN_2 was introduced to the cryopanels and the specimen was allowed to cool down. The test plan called for the control thermocouple to be at $-202^{o}F$ for at least 2.5 hours. However, as the test proceeded it became apparent that

it would require approximately 20 hours of test time to reach the -202°F temperature on the control thermocouple. Therefore, it was decided to stop the low temperature soak test when the control thermocouple temperature had decayed to -172°F. The rate of change of temperature on this thermocouple was 6°F/hr at this time.

4.5.4.3 Test No. 3 - Low Temperature Deploy and Retract

1. Following the completion of the low temperature soak period, the outboard end supports were released by the simultaneous firing of both squibs in each separation nut. Release was verified by the signal from the microswitches at each outboard end support. The temperature recorded on thermocouple number 22 located on the outboard end support adjacent to the -Y separation nut was -76°F immediately prior to firing.

2. The THERMAC controllers were set at the individual output voltage levels as determined during the deployed test at the -67°F (-55°C) temperature level. This flux level was set open-loop with the THERMAC's in the MANUAL mode, except for zone 17 (BI-STEM actuation housing) which was controlled in the set point mode at -67°F .

3. The BI-STEM was deployed. The following temperatures were recorded immediately prior to deployment:

T/C No.	Location	Temperature (^{o}F)
2 & 16	BI-STEM Motor	-63
34	Control Thermocouple (H1 module)	-75
62	BI-STEM housing	-63

A temperature rise of 37^{o}F was recorded on the motor during this deployment.

4. The BI-STEM was retracted from the fully extended position. The retraction was terminated prior to reaching the orbital stowed position due to an apparent billowing of the +Y blanket as viewed on the closed circuit T.V. camera. The deployment aid potentiometer signal was 1.29 VDC when the retraction was stopped. This indicated 77 inches of boom remained extended. At the end of this retraction the motor temperature was -70^{o}F.

5. The chamber warmup and vent phase was initiated.

6. After the chamber had reached ambient pressure and temperature, visual examination of the RA250 revealed that, in addition to the +Y blanket billowing, the -Y blanket had failed to rewrap on the storage drum and was draped on the chamber cryopanels. This problem is discussed in more detail in Section 4.5.5. It was also noted that both separation nuts had fractured at their mounting bases. This is discussed in Section 4.5.3.3.

4.5.4.4 Test No. 4 - Stowed Transient and High Temperature Soak

1. New separation nuts were installed. Only one squib was used in each separation nut and the other port was plugged with an expended squib.

2. All pull-apart thermocouple connectors were noted and checked out by manually uncaging the end support and extending the BI-STEM a short distance. Precautions were taken to avoid fouling of the separated leads.

3. The array was stowed in the launch configuration.

4. The chamber was pumped-down and LN_2 was introduced to the cryopanels.

5. The output flux level of zones 17, 18, 32, 33, 34, 35, 36, 37, 38, 39, 40, 41, and 42 was set to yield $\pm 284^{\circ}F$ ($+140^{\circ}C$) by setting the voltages determined from the deployed transient test.

6. After the cryopanel temperature had stabilized and the control thermocouple had reached $+284^{\circ}F$, the array was maintained at this temperature level for 2 hours. At the end of this time period, the IR lamp array was de-energized.

7. The stowed array was allowed to cool for 2 hours with no input flux from the lamps. After this time period, the IR lamp array was energized in zones 17, 18, 32, 33, 34, 35, 36, 37, 38, 39, 40, 41 and 42 to the flux level which yields $+284^{\circ}F$ ($+140^{\circ}C$).

8. This condition was maintained for 20 hours.

9. After 20 hours at +284°F, the array was deployed and retracted as described in Section 4.5.4.5.

4.5.4.5 Test No. 5 - High Temperature Deploy and Retract

1. All lamp zones were turned on to the output voltages recorded at the +284°F flux level during the deployed transient test.

2. Zones 16, 17, 18, 37 and 38 were turned off approximately 40 minutes prior to deployment to reduce the motor temperature.*

3. The squibs were fired to release both outboard end supports. Thermocouple No. 22 on the outboard end support adjacent to the separation nut read +117°F immediately prior to firing.

4. Zones 16, 17, 18, 37 and 38 were turned on at the +284°F flux level immediately prior to deployment.

5. The BI-STEM was deployed. The motor temperature immediately prior to deployment was +192°F. At this time the control thermocouple was reading +256°F.

* This step was taken to reduce the risk of damage to the motor/gearhead assembly. The motor/gearhead had been qualified to 71C and was quoted by the manufacture to be capable of withstanding 125°C.

6. After reaching the fully extended position the BI-STEM was immediately retracted. After reaching the orbital retract position, the motor temperature was +227°F.

7. The chamber warm-up and vent phase was initiated.

4.5.5 TEST RESULTS

4.5.5.1 Deployed Transient Test

The results of the deployed transient test are shown in Figures 4.5-9 through 4.5-20. Plots of temperature vs time have been shown for each of the solar cell modules and other significant components of the array. All active solar cell modules had similar transient response temperature histories. In all cases to warm-up to +284°F was performed by first turning on the lamps at a low voltage to heat the filaments before applying full voltage. This procedure was necessary to avoid blowing fuses as a result of the high inrush current associated with cold lamp filaments. This turn on procedure caused the step-like appearance of the temperature rise on all the active solar cell modules.

Figure 4.5-14 shows the temperature response of two thermocouples on the same module. Thermocouple No. 34 is located between the solar cells and the substrate while thermocouple No. 49 is located adjacent to the thermistors on the rear of the substrate. These two thermocouples are separated by approximately 8 inches and are in different lamp control zones. Because no evidence of instrumentation error was found, this large difference in maximum temperature is attributed to nonuniformity of illumination. The other two monitor thermocouples on this

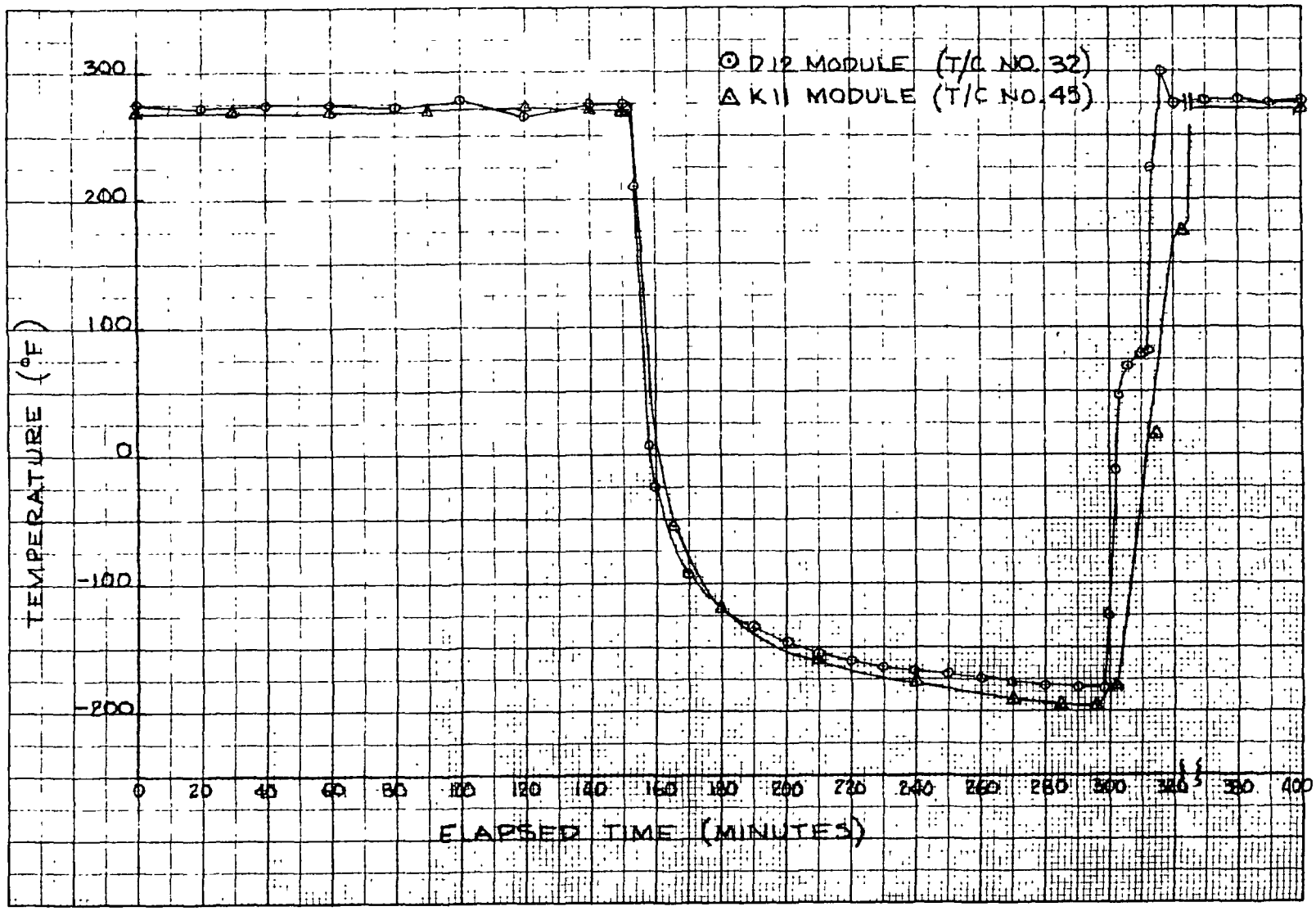

Figure 4.5-9 Deployed Transient Temperature History

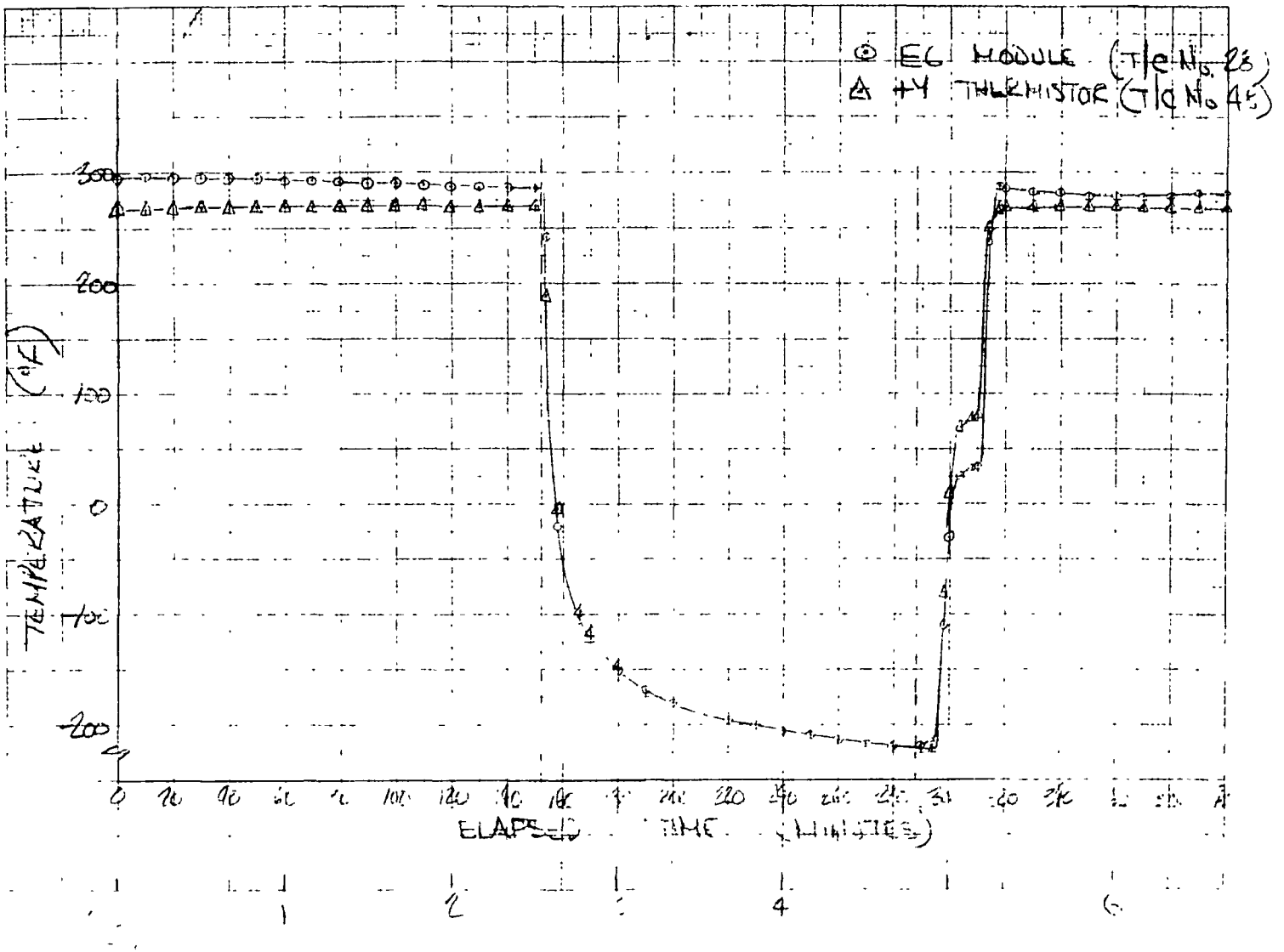

Figure 4.5-10. Deployed Transient Temperature History

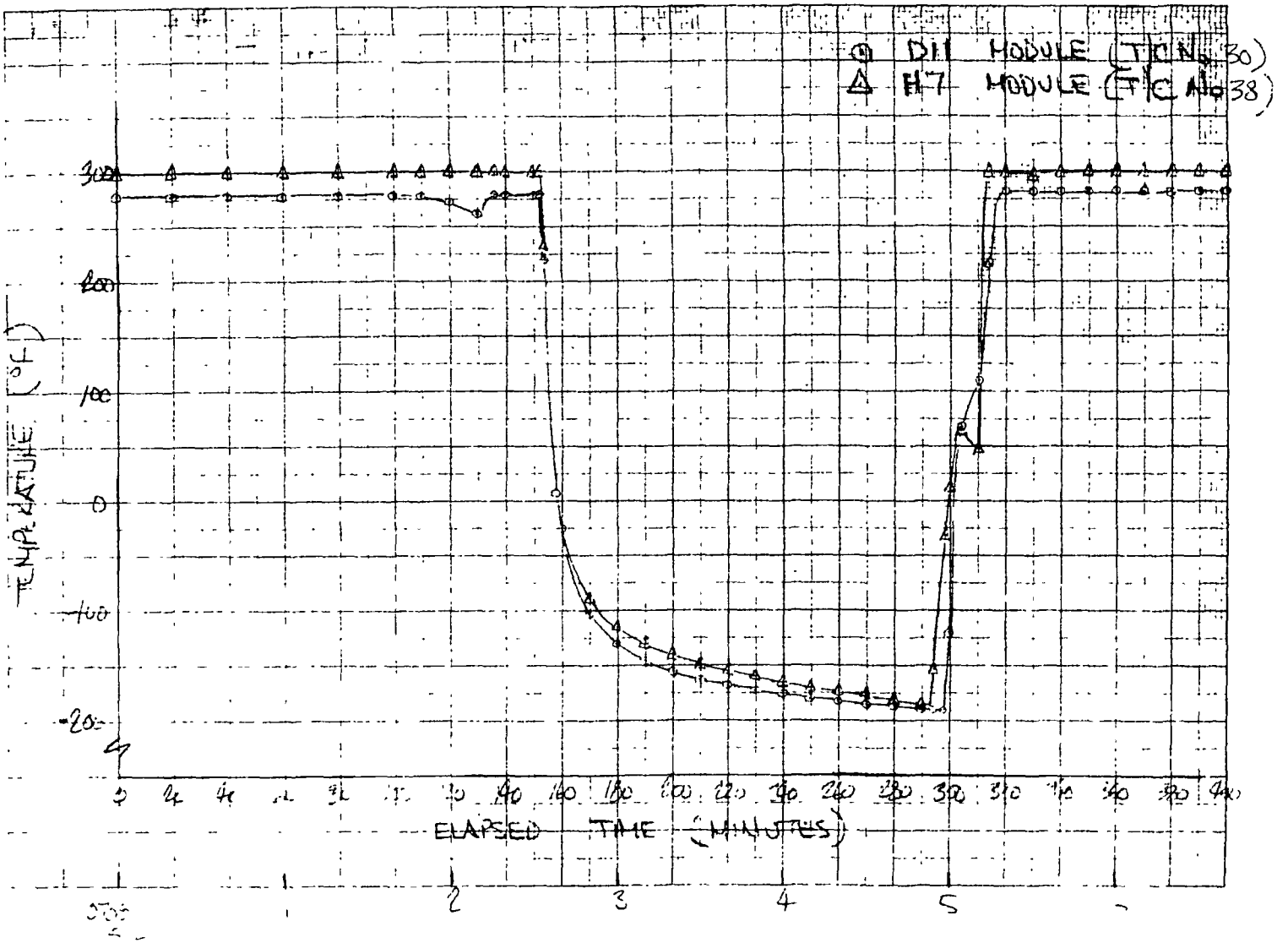

Figure 4.5-11. Deployed Transient Temperature History

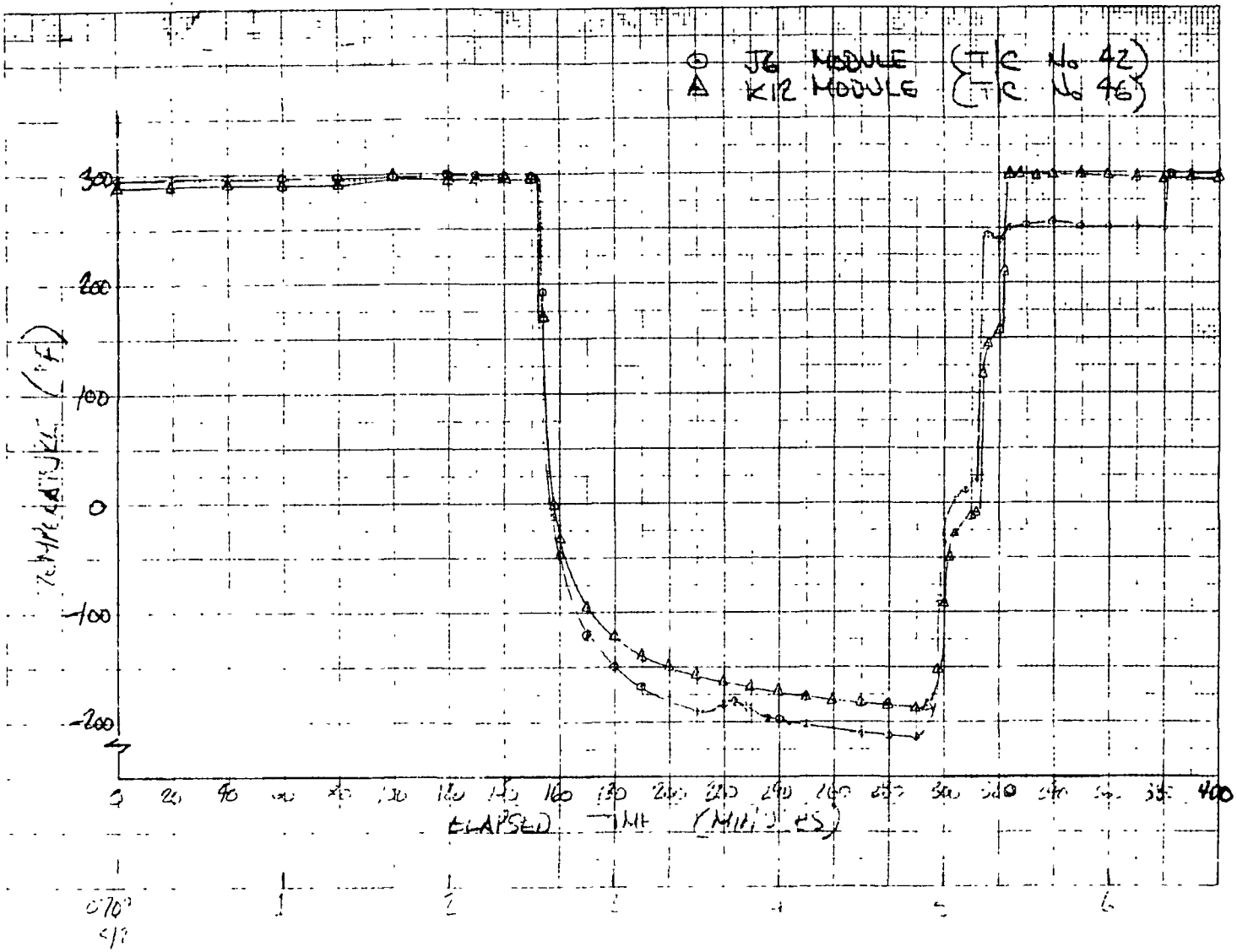

Figure 4.5-12. Deployed Transient Temperature History

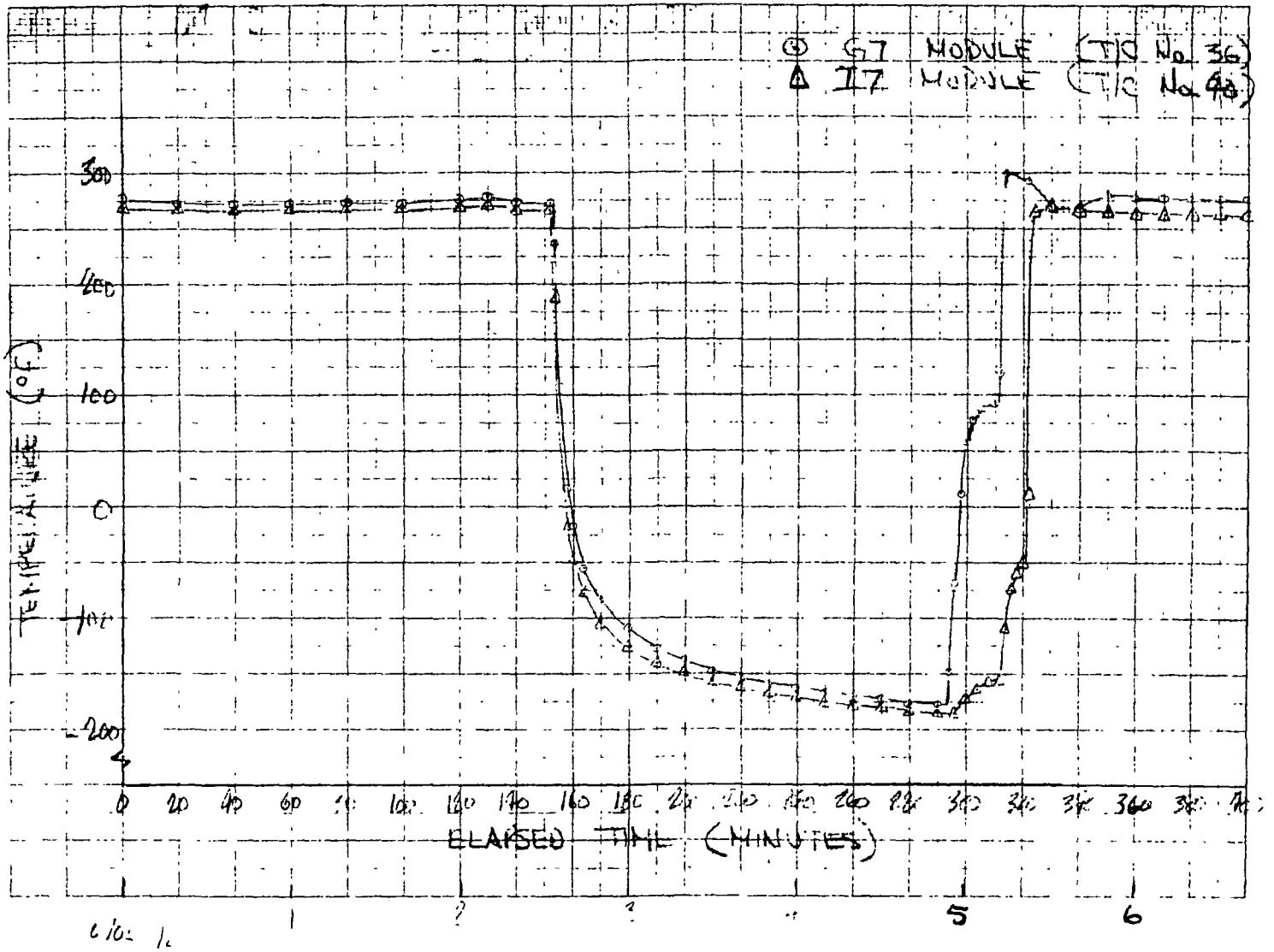

Figure 4.5-13. Deployed Transient Temperature History

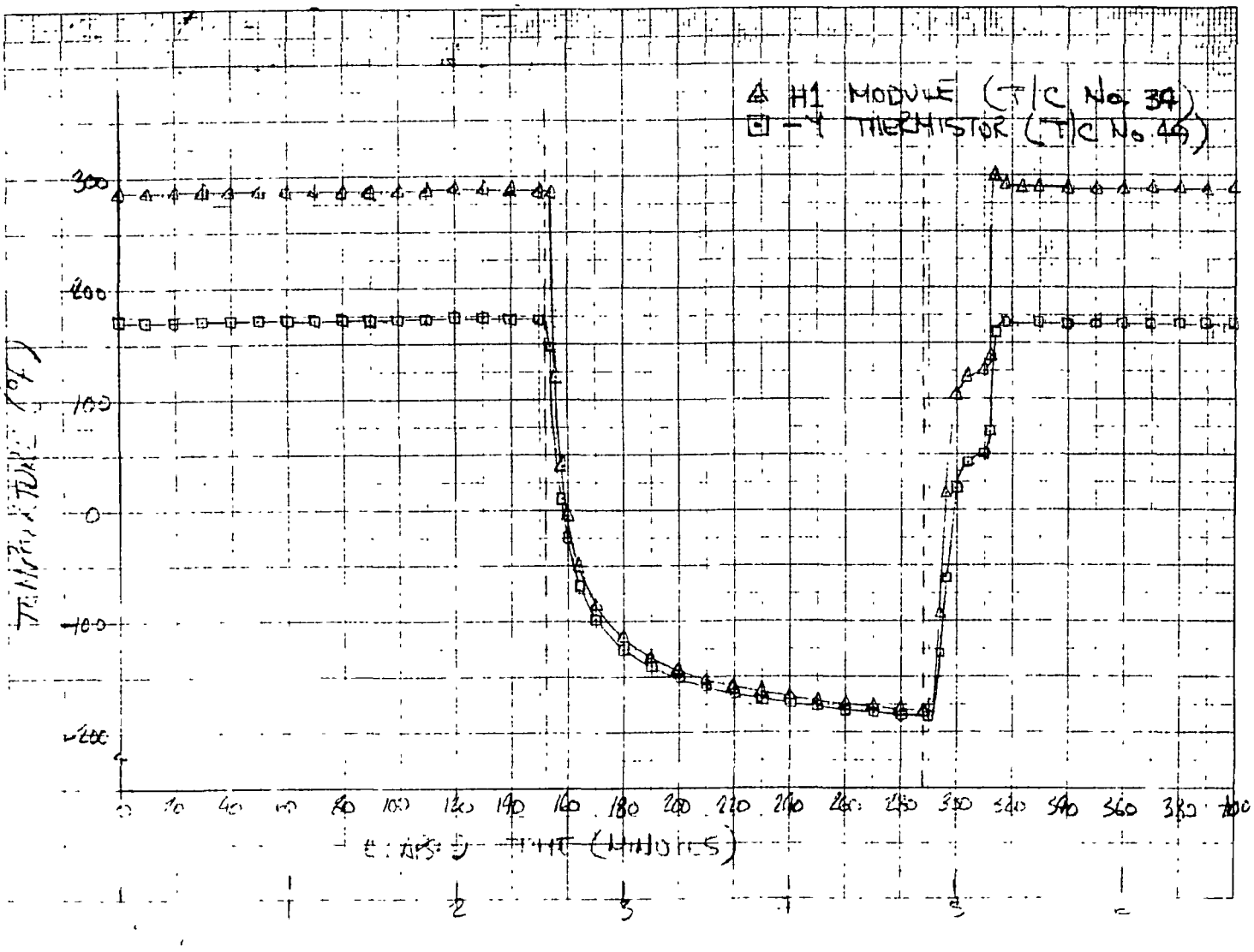

Figure 4.5-14. Deployed Transient Temperature History

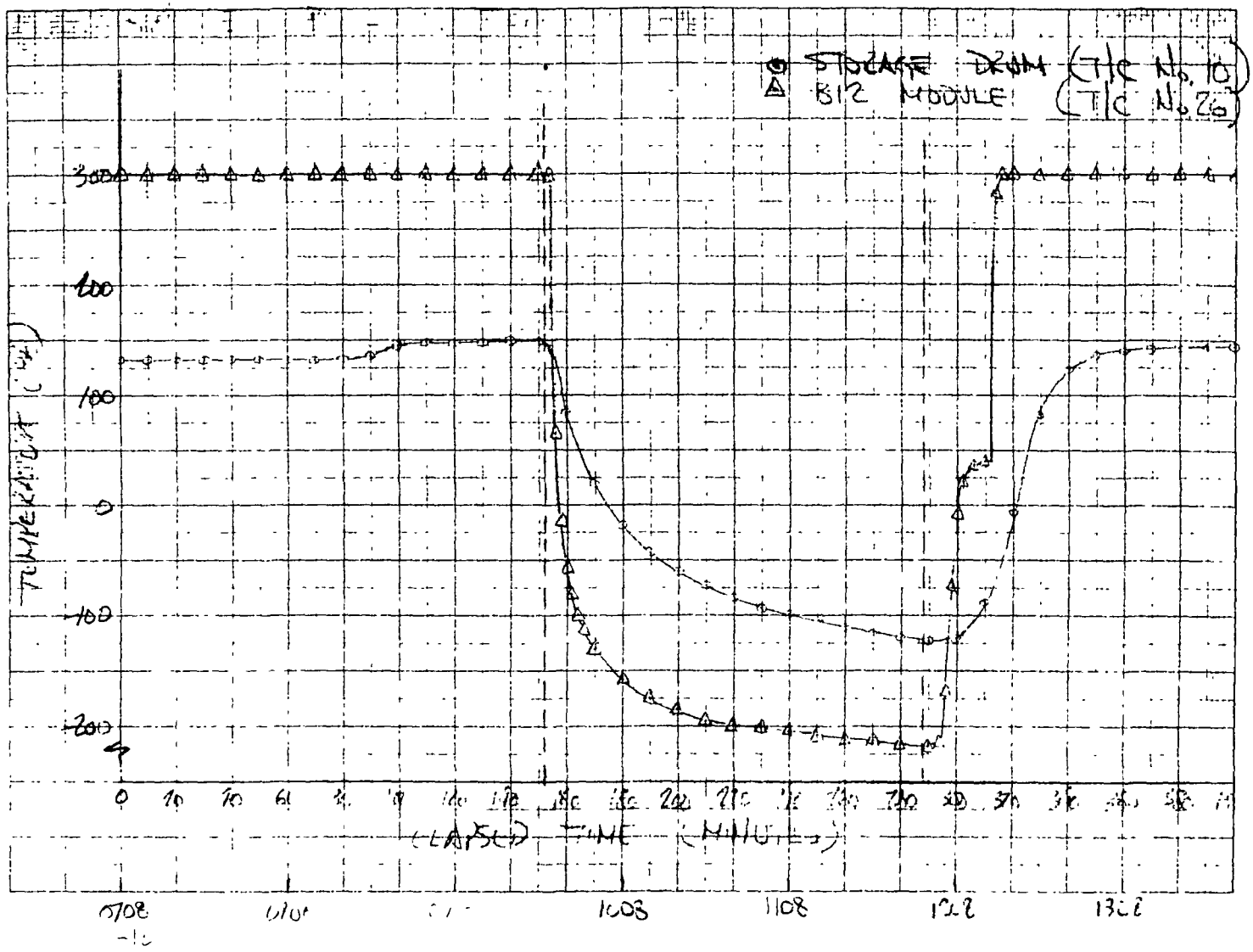

Figure 4.5-15. Deployed Transient Temperature History

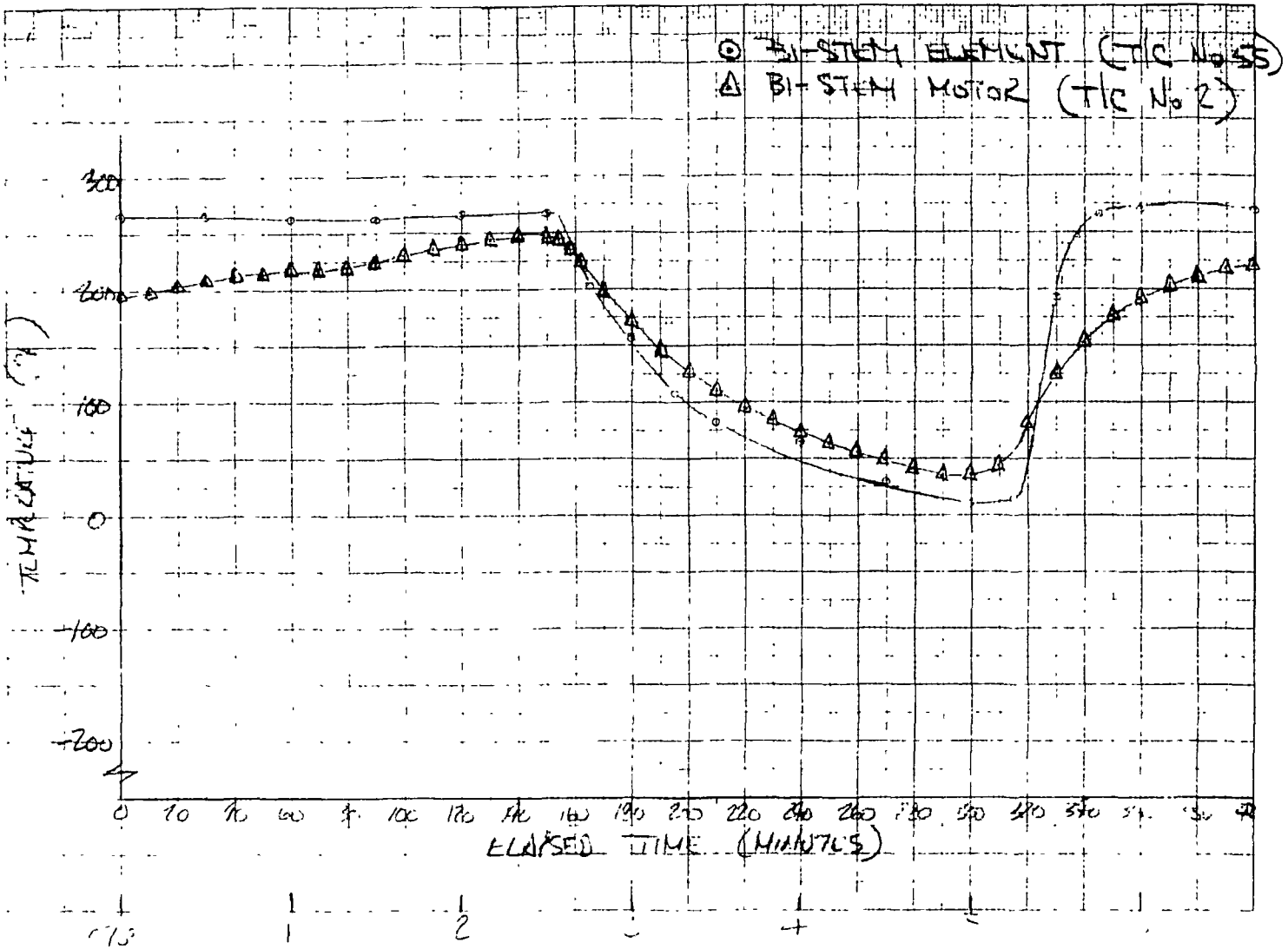

Figure 4.5-16. Deployed Transient Temperature History

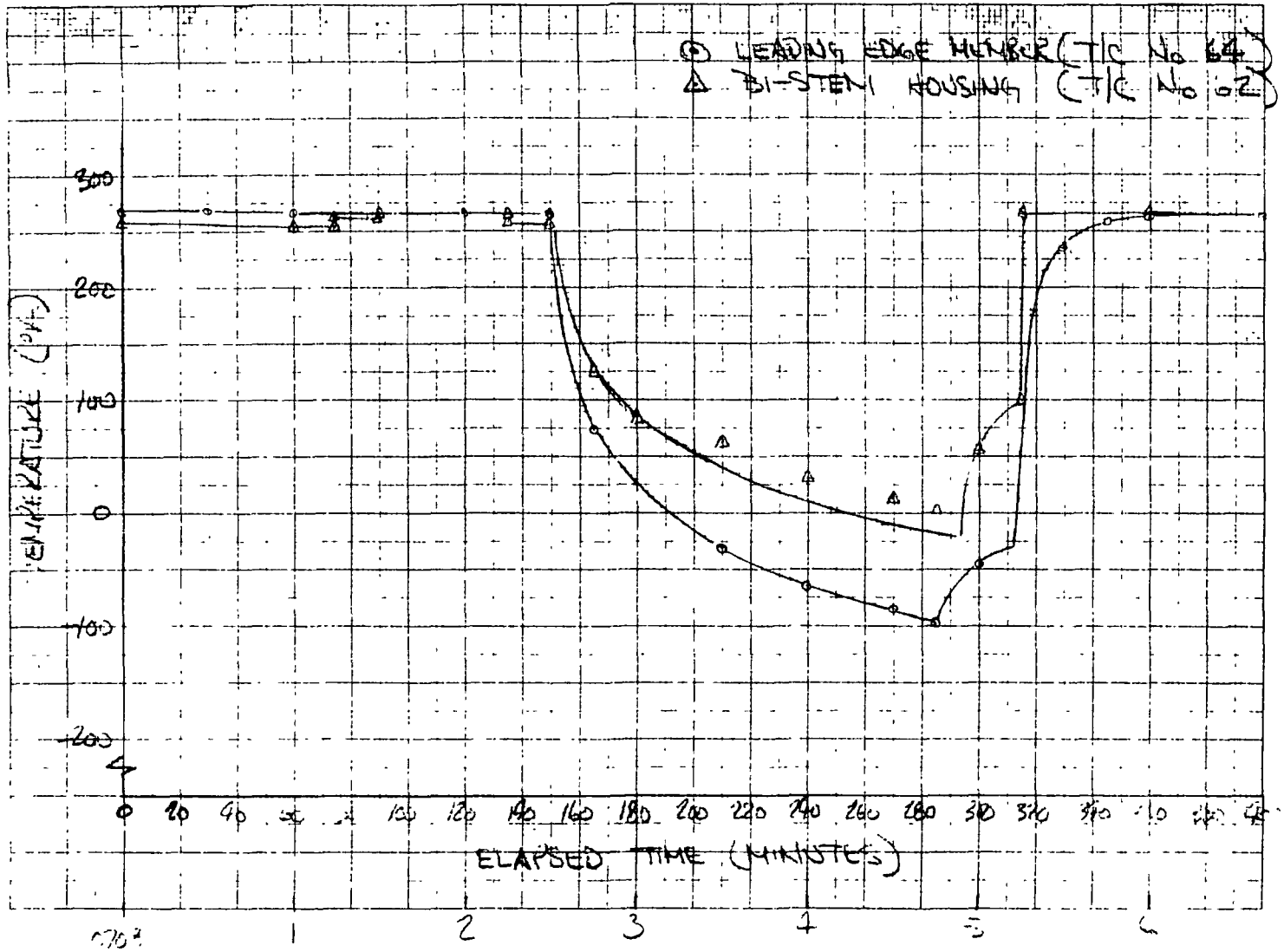

Figure 4.5-17. Deployed Transient Temperature History

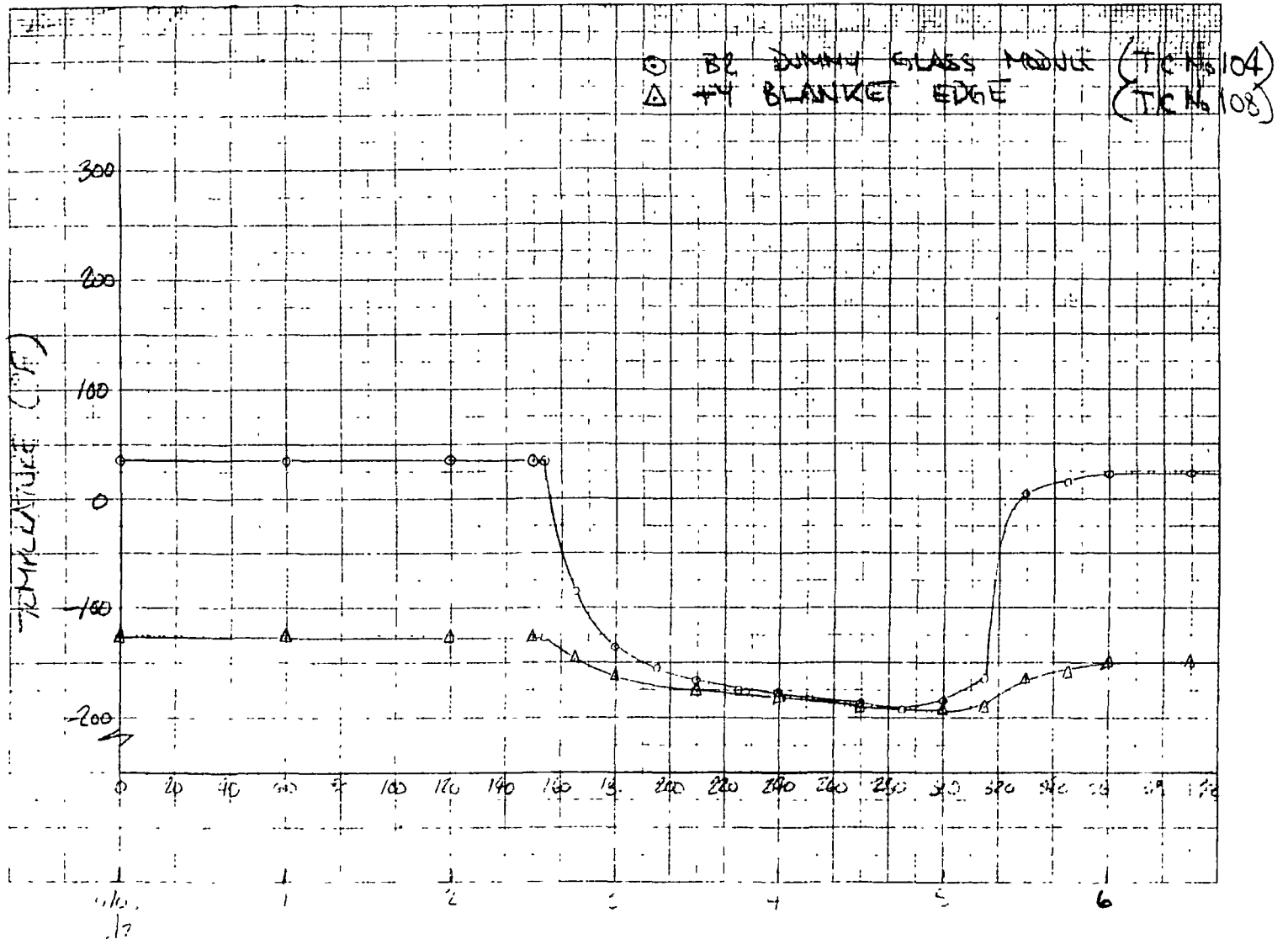

Figure 4.5-18. Deployed Transient Temperature History

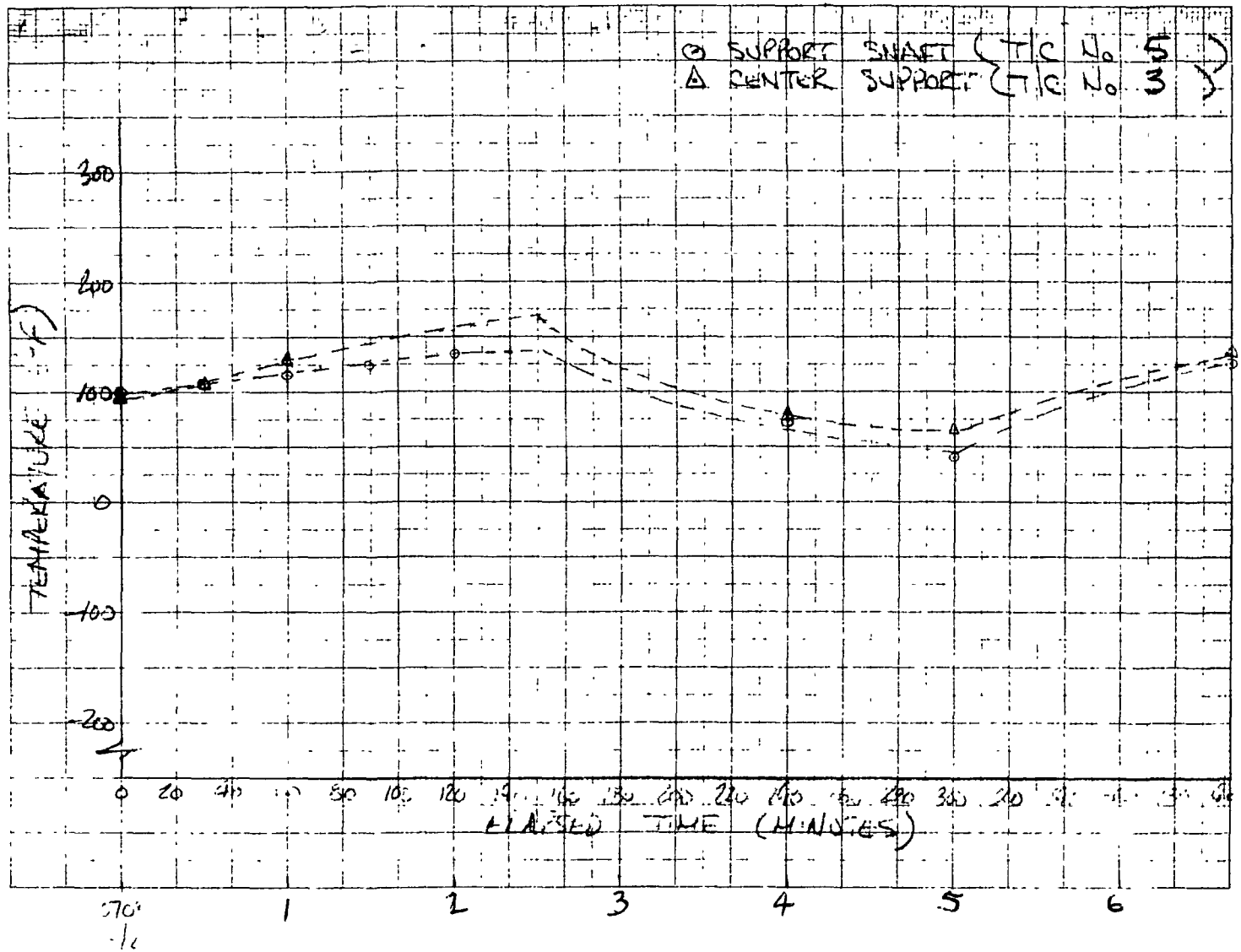

Figure 4.5-19. Deployed Transient Temperature History

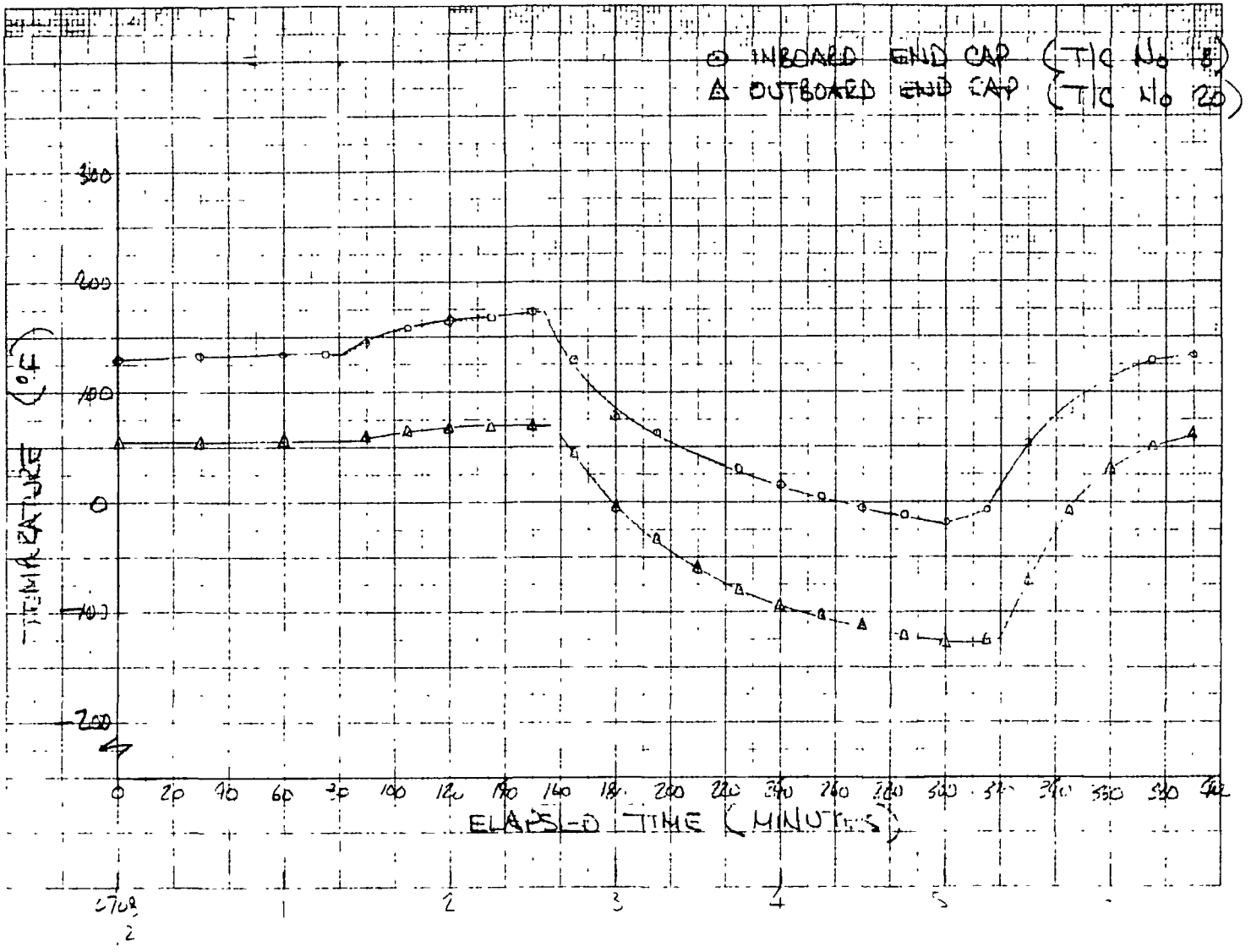

Figure 4.5-20. Deployed Transient Temperature History

module (No. 67 and 68) read maximum temperatures of 224°F and 228°F, respectively. These were the largest differences in temperature measured on any module. For example, on the E6 module (Figure 4.5-10) two widely spaced thermocouples (No. 28 and 48) separated by the Kapton substrate show a temperature difference of approximately 15°F.

Figure 4.5-19 shows the support shaft and center support temperature histories. Because of a partial failure of the K-Logger data system, the profile is based on the limited data indicated in the figures.

Figures 4.5-21 and 4.5-22 show the analytically predicted transient temperature histories for heat-up and cool-down, respectively. Comparing these predictions with the test results it can be seen that the inboard end cap is not as isolated from the adjacent structure as predicted by the analysis. The rapid array heat-up transient is confirmed by the test. The array cool-down at low temperatures is very much influenced by the sink temperature with the cryo panel temperatures of about -290°F being significantly above the absolute zero conditions used as the sink in the analysis.

4.5.5.2 Low Temperature Stowed

Figures 4.5-23 through 4.5-25 show the cool-down temperature histories of selected components of the stowed array. As seen it was not possible to reach the specified lower temperature extreme of -202°F (-130°C) on the control thermocouple (No. 34) without a long cold soak.

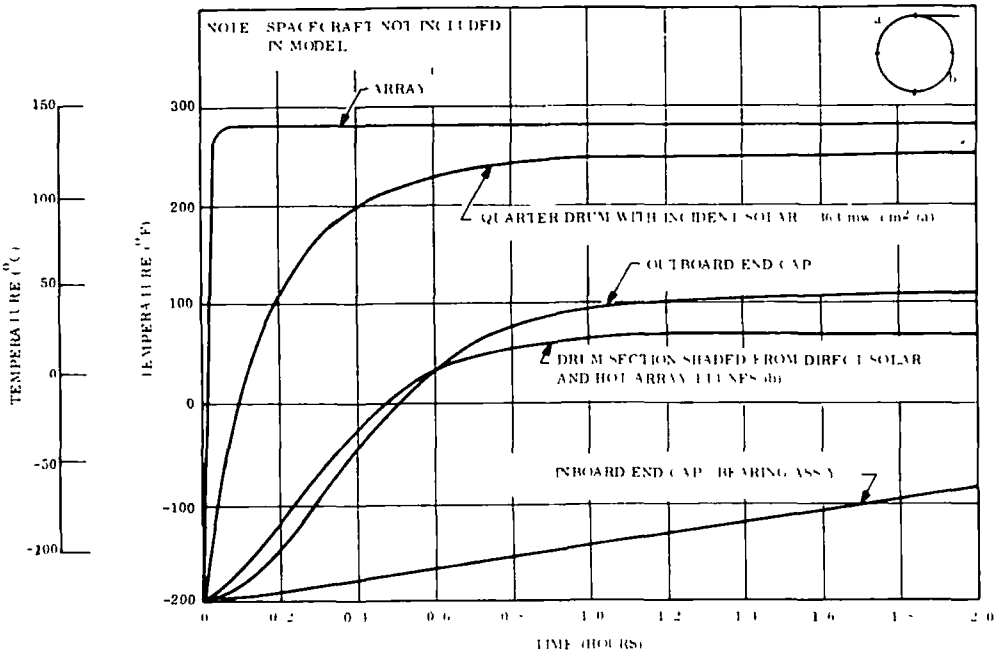

Figure 4.5-21. Deployed Array Heating Transient From -202°F (-130°C)

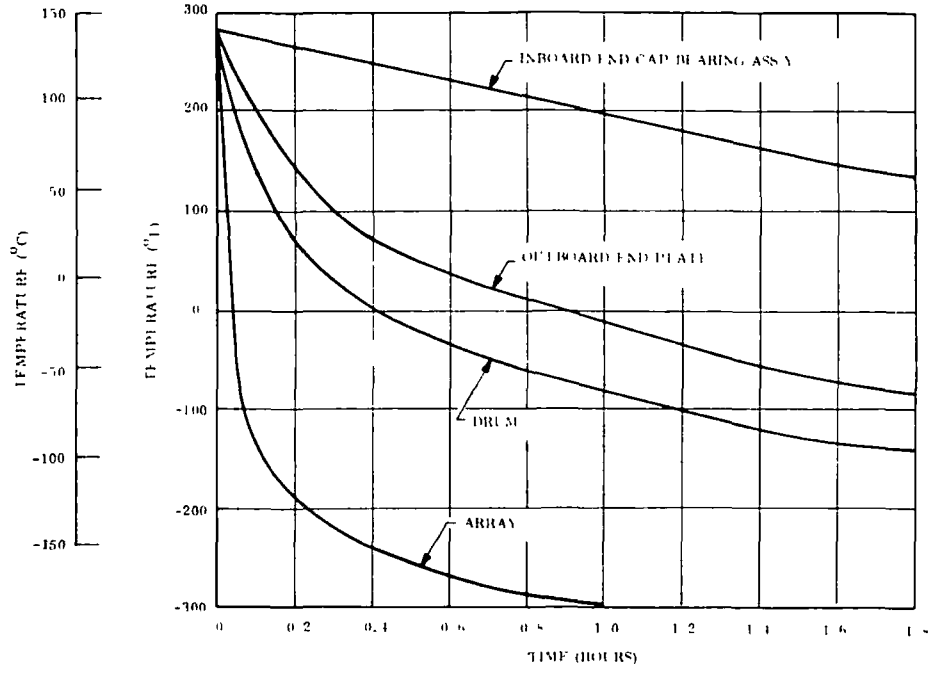

Figure 4.5-22. Deployed Array Cooling Transient From +284°F (+140°C)

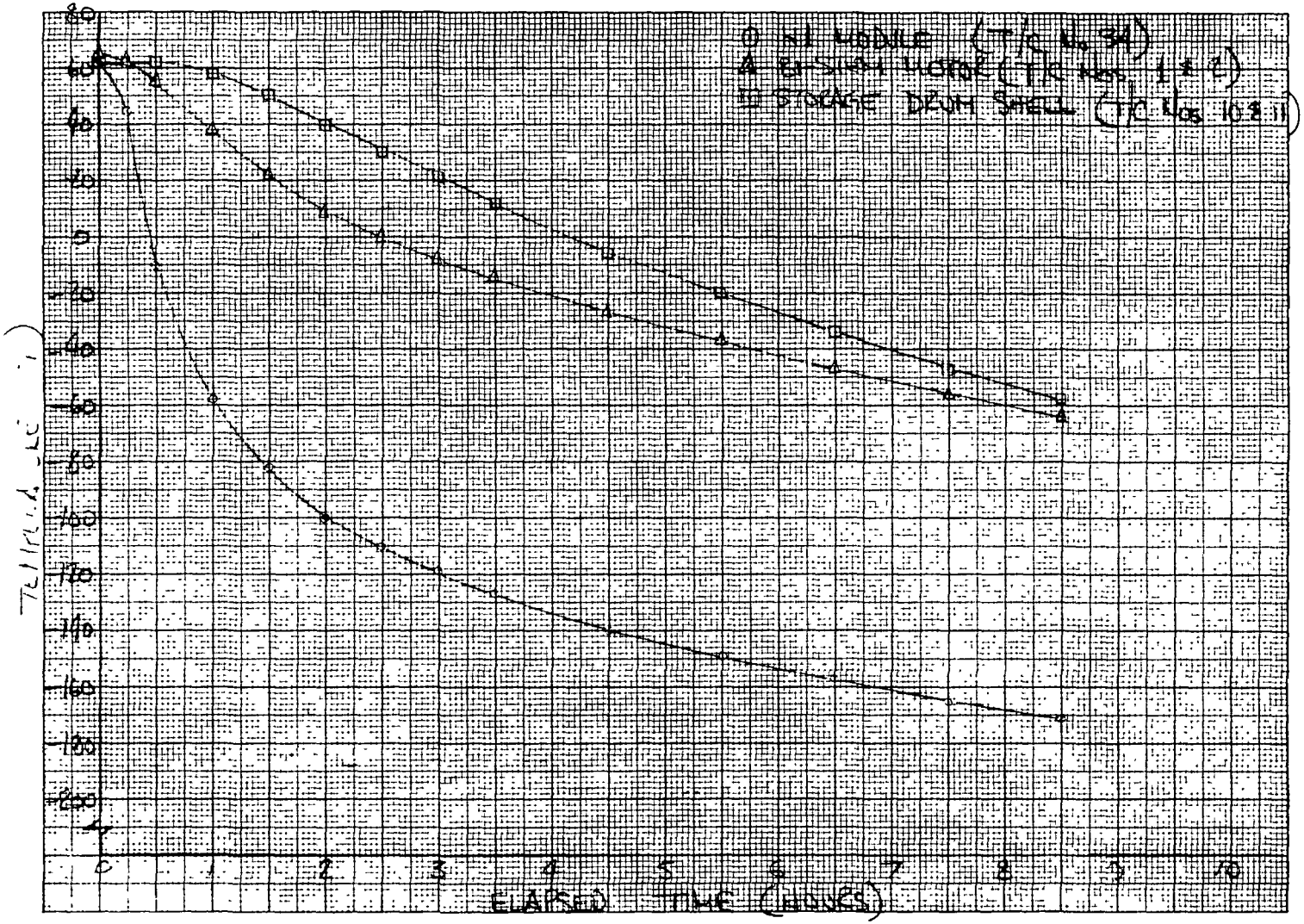

Figure 4.5-23. Low Temperature Stowed Cool-Down History

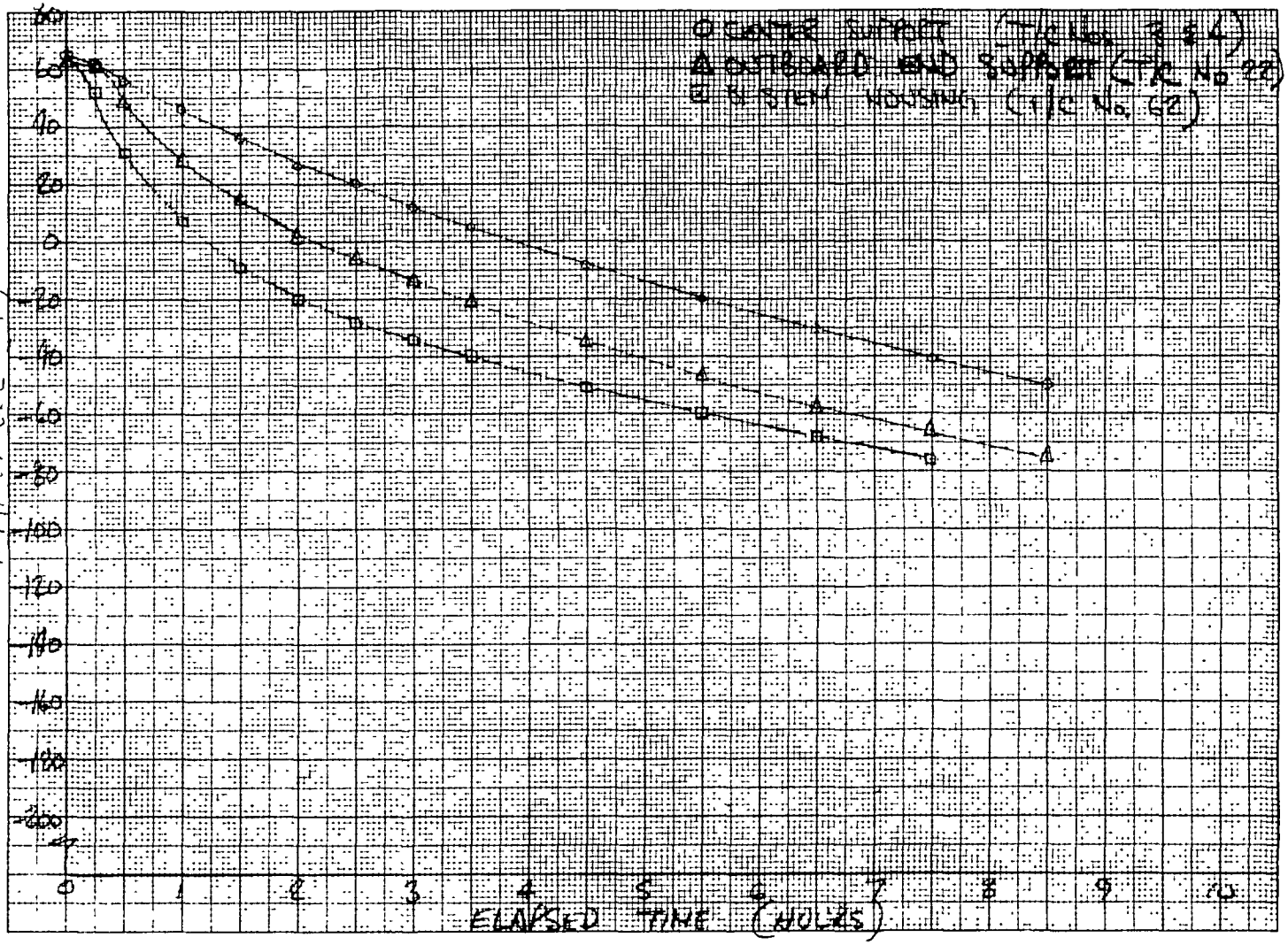

Figure 4.5-24. Low Temperature Stowed Cool-Down History

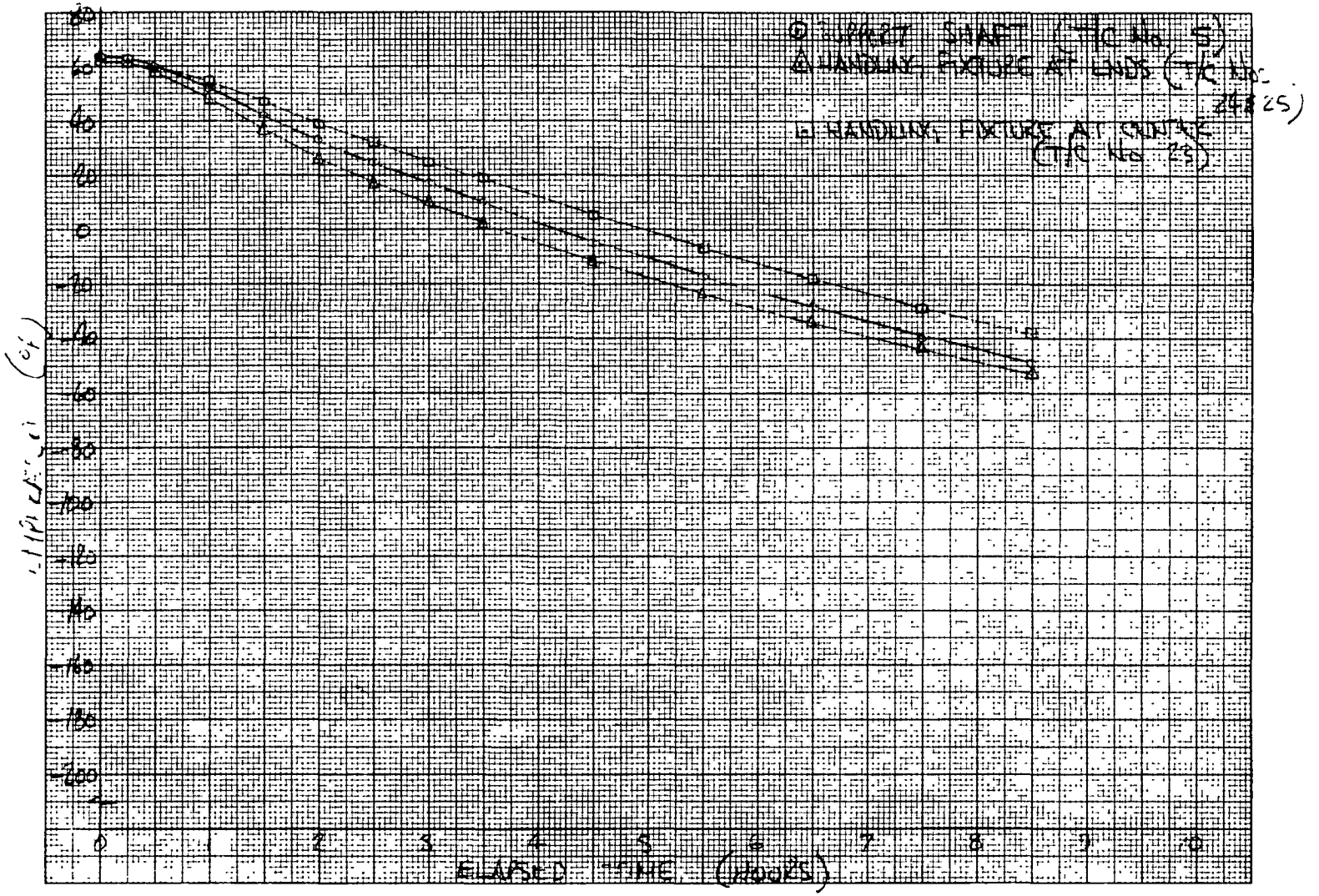

Figure 4.5-25. Low Temperature Stowed Cool-Down History

4.5.5.3 Low Temperature Deploy and Retract

The low temperature deployment of the array was initiated by the simultaneous firing of both squibs in each separation nut. The temperature recorded on thermocouple number 22 located on the outboard end support adjacent to the -Y separation nut was -76°F at the time of firing. An audible report was heard in the control room and a flash was seen on the closed circuit T.V. screen. Outboard end support release was verified by the signal from the microswitches at each end. Post test inspection of the test specimen revealed that both separation nuts had completely fractured at the mounting base (see Figure 4.5-26) and had been propelled against the cryopanels. The loose parts of the separation nut, (see Figure 4.5-27) were found laying in the bottom of the chamber completely detached from the electrical harness.

The two separation nuts, drawing no. 47C218327 P1, serial nos. 26800 and 26794, which failed were manufactured by the Hi-Shear Corporation of Torrance, California. The mode of failure in both cases was the same, i.e., the flange mounted base fractured around its complete circumference. The mounting base is made from a stainless steel 17-4PH investment casting and was subjected to a H 1075 heat treatment. Ambient and low temperature characteristics are published for 17-4 PH wrought stock.

Percentage increases and decreases for 17-4 PH investment castings should be similar to the percentage changes for the wrought stock. A matrix of approximate characteristic values for 17-4 PH stainless stell wrought stock follows:

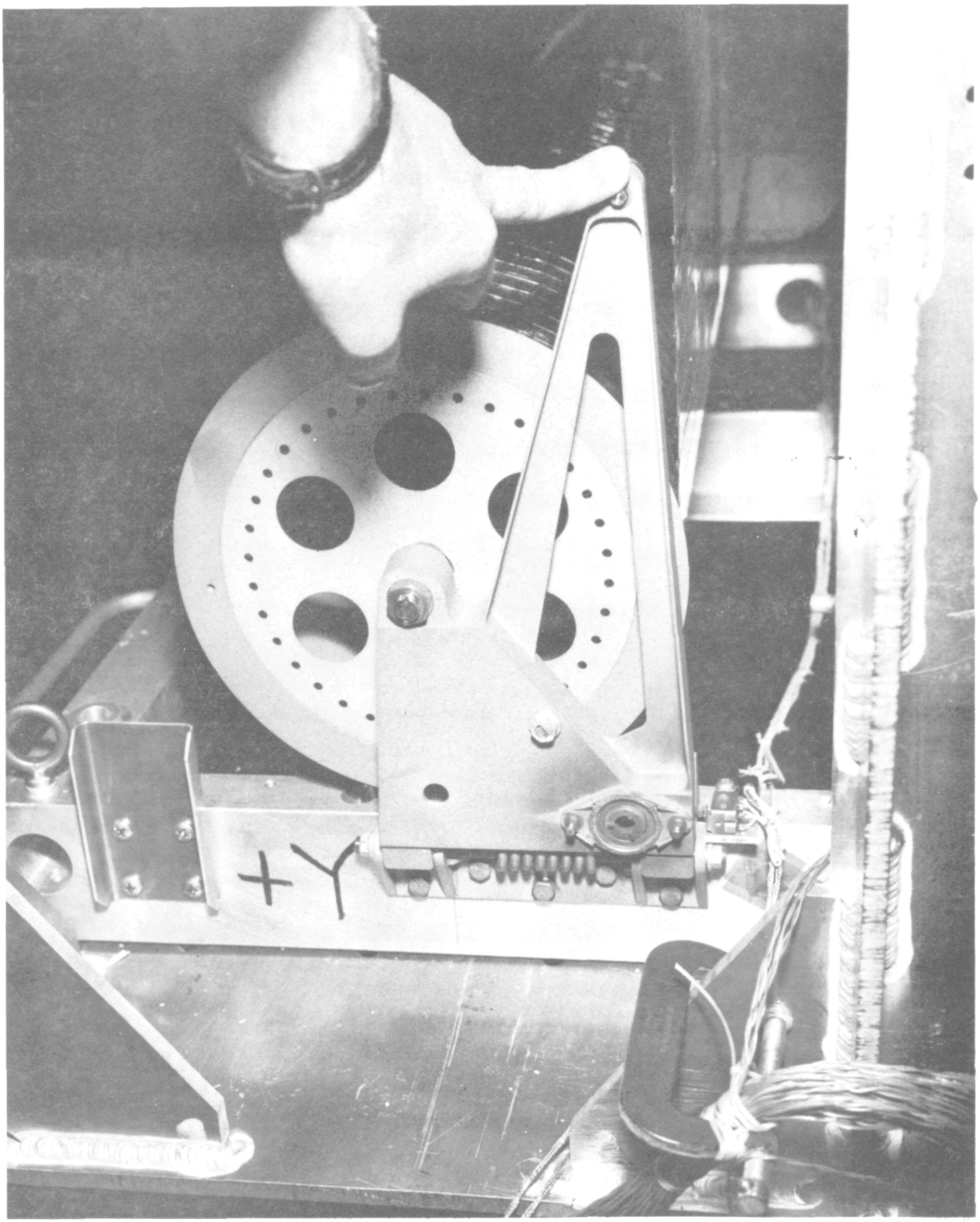

Figure 4.5-26. Outboard End Support Showing Fractured Separation Nut Mounting Base (VF 70 244B)

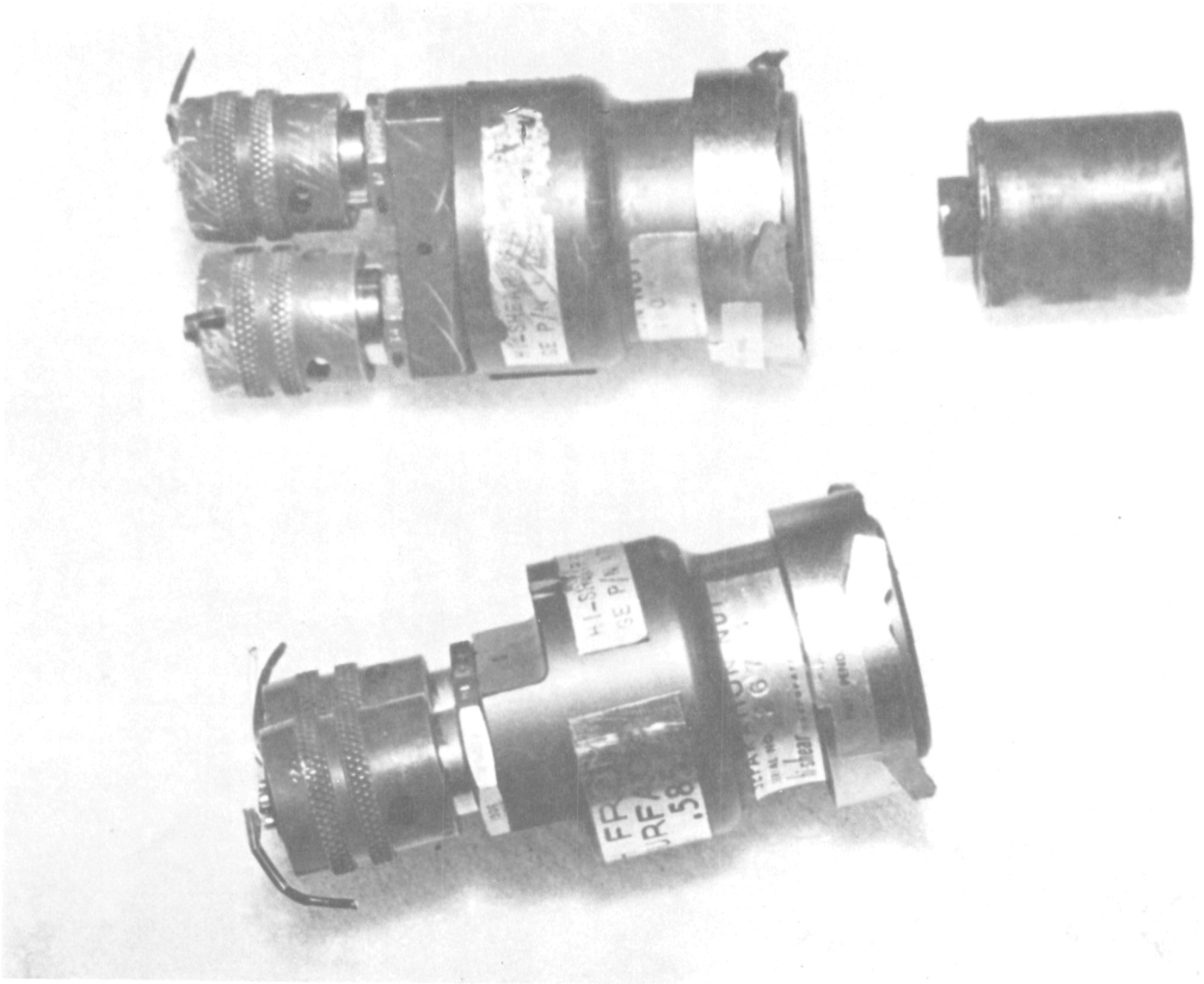

Figure 4.5-27. Both Separation Nuts With Fractured Mounting Bases (VF 70 244C)

	Ambient Temperature (72°F)	Low Temperature (-75°F)
Impact Strength	55 ft-lb.	25 ft-lb.
Yield Strength	175,000 psi	200,000 psi
Tensile Strength	187,000 psi	206,000 psi

At the low temperature to which the separation nut was subjected, -76°F, the reduced impact strength, coupled with the shock wave generated by the explosion of the squibs, caused both flange bases to fracture at their weakest points. However, to the extent that this investigation was conducted, it cannot be determined whether or not the material exhibited brittle failure. It should be pointed out that at ambient conditions, the separation nut is claimed to be capable of withstanding a pressure of 12,000 psi. The firing of the squibs creates an internal pressure stated to be 3,400 psi, which at ambient conditions allows for a significant margin of safety.

The failure was discussed with the vendor, Hi-Shear Corp. The vendor states that one of three materials is used in the manufacture of the flange base for this separation nut.

a. 7075-T6 Aluminum
b. 17-4PH Stainless Steel (Wrought Stock)
c. 17-4PH Stainless Steel Investment Casting (Heat Treat H 1075)

As previously noted, material (c) was used in the flange base for the separation nuts on the rollup solar array. Hi-Shear has stated that the nuts have been successfully operated at -100°F using two PC-42 squibs and flange bases fabricated from material (b). Hi-Shear has no low temperature data with material (c) used in the flange base.

Hi-Shear recommends that the mating structure completely support the flange base at the mounting surface. For the rollup solar array installation, the separation nut is mounted over a 0.75" diameter hole. The hole in the flange

base is 0.406" diameter. The holes are approximately centered. The flange base approximates an ellipse with a minor axis of 1.13" and a major axis of 2.25". The unsupported area is small in relation to the supported area.

Hi-Shear also recommends PC-42 squibs instead of the PC-32 squibs which were used. The vendor states that PC-42 squibs develop a pressure of 3200 psi in this installation. General Electric estimates that PC-32 squibs would develop a pressure of 200 psi more than PC-42 squibs.

Deployment of the BI-STEM element was accomplished without incident. The BI-STEM motor performance during this deployment is covered in Section 4.2. The motor temperature was -63°F immediately prior to deployment with a 37°F rise recorded during the deployment. The BI-STEM was retracted from the fully extended position, but the retraction was stopped 77 inches short of the fully stowed position because of an apparent billowing of the +Y blanket as viewed via the closed circuit T.V. camera. At the end of this retraction the motor temperature was -7°F. Upon entering the chamber to examine the test specimen, the major portion of the -Y blanket was found draped on the chamber cryopanels. Figures 4.5-28, 4.5-29, and 4.5-30 show three different views of the unwrapped -Y blanket. The +Y blanket was discovered in a billowed condition but the movement of personnel in the chamber was enough to cause the +Y drum to rotate and rewrap the blanket in its normal stowed configuration. More detailed examination of the -Y blanket revealed that the pull-apart connector for thermocouple number 34 was lodged in the wrapped blanket in such a way as to prevent the drum from rotating. The failure to secure this connector to the BI-STEM housing had evidently caused much of the -Y blanket rewrapping problem. However, this test condition in no way influenced the billowing of the other blanket.

4.5.5.4 Stowed Transient and High Temperature Soak

The results of the stowed transient test are shown in Figure 4.5-31, 4.5-32, and 4.5-33. All these curves are based on thermocouple data except the E6 module temperature (Figure 4.5-32) which was derived from the thermistor signal. During the heating period, the indicated temperature of this module exceeded the +275°F.

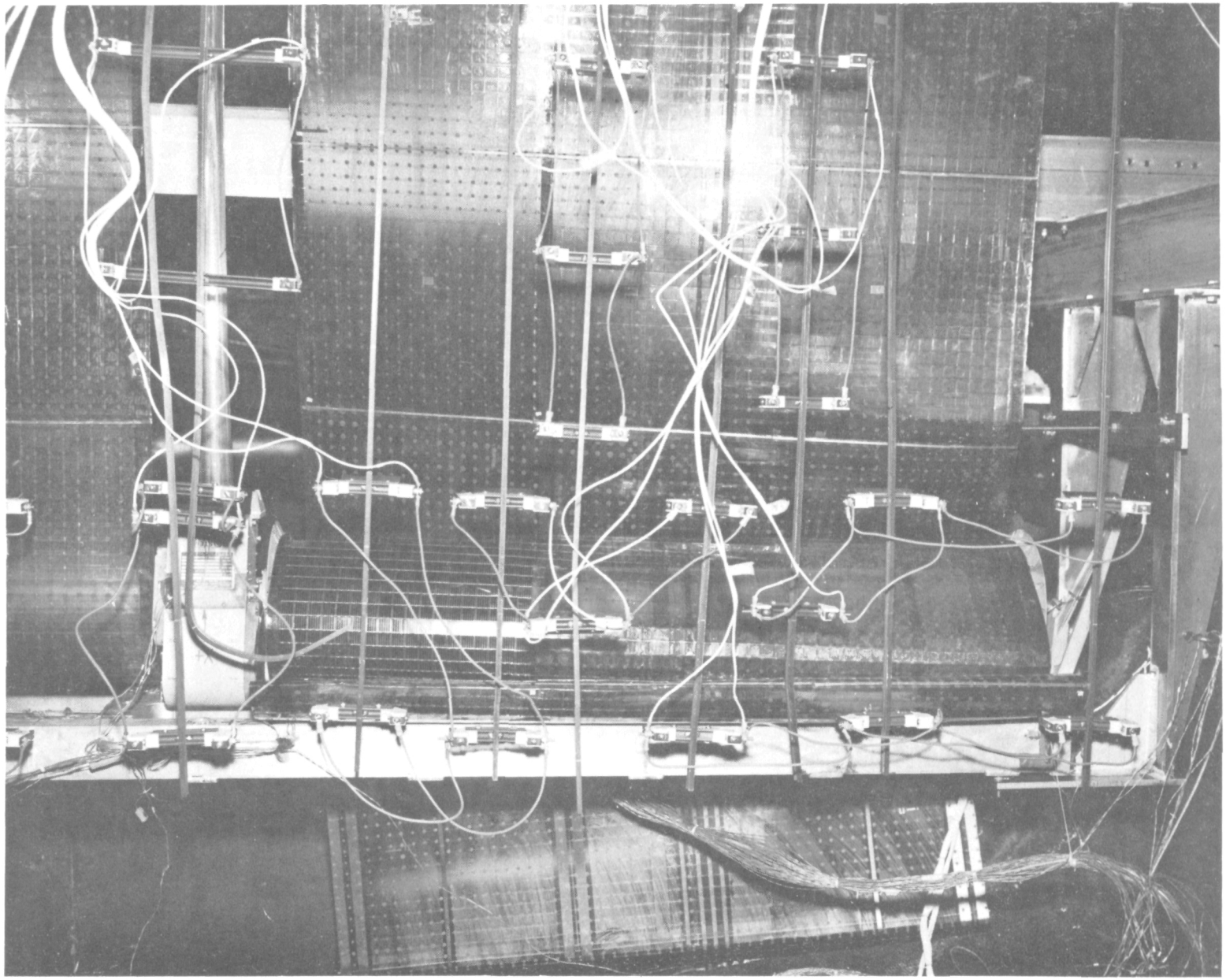

Figure 4.5-28. Unwrapped -Y Blanket as Viewed From Lamp Array Side (VF70 244A)

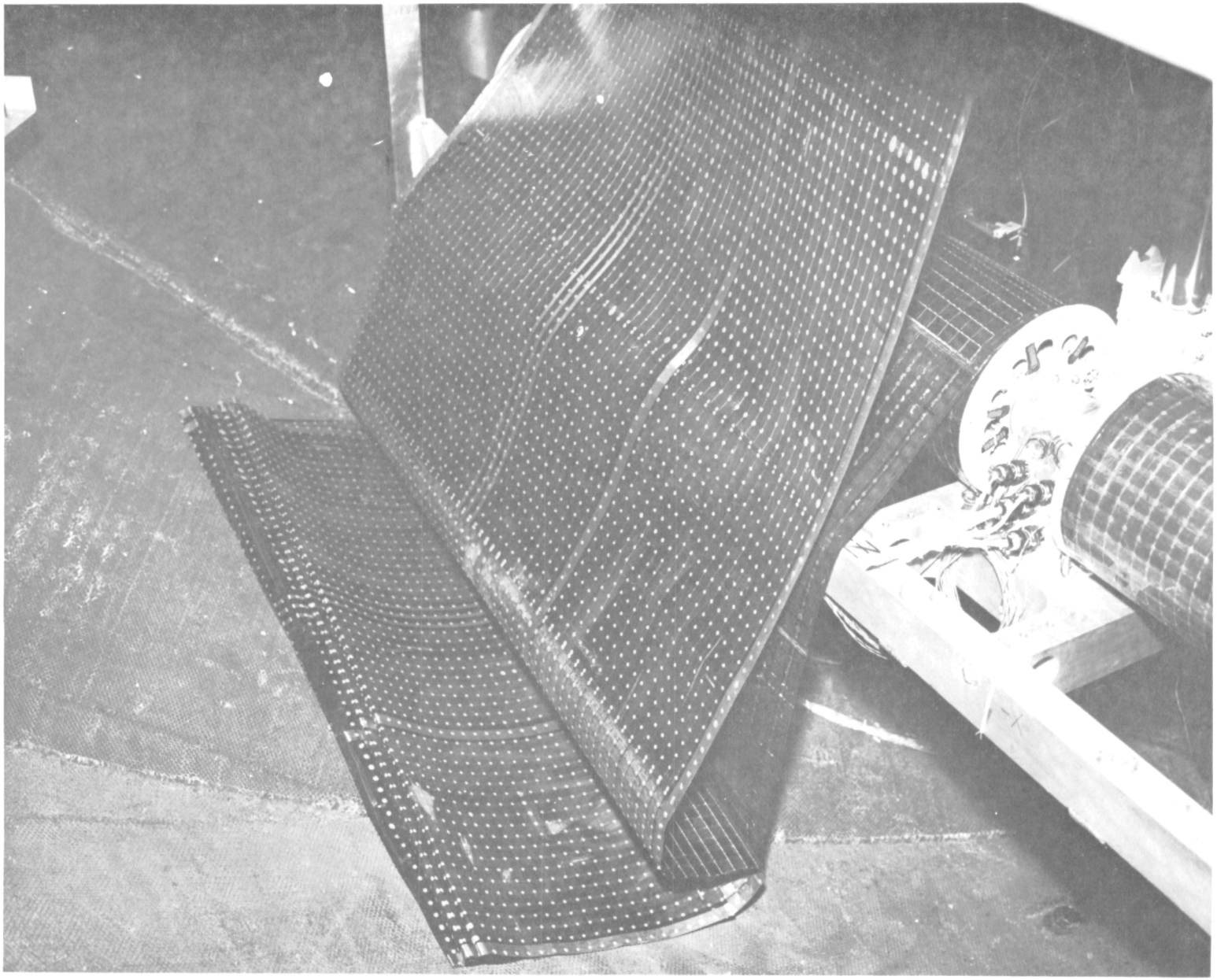

Figure 4.5-29. Unwrapped -Y Blanket as Viewed From Rear Side (VF 70 244E)

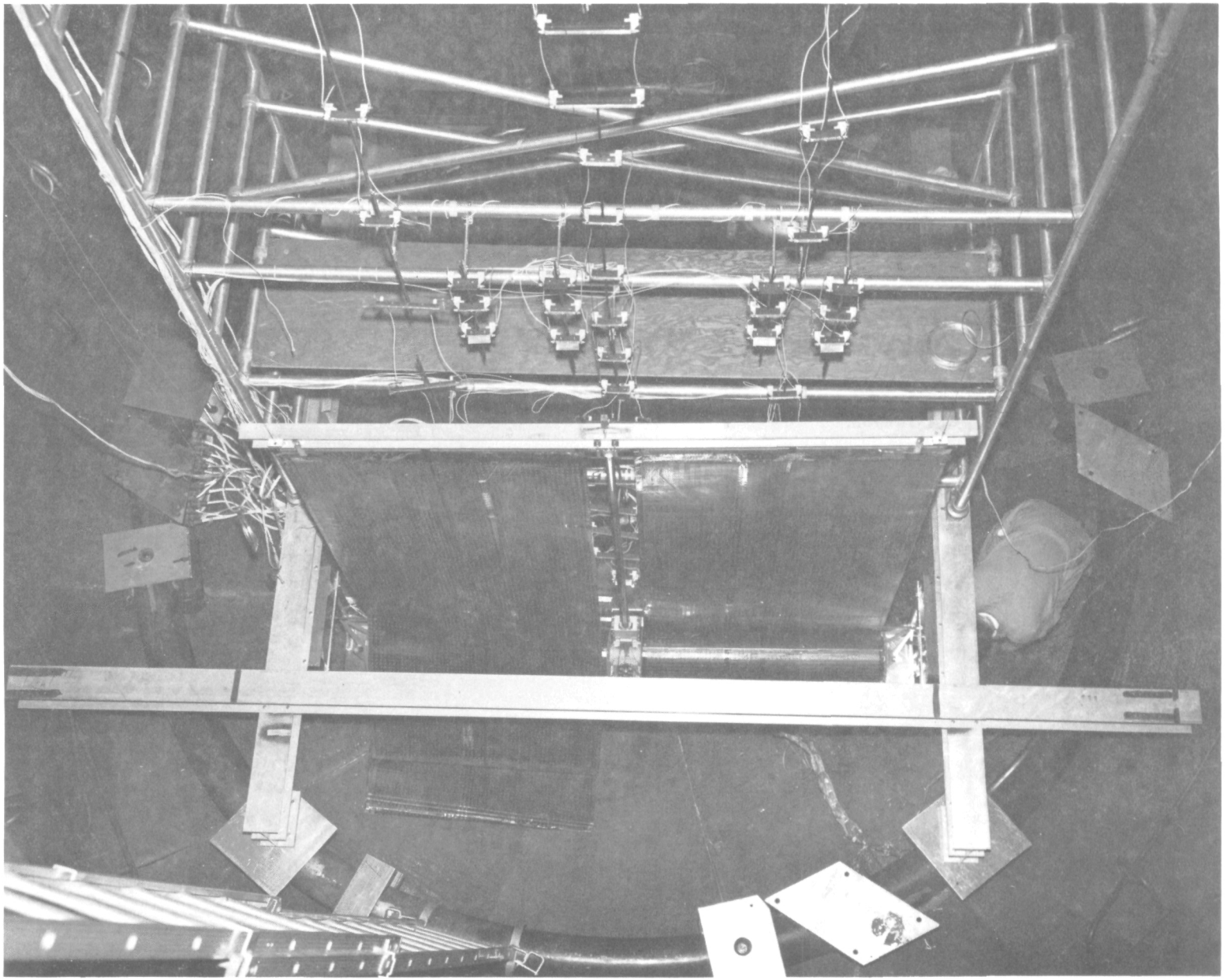

Figure 4.5-30. Unwrapped -Y Blanket as Viewed From Above (VF 70 244D)

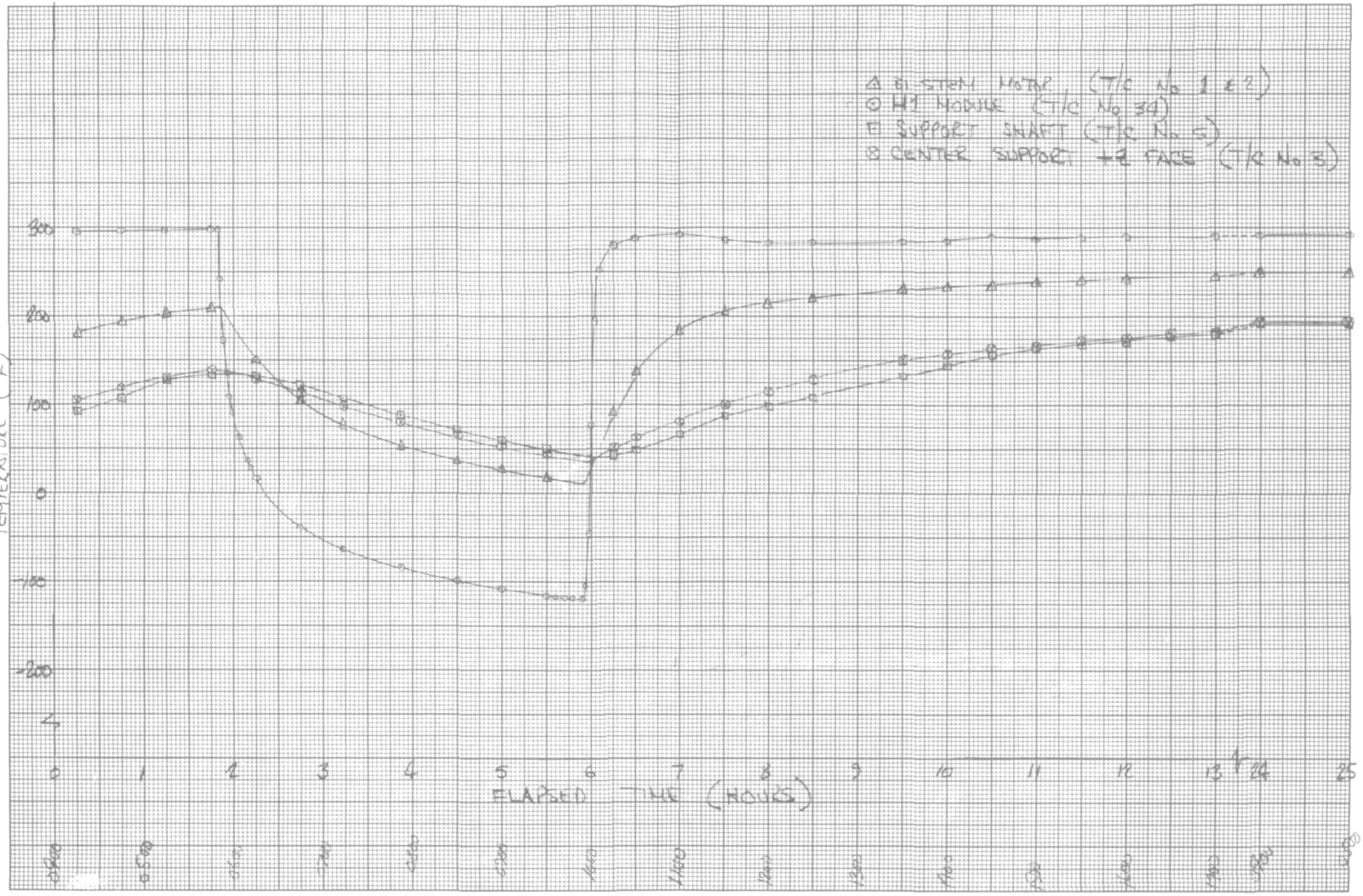

Figure 4.5-31 Stowed Transient Temperature History

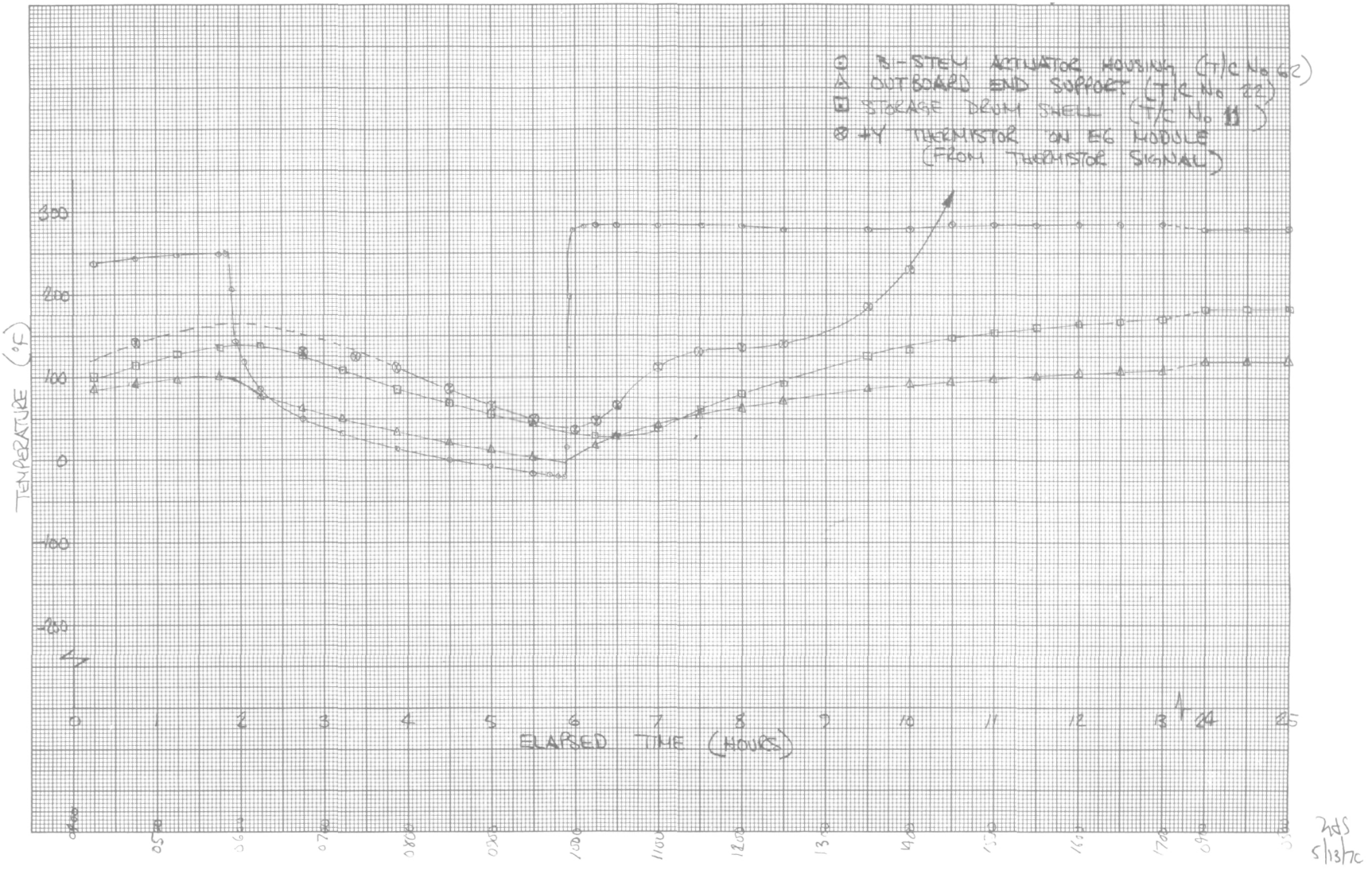

Figure 4.5-32 Stowed Transient Temperature History

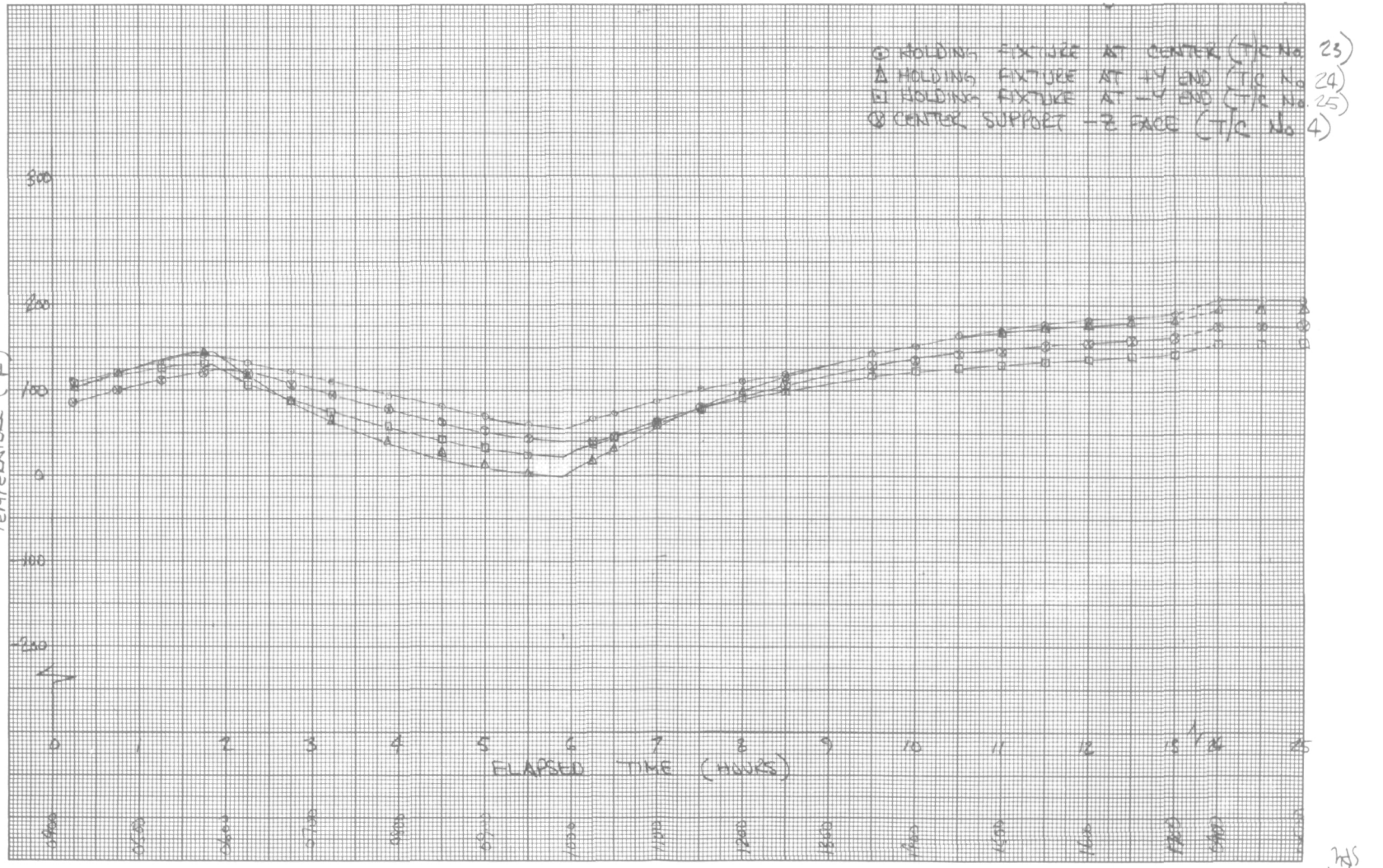

Figure 4.5-33 Stowed Transient Temperature History

upper limit of available thermistor temperature signal data. This localized heating of the inner blanket wraps is discussed in Section 4.5.5.6.

Figures 4.5-34, and 4.5-35 show the analytically predicted transient temperature responses for the stowed array. In comparing the analyses and test it should be noted the test transients were not initiated from uniform temperature conditions. The data shows that the interior of the system has long time constants. As discussed in Section 4.5.5.6, heat was introduced into the middle of the stowed blanket wraps.

4.5.5.5 High Temperature Deploy and Retract

The high temperature deploy and retract cycle was performed without failure. Post test examination of the rewrapped blankets revealed a normal condition.

4.5.5.6 Post-Test Inspection

The post test examination of the array blankets revealed localized areas where the SMRD-745 adhesive had scorched. These areas on the +Y and -Y blanket are shown in Figures 4.5-36 and 4.5-37, respectively. As shown in both figures the scorched areas are exactly one circumference apart located with the outer-most area on the side nearest to the IR lamps. The degree of scorching indicates that the areas in the middle of the blanket reached higher temperatures than either the outer wraps or the inner-most wraps. Two solar cell modules (E6 and J6) were situated within an overheated area at the same longitudinal station. J6 suffered extensive lifting of the interconnect top contact feet in the overheated areas. The fact that these connections became unsoldered indicates a localized temperature in excess of 350^{o}F. Subsequent high temperature exposure tests of specimens of glass bonded to Kapton with SMRD-745 indicated that scorching will occur at a temperature of approximately 400^{o}F.

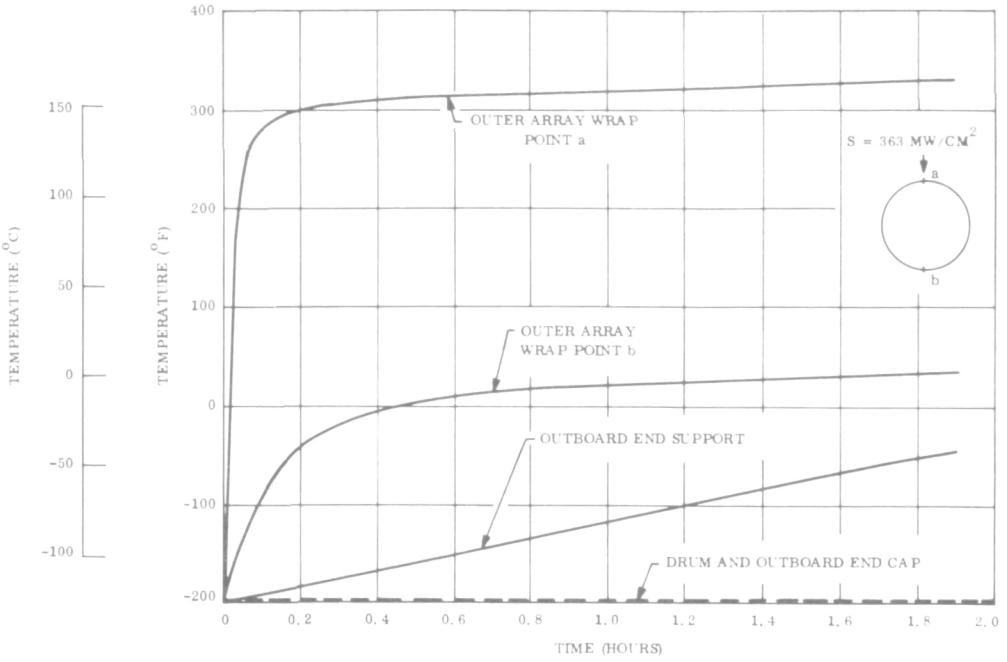

Figure 4.5-34 Stowed Array Heating Transient From -202°F (130°C)

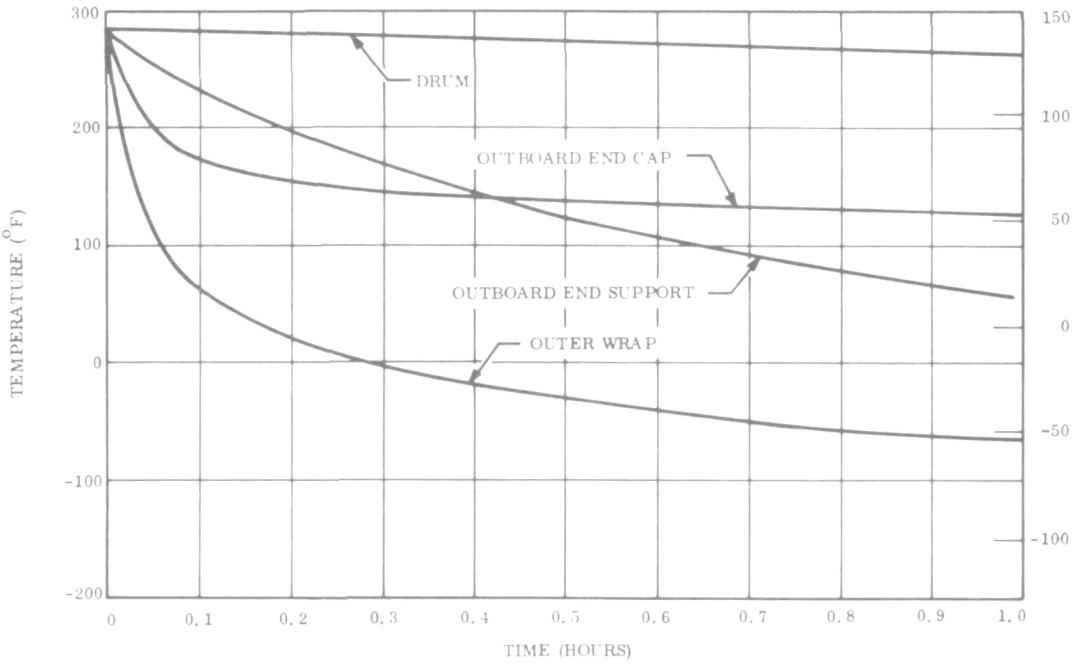

Figure 4.5-35 Stowed Array Cooling Transient From +284°F (+140°C)

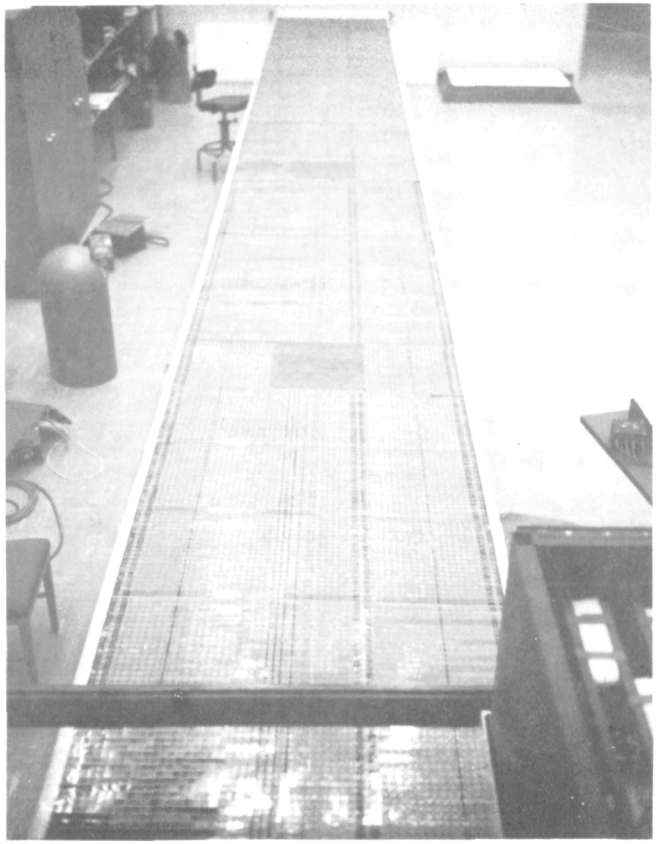

(a) Overall View

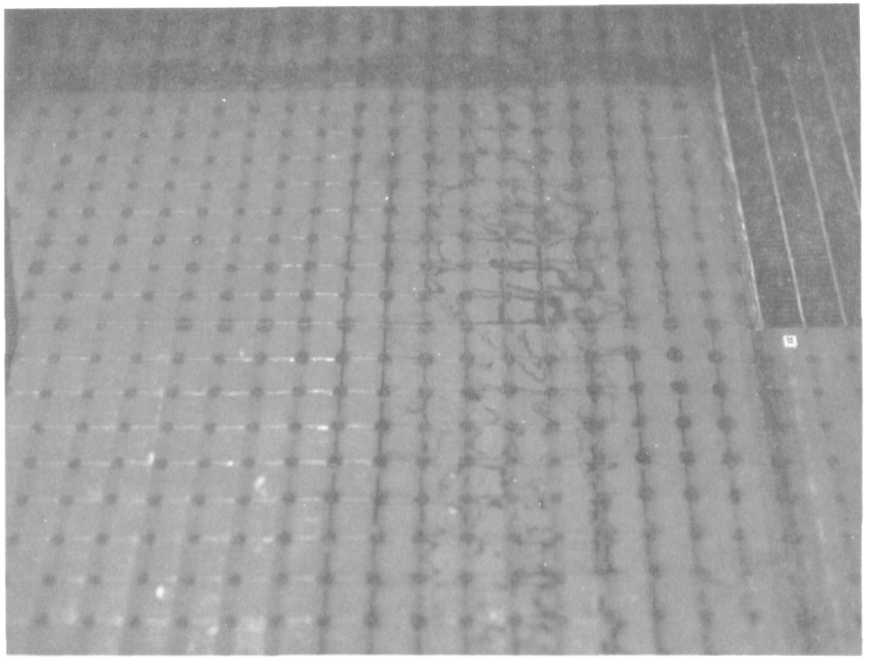

(b) Close-up of B11 Dummy Glass Module.

Figure 4.5-36 Scorch Marks on +Y Array Blanket

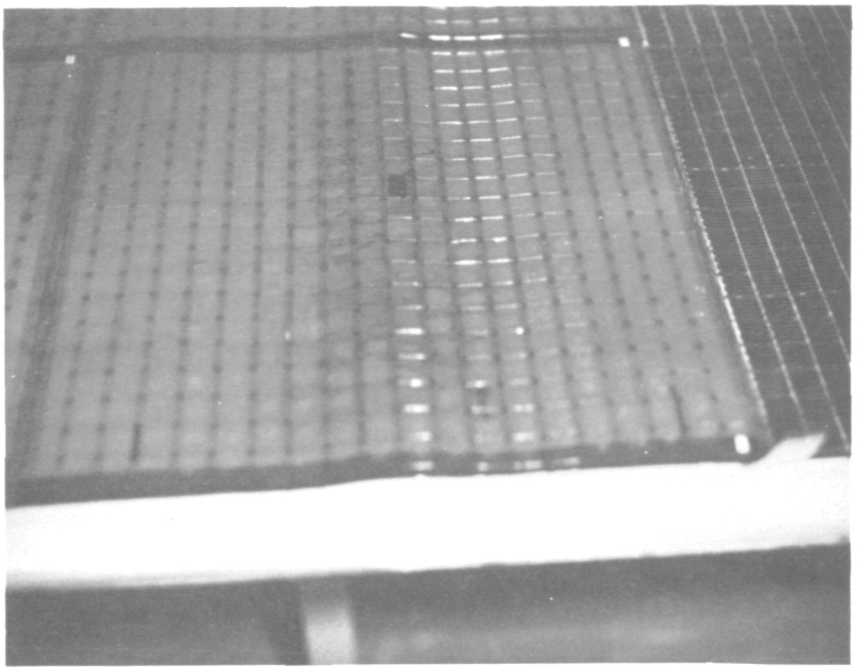

(b) Close- up of G6 Dummy Glass Module

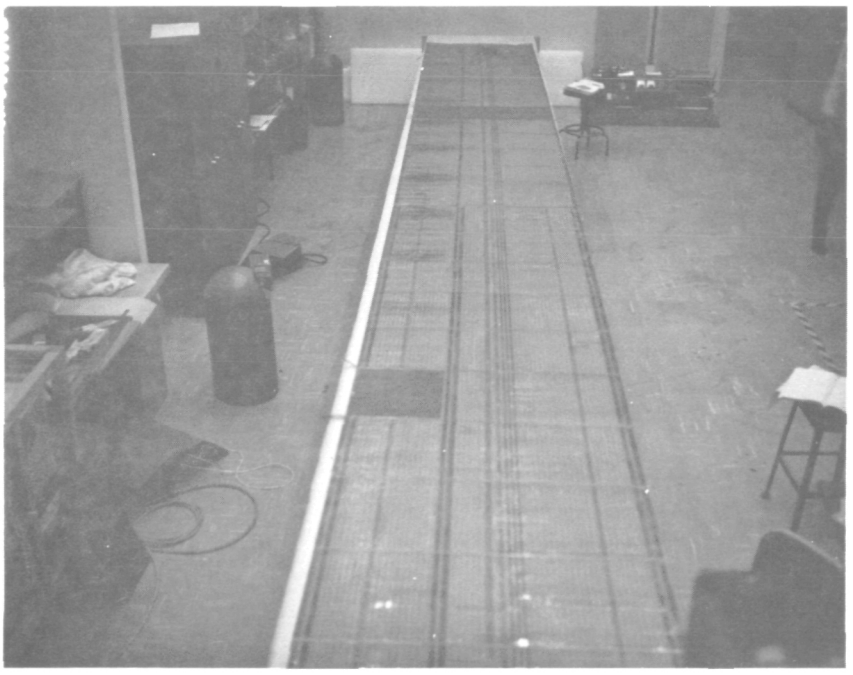

(a) Overall View

Figure 4.5-37 Scorch Marks on -Y Array Blanket

The scorching pattern which was observed immediately pin pointed the problem as a "greenhouse" effect where the energy is transmitted through the wraps, absorbed and trapped inside. In order to transfer the absorbed energy, the inner wraps increase in temperature until a sufficient temperature is established so that the absorbed heat can be re-radiated. The absorbed energy is transferred from wrap to wrap until the outer wrap is reached where all the absorbed energy is radiated to the cryowalls. The distribution of the absorbed energy is a function of the spectral distribution of the energy source and the optical properties of the wraps. Most of the blanket area is covered with glass platelets. Transmittance data for the Corning 0211 Microsheet glass platelet is shown in Figure 4.5-38. The transmittance of the thick sheet of Microsheet cuts off abruptly at about 2.8 μ. This characteristic over-rides the IR transparency of other layers in the blanket composite and causes the assembly to be opaque in the infra red spectrum.

An analysis was performed to assess the magnitude of the temperatures possible based on the available data and assumed heat fluxes. Table 4.5-2 shows the assumed composite substrate characteristices. Figure 4.5-39 presents the measured color temperature of the T3 lamps as a function of operating voltage. A review of the test data indicated that the average lamp voltage near the stowed array was about 70 volts. From Figure 4.5--39this yields a lamp color temperature of 2400^{o}K. The black body heat flux from these lamps, based on 2400^{o}K, has an energy distribution as a function of wavelength as shown in the second column of Table 4.5-2. Assuming that each wrap of the stowed array has the same optical properties and further assuming that the emittance is 1 minus the transmittance, a multinode heat balance can be obtained. Figures 4.5-40 shows the result of this analysis for 12 wraps on the storage drum. Only 12 wraps were used in the analyses since the absorbed heat was insignificant at the inner most layers. The boundary

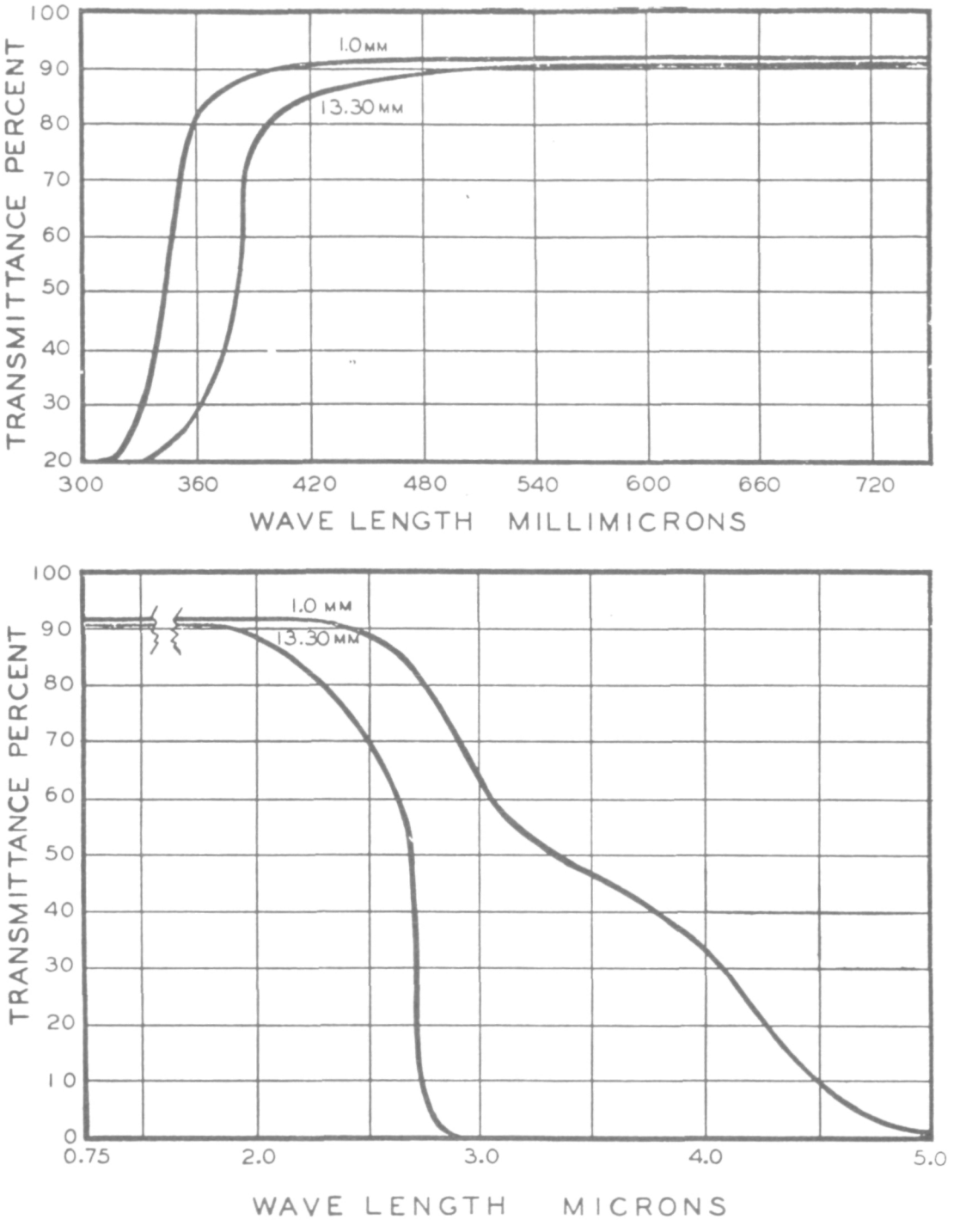

Figure 4.5-38. Transmittance of Corning 0211 Microsheet

Table 4.5-2 Composite Optical Properties of Roll Up Array Blanket

% Tot. Energy (Microns) λ	% Tot. Energy* $\frac{W_{o-\lambda}}{W_{o-\infty}}$	Glass Transmittance T_G	Kapton Transmittance T_K	Composite Transmittance T_G T_K	Composite Absorptance $\alpha = 1 - (T_G T_K)$
.6	1	.9	.9	.81	.19
.78	5	.9	.88	.792	.208
.91	10	.9	.86	.775	.225
1.1	20	.9	.84	.755	.245
1.3	30	.9	.82	.738	.262
1.5	40	.9	.80	.72	.28
1.7	50	.9	.79	.711	.289
1.97	60	.9	.79	.711	.289
2.3	70	.7	.79	.553	.447
2.53	75	.67	.72	.482	.518
2.85	80	0	.65	---	1.0
3.9	90	0	---	---	1.0

* Energy distribution for T3 Lamp at 70V (Color Temperature 2400K)

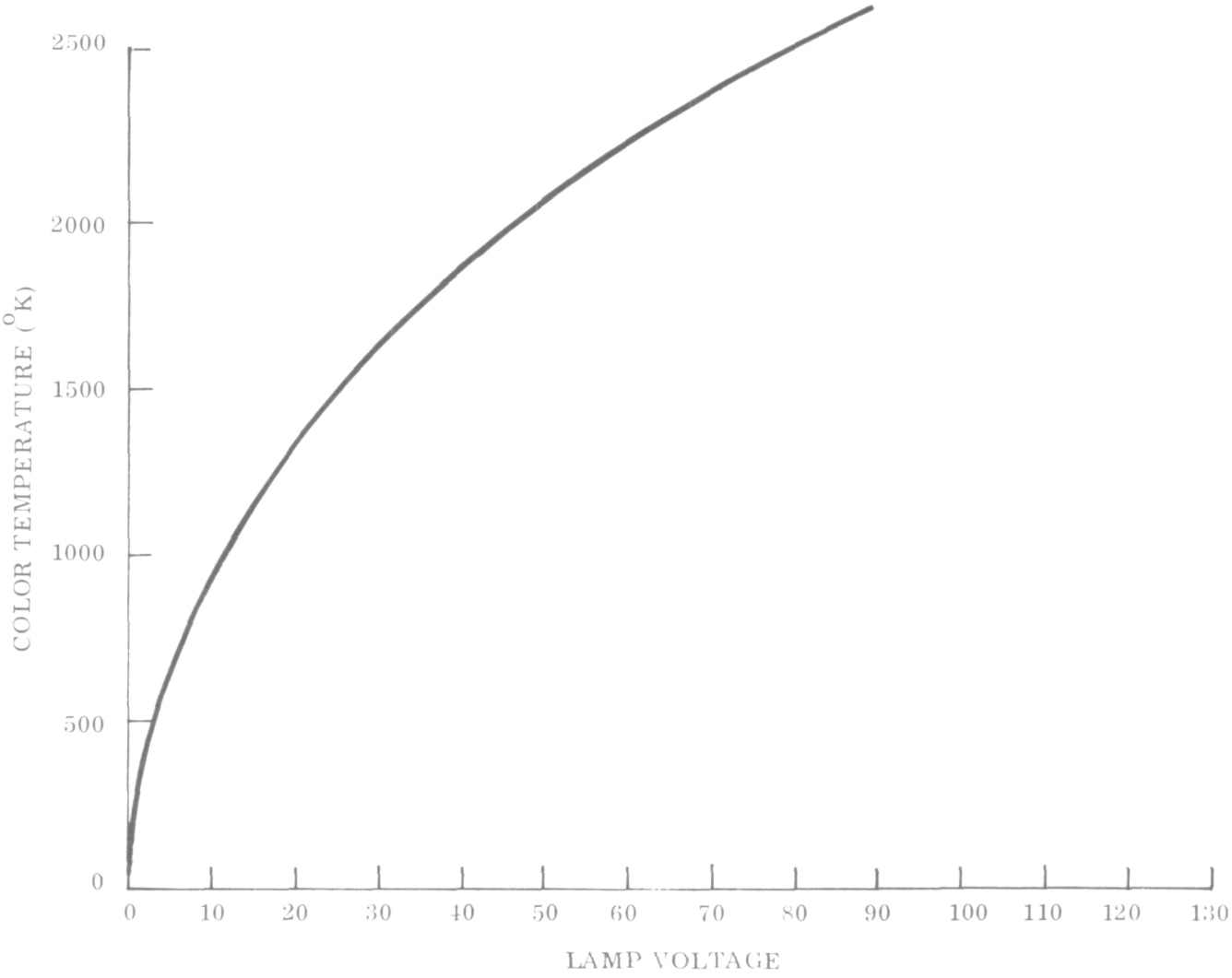

Figure 4.5-39. Color Temperature Versus Voltage For Quartzline Lamp - Tungsten T3-500 Watt

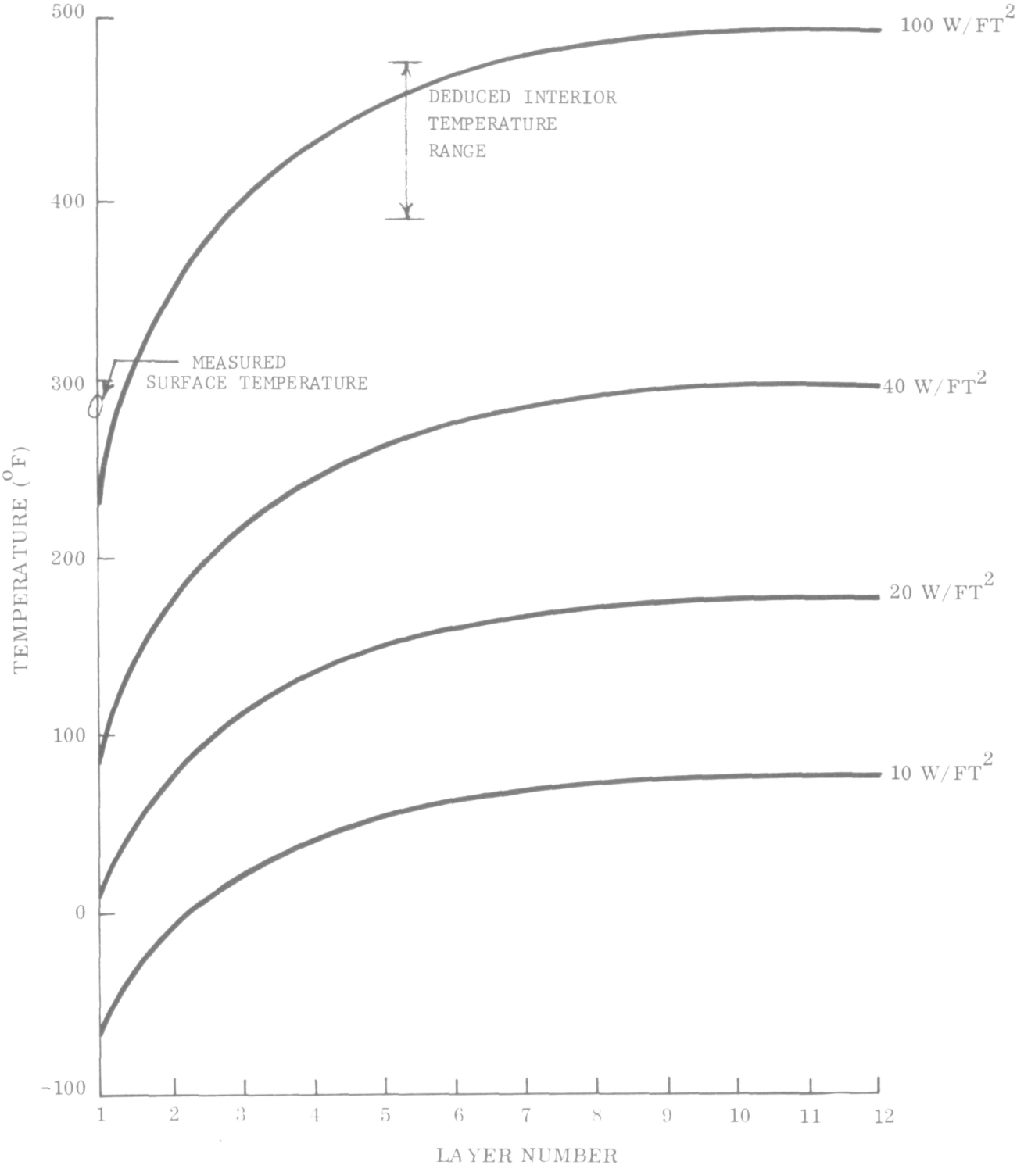

Figure 4.5-40. Temperature Distribution in Stowed Rollup Array Blanket With Glass Simulated Solar Cells.

condition at the inner most wrap was assumed to be abiabatic for this analysis. The curves on this figure were generated for four incident heat fluxes and a 2,400°K color temperature. The distribution of absorbed heat is propotional to the incident heat flux. The temperature distribtuion through the layers shows the highest gradient in the outer layers and the smallest in the inner layers. Heat losses through the storage drum shell will cause the inner wraps to be cooler than predicted by this analysis. 100 watts/ft^2 is sufficient to cause interior temperatures that would melt solder. The incident heat flux was planned to be at least this high. It is concluded the "greenhouse" effect caused the problem.

4.5.6 CONCLUSIONS AND RECOMMENDATIONS

The following conclusions and recommendations are presented as a result of this thermal vacuum test series.

1. The array system survived the thermal vacuum test conditions. The identified problems with excessive test blanket temperatures, does not exist on a blanket 100% covered with active solar cells. Other problems are discussed as separate items.

2. The analytical models of the array (both stowed and deployed) were generally confirmed by test. It was not possible to exactly duplicate the initial and boundary conditions used in the analysis. For example, a uniform temperature for the initiation of the stowed transients was not possible.

3. The actuaton was successfully operated at both high and low temperature conditions. Note that the maximum operating temperature of 100°C is 39 degrees above the temperature to which the motor gearhead had been qualified.

4. The high temperature deployment/retraction was successful as was the low temperature deployment. The verification of low temperature retraction was clouded by a fouled thermocouple wire. However, the present storage drum

constant torque Negator spring system may be marginal to overcome the increased blanket rewrap forces at low temperatures. Further experimental investigations of blanket bending stiffness at low temperature are necessary to enable the selection of the proper Negator spring.

5. Separation nut corrective action is necessary if low temperature outboard end support release is required. This action should include the selection of a mounting flange material which is satisfactory for low temperature impact type loading. The size of the hole in the movable arm can be reduced to 0.406 inches to provide support under the entire flange base area. Those changes should be followed by a component level testing program to qualify the device for low temperature activation.

6. The temperature cycling of the active solar cell modules was not the most damaging environment of the environmental test series. However, failures typical of those caused by thermal cycling were observed. Additional thermal cycling tests are needed but should be run on a sample basis rather than a system basis. The total array system is difficult to thermal cycle.

4.6 ACOUSTIC TEST

4.6.1 INTRODUCTION

The Acoustics Test was performed in the General Electric Reentry and Environmental Systems Division facility at 3198 Chestnut Street, Philadelphia, Pennsylvania. The array in the stowed configuration was subjected to the following exposures to an acoustic environment:

Run 1	40 second checkout run at	130 db nominal
Run 2	30 second full level run	150 db nominal
Run 3	30 second full level run	150 db nominal
Run 4	30 second full level penalty run	150 db nominal
Run 5	30 second full level penalty run	150 db nominal

The penalty runs were made because the level of the second full level run was slightly below 150 db. Post test inspection showed no visible or operational damage. Details of the post test health check are given in Section 4.2.

4.6.2 OBJECTIVES

The objectives of this test were as follows:

1. Prime

   a. To demonstrate array structural and functional integrity following exposure to 60 seconds of random incidence, reverberant sound with an overall sound pressure level of 150 db as specified in Reference 1-2.

2. Secondary

   a. To define the acoustic environment at various locations in the array for future use in planning test and development programs.

   b. To provide information on the response of the array system for the evaluation of acoustic testing in future programs.

4.6.3 RESULTS AND CONCLUSIONS

4.6.3.1 Results

The overall levels are shown in Tables 4.6-1 and 4.6-2. Microphone locations are shown in Figure 4.6-1. Selected spectrograms of the noise field are shown in Figures 4.6-2 and 4.6-3 and power spectral density plots of accelerometer responses are shown in Figures 4.6-4 through 4.6-15. The noise field data shown is typical of that generated in the test runs. It tracks the lower boundary of the specified environment. The penalty runs were made to compensate for the slightly less than nominal environment. The accelerometer plots were selected to show blanket response at mid-span, drum response at mid-span and the response of the structure as measured at the hearing housing inside the drums. The overall pressure level inside the drums was approximately equal to the external environment though some attenuation of the high frequency environment was noted.

The array response to acoustic excitation was lower in the Y axis direction than in X or Z which were equal. This is expected because the specimen shape has its largest exposed surfaces parallel to the Y axis.

4.6.3.2 Conclusions

The RA 250 Solar Array Assembly survived exposure to the specified acoustic test environment. The acoustic test should be retained as a system test environment for light weight stowed configuration solar array assemblies. This recommendation is based on the fact that as a subsystem of a spacecraft the array will be isolated from the structure above 200 Hz except as coupled acoustically with the launch vehicle. Due to mechanical isolation of the array from the

Table 4.6-1 Transducer Locations and Levels

Item No.	Transducer	Sta. No.	Location	Run	Overall Level
1	Microphone	D, Trk 3	Outside +Y Drum, 50% Span $\theta = 0^{o}$	3	149.0 db
2		B, Trk 6	Outside +Y Drum, 50% Span $\theta = 90^{o}$	3	150.0
3		C, Trk 1	Outside +Y Drum, 0% Span $\theta = 0^{o}$	3	150.0
4		F, Trk 4	Outside -Y Drum, 100% Span $0 = 180^{o}$	3	147.5
5		A, Trk 5	Outside -Y Drum, 100% Span $0 = 270^{o}$	3	150.5
6	Microphone	E, Trk 2	Inside +Y Drum, 50% Span on Y Axis	3	151.5 db
7	Accelerometer	2X	LEM +Y Side Center Coup.	3	7.4 GRMS
8		2Z	LEM +Y Side Center Coup.	3	4.8
9		4X	LEM 50% Span +Y Side	5	8.0
10		4Z	LEM 50% Span +Y Side	5	5.5
11		7Y	+Y End Support on Drum Plug	5	3.6
12		11Y	+Y Blanket 100% Span 180^{o}	3	5.6
13		11Z	+Y Blanket 100% Span 180^{o}	3	10.2
14		13X	+Y Drum 100% Span 90^{o}	5	3.3
15		14Y	+Y Drum 100% Span 180^{o}	5	2.8
16		14Z	+Y Drum 100% Span 180^{o}	5	5.2
17		15X	+Y Bearing Housing	3	1.5
18		15Y	+Y Bearing Housing	3	0.9
19		15Z	+Y Bearing Housing	3	1.4
20		16X	+Y Blanket 50% Span 0^{o}	3	10.5
21		18Z	+Y Blanket 50% Span 90^{o}	3	15.6
22		24X	+Y Drum 50% Span 0^{o}	3	4.0
23		26Z	+Y Drum 50% Span 90^{o}	3	4.9
24		36Z	+Y Blanket 0% Span 0^{o}	3	6.3
25		37Z	+Y Blanket 0% Span 90^{o}	3	6.6
26		38Z	+Y Drum 0% Span 0^{o}	5	14.3
27		40Y	+Y Drum 0% Span 180^{o}	5	2.1
28		41Y	+Y Blanket 0% Span 180^{o}	3	3.6
29	Accelerometer	42X	-Y Blanket 50% Span 0^{o}	3	10.0 GRMS

NOTE: Accelerometer locations and coordinates are shown in Figure 4.7-7.

spacecraft, the blanket assembly (cover glass, interconnects and solar cells) would not be excited by mechanical means in the high frequency (above 200 Hz) spectrum.

Table 4.6-2 Microphone Overall Levels (db reference to 0.0002 dynes/cm^2)

Track	Run 2	Run 3	Run 4	Run 5
1	149.0	150.0	147.0	148.5
2	151.5	151.5	149.0	151.5
3	149.0	149.0	146.5	149.0
4	147.5	147.5	145.5	147.5
5	150.5	150.5	147.0	149.5
6	149.5	150.0	147.0	149.5
Average of 6 Tracks	149.5	149.7	147.0	149.2

4.6.4 DISCUSSION OF TESTING

The acoustic horns were arranged in the chamber with baffles as shown in Figure 4.6-1. A preliminary test was performed to shape acoustic spectrum using the solar array dust cover as a dummy test specimen.

The test specimen, fully instrumented and secured in its handling frame was suspended from a spreader bar using shock cord (bungee) and a turnbuckle for adjustment. The natural frequency of the suspension system was less than 5 CPS. The instrumentation was connected to the signal conditioning equipment. Photographs of the test setup are shown in Figures 4.6-16 and 4.6-17.

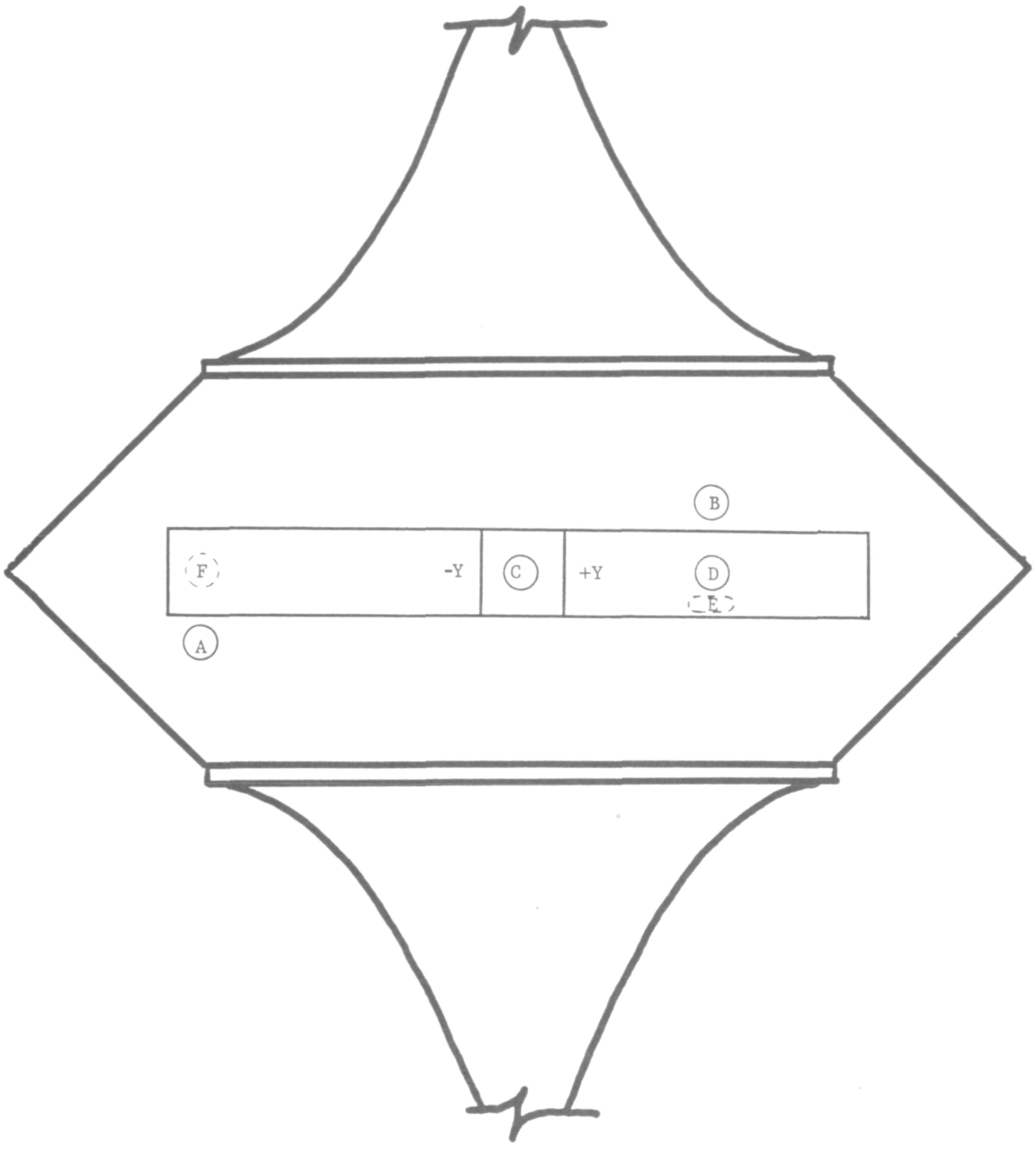

Figure 4.6-1. Test Set Up

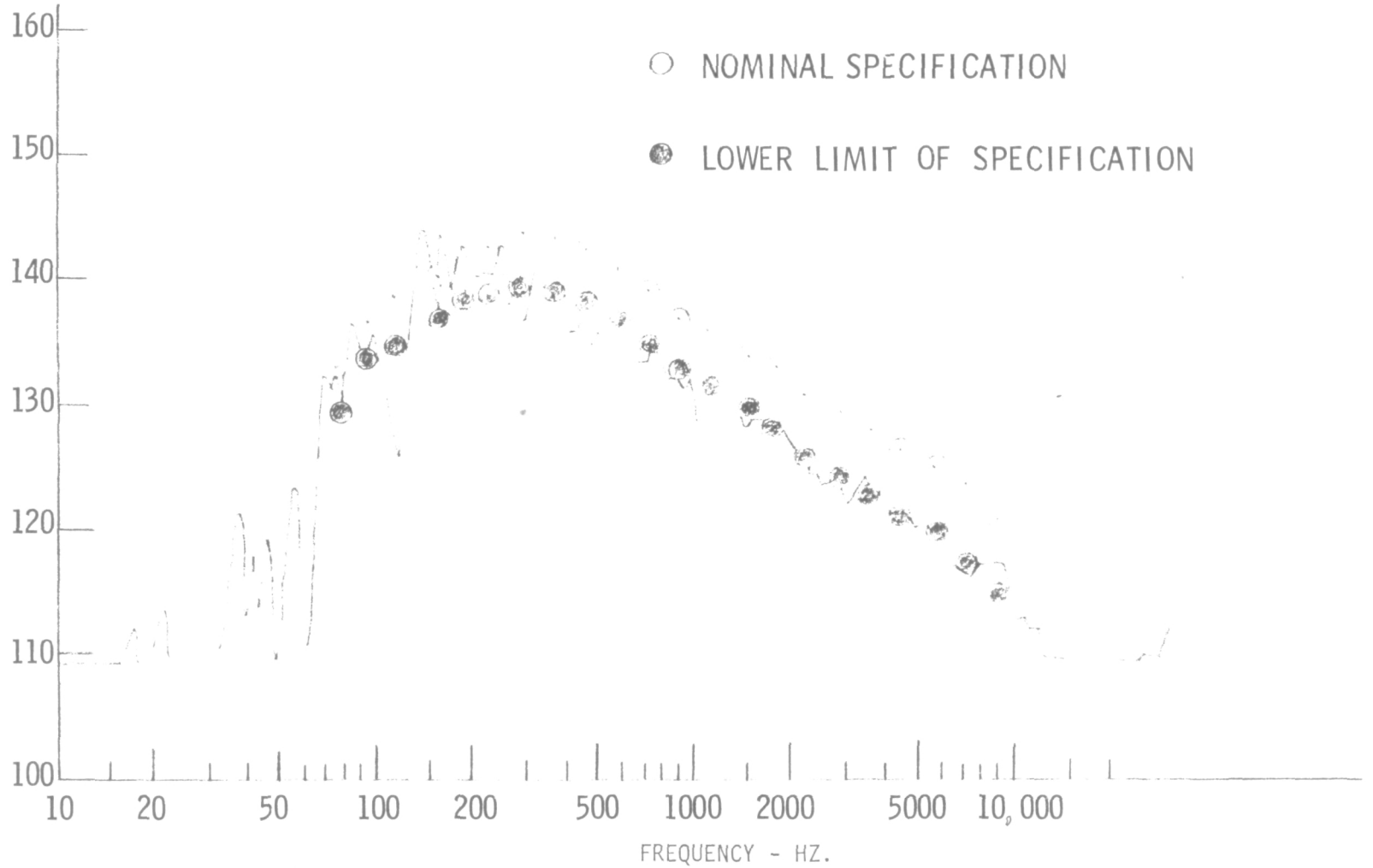

Identification R271
Outside +Y Drum
0% Span
$\theta = 0°$

Run No. 2
Date 5/15/70

Figure 4.6-2. Spectrogram of Input Acoustic Field During Run 2

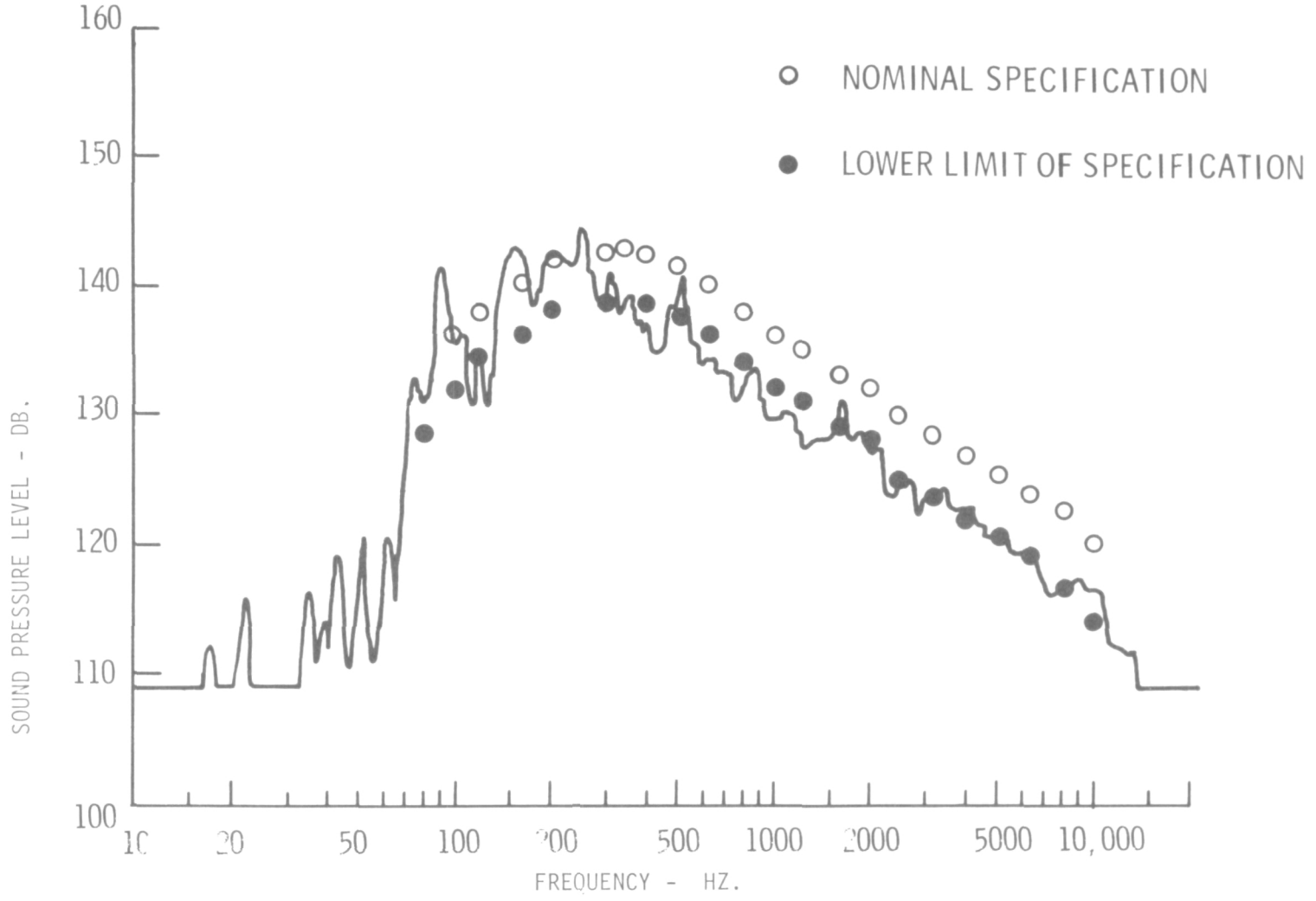

Identification R371
Outside +Y Drum
0% Span
0 = 0

Run No. 3
Date 5/15/70

Figure 4.6-3 Spectrogram of Input Acoustic Field During Run 3

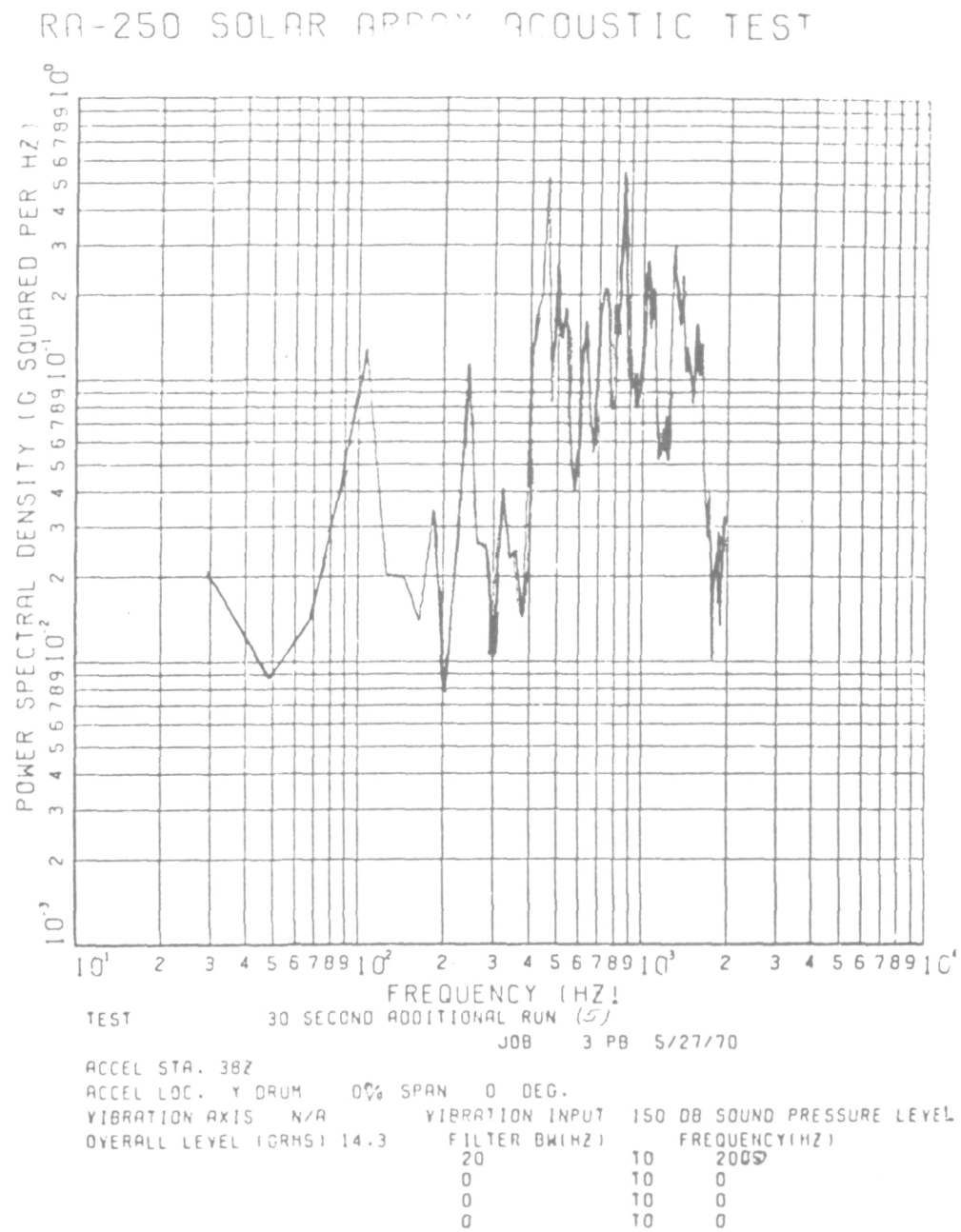

Figure 4.6-4. Acoustic Test Results

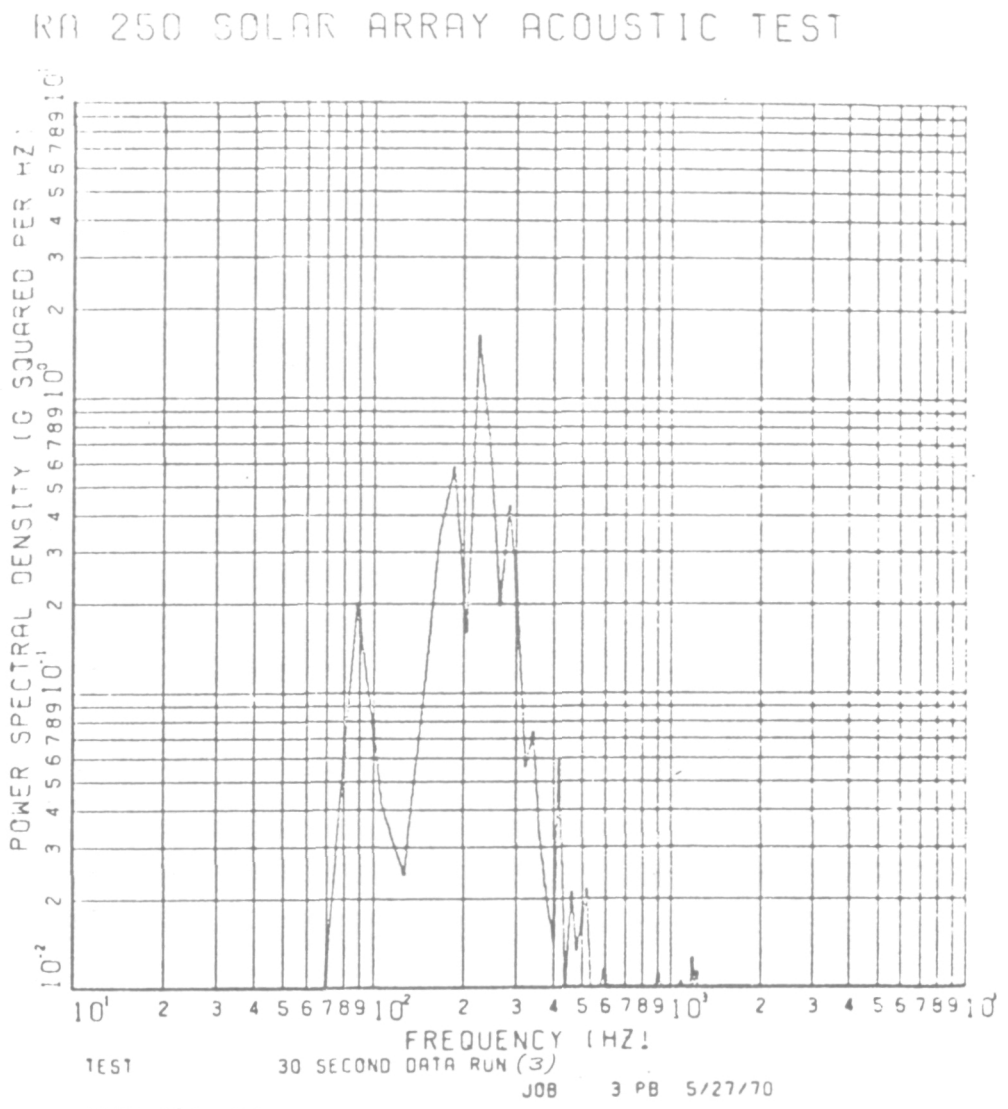

Figure 4.6-5. Acoustic Test Results

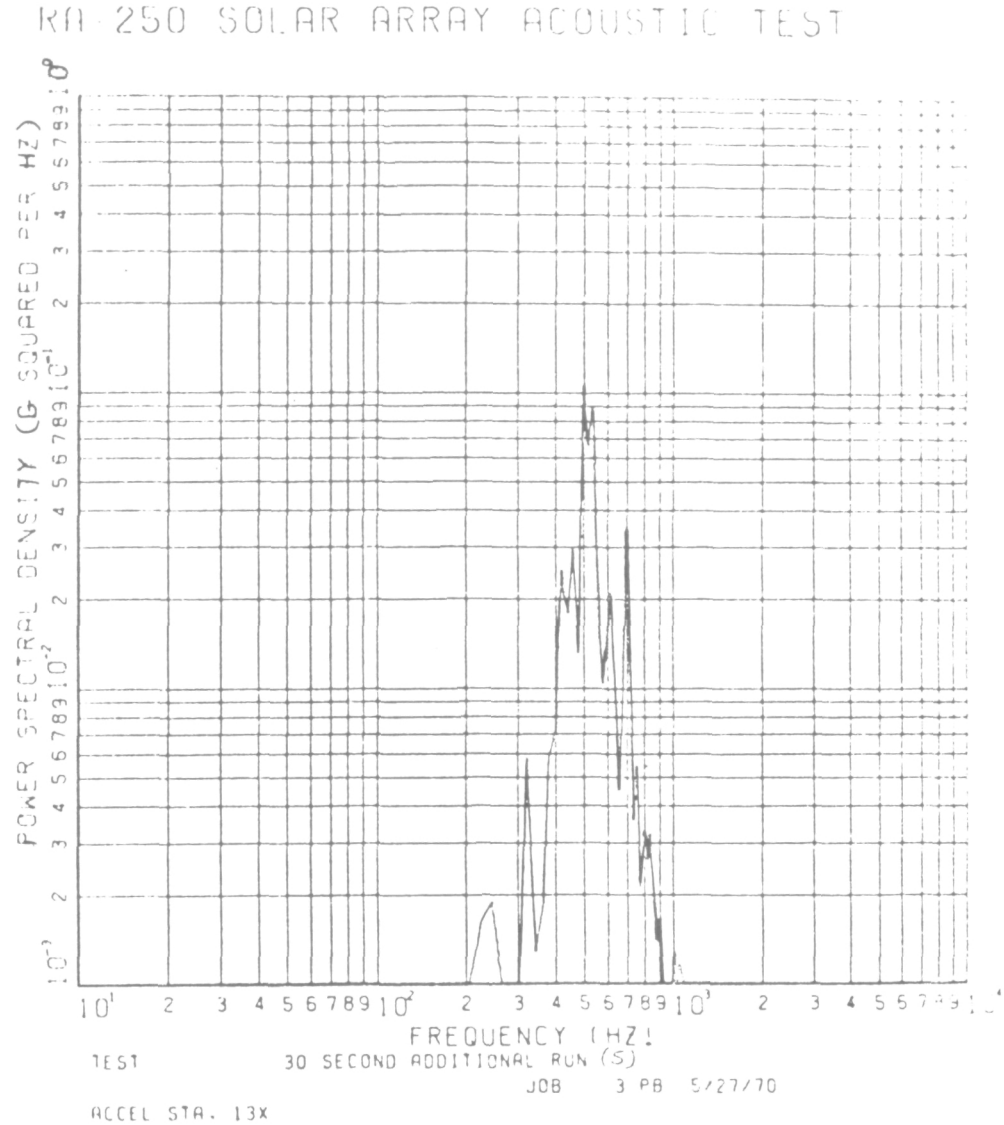

Figure 4.6-6. Acoustic Test Results

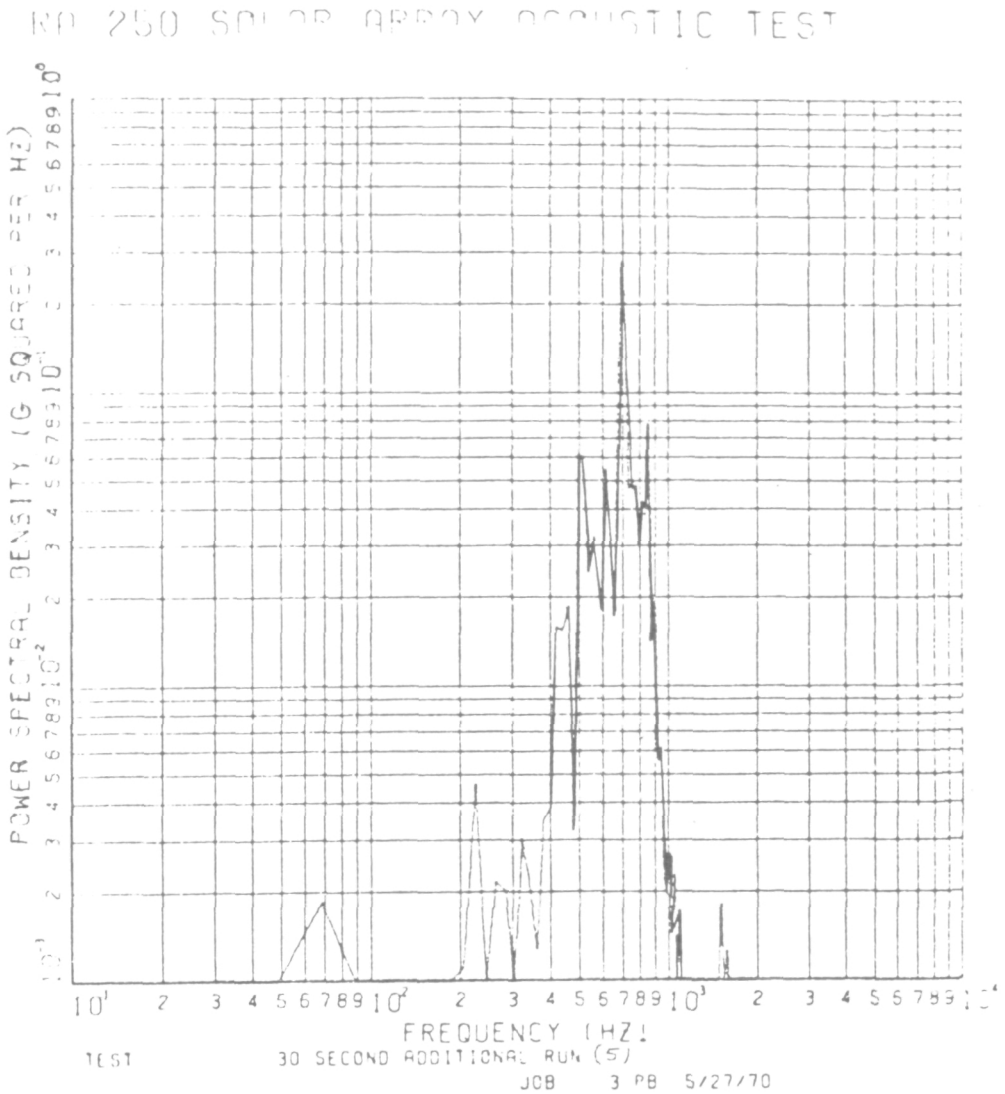

Figure 4.6-7. Acoustic Test Results

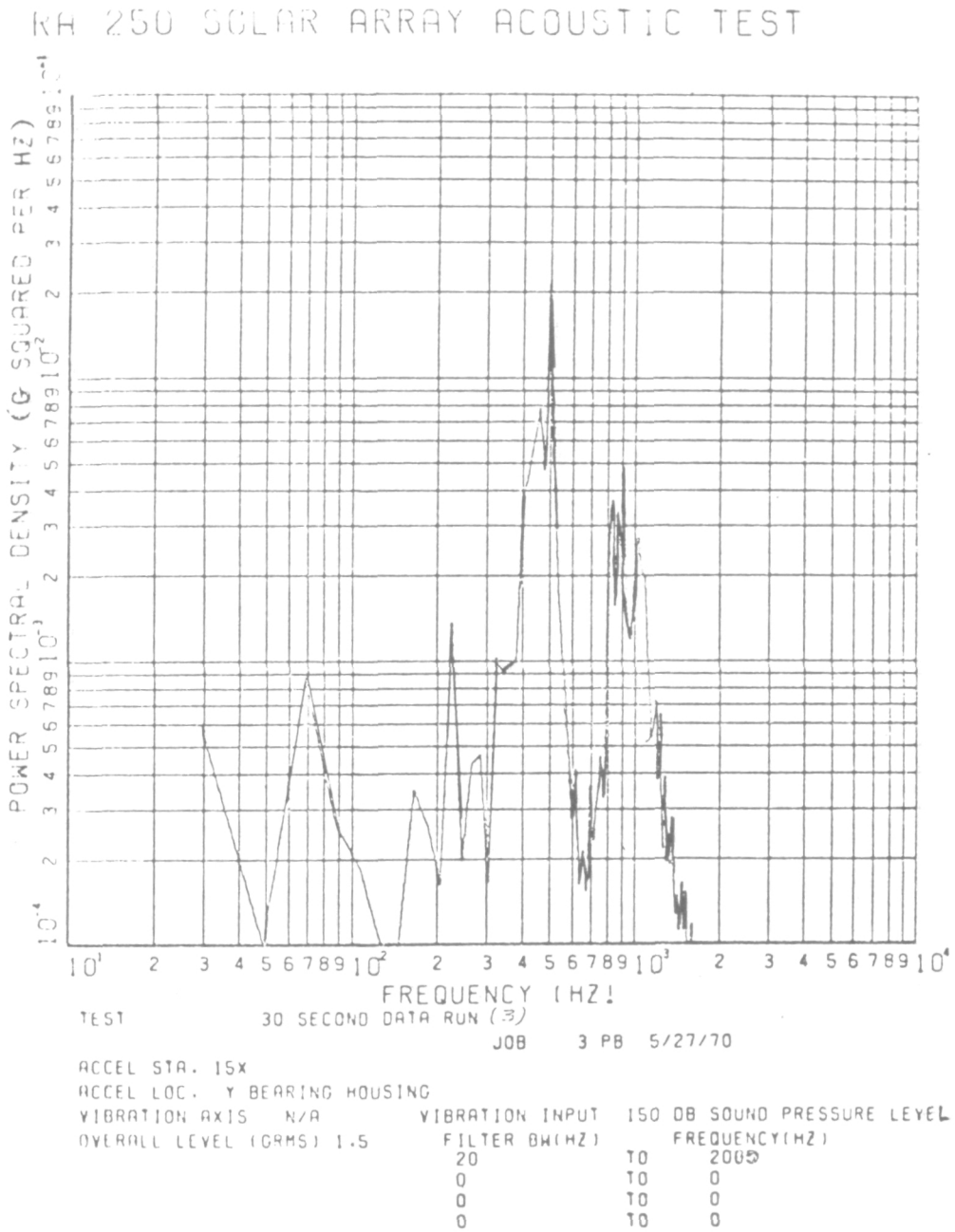

Figure 4.6-8. Acoustic Test Results

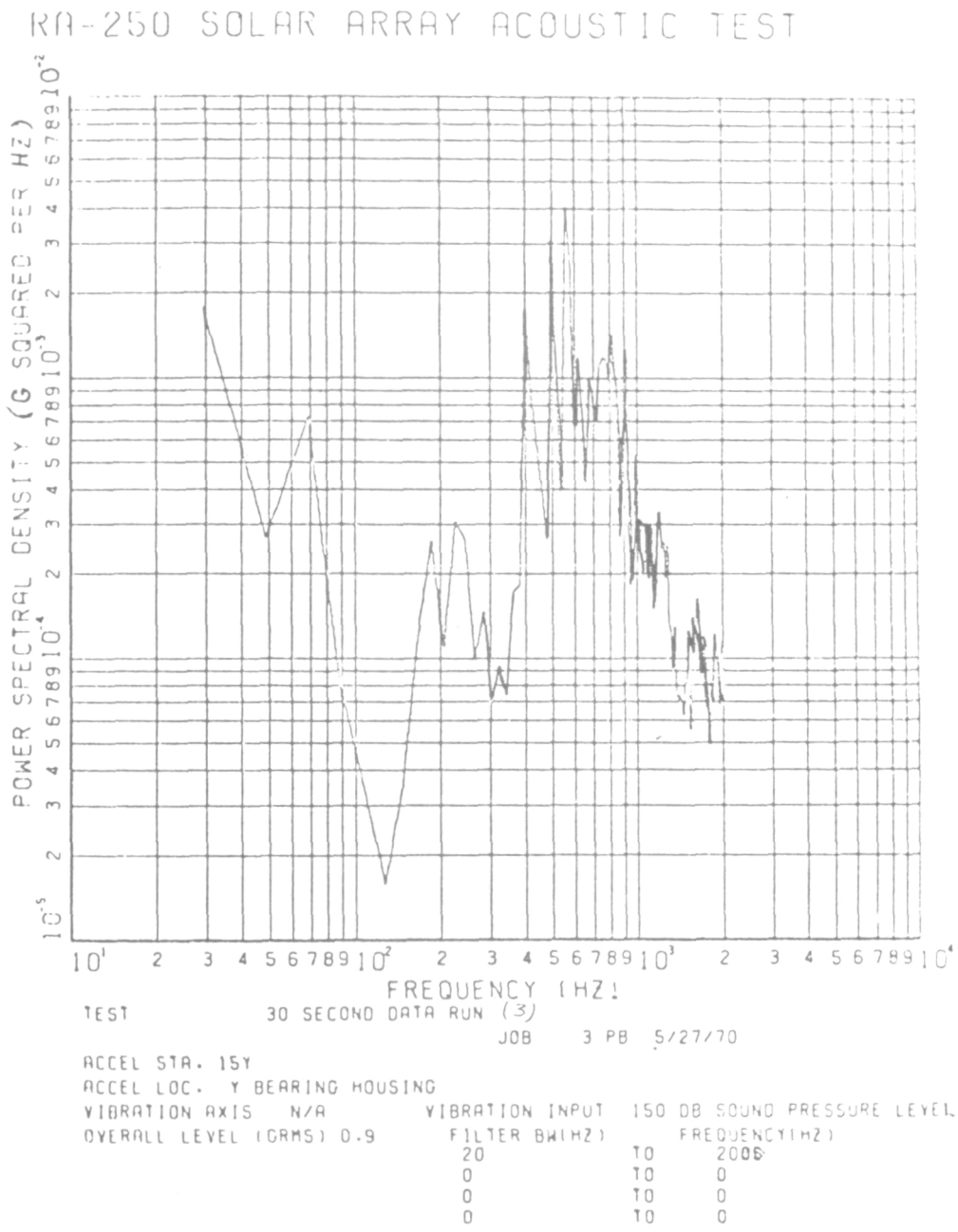

Figure 4.6-9. Acoustic Test Results

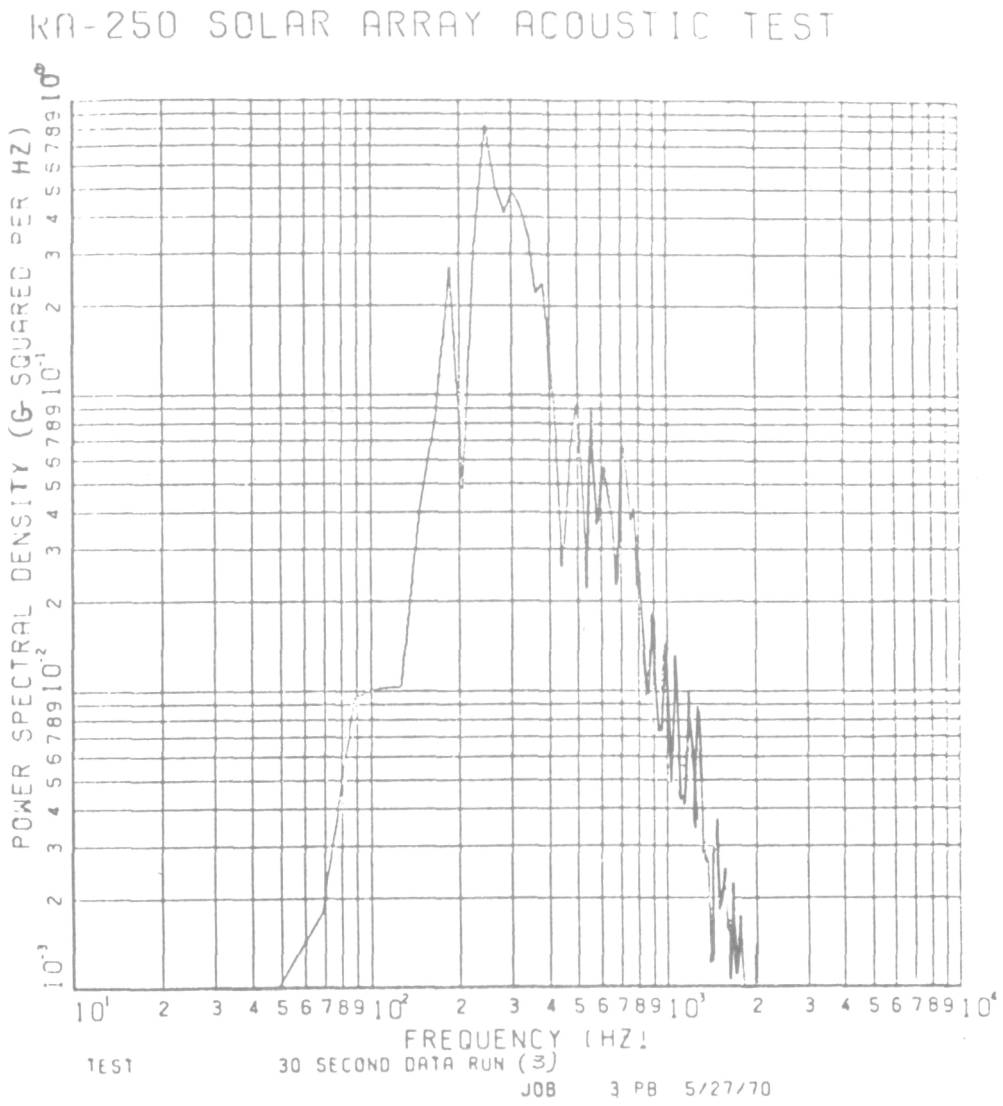

Figure 4.6-10. Acoustic Test Results

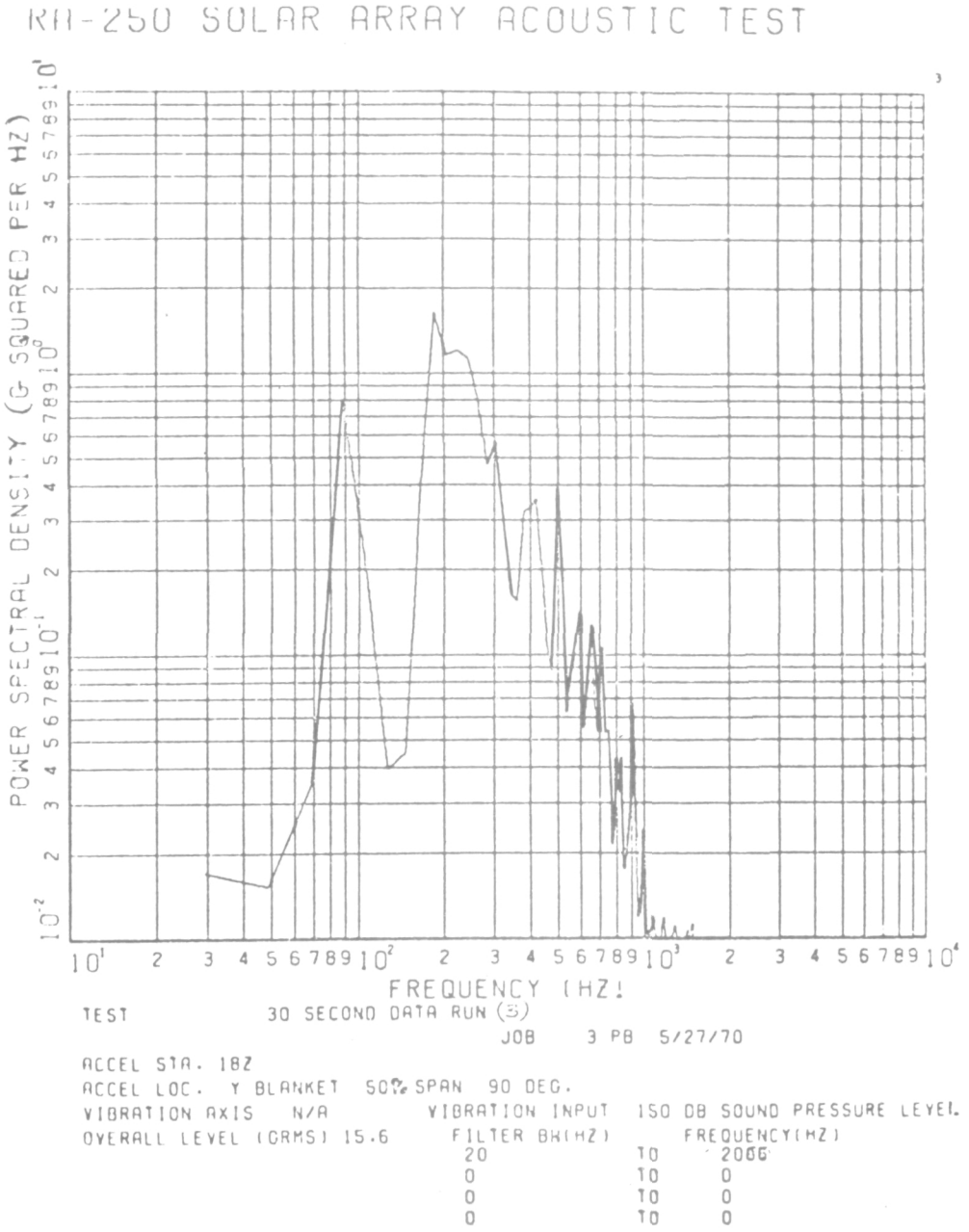

Figure 4.6-11. Acoustic Test Results

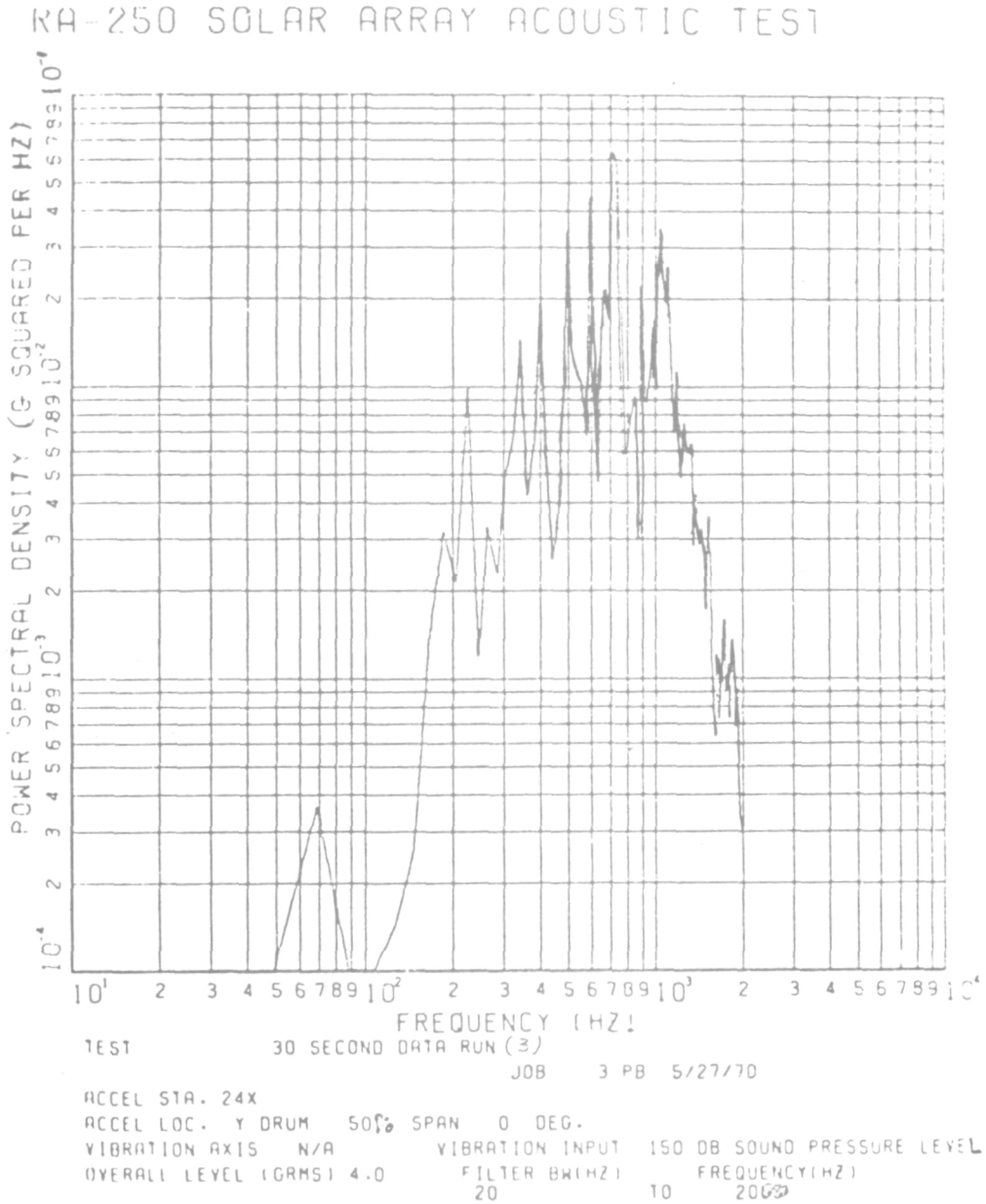

Figure 4.6-12. Acoustic Test Results

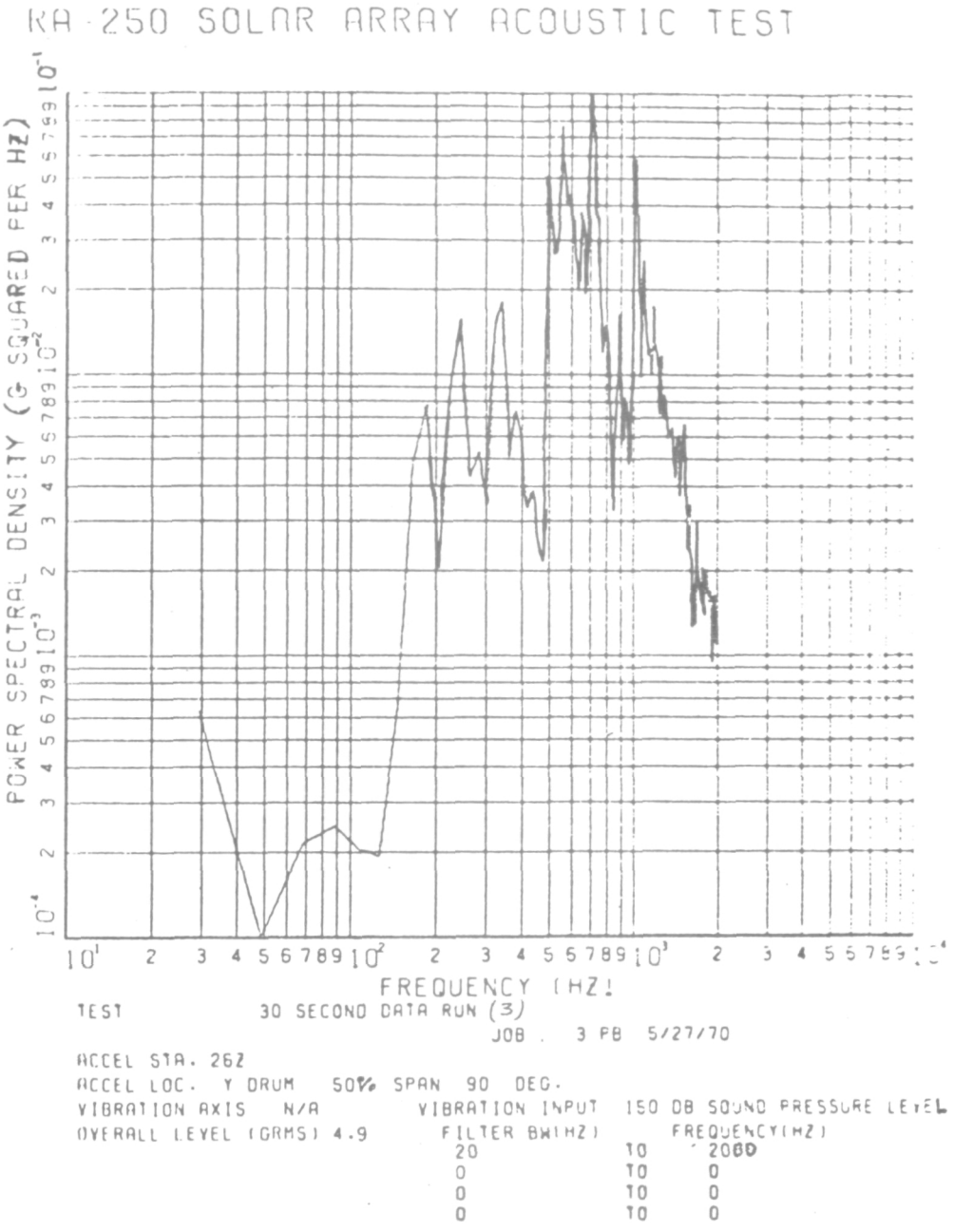

Figure 4.6-13. Acoustic Test Results

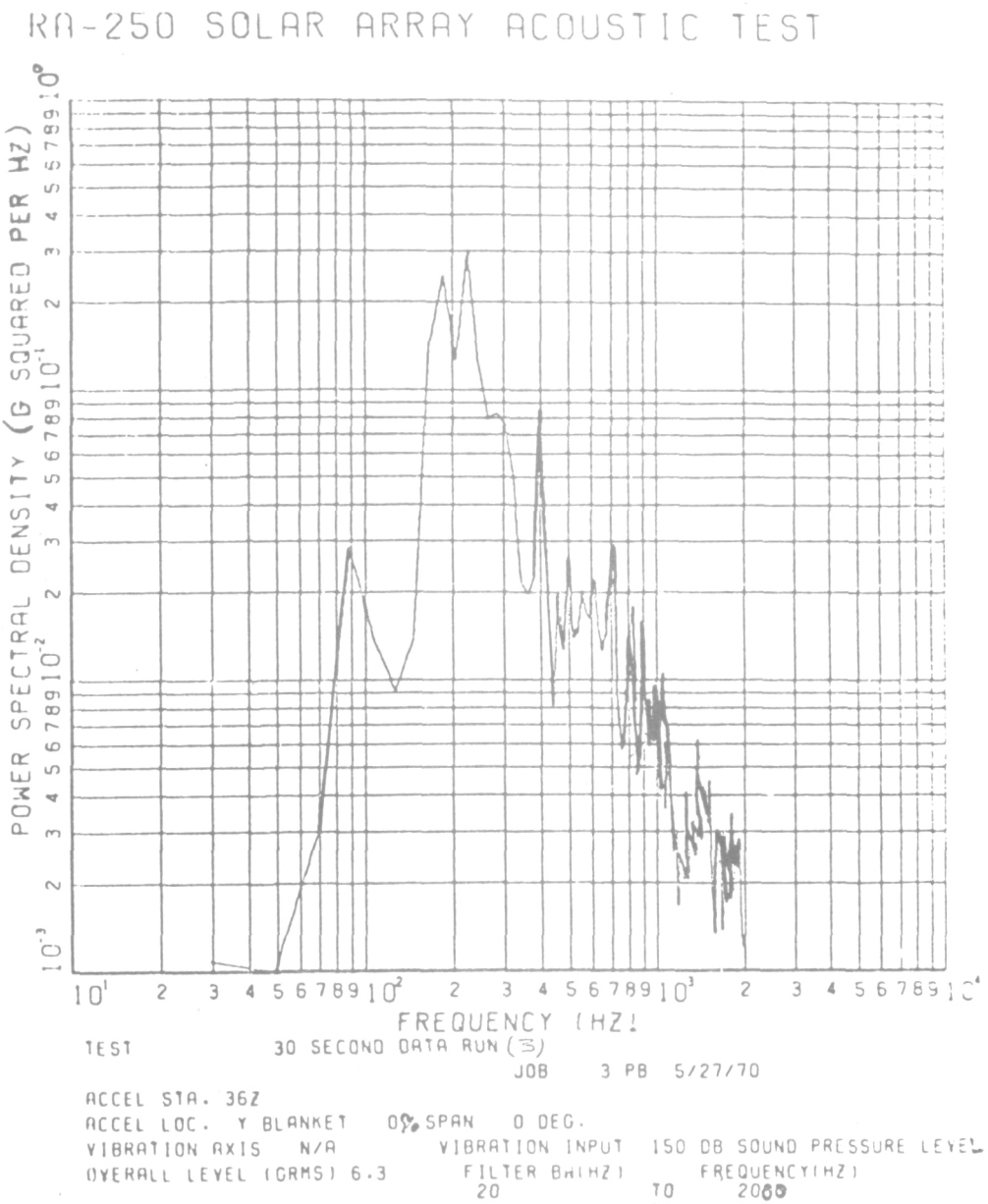

Figure 4.6-14. Acoustic Test Results

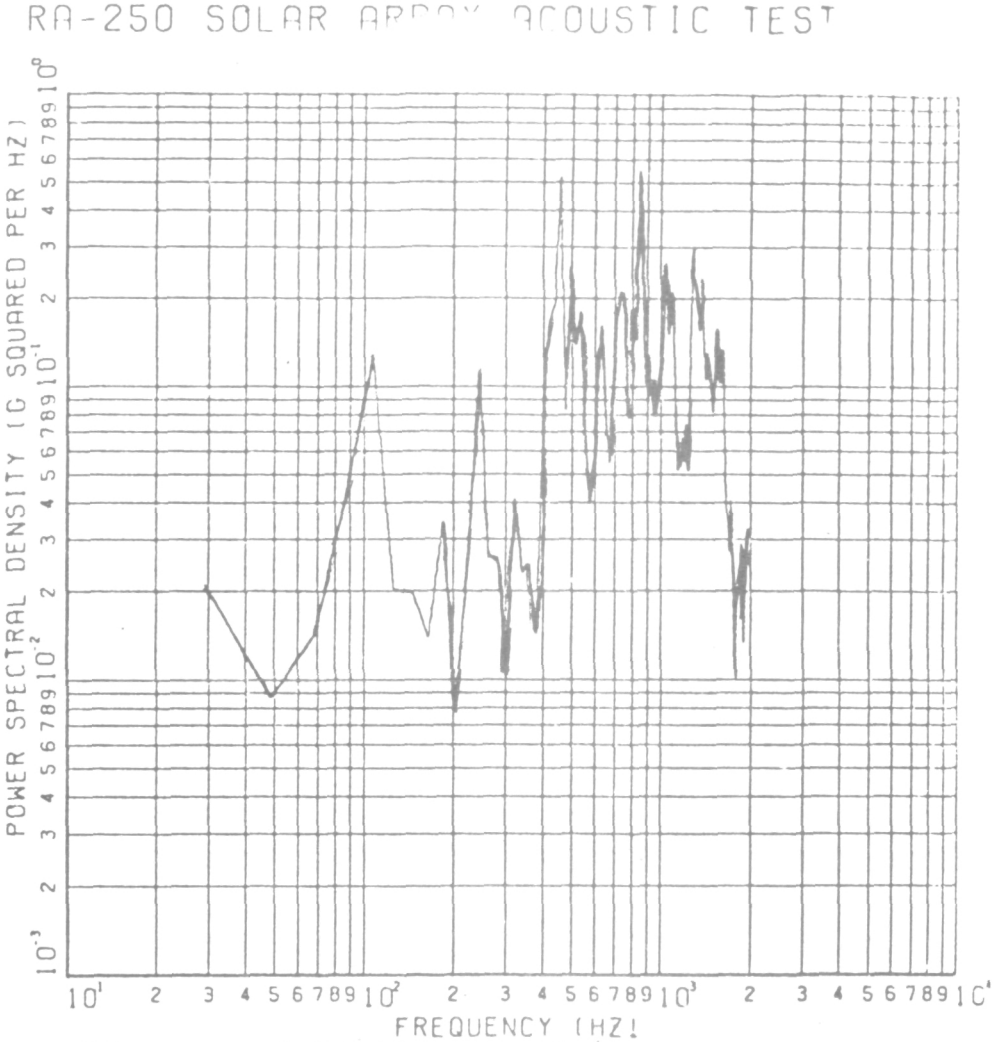

Figure 4.6-15. Acoustic Test Results

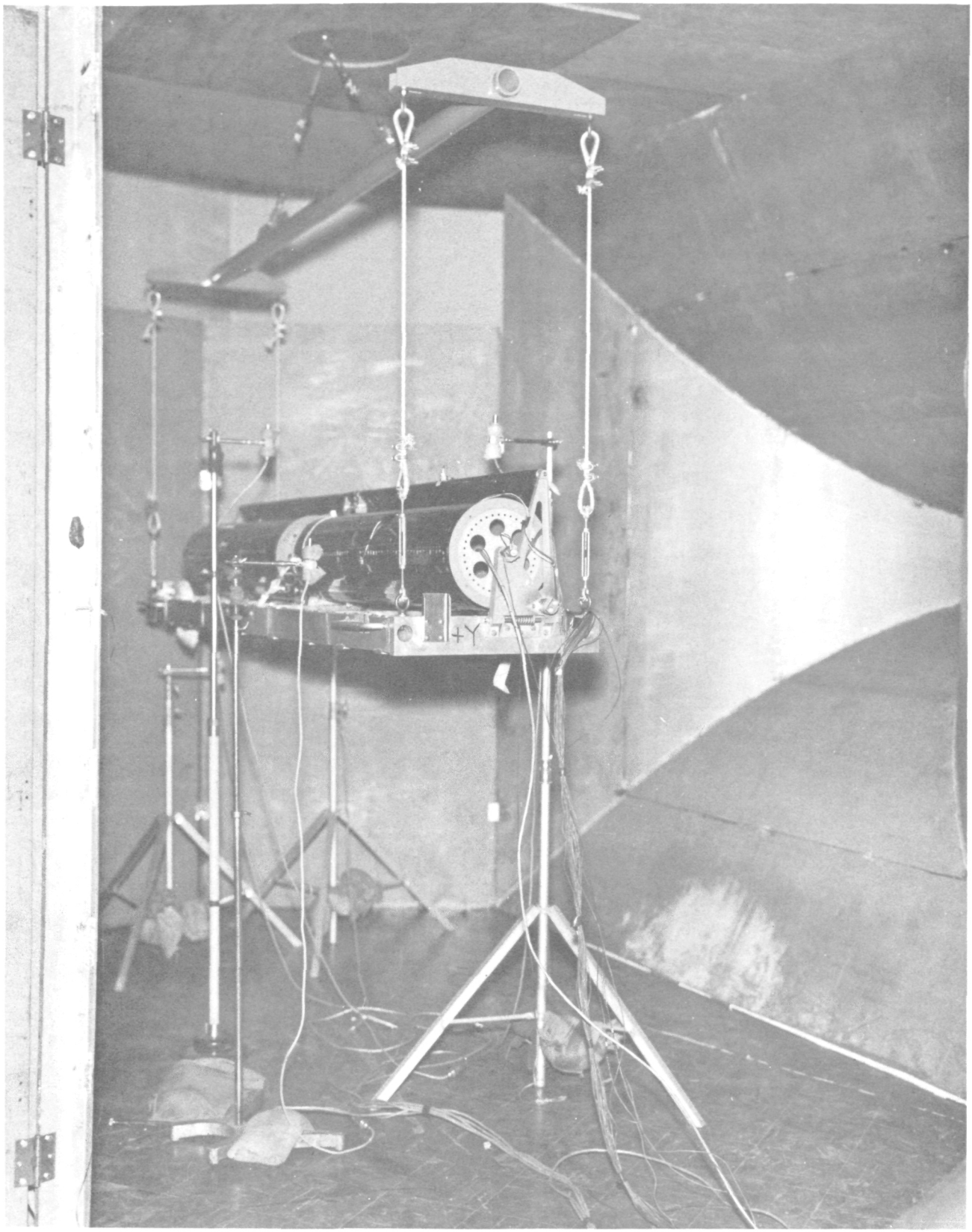

Figure 4.6-16 View of Rollup Solar Array Installed in the Acoustic Chamber

(C-70-0115-A)

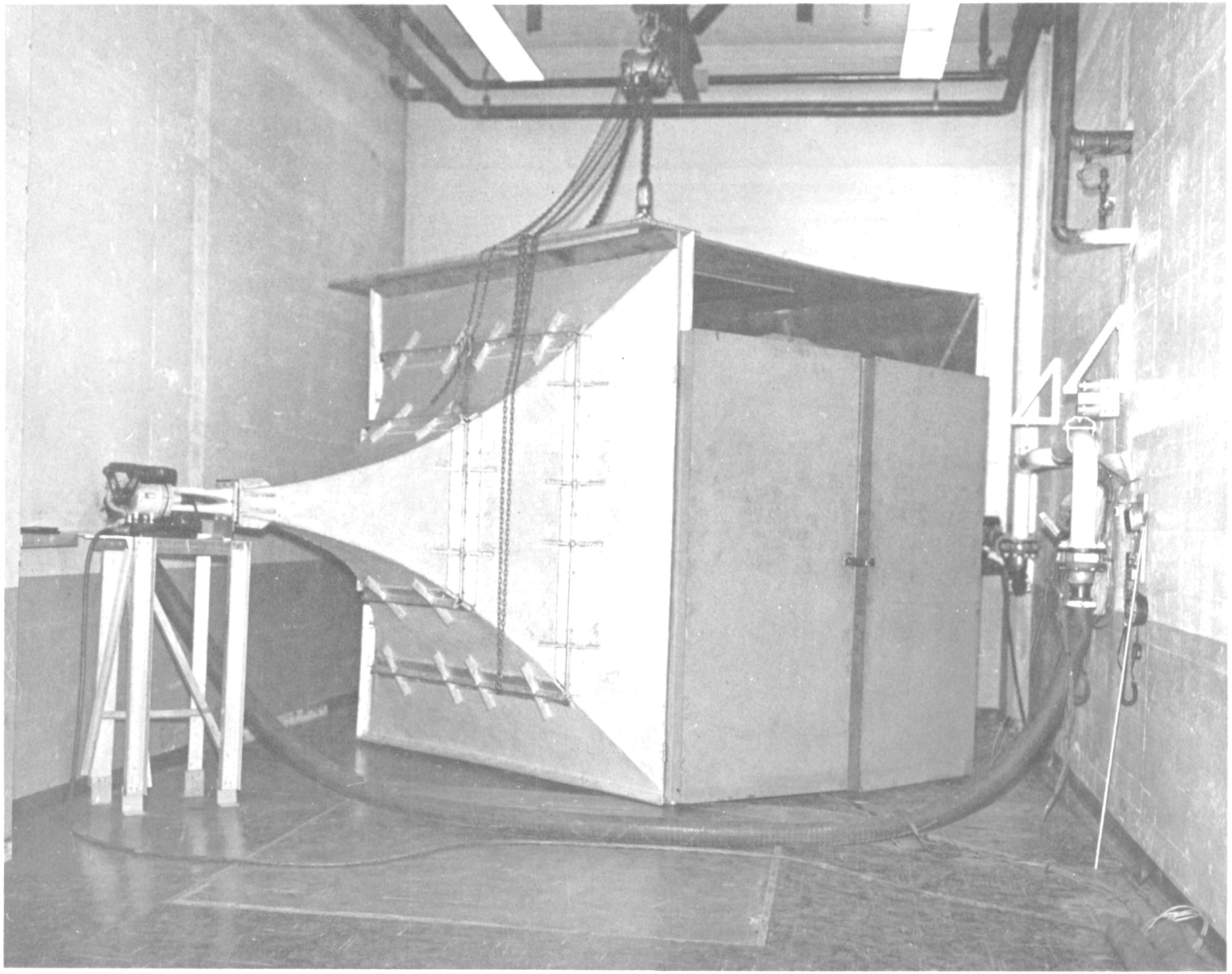

Figure 4.6-17 Test Facility for Rollup Solar Array Acoustic Test
(C-70-0115-A)

A test run at 130 db was made to insure the spectrum shape with the actual test hardware was satisfactory. Runs for data followed. The test environment was at the lower limits of the specified environment as shown in Table 4.6.2 and Figures 4.6-2 and 4.6-3. Since the environment level could not be increased without extensive effort a penalty run was made to substitute additional test time for the less than nominal environment. For unknown reasons the first penalty run resulted in a 147 db environment so a second penalty run was carried out.

4.7 STOWED DYNAMICS TEST

4.7.1 SUMMARY

The RA 250 Solar Array stowed vibration test was performed in the GE Structural Dynamics Laboratory, Building 400 at the Valley Forge Space Center. The array qualification testing resulted in the failure of one BI-STEM actuator limit switch. No structural modes were noted below 100 Hz and blanket resonances noted between 15 and 100 Hz were highly localized and are not considered true modes.

4.7.2 TEST OBJECTIVES

The test involved two distinct areas of interest, modal data and structural verification (qualification).

4.7.2.1 Modal

1. Determine frequency, mode shape, and critical damping ratios of all stowed array resonant modes occurring below 100 Hz.

2. To investigate blanket wrap modes which occur below 100 Hz.

4.7.2.2 Qualification

1. To demonstrate survival following exposure of the stowed array to qualification level sinusoidal and random vibration spectra.

2. To obtain data for definition of component vibration test specifications for future flexible array systems and components.

4.7.3 RESULTS

4.7.3.1 Modal

1. No significant structural modes were noted below 100 Hz and hence none were investigated or defined.

2. Blanket modes with a classical response (peak quadrature response at a zero in-phase response) were not noted during this test.

3. Amplification factors throughout the array were relatively low, falling between 1:1 and 4:1 up to 200 Hz.

4. No blanket modes were noted during Y axis testing but random blanket motion resulted in centering the rolled blankets on the drums and generation of blanket slack.

5. Blanket motion due to Z and X excitation were similar and data reduction and investigation emphasized X axis response.

4.7.3.2 Qualification Testing

1. The array was subjected to the sinusoidal vibration profile shown in Figures 4.7-1, 4.7-2, and 4.7-3 in the Y, Z and X axes.

2. The array was subjected to a random vibration test spectrum for the specified 60 seconds in Y and X axes of test. In the Z axis of test, the specified input was applied in the range from 20 to 350 Hz. Roll-off at -12 db per octave starting at 350 Hz was required because of fixture resonances above 350 Hz (Figures 4.7-4, 4.7-5, and 4.7-6).

3. The array experienced one component failure, which was detected during the inspections made after each axis of testing was completed. Following Z axis testing, the solar panel actuator did not operate when power was applied. The "fully extended" limit switch roller actuator failed. The BI-STEM was successfully deployed after removal of the broken component and electrically bypassing the limit switch.

4. Results of post test inspection such as cell and coverglass chip and crack mapping, limit switch bracket failure, and description of a BI-STEM fatigue crack are covered in Section 4.2.

5. It is considered that the RA250 array design structure and configuration successfully survived the qualification level vibration environment.

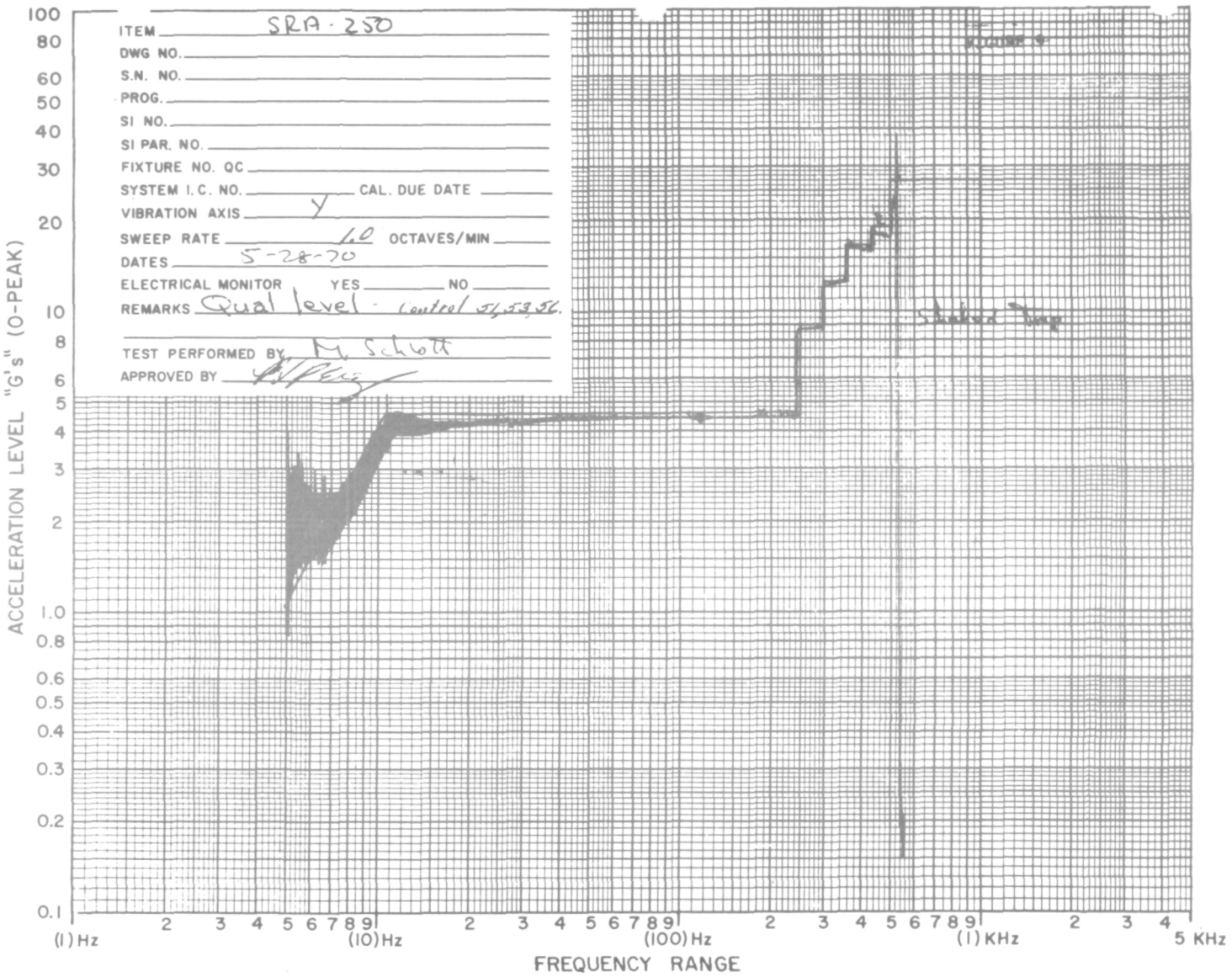

Figure 4.7-1, Control Signal for Y Axis Sinusoidal Vibration - Qualification Level Run

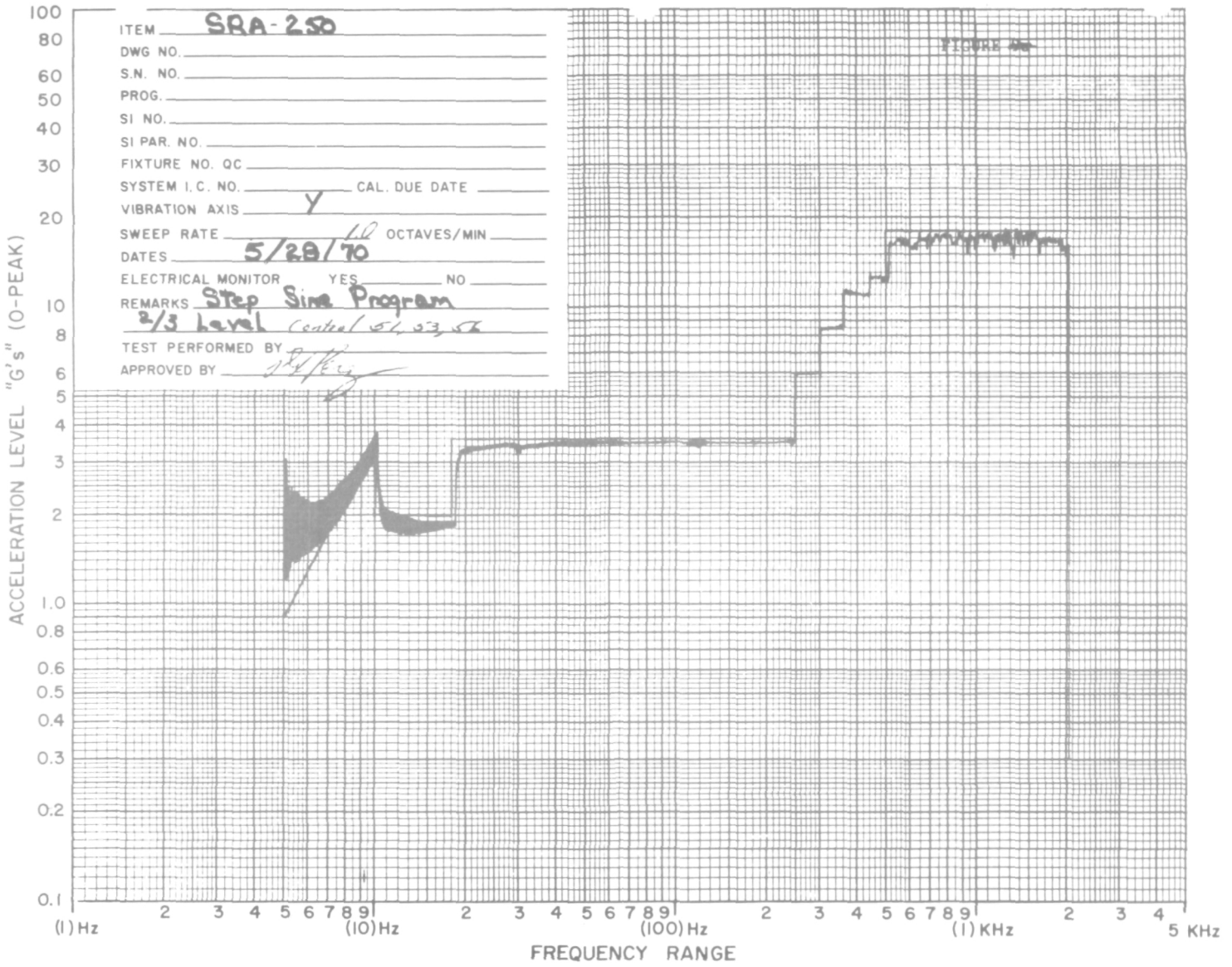

Figure 4.7- 2. Control Signal for Y Axis Sinusoidal Vibration - Qualification Level Run

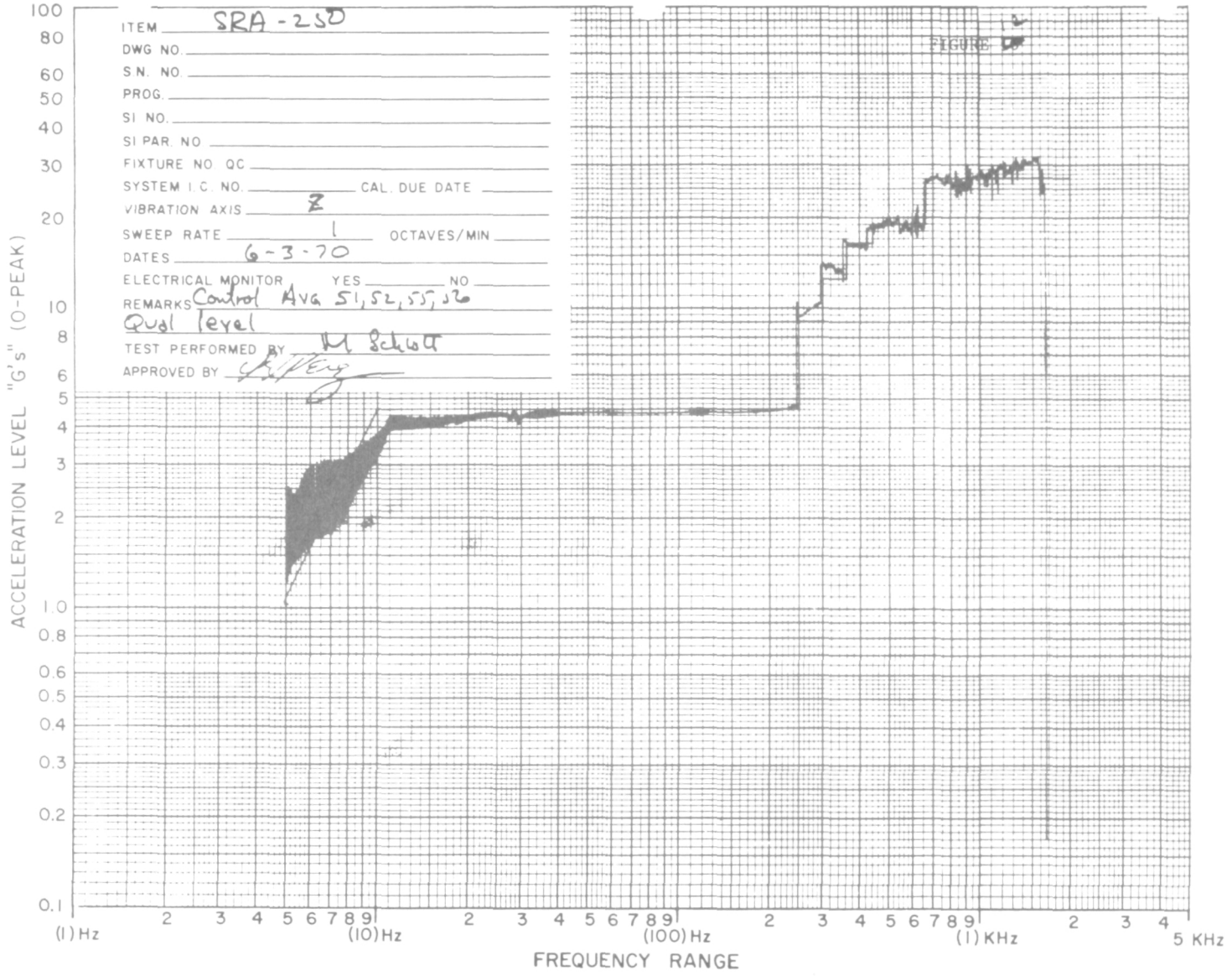

Figure 4.7- 3. Control Signal for Z Axis Sinusoidal Vibration - Qualification Level Run

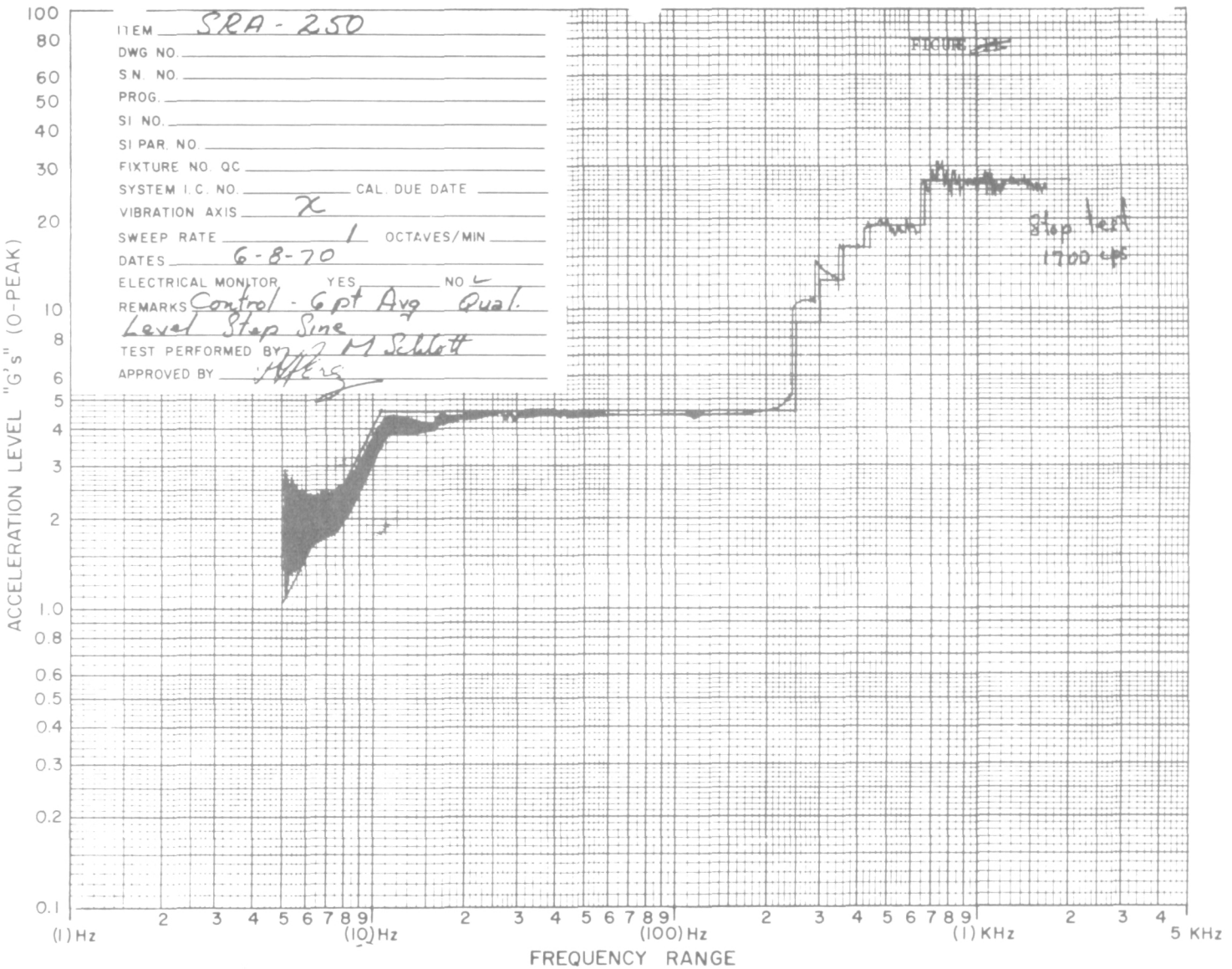

Figure 4.7-4. Control Signal for X Axis Sinusoidal Vibration - Qualification Level Run

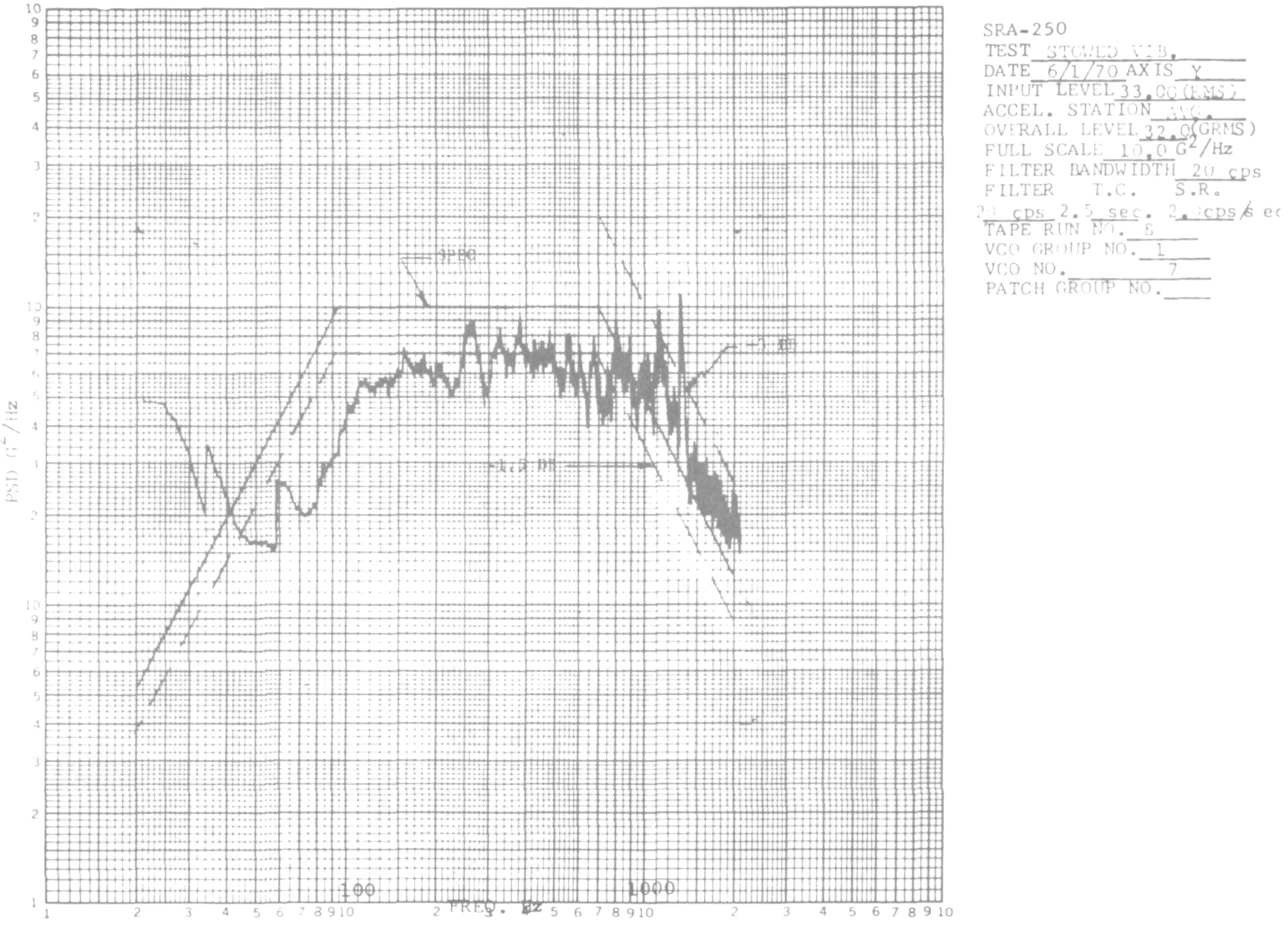

SRA-250
TEST STOWED V.B.
DATE 6/1/70 AXIS Y
INPUT LEVEL 33.00 (RMS)
ACCEL. STATION AVG.
OVERALL LEVEL 32.0 (GRMS)
FULL SCALE 10.0 G^2/Hz
FILTER BANDWIDTH 20 cps
FILTER T.C. S.R.
20 cps 2.5 sec. 2 cps/sec
TAPE RUN NO. 8
VCO GROUP NO. 1
VCO NO. 7
PATCH GROUP NO.

Figure 4.7-5. Power Spectral Distribution of Control Signal for X Axis Random Vibration - Qualification Level Run

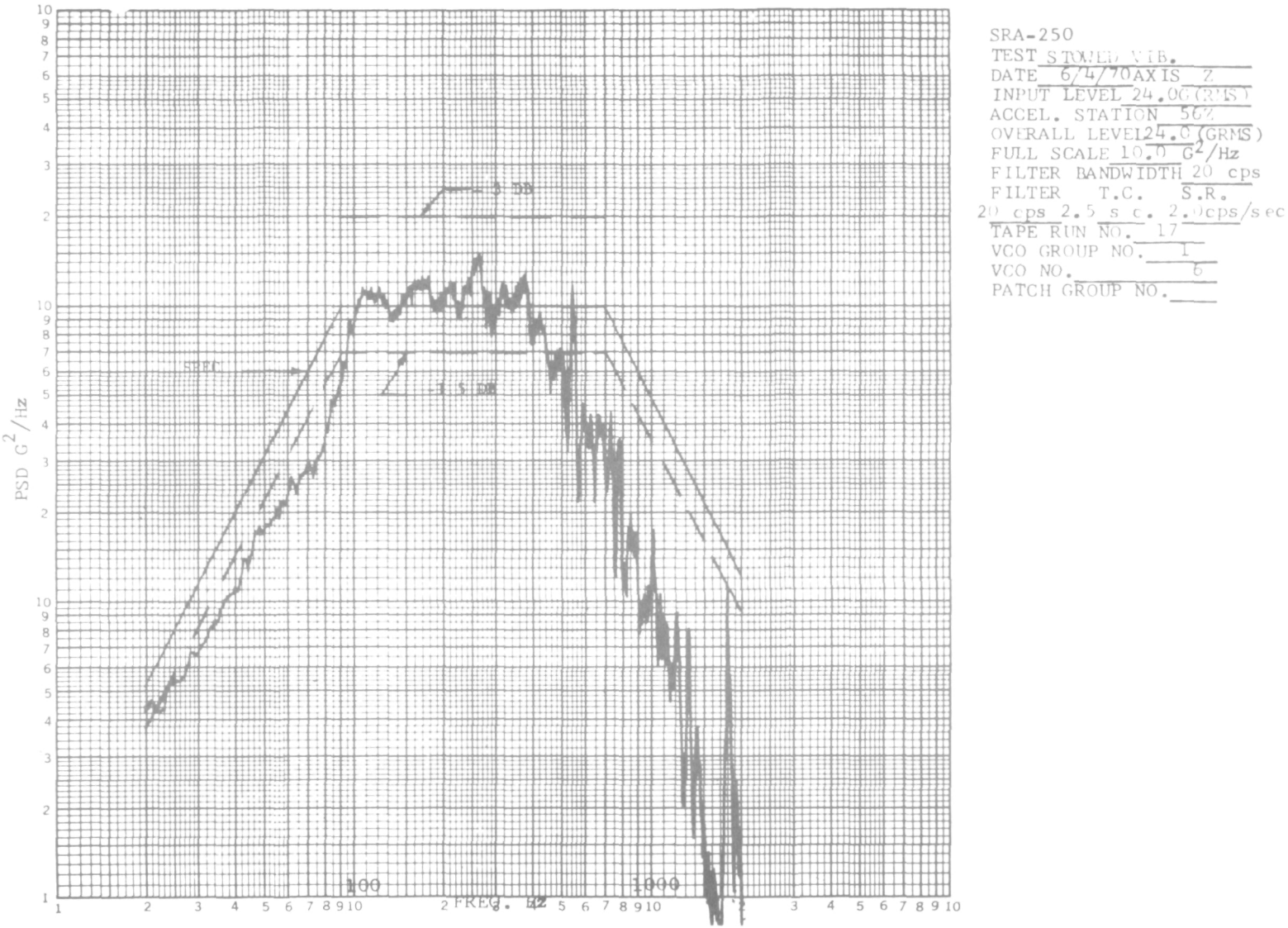

Figure 4.7-3. Power Spectral Distribution of Control Signal for Z Axis Random Vibration - Qualification Level Run

4.7.4 TEST SETUP AND TEST CONDUCTION

The test sequence, (motion study, sine and random qualification vibration) was conducted along each geometric axis (X, Y, & Z) of the stowed array. Figure 4.7-7 presents a sketch of the test specimen indicating the system of axes, and transducer locations. In brief, the Y axis was coincident with the drum rotational axis; the X axis was parallel to the BI-STEM axes of symmetry and bisected the Y axis; and the Z axis was perpendicular to both the X and Y axes and also bisected the Y axis.

4.7.4.1 Instrumentation, Data Recording, and Playback

The array and handling frame were instrumented with 75 accelerometers and 36 strain gage circuits located as defined in Table 4.7-1 and Figure 4.7-7. Figure 4.7-8 presents block diagrams of the data recording and playback system.

4.7.4.2 Test Setup

In each axis of test, the array-handling frame assembly was hard mounted on the array stowed vibration fixture and driven by a single MB-220 exciter. The test fixture was supported on hydrostatic slip bearings. Figures 4.7-9, 4.7-10, and 4.7-11 present photographs of the array setup for Y, Z, and X axes testing, respectively.

4.7.4.3 Test Conduction

Testing in each of the three (X,Y, Z) array geometric axes was substantially identical and consisted of the following:

1. Several low level sinusoidal sweeps at 0.46G at 1 octave/min. from 5 Hz to 2 KHz. These sweeps were run to set initial recording gain factors and to obtain array response to a constant level base excitation

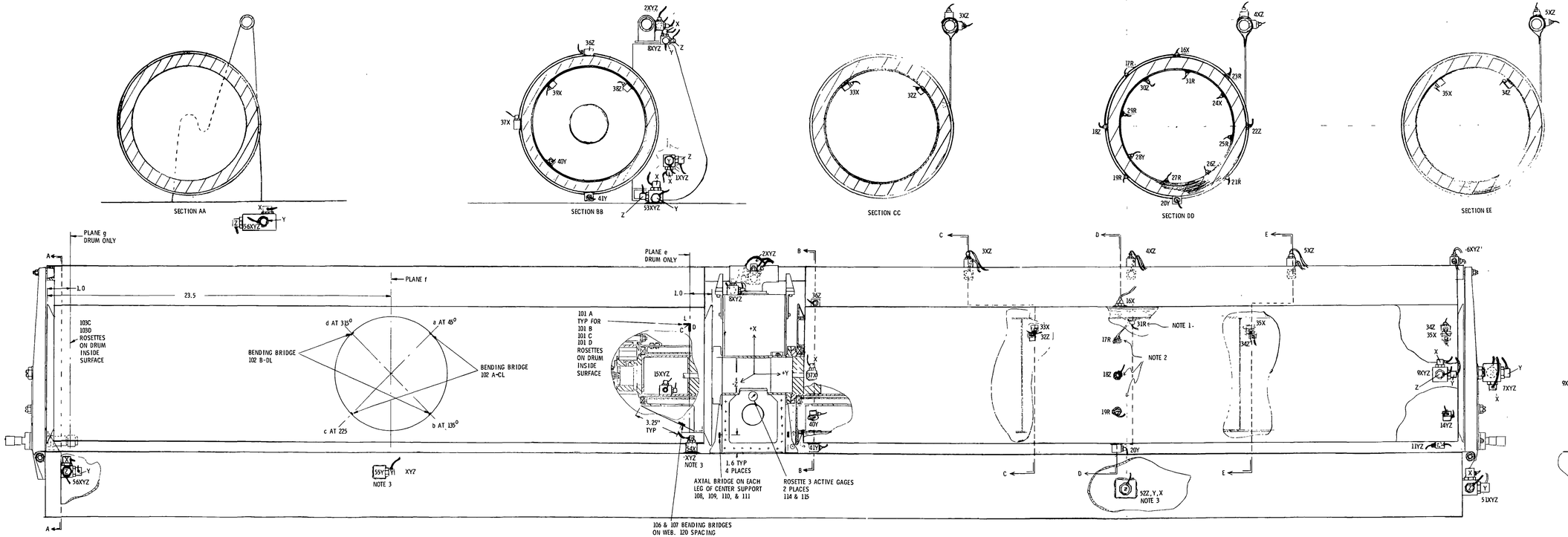

Figure 4.7-7 RA250 Stowed Vibration Test Instrumentation

Table 4. 7-1. RA250 Stowed Vibration Test Instrumented Locations

STATION NO.	LOCATION	STATION NO.	LOCATION	STATION NO	LOCATION
1X	BISTEM ACTUATOR MOUNT	19R	+Y BLKT., 50% SPAN @ 135°	56X	HANDLING FIXT., 100% SPAN, -Y
1Y	BISTEM ACTUATOR MOUNT	20Y	+Y BLKT., 50% SPAN @ 180°	56Y	HANDLING FIXT., 100% SPAN, -Y
1Z	BISTEM ACTUATOR MOUNT	21R	+Y BLKT., 50% SPAN @ 225°	56Z	HANDLING FIXT., 100% SPAN, -Y
2X	LEM @ BISTEM I. F.	22Z	+Y BLKT., 50% SPAN @ 270°	101AC	QUAD A PLANE E
2Y	LEM @ BISTEM I. F.	23R	+Y BLKT., 50% SPAN @ 315°	101AD	QUAD A PLANE E
2Z	LEM @ BISTEM I. F.	24X	+Y DRUM, 50% SPAN @ 0°	101AL	QUAD A PLANE E
3X	LEM +Y SIDE, 25% SPAN	25R	+Y DRUM, 50% SPAN @ 45°	101BC	QUAD C PLANE E
3Z	LEM +Y SIDE, 25% SPAN	26Z	+Y DRUM, 50% SPAN @ 90°	101BD	QUAD C PLANE E
4X	LEM +Y SIDE, 50% SPAN	27R	+Y DRUM, 50% SPAN @ 135°	101BL	QUAD C PLANE E
4Z	LEM +Y SIDE, 50% SPAN	28Y	+Y DRUM, 50% SPAN @ 180°	101CC	QUAD C PLANE E
5X	LEM +Y SIDE, 75% SPAN	29R	+Y DRUM, 50% SPAN @ 225°	101CD	QUAD C PLANE E
5Z	LEM +Y SIDE, 75% SPAN	30Z	+Y DRUM, 50% SPAN @ 270°	101CL	QUAD C PLANE E
6X	LEM +Y SIDE, 100% SPAN	31R	+Y DRUM, 50% SPAN @ 315°	101DC	QUAD D PLANE E
6Y	LEM +Y SIDE, 100% SPAN	32Z	+Y DRUM, 33% SPAN @ 0°	101DD	QUAD D PLANE E
6Z	LEM +Y SIDE, 100% SPAN	33X	+Y DRUM, 33% SPAN @ 90°	101DL	QUAD D PLANE E
7X	OUTB'D END SUPPORT +Y DRUM I. F	34Z	+Y DRUM, 75% SPAN @ 0°	102A-CL	QUAD A-C PLANE F
7Y	OUTB'D END SUPPORT +Y DRUM I. F.	35X	+Y DRUM, 75% SPAN @ 90°	102B-DL	QUAD B-D PLANE F
7Z	OUTB'D END SUPPORT +Y DRUM I. F.	36Z	+Y BLKT., ZERO SPAN @ 0°	103CC	QUAD C PLANE G
8X	TOP OF CEN. SUPPORT NEAR BISTEM	37X	+Y BLKT., ZERO SPAN @ 90°	103CD	QUAD C PLANE G
8Y	TOP OF CEN. SUPPORT NEAR BISTEM	38Z	+Y DRUM, ZERO SPAN @ 0°	103CL	QUAD C PLANE G
8Z	TOP OF CEN. SUPPORT NEAR BISTEM	39X	+Y DRUM, ZERO SPAN @ 90°	103DC	QUAD D PLANE G
9X	+Y BLKT , 100% SPAN @ 90°	40Y	+Y DRUM, ZERO SPAN @ 180°	103DD	QUAD D PLANE G
9Y	+Y BLKT., 100% SPAN @ 90°	41Y	+Y BLKT., ZERO SPAN @ 180°	103DL	QUAD D PLANE G
9Z	+Y BLKT., 100% SPAN @ 90°	51X	HANDLING FIXT., 100% SPAN, +Y	104	OUTB'D END CAP.
11Y	+Y BLKT., 100% SPAN @ 180°	51Y	HANDLING FIXT., 100% SPAN, +Y	105	OUTB'D END CAP
11Z	+Y BLKT., 100% SPAN @ 180°	51Z	HANDLING FIXT., 100% SPAN, +Y	106	INB'D END CAP.
12X	+ DRUM, 100% SPAN @ 0°	52X	HANDLING FIXT., 50% SPAN, +Y	107	INB'D END CAP.
12Z	+ DRUM, 100% SPAN @ 0°	52Y	HANDLING FIXT., 50% SPAN, +Y	108	SUPPORT STRUCT. +Z SIDE -Y CORNER
13X	+ DRUM, 100% SPAN @ 90°	52Z	HANDLING FIXT., 50% SPAN, +Y	109	SUPPORT STRUCT. +Z SIDE +Y CORNER
13Z	+ DRUM, 100% SPAN @ 90°	53X	HANDLING FIXT., 0% SPAN, +Y	110	SUPPORT STRUCT. -Z SIDE -Y CORNER
14Y	+ DRUM, 100% SPAN @ 180°	53Y	HANDLING FIXT., 0% SPAN, +Y	111	SUPPORT STRUCT -Z SIDE +Y CORNER
14Z	+ DRUM, 100% SPAN @ 180°	53Z	HANDLING FIXT., 0% SPAN, +Y	112	MOVEABLE ARM ANGLE SECTION
15X	BEARING HOUSING INSIDE -Y DRUM	54X	HANDLING FIXT., 0% SPAN, -Y	113	MOVEABLE ARM BOX SECTION
15Y	BEARING HOUSING INSIDE -Y DRUM	54Y	HANDLING FIXT., 0% SPAN, -Y	114C	SUPPORT STRUCT. -Z SIDE
15Z	BEARING HOUSING INSIDE -Y DRUM	54Z	HANDLING FIXT., 0% SPAN, -Y	114D	SUPPORT STRUCT -Z SIDE
16X	+Y BLKT., 50% SPAN @ 0°	55X	HANDLING FIXT., 50% SPAN, -Y	114L	SUPPORT STRUCT. -Z SIDE
17R	+Y BLKT., 50% SPAN @ 45°	55Y	HANDLING FIXT., 50% SPAN, -Y	115C	SUPPORT STRUCT. +Z SIDE
18Z	+Y BLKT., 50% SPAN @ 90°	55Z	HANDLING FIXT., 50% SPAN, -Y	115D	SUPPORT STRUCT. +Z SIDE
				115L	SUPPORT STRUCT. -Z SIDE

ABBREVIATIONS

LEM	LEADING EDGE MEMBER
BLKT	BLANKET
I.F.	INTERFACE
FIXT	FIXTURE

NOTES:

1. Suffix X, Y, or Z indicates accelerometer axis of response referenced to array axes.
2. Suffix R. Accelerometer indicates response axis set radially to array surface, drum, or blanket.
3. Suffix C, D, L rosette gage legs
   - 3.1. C-Cross axis, perpendicular to array Y axis
   - 3.2. D-Diagonal axis, 45° to array Y axis
   - 3.3. L-Longitudinal axis. parallel to array Y axis
4. Suffix A-CL or B-DL Bending bridges longitudinal output gage in Quad A minus output gage in Quad C (180° spaced).
5. Drum rotated 50° for Y qualification and all X and Z testing hence drum X and Z and R station are rotated back 50°., i.e., a drum accelerometer station 24X defined at 0° moved to 310°

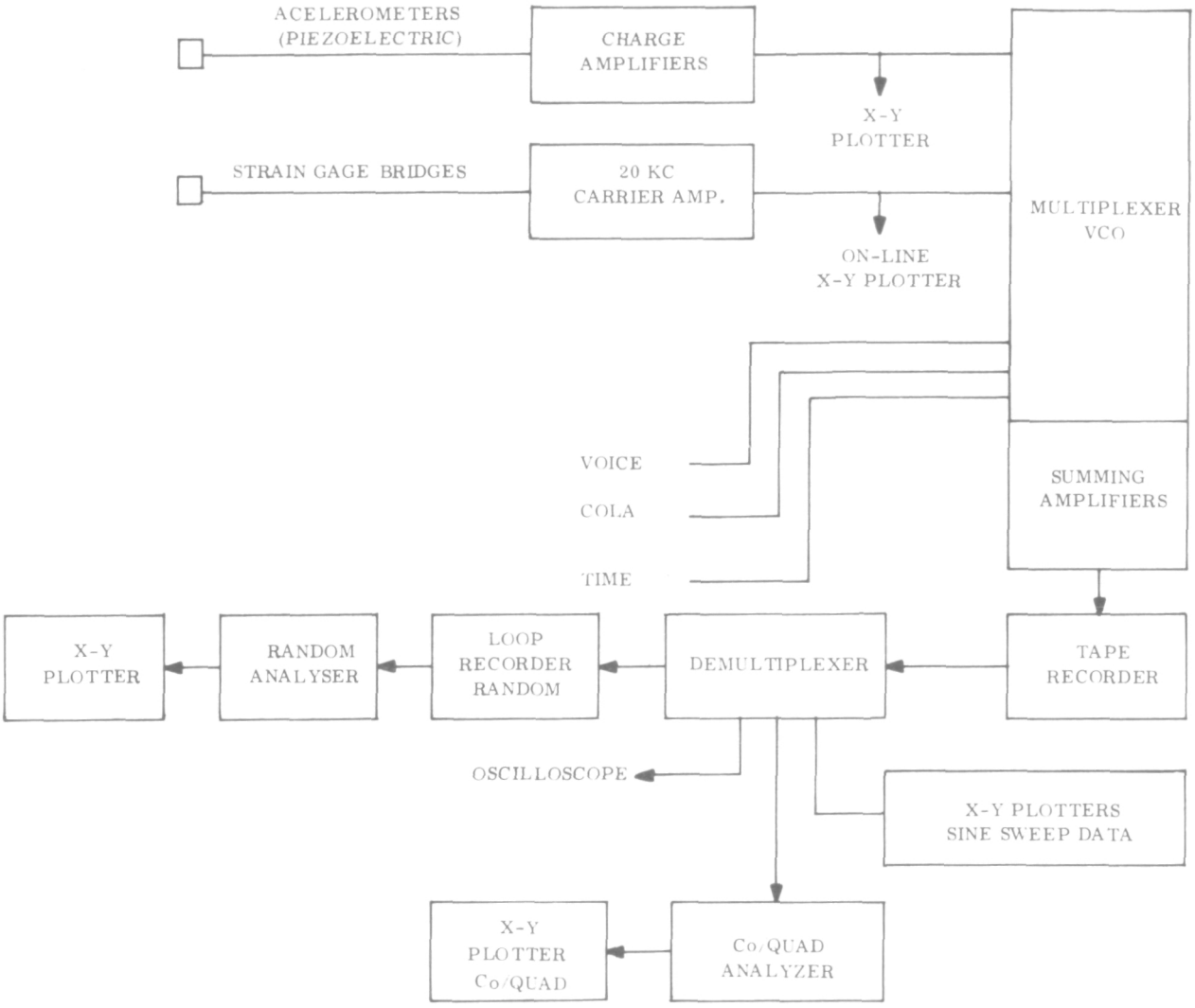

Figure 4.7-8. Data Processing System

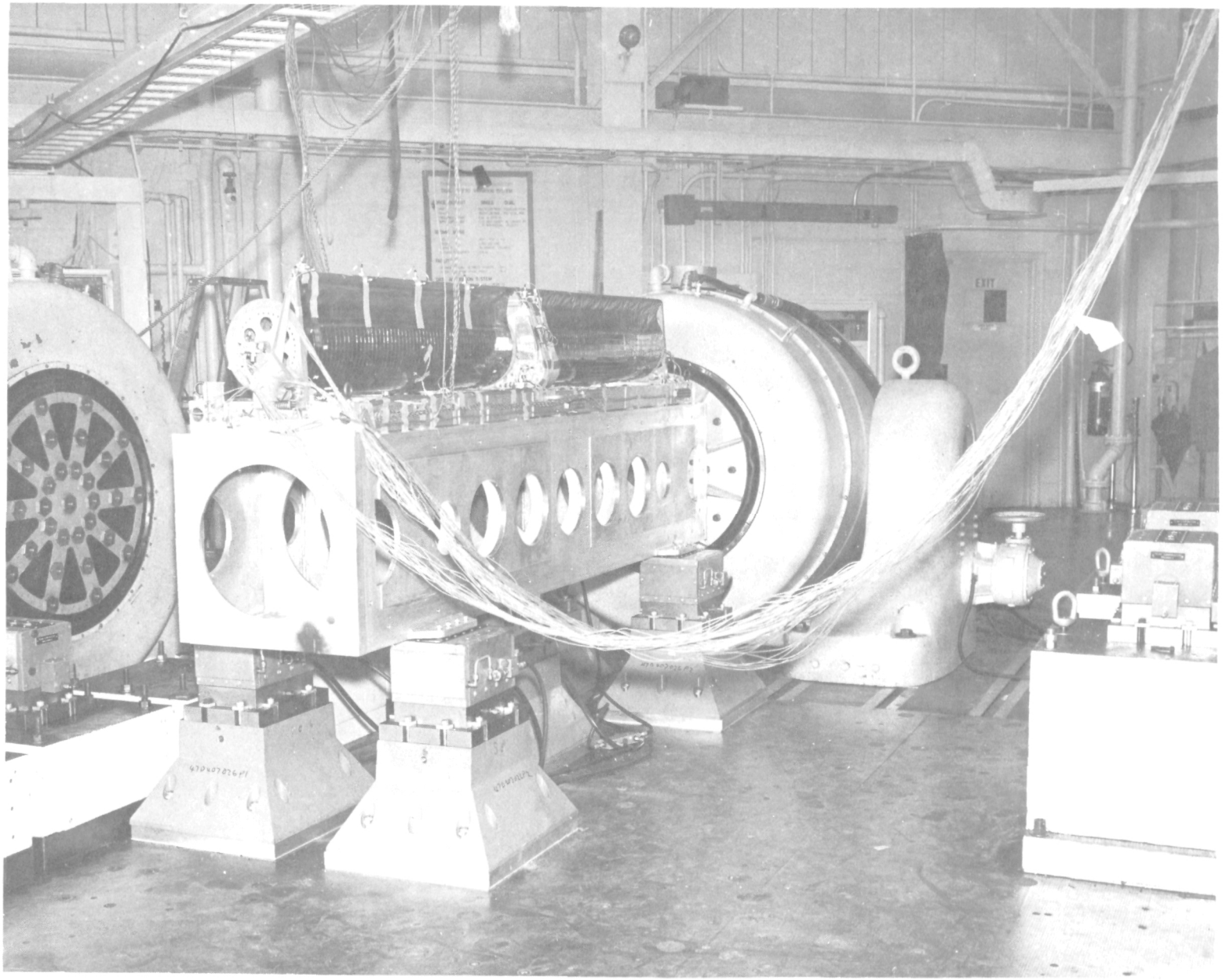

Figure 4.7-9 Y Axis Test Setup (VF 70271B)

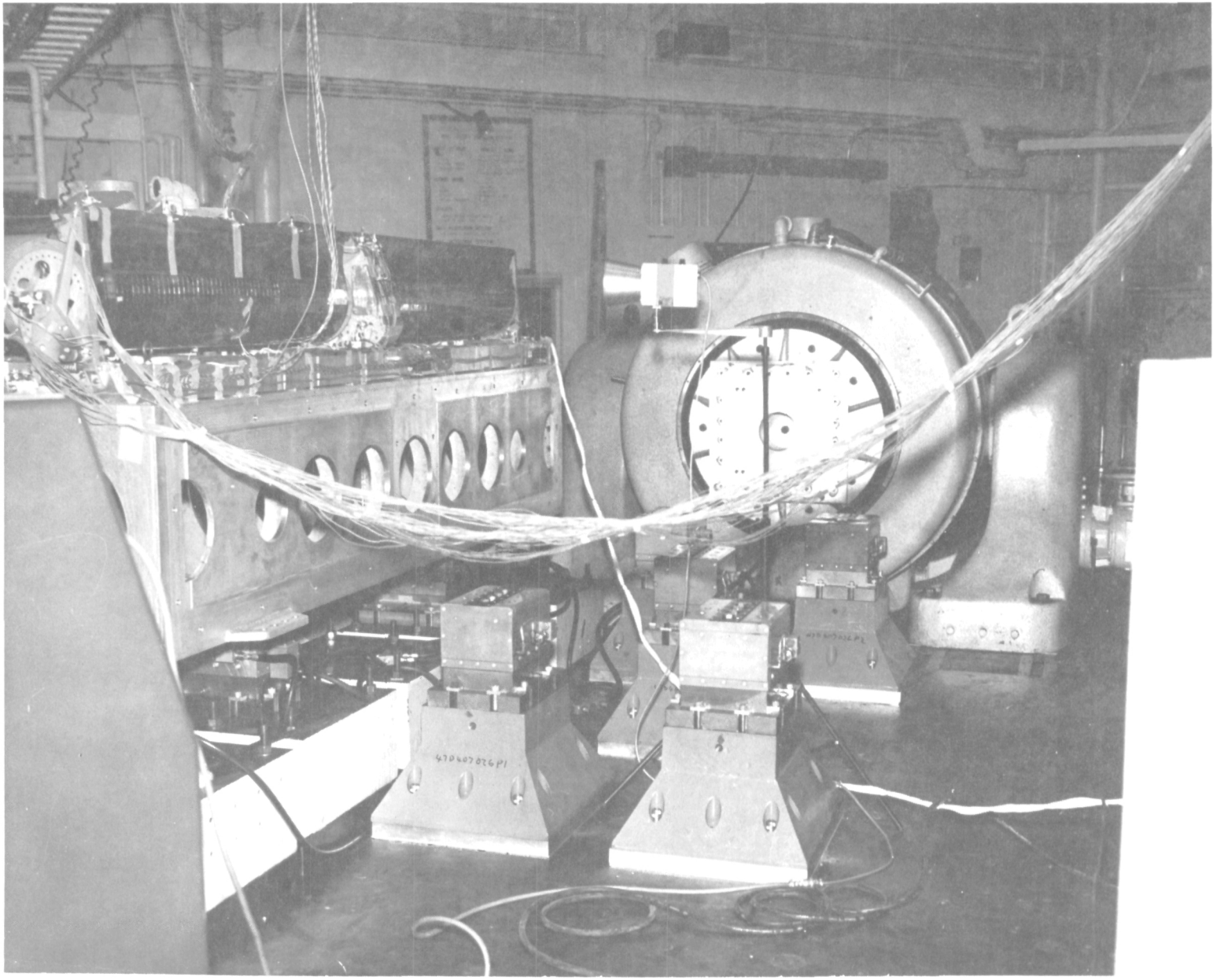

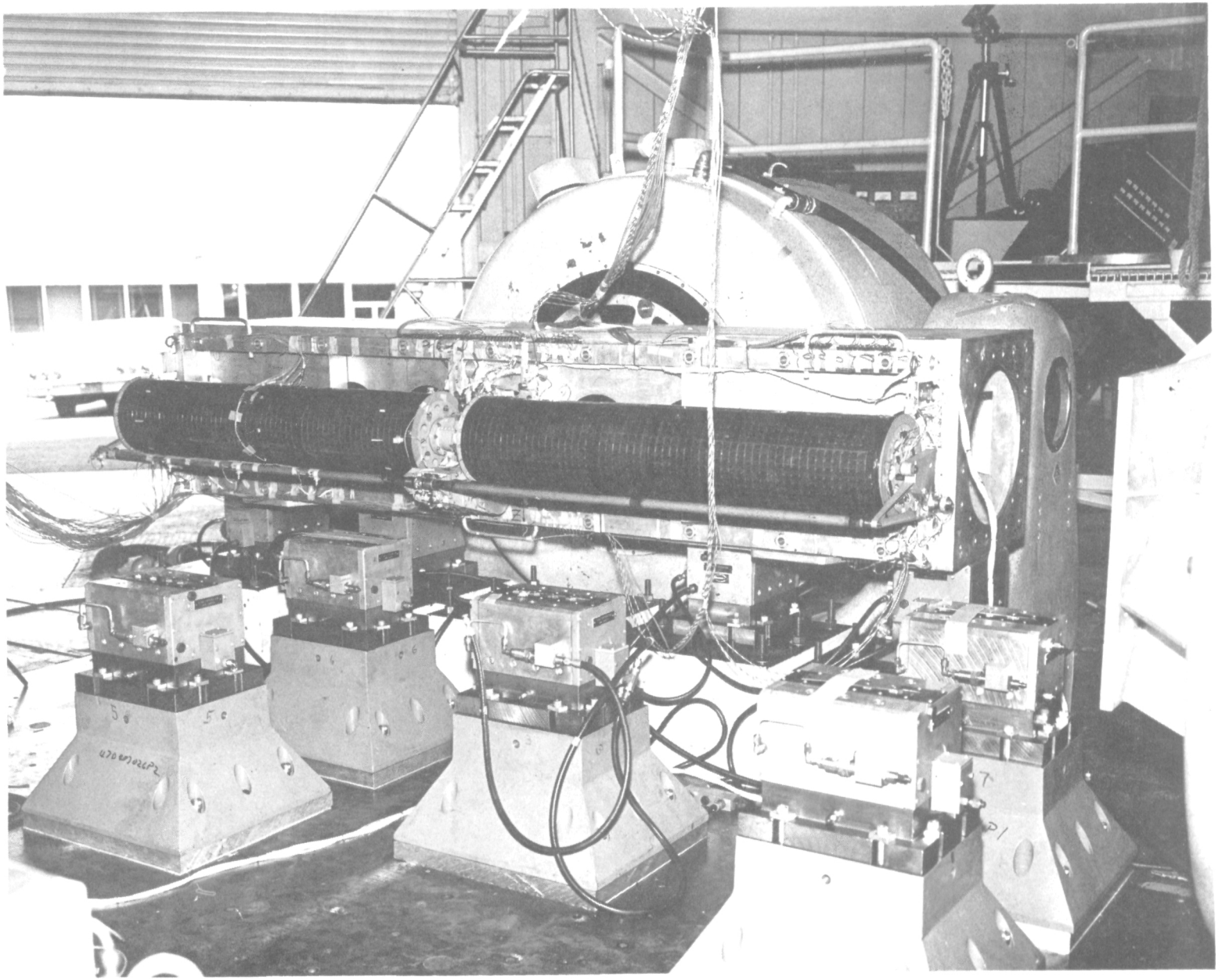

Figure 4.7-11 X Axis Test Setup (VF 70278)

input to determine amplification factors. During these runs the array was visually observed under strobe lighting to obtain an appreciation of blanket motion. Selected channels of the low level sweeps were analyzed for colinear and quadrature response for identification of blanket and structural modes occurring below 100 Hz. In addition, selected strain or accelerometer channels were analyzed to determine the risk of damage as the input levels were progressively increased to the qualification level.

2. An acceptance level sinusoidal sweep at two thirds of the specification level was performed to evaluate linearity of system response and to provide a prediction of the stress levels for the qualification run. The array blanket was visually studied under strobe light illumination during the constant level portion of the sweep between 10 and 250 Hz.

3. The sinusoidal qualification sweep was performed with selected channel responses reviewed during preparation for random testing.

4. Random testing followed the same sequence, that is low level, acceptance level and qualification level testing in the current axis of test. Selected strain channels were evaluated on line to evaluate the risk of damage.

5. On completion of any axis vibration testing the array was visually inspected and the BI-STEM actuator was operationally checked.

6. The tests were performed in the following axis order: Y, Z, and X.

4.7.5 DISCUSSION OF RESULTS

4.7.5.1 Motion Study

Table 4.7-2 lists array resonant frequencies and amplification factors. It can be seen that no structural modes were noted below 100 Hz. Leading edge member accelerometers indicated resonant behavior in 30 to 80 Hz band during X and Z excitation, but these were not investigated by dwell runs because of the low mass of the leading edge member; and because the accelerometers were mounted on the Kapton loop instead of the leading edge member surface. Visual observation of the leading edge member using strobe lights indicated decoupling between the Kapton and the leading edge member. Direct mounting of accelerometers had been ruled out prior to test due to the need to cut the Kapton or bond the Kapton locally to the leading edge member to obtain a more positive accelerometer mounting on the leading edge member.

Table 4.7-3 with its associated sketches present quadrature response of the 50% span blanket accelerometers. Figures 4.7-12, 4.7-13, 4.7-14 and 4.7-15 present representative co-quad plots of blanket accelerometers. Inspection of the co-quad plots indicates the absence of pure modal motion in the tabulated data; (i.e., plots indicate flat quad peaks, non-symmetrical functions about zero and significant co-linear component at maximum quadrature response). Visual observation of the blankets under strobe lights indicate the following:

1. During Y axis excitation no established describable motion of the blankets occurred either during low level (.4 g) or high level (4.6g) sinusoidal excitation. Motion was random, intermittent and resulted in elimination of wrap edge misalignments. Prior to Y excitation the

Table 4.7-2 RA250 Amplification Factors

Location	Station	Input & Resp. Axis	F_s (Hz)	A_s	F_q (Hz)	A_q
Actuator at	1	X	125	2.4	125	1.6
Center of Spool	1	Y	160	3.4	120	2.3
	1	Z	300	3.9	300	2.0
Center Support	8	X	120	2.1	120	1.6
Top	8	Y	160	5.5	120	3.5
	8	Z	160	3.7	100	3.8
Bearing Housing	15	X	440	4.2	440	3.5
	15	Y	140	1.0	110	1.2
	15	Z	350	4.3	350	2.1
Leading Edge	2	X	125	2.0	125	2.4
Member at Bistem	2	Y	160	5.7	125	4.2
	2	Z	160	4.3	100	4.2
L.E.M. 50% Span	4	X	125	2.2	130	1.7
	4	Z	130	5.1	125	6.0
L.E.M. 75% Span	5	X	130	5.1	130	1.1
	5	Z	130	4.5	120	3.3
Outboard Drum Support	7	X	270	2.4	270	2.3
	7	Y	260	1.7	270	2.8
	7	Z	280	1.5	280	3.8
Drum	25	X	140	2.2	No Data	
	40 & 28	Y	140	1.5	110	1.3
	27 & 31	Z	150	1.9	150	1.9
Blanket	16	X	40 to 60	1.8	40 to 60	1.3
	20	Y	30 to 80	1.3 to 1.9	10 to 16	2.2
	22 & 18	Z	30 to 100	1.3 to 3.7	10 to 50	1.3-1.8

F_s, A_s frequency and amplification factor based on survey level excitation, .46G

F_q, A_q frequency and amplification factors based on qualification level excitation.

Table 4.7-3 RA 250 - Stowed Blanket Quadrature Response
(Data is at 50% Span on +Y Drum)

a. 26 Hz X Excitation

Station	θ DEGR	QUAD G	f_1 Hz	f_2 Hz	c/c_c
16X	0	-3.0	----	----	
17R	45	+0.3	----	----	
18Z	90	0.0	----	----	
19R	135	-0.3	----	----	
20Y	180	----	----	----	----
21R	225	+3.4	17	30	0.26
22Z	270	+3.3	16	37	0.41
23R	315	-3.3	20	30	0.19
				Avg.	0.28

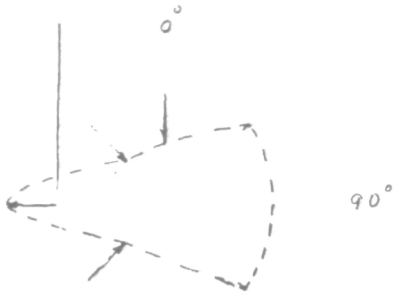

26 Hz Blanket Shape
c/c_c=0.28

b. 37 Hz X excitation

16X	0	-6.5	26	44	0.24
17R	45	+1.5	----	----	----
18Z	90	0.0	----	----	-----
19Y	135	-1.2	----	----	----
20Y	180	----	----	----	----
21R	225	+1.2	----	----	----
22Z	270	0.3	30	42	.16
			AVG.		0.20

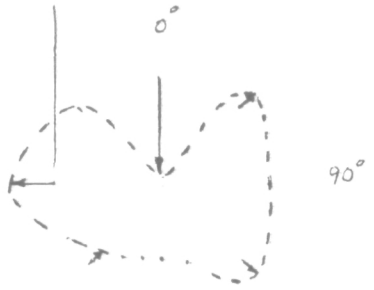

37 Hz Blanket Shape
c/c_c = 0.20

c. 52 Hz X excitation

16X	0	-2.6	----	----	----
17R	45	+4.0	----	----	----
18Z	90	+0.0			
19R	135	-5.0	41	67	0.23
20Y	180	----	----	----	-----
21R	225	+3.4	38	56	0.18
22Z	270	-0.8	46	56	0.10
23R	315	-3.0	44	56	0.12
				AVG.	0.18

52 Hz Blanket Shape
c/c_c = 0.18

$$C/C_c \text{ , Damping Ratio, } \frac{1}{2}\left[\frac{(f_2/f_1)^2 - 1}{(f_2/f_1)^2 + 1}\right]$$

f_1 In-phase peak response frequency immediately preceding the resonant frequency
f_2 In-phase peak response frequency immediately following the resonant frequency

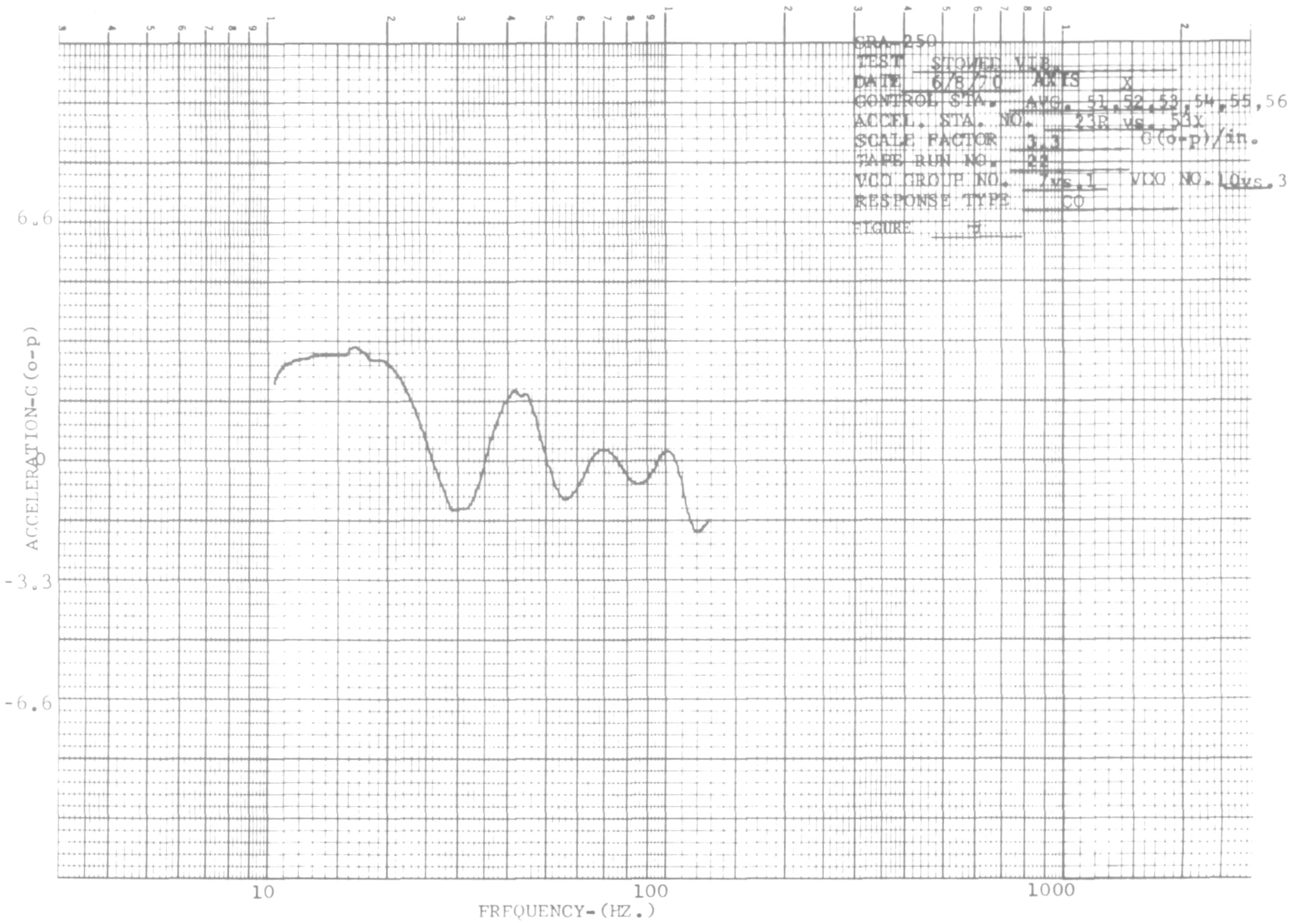

Figure 4.7-12. Frequency Sweep - Excitation Axis-X

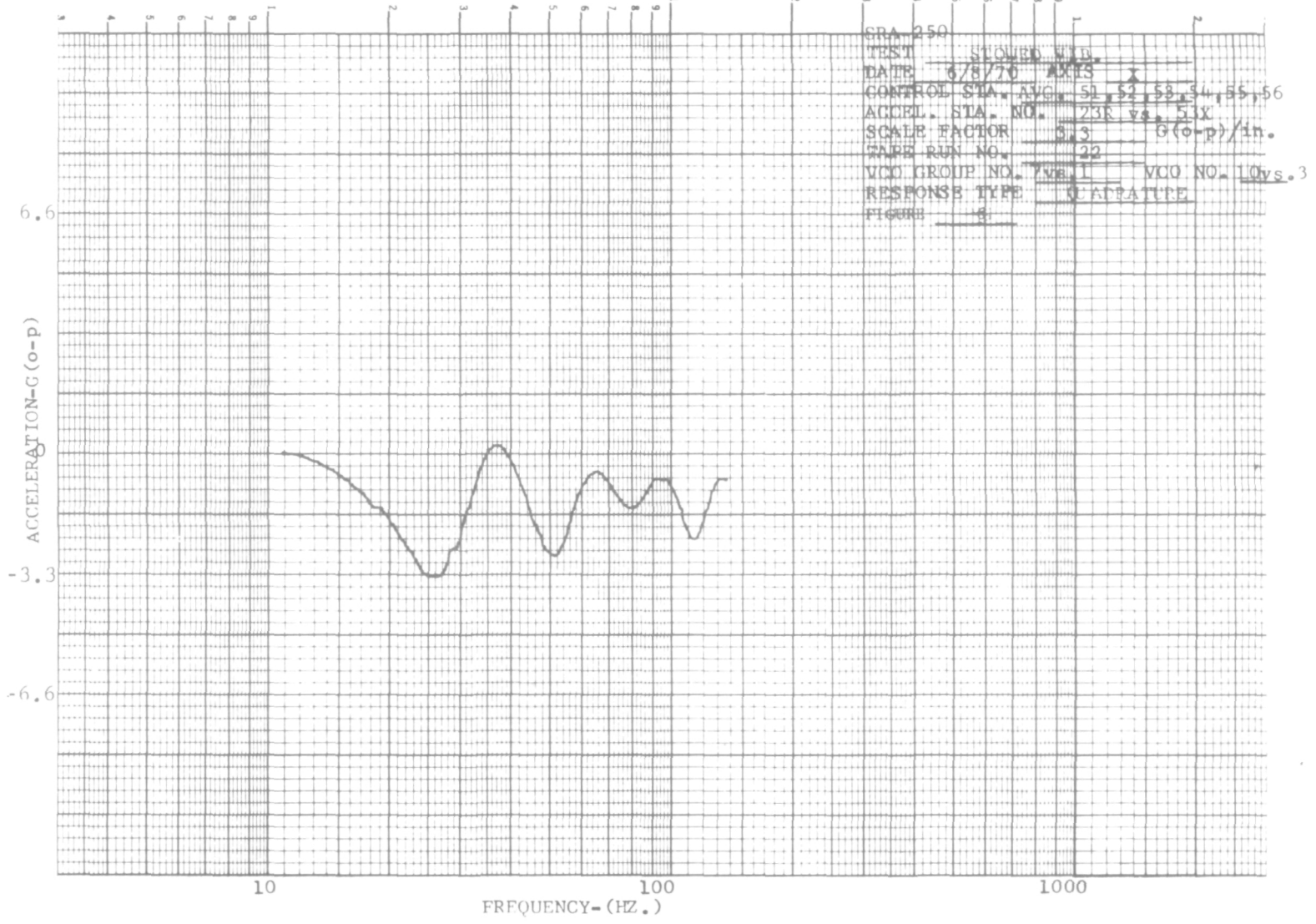

Figure 4.7-13. Frequency Sweep - Excitation Axis-X

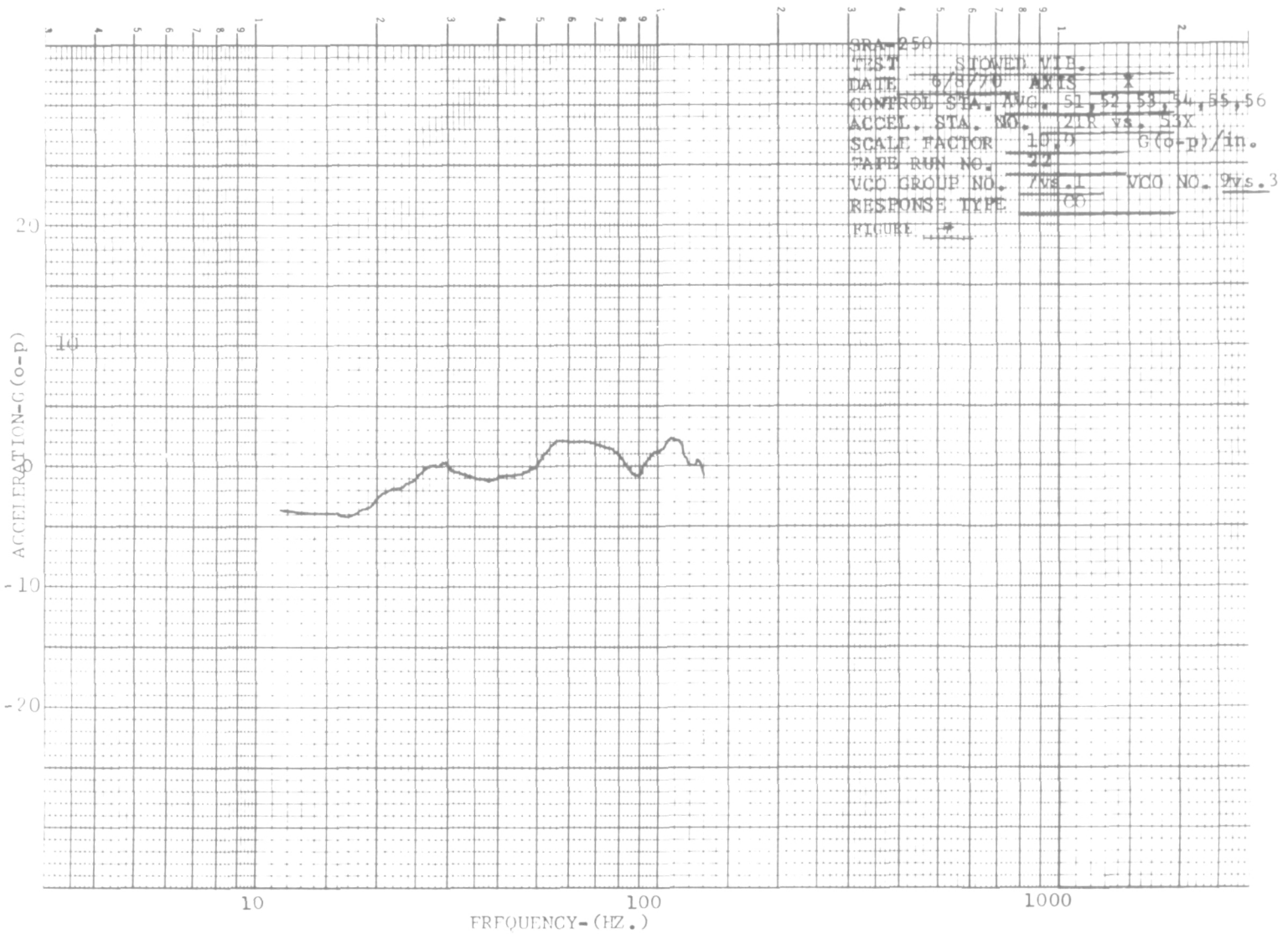

Figure 4.7-14. Frequency Sweep - Excitation Axis-X

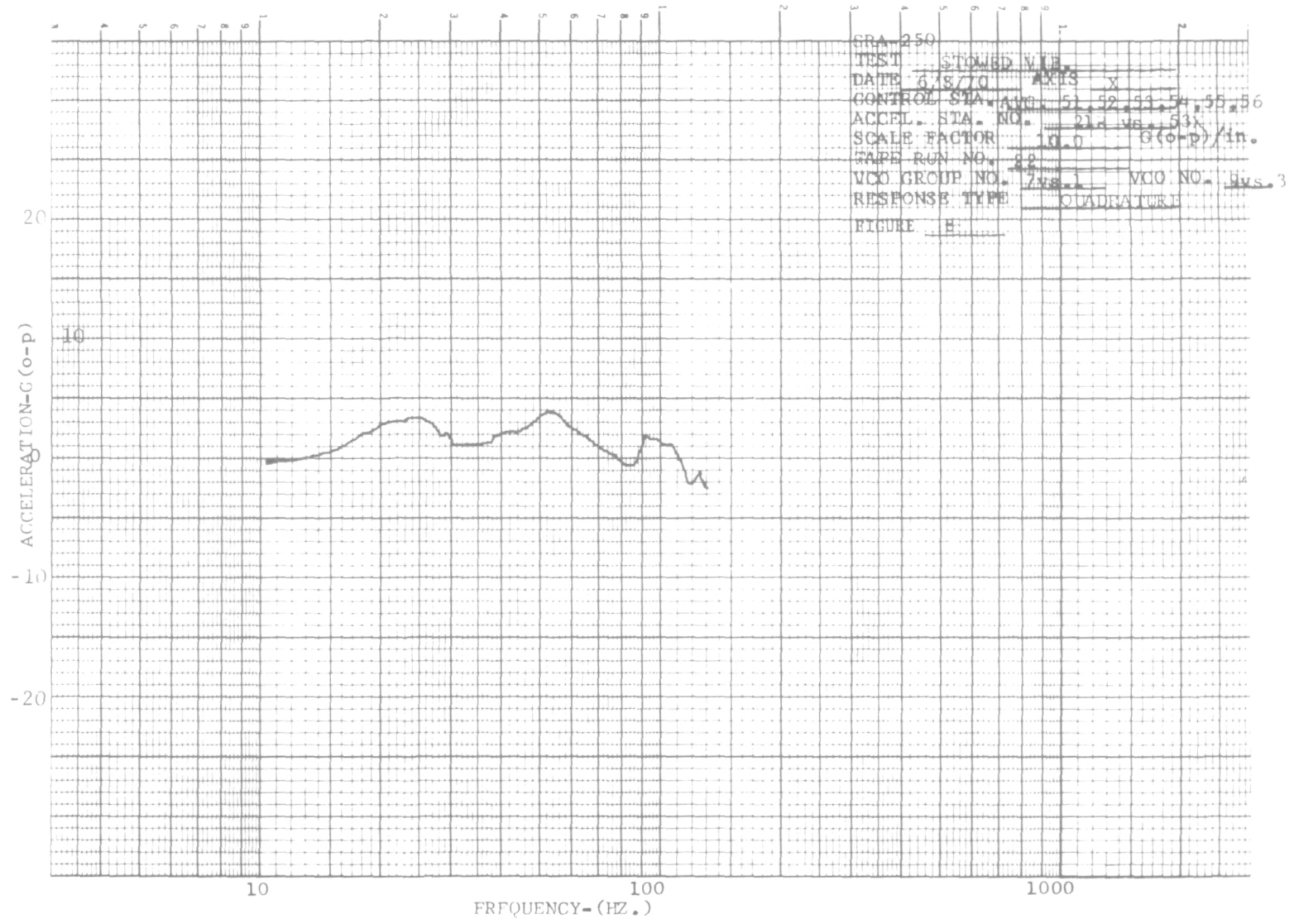

Figure 4.7-15. Frequency Sweep - Excitation Axis-X

blanket outer edges did not form a plane surface normal to the drum axis. Following excitation all edges were aligned normal to the drum axes and the blanket was centered on the drums. Significant blanket slack was generated between the leading edge member and drums. This slack was removed by uncaging the drum and rotating the drums 50 degrees to tighten the wraps.

2. During Z and X excitation blanket motion was identical and reflected in Table 4.7-3. At the start of Z axis testing, the drum wrap had already been tightened a total of 50 degrees producing a blanket wrap O.D. of 9.36 inches. No additional blanket slack was generated during Z and X axis testing.

3. During Z and X testing blanket motion was found to be affected by excitation level. At 0.46g input blanket motion both in amplitude and band width was significantly less than that at 3.0 G or 4.6 G.

4. Blanket motion during X excitation with array properly tight (9.36 inch O. D.) was of the order of 0.07 inches and thus always remained inside the edge guide envelope. No interference problems is foreseen with the spacecraft or launch configuration shroud.

4.7.5.2 Qualification Testing

In each axis of test on completion of the low level modal sweep an intermediate level sinusoidal and random run at 2/3 specified qualification test levels were performed. This 2/3 level test run is referred to as an acceptance level. It

was performed to determine linearity of array response and to provide a prediction of stress levels for the qualification runs. It was planned to reduce the qualification and acceptance test levels by reducing the input in selected frequency resonant bands if excessive risk of damage was indicated. In all axes of test the specified qualification level input profile was as listed below.

SINUSOIDAL QUALIFICATION SINUSOIDAL INPUT

Frequency	Level	Sweep Rate
5 to 10 Hz	0.90" DA	1 octave/minute
10 to 225 Hz	± 4.6 G	
225 to 550 Hz	0.00176 DA	
550 to 2000 Hz	± 27.0 G	

Figures 4.7-16, 4.7-17 and 4.7-18 present the plots of the input control signals during sinusoidal qualification testing.* Figure 4.7-7 presents the location of input accelerometers identified in Figures 4.7-16, 4.7-17, and 4.7-18 as being averaged for input control. Low frequency, below 7 Hz, deviation from input specification is a plotting error due to log converter low frequency roll-off characteristics.

Input levels were monitored by on line peak G meters in the exciter servo loop. Due to fixture response characteristics, different control accelerometers were averaged in each axis of test.

* Constant displacement profile between 225 and 550 Hz was approximated by multiple acceleration steps due to control equipment limitation.

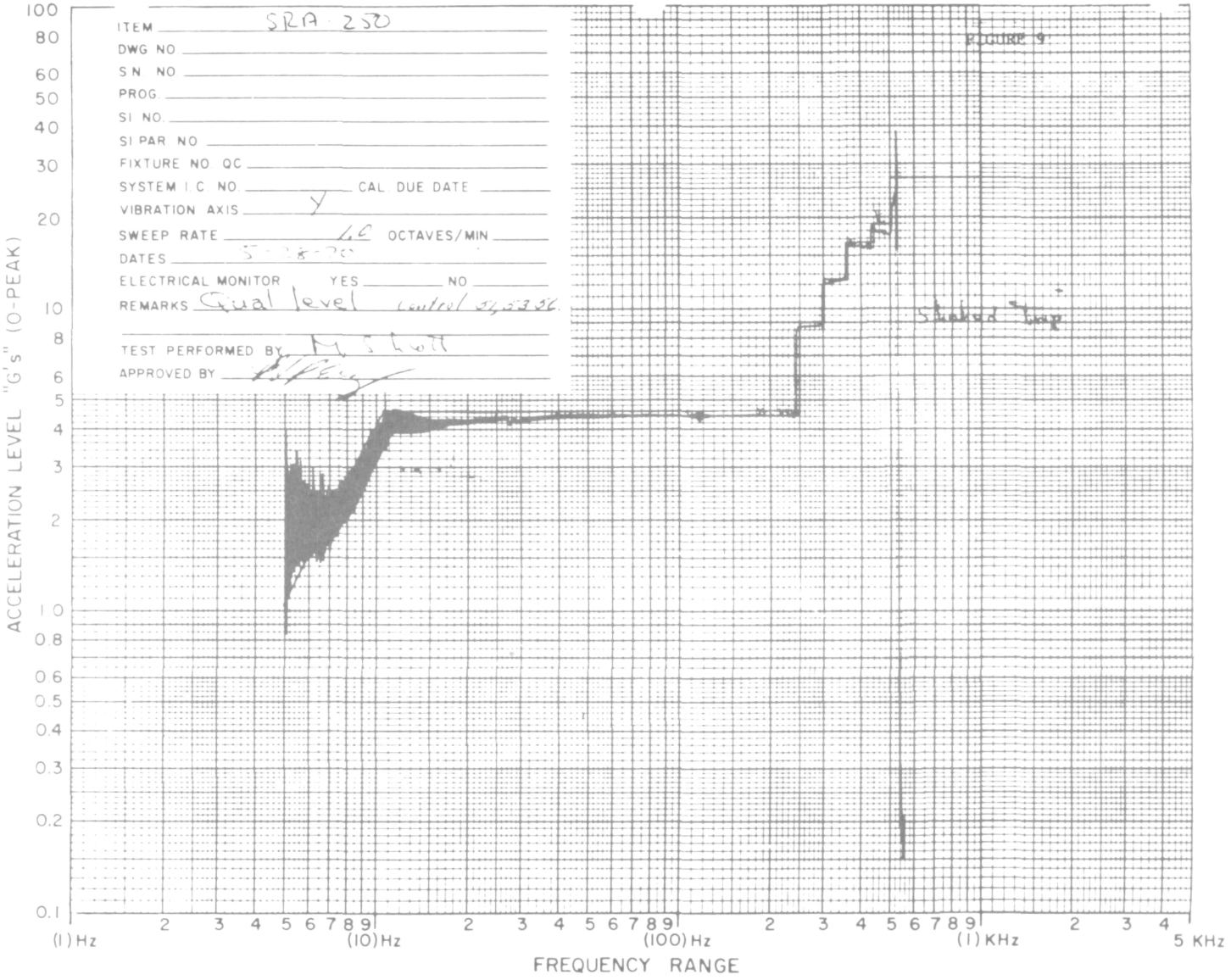

Figure 4.7-16 Control Signal for Y Axis Sinusoidal Vibration - Qualification Level Run

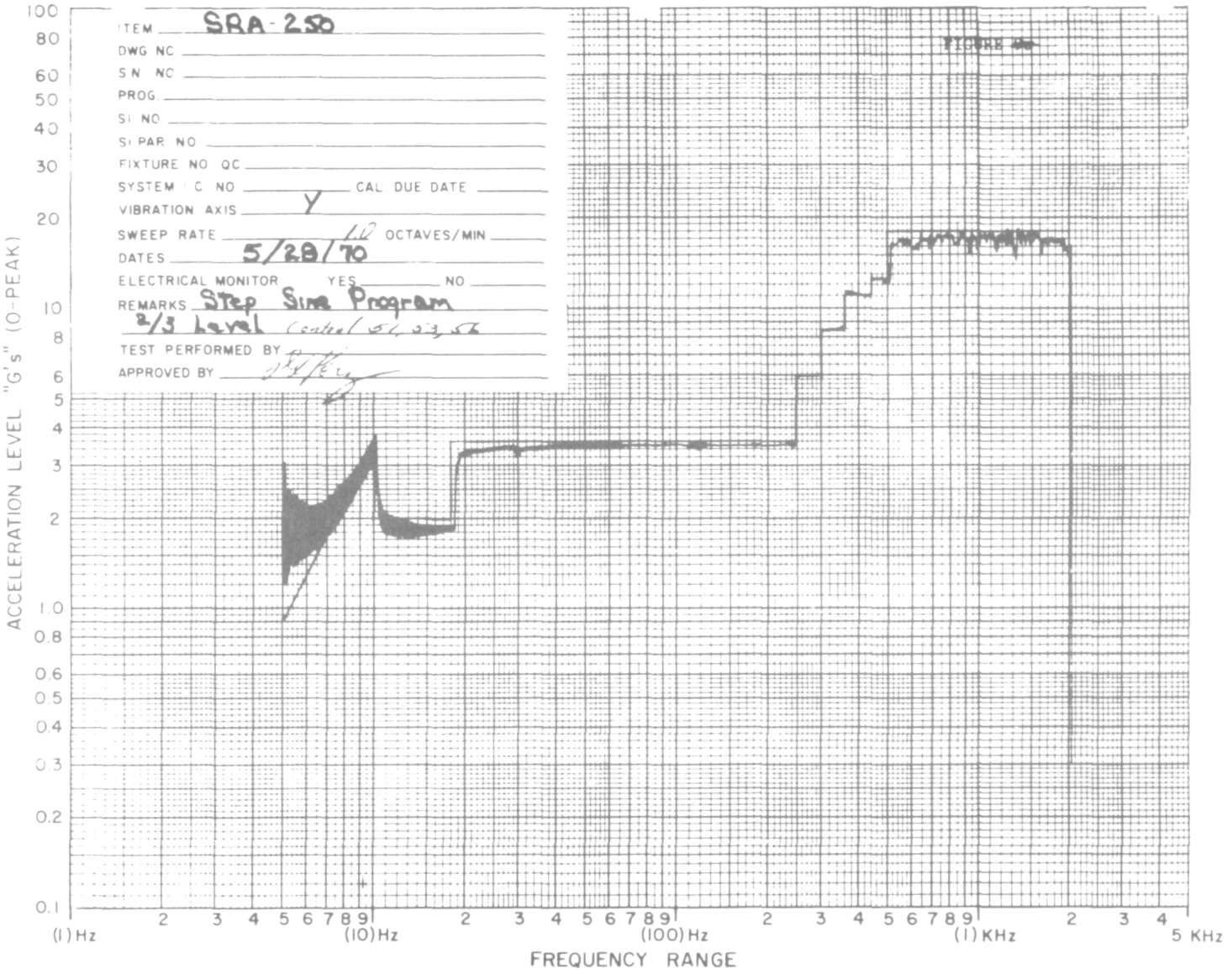

Figure 4.7-17 Control Signal for Y Axis Sinusoidal Vibration - ACCEPTANCE LEVEL RUN

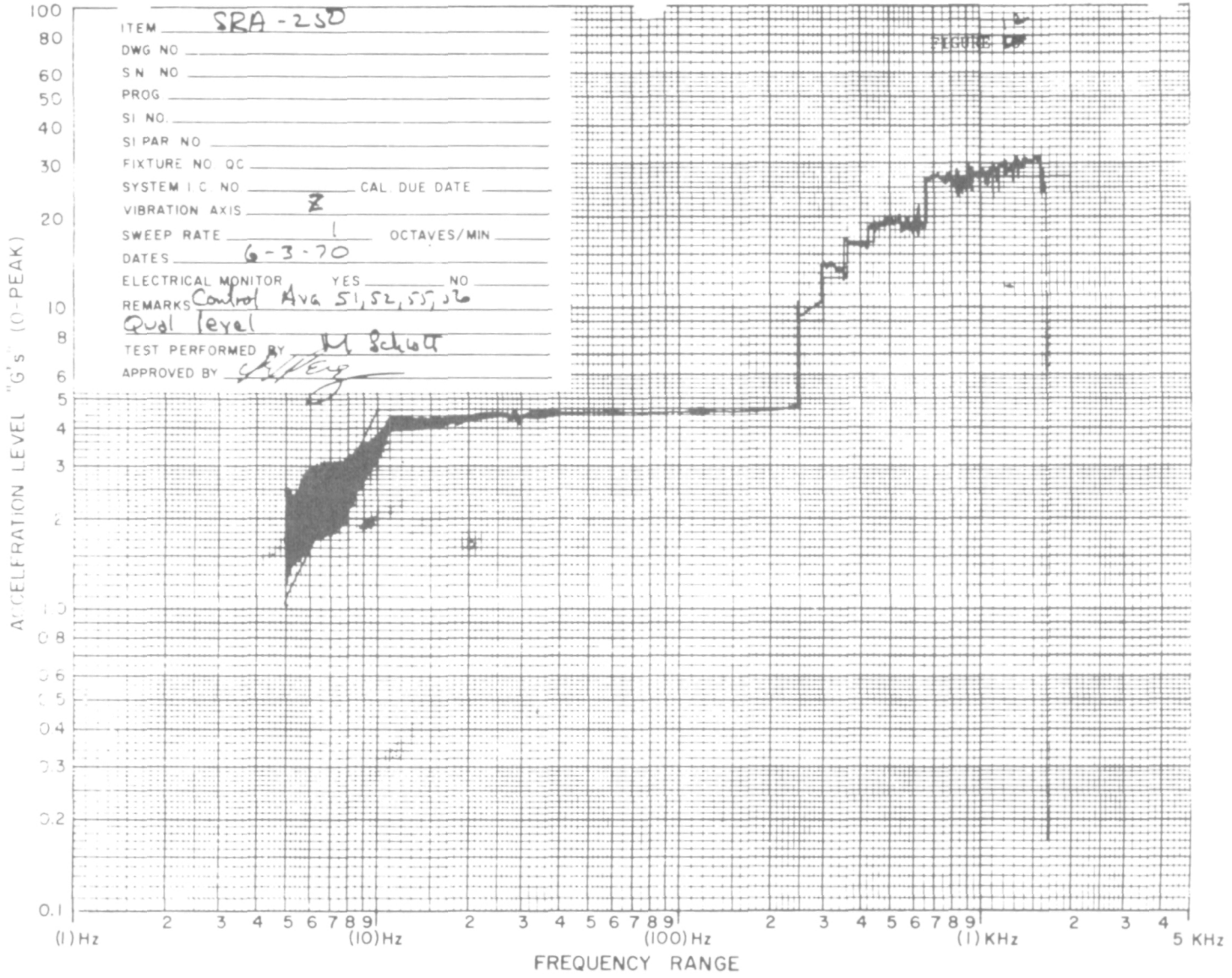

Figure 4.7-18 Control Signal for Z Axis Sinusoidal Vibration - Qualification Level Run

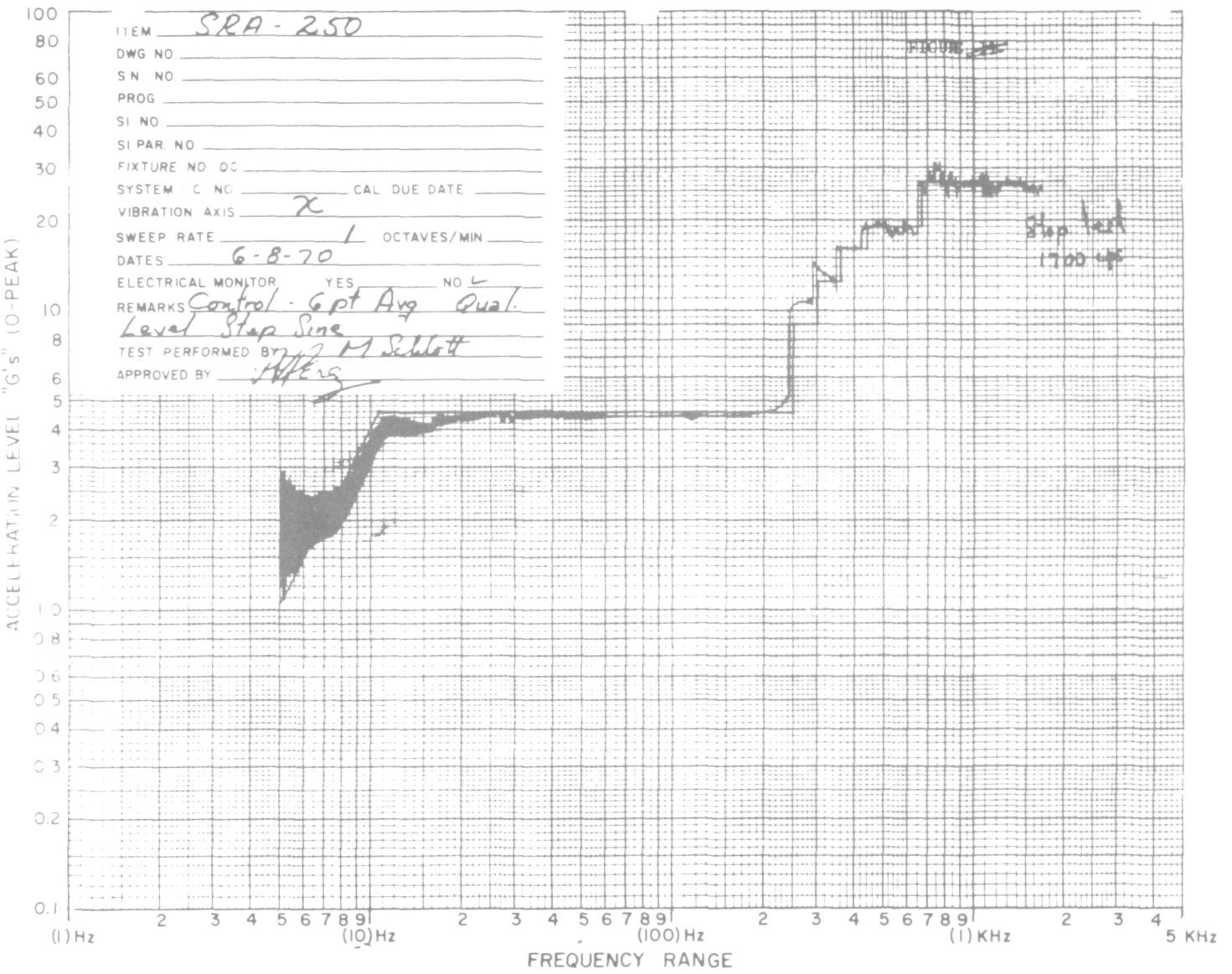

Figure 4.7-19 Control Signal for X Axis Sinusoidal Vibration - Qualification Level Run

Figure 4.7-16 presents the Y axis qualification run. Input control was average of stations 51Y, 53Y and 56Y. This sweep was terminated at a 530 Hz fixture resonance by operation of power amplifier circuit breaker. The qualification run was not completed as the acceptance run Figure 4.7-17 was successfully run and indicated no significant strain loads in the array above 500 Hz. The notched input in Figure 4.7-17 between 10 and 18 Hz was programmed due to a false indication of strain at station 113 at qualification input. This notch was removed on the basis of the acceptance run when it was determined that the high indicated strain was due to a signal conditioner malfunction.

Figure 4.7-18 presents the Z axis qualification run input. Input control was the average of station 51Z, 52Z, and 56Z. Testing was terminated at 1,650 Hz due to saturation of exciter servo dynamic response range. Shutdown was directed to preclude tripping amplifier safety overload circuits. The level change to 27G was shifted from 500 Hz to 650 Hz to prevent loss of servo control in the 550-600 Hz fixture resonant band.

Figure 4.7-19 presents the X axis qualification run. Input control was the average of stations 51X, 52X, 53X, 54X, 55X, and 56X. For the same reasons discussed previously, the 27G step level change was shifted to 650 Hz and testing was terminated at 1700 Hz.

Following qualification sinusoidal testing in each axis of test a qualification random test was performed. The specified test spectrum is presented below.

RANDOM QUALIFICATION TEST INPUT

Frequency	PSD +3 DB -1.5DB	
20 to 40 Hz	+ 6 db/octave	overall level 33G RMS ±10%
40 to 700 Hz	1.0 G^2/Hz	
700 to 2000 Hz	-6 db/octave	exposure 60 sec. ± 1 sec.

Figure 4.7-20 presents the Y axis qualification input control PSD plot. The analyzed signal is the average of stations 51Y, 53Y, 54Y, and 56Y. The specification limits are overlaid on the control plot. The overall RMS level indicates that significant energy above 2 KHz was present since the overall level and shaping are in specification but the spectral density is low.

Figure 4.7-21 presents the Z axis qualification input control PSD plot. The analyzed signal is station 56Z, the only station on which operational control was possible with the test fixture. Equalization to specified spectrum shape was possible only to 22 G RMS where the high frequency, above 550 Hz, spectrum broke up and specified spectral distribution could not be controlled. It was decided to reshape the qualification spectrum by rolling off at 12 db/octave above 350 Hz. This resulted in a 24G RMS overall level input at station 56Z with an average input of 26G RMS considering stations 51, 53, 54, and 56 inputs.

Figure 4.7-22 presents the X axis qualification input control PSD plot. The analyzed signal is the average of stations 51X, 54X, and 56X. The specification density distribution is overlaid on the input plot indicating again that energy was present above 2 KHz as the indicated overall level read during analysis was 37 G RMS and the computed level from the spectral density plot is 31 G RMS.

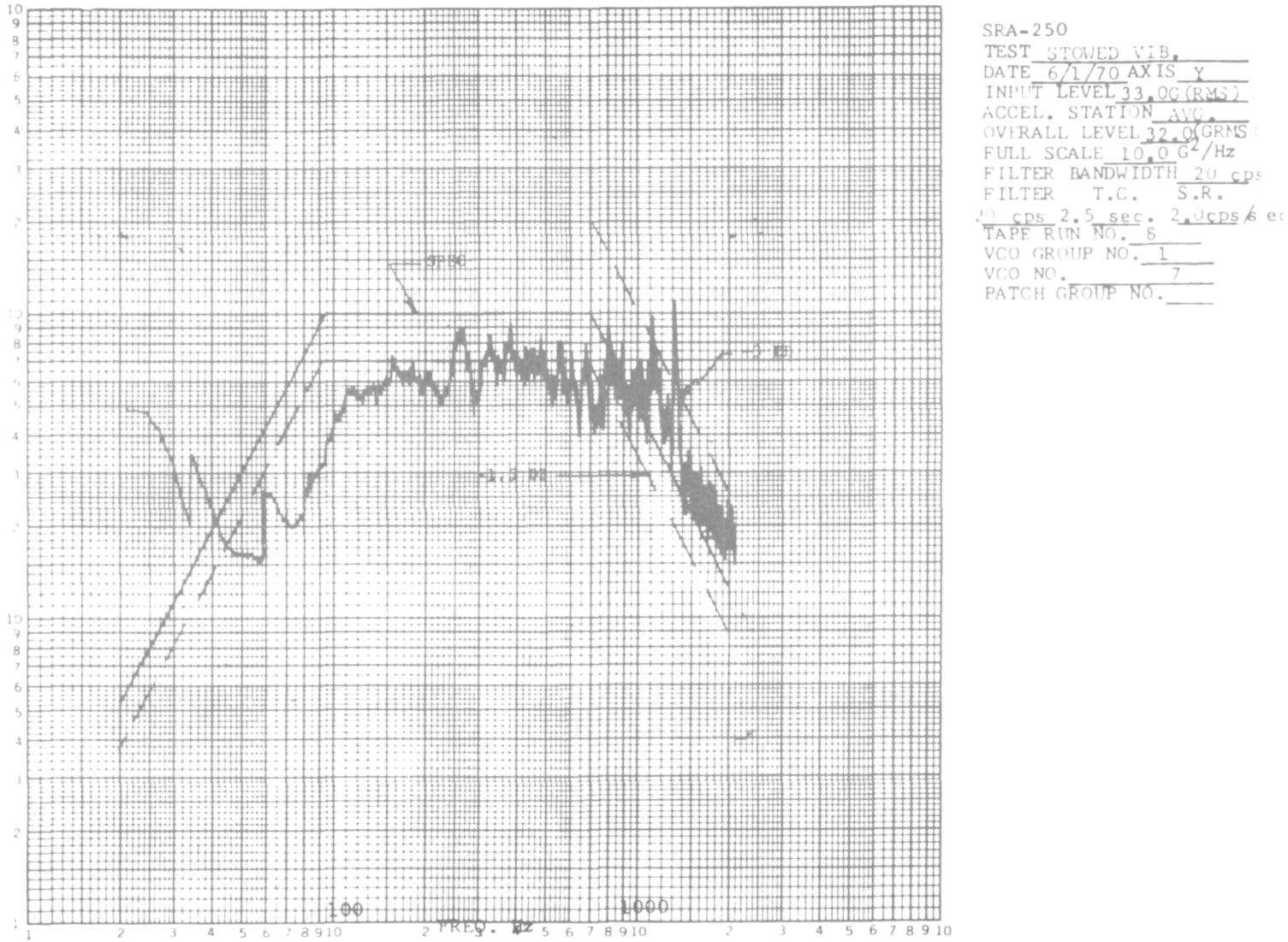

Figure 4.7-20 Power Spectral Distribution of Control Signal for X Axis Random Vibration - Qualification Level Run

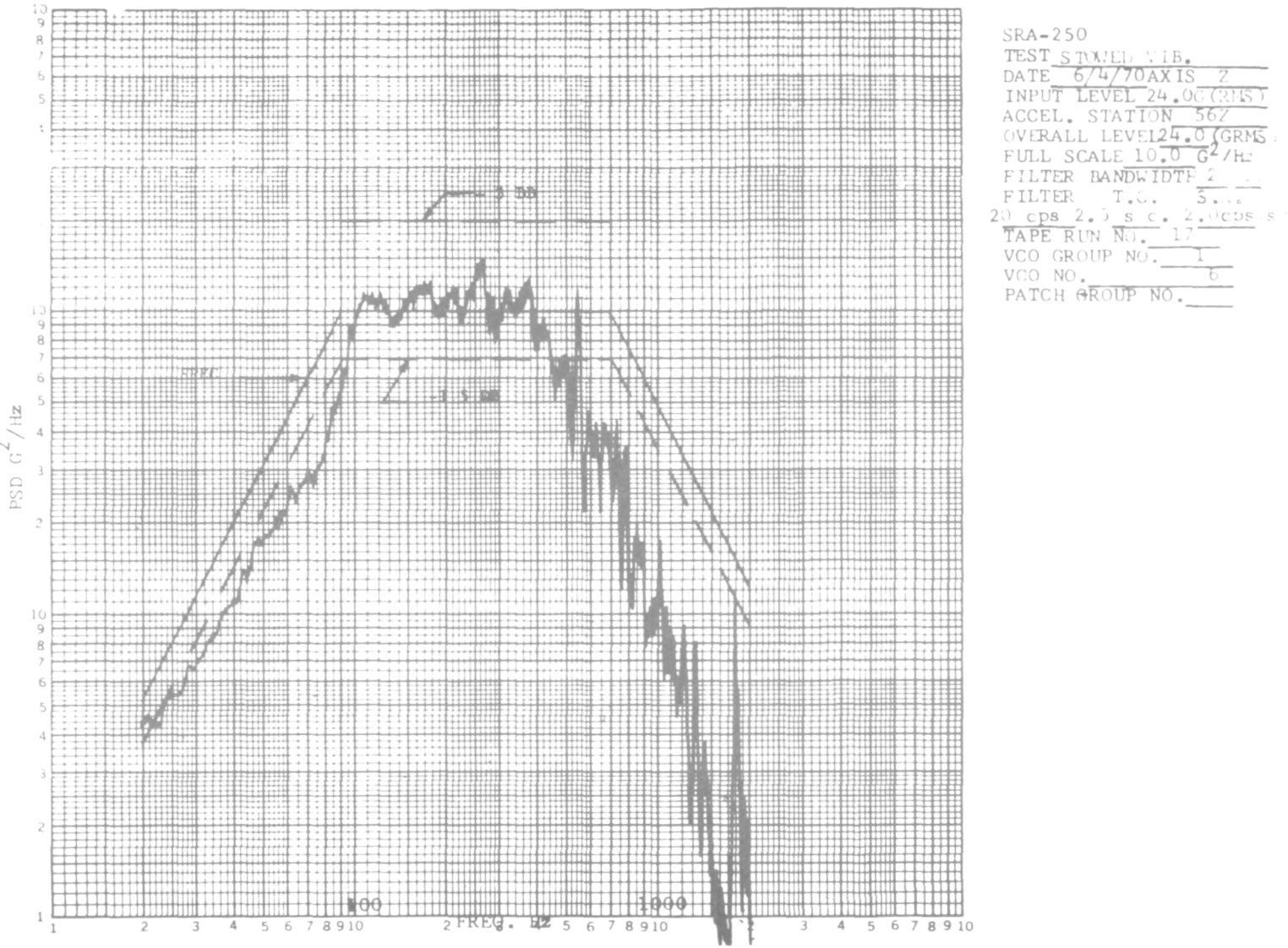

Figure 4.7-21 Power Spectral Distribution of Control Signal for Z Axis Random Vibration - Qualification Level Run

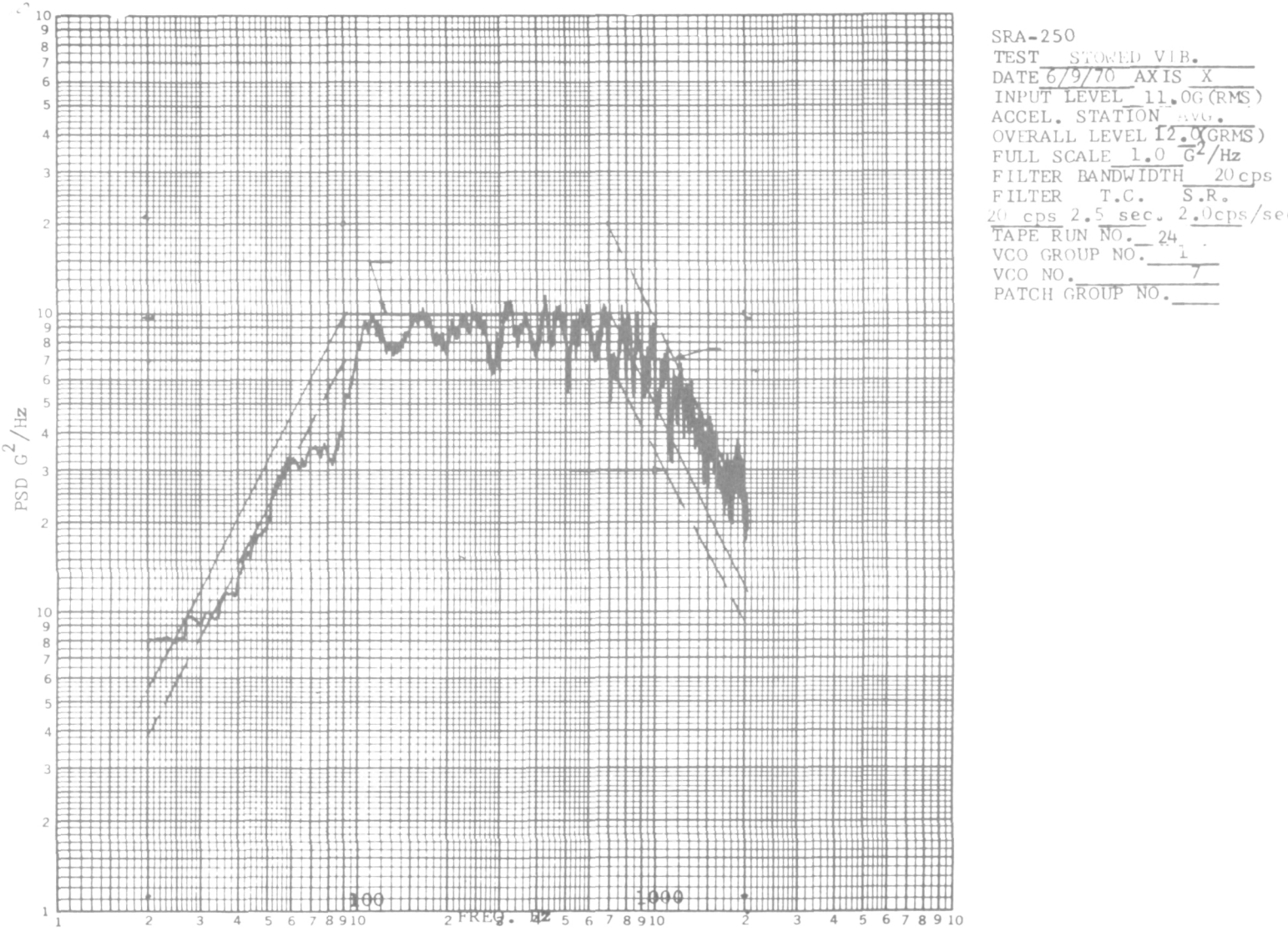

Figure 4.7-22 Power Spectral Distribution of Control Signal for X Axis Random Vibration - Qualification Level Run

4.7.5.3 Dynamic Loads

The qualification environment involved high input levels both for the sinusoidal and random inputs. It was believed that these high input levels involved considerable risk of structural damage to the array system. Consequently, the analyses of the dynamic loads and resulting stresses was emphasized. There was no established technique for predicting the dynamic loads due to the solar array blankets so results from previous tests were utilized (Reference 1.9, "Deployable Large Area Solar Cell Array Testing, Ryan Report No. 20869-4, 15 August 1968, JPL Contract 951107.). Based on the reference results, the natural frequency of the stowed array blanket was assumed to be 50 Hz. Thus the mass of the solar cell blankets was assumed to be attached to the drums via springs with a stiffness that was selected to provide the desired frequency. A Q of 12 was used. This approach was grossly conservative in that the observed amplification factors were very much lower (See Table 4.7-2) and consequently the dynamic loads were lower than predicted by the analysis. The expected high stress were not developed. The stowed array system did not exhibit sharp resonances and high amplifications. Consequently it sustained the high vibration levels without damage.

SECTION 5

REFERENCES

1-1. Feasibility Study 30 Watts Per Pound Rollup Solar Array Final Report

Report No. 68SD4301, 21 June 1968, JPL Contract 951970, General Electric Company, Philadelphia, Pa.

1-2. Detail Specification for 30 Watts Per Pound Rollup Solar Cell Array, Rev. E, JPL Specification SS501407.

1-3. Quarterly Report No. 1, Rollup Subsolar Array. Report No. GE-SSO-69SD4282, 12 June 1969. JPL Contract 952314. General Electric Company, Philadelphia, Pa.

1-4. Quarterly Report No. 2, Rollup Subsolar Array. Report No. GE-SSO-69SD4351, 15 September 1969. JPL Contract 952314. General Electric Company, Philadelphia, Pa.

1-5. Quarterly Report No. 3, Rollup Subsolar Array, Report No. GE-SSO-69SD4373, 15 December 1969. JPL Contract 952314. General Electric Company, Philadelphia, Pa.

1-6. Quarterly Report No. 4, Rollup Subsolar Array. Report No. GE-SSO-70SD4225, 13 March, 1970. JPL Contract 952314. General Electric Company, Philadelphia, Pa.

1-7. Hok, Gunnar, "Response of Linear Resonant Systems to Excitation of a Frequency Varying Linearly with Time", Journal of Applied Physics, August, 1947.

1-8. Final Program Briefing - Lightweight Solar Panel Development Program. 15 July 1970. JPL Contract 952571. The Boeing Company, Seattle, Wash.

1-9. Deployable Large Area Solar Cell Array Testing. Report No. 20869-4. JPL Contract 951107. Ryan Aeronautical Company, San Diego, California.

GENERAL ELECTRIC
SPACE DIVISION
SPACE SYSTEMS ORGANIZATION